THE UNIVERSITY
of EDINBURGH

Constraining bedrock erosion during extreme flood events

Edwin R.C. Baynes

Thesis submitted for the degree of Doctor of Philosophy

The University of Edinburgh

2015

Declaration

This thesis has been composed by myself and represents my own work. I have carried out all of the research presented herein. I acknowledge my co-authors in Sub-Chapters 2.3 and 2.4, which are written in research paper format, but I am the first author on both of these and as such wrote the text, prepared all the diagrams and developed the intellectual arguments presented. The contributions of the co-authors are documented where appropriate.

This work has not been submitted for any other degree or professional qualification.

Edwin Richard Crews Baynes

2015

‘The great cataract is the embodiment of power … It is a spectacle of great beauty. The clear, green, pouring stream, forced with growing speed against the air, parts into rhythmic jets which burst and spread till all the green is lost in a white cloud of spray, on which the rainbow floats … but the fascination of its ever-varied yet continuous motion, and the awe that waxes rather than wanes with familiarity, are not to be felt at second-hand; and so the world, in long procession, goes to see … but its geographical significance is too little appreciated. This paper endeavours to tell some of the lore of the professional geographer and geologist, in order that the layman may gain pleasure not only from the beauty and grandeur of the scene, but through understanding its meaning as part of the great drama of nature … Every element of the landscape has an origin and a history. To relate these is to explain it.’

G.K. Gilbert (1896) - *Niagara Falls and their History*

Abstract

The importance of high-magnitude, short-lived flood events in controlling the evolution of bedrock landscapes is not well understood. During such events, erosion processes can shift from one regime to another upon the passing of thresholds, resulting in abrupt landscape changes that can have a long lasting legacy on landscape morphology.

Geomorphological mapping and topographic analysis document the evidence for, and impact of, extreme flood events within the Jökulsárgljúfur canyon (North-East Iceland). Surface exposure dating using cosmogenic ^{3}He of fluvially sculpted bedrock surfaces determines the timing of the floods that eroded the canyon and helps constrain the mechanisms of bedrock erosion during these events. Once a threshold flow depth has been exceeded, the dominant erosion mechanism becomes the toppling and transportation of basalt lava columns and erosion occurs through the upstream migration of knickpoints. Surface exposure ages allow identification of three periods of rapid canyon cutting during erosive flood events about 9, 5 and 2 ka ago, when multiple active knickpoints retreated large distances (> 2 km), each leading to catastrophic landscape change within the canyon. A single flood event ~9 ka ago formed, and then abandoned, Ásbyrgi canyon, eroding 0.14 km^3 of rock. Flood events ~5 and ~2 ka ago eroded the upper 5 km of the Jökulsárgljúfur canyon through the upstream migration of vertical knickpoints such as Selfoss, Dettifoss and Hafragilsfoss. Despite sustained high discharge of sediment-rich glacial meltwater (ranging from 100 to 500 m^3 s^{-1}); there is no evidence for a transition to an abrasion-dominated erosion regime since the last erosive flood: the vertical knickpoints have not diffused over time and there is no evidence of incision into the canyon floor. The erosive signature of the extreme events is maintained in this landscape due to the nature of the bedrock, the discharge of the river, large knickpoints and associated plunge pools. The influence of these controls on the dynamics of knickpoint migration and morphology are explored using an experimental study. The retreat rate of knickpoints is independent of both mean discharge, and temporal variability in the hydrograph. The dominant control on knickpoint retreat is the knickpoint form which is set by the ratio of channel flow depth to knickpoint height. Where the knickpoint height is five times greater than the flow depth, the knickpoints developed undercutting plunge pools, accelerating the removal of material from the knickpoint base and the overall retreat

rate. Smaller knickpoints relative to the flow depth were more likely to diffuse from a vertical step into a steepened reach or completely as the knickpoint retreated up the channel. These experiments challenge the established assumption in models of landscape evolution that a simple relationship exists between knickpoint retreat and discharge/drainage area. In order to fully understand how bedrock channels, and thus landscapes, respond and recover to transient forcing, further detailed study of the mechanics of erosion processes at knickpoints is required.

Lay summary

The importance of high-magnitude, short-lived events in controlling the evolution of landscapes is not well understood. This matters because during such events, erosion processes can surpass thresholds and cause abrupt landscape changes that have a long lasting legacy on landscape morphology. In this PhD, I use a study of the formation and evolution of the large (28 km long) Jökulsárgljúfur canyon in northeast Iceland, and an experimental flume tank in the laboratory to study the impact of the extreme flood events on the landscape and also the complexities of the erosion processes at work during such events.

In Iceland, I used a broad range of methods from the fields of geomorphology, geochemistry and geophysics, to develop a detailed evolution history of the Jökulsárgljúfur canyon since the last Ice Age. In particular I use a dating technique known as surface exposure dating using cosmogenic nuclides to identify the timing of erosion within the canyon. This technique is based on the concept that the Earth's surface is constantly being bombarded with cosmic rays which, in some minerals present on the Earth's surface, produce 'cosmogenic nuclides' through time. I collected rock samples from eroded surfaces within the canyon and measured the concentration of cosmogenic nuclides within them, allowing the age of the eroded surfaces, and hence the timing of the extreme floods to be determined. I show that in the last 10,000 years, there have been three periods where extreme flood events have eroded the canyon are the dominant control on the evolution. During the floods, which can be triggered by volcanic activity beneath the large ice cap, Vatnajokull, the flow depth exceeds the threshold for erosion through plucking rather than abrasion at large vertical waterfalls, leading to rapid upstream retreat of waterfalls over distances greater than 2.5 km in very short periods of time (days to weeks), These flood events have a long-term legacy on the landscape with the erosive signature maintained for thousands of years, emphasizing the importance of episodic extreme events in shaping landscapes.

Using the experimental flume tank, I also identify the role of thresholds in controlling how waterfalls erode during background time-periods between the extreme flood events. I carried out a series of experiments that showed that taller waterfalls are more likely to retreat upstream faster than smaller waterfalls, when keeping everything else the same. The discharge in the channel does not affect the

upstream retreat rate of the waterfall but does make the channel wider, thus eroding more material as the waterfall retreats upstream.

These results show that the action of extreme flood events, complex erosion processes and thresholds between different erosion regimes must be considered in order to fully understand how landscapes evolve through time, with common simplifications such as a scaling of erosion with drainage area insufficient in accurately predicting the response of landscapes to dynamic forcing mechanisms.

Acknowledgements

I'm told that this is often the most read page of a PhD thesis (hello!). It is also one of the hardest sections to write… how can you appropriately acknowledge the multitude of support one receives during the course of a PhD? Having said that, here's an attempt anyway:

Of course, I am indebted to my supervisors for all of the guidance, encouragement and feedback I have received throughout the PhD. In particular, I sincerely thank Mikaël Attal for his academic guidance in helping me shape my ideas and for his infectious enthusiasm that can do nothing other than provide motivation even during the tougher times. Amnesia apart, it has always been a pleasure to work with Mikaël. Andrew Dugmore's experience, calming influence and constructive advice have proved invaluable throughout, as did use of the Land Rover while in Iceland. Linda Kirstein demonstrated far more patience than was warranted while guiding this total novice through the fundamental basics of geology and geochemistry. I hope she is proud that I now confidently know my olivines from my basalts! Additionally, I am thankful to Samuel Niedermann and Dimitri Lague, without whom major parts of this PhD would not have been possible, and also for making me welcome in Potsdam and Rennes, respectively.

In addition to my supervisory team, I am grateful to Enzio Schnabel (GFZ) and Jean-Jacques Kermarrec (Rennes) who offered invaluable help and technical expertise during my laboratory work. Kathy Whaler is thanked for introducing me to and guiding me through the ERT method. Noel Gourmelen is thanked for helping to obtain the DEM, and the DLR are thanked for providing the data. Katie Whitbread, Andrew Tedstone and Alex Ingle are thanked for all their assistance in the field and for battling with some less than ideal Icelandic weather. Alex's fantastic skills behind the camera also brought Iceland and my work to a wider audience through the wonders of youtube. Catriona Kelly in the University of Edinburgh Press Office is thanked for writing an excellent press release that helped my research receive exposure on the BBC website.

I gratefully acknowledge my funders: a NERC PhD studentship, the Carnegie Trust for the Universities of Scotland grant (awarded to M. Attal), the BSG, IAS and QRA for supporting conference attendance and the EDUCT for paying for my flights to

Potsdam. The Vatnajökull National Park Authority is thanked for giving permission to work in such a stunning location as well as providing invaluable logistical support.

I am grateful to the collective Edinburgh Geoscience community who have provided some fantastic moments over the last three (almost four) years; I wouldn't have had it any other way. In particular, I am grateful to all members of Lower Lewis for putting up with me and my attempts to establish numerous office 'traditions' over the years. Specific mentions must be made to Sophie for blending in well with our housing arrangements, Martin for introducing me to the Hibees, The General for his sub-optimal map-reading skills through Berwick-Upon-Tweed, and Donald for his help with the crossword. I wish the Drummond Bears every success in future derby matches, and hope the win/loss record improves under the new leadership of Gabriel Agbenlahor and Radamel Philcao. Finally, I would like to thank Alan and co for turning things around and making trips to Leith on a Saturday afternoon much more enjoyable over recent months. It's time to head to that Beach Bar & Spa…

E.R.C.B

May, 2015

Update (November, 2015): I am thankful to Prof Andy Russell (Newcastle) and Dr. Andy Hein (Edinburgh) for examining this thesis and for the enjoyable discussion during my viva. The suggested revisions have improved the thesis from its initial version.

Contents Page

Chapter 1: Introduction

1.1 Overview

This thesis addresses the issue of bedrock erosion during extreme flood events and aims at developing a greater understanding of the importance of high-magnitude, low-frequency events in landscape evolution. An integrated, multi-disciplinary approach is employed, combining topographic analysis and field observations with geochemical and geophysical analyses of a spectacular landscape in northeast Iceland, the Jökulsárgljúfur canyon (Chapter 2). This work is complemented with an experimental modelling study of fluvial processes carried out at the Université de Rennes 1, France (Chapter 3).

In the introduction, I present the context and rationale for the study of bedrock erosion during extreme flood events (Section 1.2) before documenting the specific aim and objectives of this research (Section 1.3). This chapter concludes with a detailed outline of the structure of this thesis (Section 1.4).

The central body (Sub-Chapters 2.3 and 2.4) of this thesis are in the form of research papers, either already published or *in press*, as noted at the start of each Sub-Chapter. These papers discuss individual aspects of this research and can be read as self-contained units. Chapter 4 provides a holistic synthesis of what has been shown in the course of this research and discusses the implications of the findings in the wider study of fluvial geomorphology and landscape evolution.

1.2 Background & Justification

The understanding of fluvial bedrock channel erosion is fundamental to determining both the short-term and long-term evolution of mountain topography (e.g. Howard *et al.*, 1994; Whipple and Tucker, 1999; Whipple *et al.,* 2000; Lague *et al.*, 2005; Reusser *et al.,* 2006; Wobus *et al.*, 2006; Turowski *et al*., 2006; 2007; 2008; 2009; Lamb *et al*., 2008a; Attal and Lavé, 2006; 2009; Whittaker *et al.*, 2007; Yanites and Tucker, 2010; Cook *et al.*, 2013; Lague, 2014). Bedrock channels occur in mountain environments wherever sediment transport capacity of the river exceeds the supply of sediment from hillslopes, leading to exposed bedrock reaches within the channel system (Howard *et al*., 1994; Whipple *et al.*, 2000). As the link between the fluvial network and hillslopes, bedrock channels mediate the response of the landscape to changing boundary conditions, such as tectonics and climate (Howard *et al.,* 1994; Whipple *et al*., 2000; Lague *et al.*, 2005; Reusser *et al.*, 2006; Attal *et al*., 2011; Lague, 2014) through vertical erosion and changing channel bed slope and/or channel width (Lavé and Avouac, 2001; Hartshorn *et al.,* 2002; Finnegan *et al.*, 2005; Whittaker *et al.*, 2007; Turowski *et al*., 2008). Therefore, the study of bedrock erosion processes is fundamentally important in order to fully understand how landscapes evolve through time.

1.2.1 The processes of bedrock erosion

Erosion of bedrock occurs through three main physical processes: abrasion, plucking and cavitation. Erosion by abrasion occurs through the breaking down of intact bedrock by repeated impact from sediment transported by the river as bedload and in suspension (Fig. 1.1; Whipple *et al*., 2000; Sklar and Dietrich, 2001). For objects protruding into the channel, suspended load is the dominant mechanism of erosion, producing sculpted bedforms such as flutes, furrows and potholes across centimetre to metre scales (Richardson and Carling, 2005; Wilson *et al.*, 2013).

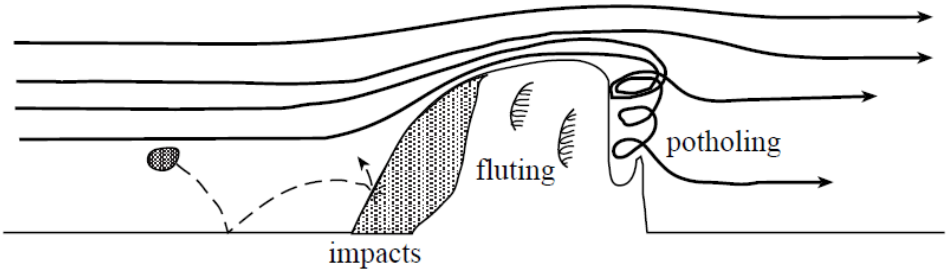

Fig. 1.1: Schematic diagram of the process of abrasion of objects protruding into the channel by bedload and suspended sediment. Bedload impacts the upstream side of protruding bedrock, creating a smooth 'aerodynamic' appearance while suspended sediment is caught in eddy currents and impacts the downstream side of the protrusion. This dichotomy creates asymmetrical features in the bedrock channel (Richardson and Carling, 2005; Wilson *et al.,* 2013). *Diagram source: Whipple et al. (2000)*.

The rate of erosion by abrasion by suspended sediment ($\varepsilon_{\mathrm{abr}}$) is proportional to the flux of energy during the impact of the sediment on the bedrock surface per unit time (q_{ke}) (Whipple *et al.,* 2000; Anderson, 1986):

$$\varepsilon_{\mathrm{abr}} = \frac{S_a q_{ke}}{\rho_r} \qquad \text{(Eqn. 1.1)}$$

Where S_a is the susceptibility of the substrate to erosion and ρ_r is the rock density. The flux of kinetic energy is defined as:

$$q_{ke} = \frac{1}{2}\,\rho_S C_{vr} U^3 \qquad \text{(Eqn. 1.2)}$$

Where ρ_S is the sediment density, C_{vr} is the volumetric concentration of sediment of size *r* and U is the fluid velocity (Whipple *et al.,* 2000). In turn, the suspended sediment concentration scales with the fluid velocity squared (Anderson, 1986):

$$C_{vr}\ \alpha\ U^2 \qquad \text{(Eqn. 1.3)}$$

Hence, in a transported-limited setting (where there is an unlimited supply of suspended sediment to erode with), the erosion rate by abrasion (ε_{abr}) is proportional to the fluid velocity (*U*) to the fifth power:

$$\varepsilon_{abr} \propto U^5 \quad \text{(Eqn. 1.4)}$$

Bedload is thought to provide the most efficient tools for river downcutting by abrasion: when put in motion during floods, bedload impacts the exposed bedrock, leading to erosion that is a function of both lithology and the energy released during the impacts (e.g. Gilbert, 1877; Sklar and Dietrich, 2001; 2004). However, recent experimental work demonstrated that the significance of abrasion by suspended sediment is often underestimated, particularly in oversteepened reaches and during large floods (Scheingross *et al.*, 2014).

Where the bedrock structure is heavily jointed, the removal or "plucking" of large rocks directly from the intact bedrock surface is also an important erosion process (Fig. 1.2) which occurs in a two-stage process (Snyder *et al.*, 2003a). Firstly, weakness planes within the rocks are developed and exacerbated through chemical and physical weathering, hydraulic wedging of fine-grained material in the cracks, impact by saltating sediment (abrasion) and pressure fluctuations during highly turbulent flow (cavitation) (Whipple *et al.*, 2000). Secondly, a high-magnitude flood event, with a shear stress above the threshold value for entrainment of the blocks (Buffington and Montgomery, 1997), occurs to dislodge, entrain and transport the loosened blocks from their *in situ* position (Snyder *et al*., 2003a). The amount of plucking is therefore set by the joint-spacing of the bedrock and the size of the loosened blocks, the rate of block loosening, as well as the regularity of flow events of sufficient magnitude to entrain them (Whipple *et al.*, 2000; Snyder *et al.*, 2003a).

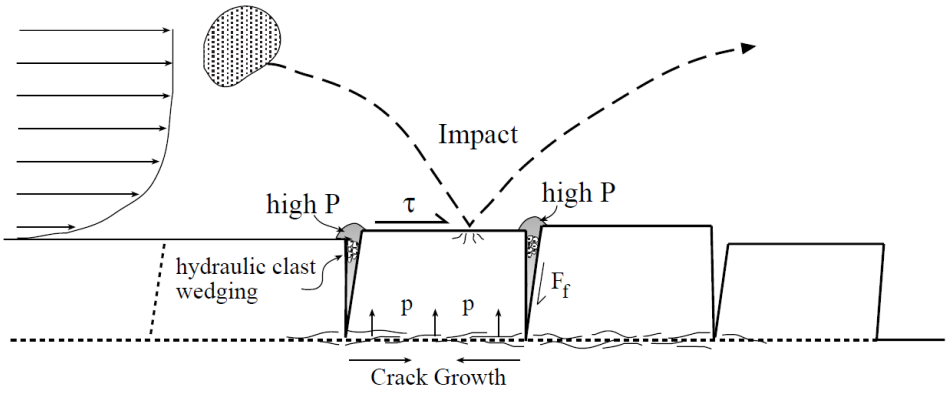

Fig. 1.2: Schematic diagram of the process of bedrock plucking. Fractures and joints between blocks at a sub-metre scale grow until the blocks become loose enough to be entrained and transported by the flow. The rate of block removal is a function of the block loosening rate and the frequency of floods of a magnitude great enough to entrain them. τ = shear stress acting on the surface of the block, F_f = friction force acting to resist entrainment, p = instantaneous pressure force acting on the base of the block, P =hydraulic pressure acting on cracks between joints. *Diagram source: Whipple et al. (2000).*

When the fluid pressure of fast-flowing water drops below the vapour pressure of the dissolved air, water vapour and air bubbles are formed, leading to reaches of 'white water'. When these bubbles are advected into regions of higher pressure, they can implode, producing a high energy pulse in the direction of the implosion, leading to erosion when this occurs close to the bedrock surface (Barnes, 1956). This process, known as cavitation, occurs only above a cross-sectionally averaged threshold flow velocity required for the air bubbles to form, given by:

$$U_{cav} = \sqrt{gd} \qquad \text{(Eqn. 1.5)}$$

where g = acceleration due to gravity (9.81 m s^{-2}) and d = flow depth (in metres).

There remains uncertainty regarding the significance of erosion through cavitation, although it is thought the erosion rate (ε_{cav}) may be characterised by a non-linear relationship with the flow velocity, rapidly increasing as

cavitation proceeds from the initial inception of air bubbles to increasingly full development (Arndt, 1981; Whipple *et al.,* 2000):

$$\varepsilon_{cav} \; \alpha \; (U - U_{cav})^q \qquad \text{(Eqn. 1.6)}$$

where U = flow velocity and q is a dimensionless constant. Values of up to 7.2 have been reported for q (Murai *et al.*, 1997), but further studies are required to better constrain this value (Whipple *et al.*, 2000).

Cavitation can act in concert with both abrasion and plucking; while there are no definitive bedforms that can be attributed to the cavitation process, it is likely that localised cavitation around bedforms such as flutes and potholes could accentuate these erosional features (Arndt and Maines, 1994). The high pressure impact of imploding bubbles may exploit weaknesses in the bedrock structure which bedload and suspended sediments then erode through successive impacts (Whipple *et al*., 2000), thus accelerating the first stage of the plucking process (Snyder *et al.*, 2003a).

Abrasion, plucking and cavitation rarely occur independently of each other, although the relative importance of each process varies both spatially and temporally between, and within, channels. Flows that surpass threshold conditions entrain sediment needed for abrasion, to dislodge and entrain entire blocks via plucking and for air bubbles to form that may lead to erosion through cavitation. Abrasion can only occur where sediment is available for transport; plucking can only occur where loosened blocks exist, set by the degree of bedrock fracturing. Thus, thresholds are important in controlling the spatial and temporal variability of erosion processes in bedrock channels, although many models of landscape evolution (e.g. Fastscape; Braun and Willett, 2013) do not consider the role of thresholds in erosion processes.

1.2.2 Models of bedrock erosion

1.2.2.1 The stream power law

Given the importance of bedrock channels in long-term landscape evolution, attempts have been made to develop models of the fluvial system that

establish a quantitative link between the temporal evolution of channel geometry and perturbations such as changes in climate or tectonic activity (Tucker and Hancock, 2010; Lague, 2014). The most commonly applied model that uses mechanistic transport/erosion laws is based on the assumption that the erosion rate in the bedrock channel is proportional to the stream power (e.g. Seidl and Dietrich, 1992; Craddock *et al.*, 2007) or the fluvial shear stress (e.g. Howard and Kerby, 1983; Willgoose *et al*., 1991; Stock and Montgomery, 1999). Under these models, the rate of bedrock erosion (ε) is modelled as a power law function of drainage area (a proxy for discharge) (A) and local channel gradient (S):

$$\varepsilon = KA^m S^n \qquad \text{(Eqn. 1.7)}$$

where m and n are positive constants and K is an erodibility coefficient that includes parameters such as rock strength, sediment supply, grain size and climate variability. The values used for the exponents m and n and the erodibility coefficient K vary between different models and different landscape settings (Howard *et al*., 1994; Attal *et al.*, 2011; Lague, 2014; Mudd *et al.*, 2014), and uncertainty remains regarding the controls on the correct values for these constants.

Landscape evolution models utilising the stream power law (e.g. CHILD; Tucker *et al.,* 2001; Fastscape; Braun and Willett, 2013) are widely used in studies of long term landscape evolution because they are able to reproduce many elements of steady state and transient river profiles with a simple model formulation based on topographic parameters (channel slope and drainage area) that can be easily extracted from digital elevation models (DEMs) (Lague, 2014). However, many studies suggest that stream power is likely to be too simple to be universal as, for example, it is unable to resolve variations in channel width associated with changes in incision rate (Lavé and Avouac, 2001).

Stream power models have often oversimplified the physical processes of erosion (Berlin and Anderson, 2007; Lamb *et al.,* 2008a; Turowski *et al.,*

2009; DiBiase *et al.*, 2015) and typically make the assumption that bedrock erosion occurs when boundary shear stress is far greater than the threshold value necessary to initiate incision so the threshold value can be neglected from the model (Snyder *et al.,* 2003a). Threshold values are very important for the initiation of erosion by abrasion, plucking and cavitation (see Section 1.2.1) and therefore stream-power based models that neglect thresholds have led to the development of models that have little bearing upon what is actually observed within the fluvial system (Howard *et al*., 1994; Jerolmack and Paola, 2010; Lague, 2014). In addition to the complexities in the physics of the erosion processes, stream power incision models also fail to accurately consider the large heterogeneity of natural systems and the inherent stochasticity of forcing mechanisms such as flooding and sediment supply from hillslopes (Lague, 2014). Lague (2014) reviewed the understanding of the complexity of bedrock incision processes in the context of upscaling from a reach scale to a landscape scale, and showed that the traditional approach employed in many studies of landscape evolution has resulted in incorrect formulations of the stream power model. Therefore, while stream power models continue to be used extensively in studies of landscape evolution (e.g. Braun and Willett, 2013); it is also important to acknowledge the caveats and assumptions therein.

1.2.2.2 The role of sediment

The stream power model does not take into account the physics of the bedrock erosion processes, leading to the role of sediment being ignored, despite it being known to control erosion through abrasion (Section 1.2.1; Whipple *et al.*, 2000). Under low sediment supply rates, sediment contained within the channel acts as the 'tools' for bedrock erosion through abrasion. Under high sediment supply rates, the sediment acts to protect the bed as bedrock is progressively buried beneath sediment which thus acts as a protective 'cover' (Fig. 1.3; Gilbert, 1877; Sklar and Dietrich, 2001; 2004). Sediment grain size is also important as, under experimental conditions where flow speed and sediment load are kept constant, coarser grained

sediment lead to higher erosion rates. Under these conditions (*v* remains constant), smaller grained particles have lower kinetic energy upon impact due to their lower mass *m*, regardless of the transport mode (Equation 1.2; Fig. 1.4; Sklar and Dietrich, 2001; Scheingross *et al.,* 2014). However, this is only true up to an intermediate grain size, as if grains are too large they are not entrained and thus do not cause erosion. Scheingross *et al.* (2014) showed that erosion by suspended sediment can dominate channel incision in coarse-grained rivers during large floods and in steep channels such as overly steepened knickzones, resulting in faster transmission of changes in base-level and landscape adjustment than observed with saltation-abrasion models (e.g. Crosby *et al.,* 2007; Gasparini *et al.*, 2007).

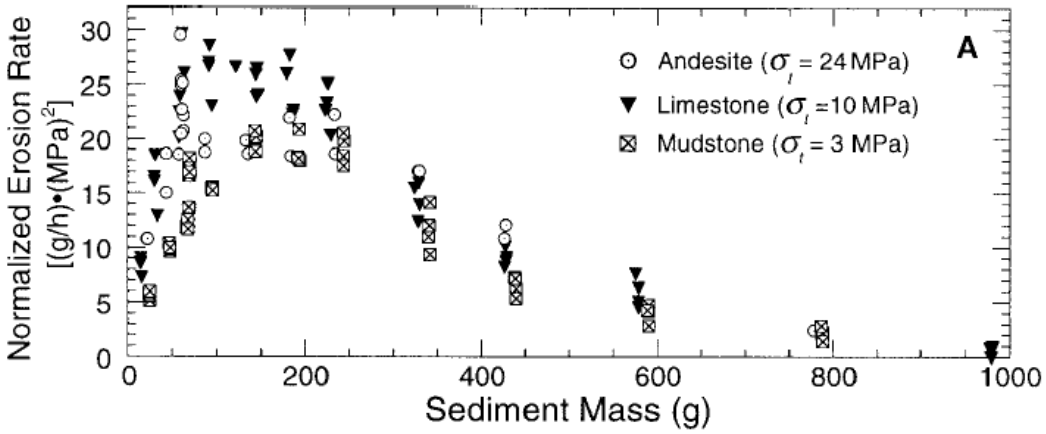

Fig. 1.3: Experimental demonstration of the 'tools and cover effect' of sediment supply on bedrock abrasion rates, carried out using an abrasion mill designed to replicate the interaction coarse bed load with the rock floor of an actively incising river channel (Sklar and Dietrich, 2001). Disks of rock were bolted to the bottom of water filled cylinders in which water-driven propellers circulated water. Sediment, of various size and amounts, were circulated in response to the tractive force of the rotating water, impacting the bedrock disks leading to erosion through abrasion. At low sediment masses (0-150 g), erosion increases with increasing sediment mass as the number of collisions between the sediment and the bed increases. Above a threshold value (~150-200 g), increasing the sediment mass simply adds to the mass of sediment of the stationary deposit at the base of the abrasion mill, thus protecting the bedrock from erosion. *Diagram source: Sklar and Dietrich (2001).*

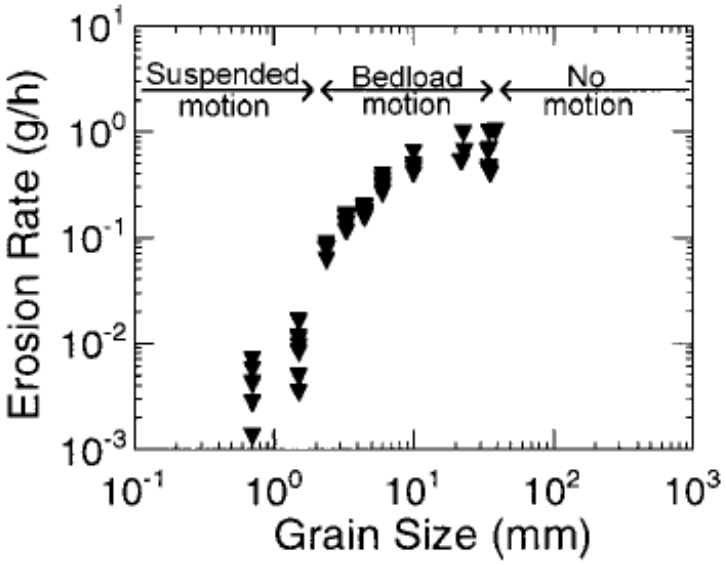

Fig. 1.4: Experimental results by Sklar and Dietrich (2001) showing effect of sediment grain size on rate of bedrock erosion in an abrasion mill. Smaller particles are transported in suspension, limiting the number of collisions with the bed and therefore lead to a lower overall erosion rate. Peak erosion rates are associated with larger particles that are transported as bedload. However, above a threshold grain size, the flow is no longer able to entrain the largest particles and therefore no erosion occurs. *Diagram source: Sklar and Dietrich (2001).*

1.2.2.3 Quantification of controls on erosion by plucking

In landscapes that contain heavily jointed bedrock, plucking is likely to contribute significantly to the overall bedrock erosion due to the availability of blocks during periods of high flow (Snyder *et al.*, 2003a). One of the dominant mechanisms for block loosening, the first stage of the plucking process, is the impact of coarse-grained sediment transported as bedload (Section 1.2.2). The loosening rate of the in situ blocks (L) is therefore a function of the bedload sediment flux (q_s) which itself is a function of the critical shear stress (τ_c) required to entrain coarse bedload (Whipple *et al.,* 2000):

$$L \ \alpha \ q_s^p \ \alpha \ (\tau_b - \tau_c)^{\frac{3p}{2}} \qquad \text{(Eqn. 1.8)}$$

where τ_b is the basal shear stress and p is an unknown positive constant probably close to one (Whipple *et al.*, 2000). Block loosening by other processes such as chemical weathering or hydraulic wedging is expected to be less non-linear than the loosening rate by the impact of coarse bedload so equation 1.8 represents an end-member case for the loosening rate *of in situ* blocks (Whipple *et al.,* 2000). Once the block has become detached from the surface, the second phase of the plucking process will entrain the block from its initial position, once all resisting forces are overcome (Snyder *et al.*, 2003a). For the case of a block wedged between adjoining blocks (e.g. Fig. 1.2), these forces include the normal component of the block weight, friction between the lateral ($F_{fy}|_l$), upstream ($F_{fy}|_u$) and downstream ($F_{fy}|_d$) block edges and the instantaneous pressure force averaged across the upper surface of the block ($\dot{p}'_s$) (Whipple *et al.,* 2000). For a block with thickness *h,* width *w*, length *l* and density ρ_s, ignoring the possible effects of through flow, the condition for entrainment is:

$$\dot{p}'_b - \dot{p}'_s \geq g(\rho_s - \rho)h + \left(F_{fx}|_u + F_{fx}|_d\right)\frac{h}{l} + 2(F_{fx}|_l)\frac{h}{w} \qquad \text{(Eqn. 1.9)}$$

Where ρ is the density of the flow and $\dot{p}'_b$ is the instantaneous pressure at the averaged across the base of the block (Whipple *et al.*, 2000). Graf (1977) demonstrated that the mean dynamic pressures scale with the mean shear stress; assuming that the magnitude of the instantaneous pressure fluctuations also scale with mean shear stress, the initial block extraction rate (*E*) is a function of the basal shear stress (τ_b) above a critical value (τ_e):

$$E\ \alpha\ (\tau_b - \tau_e) \qquad \text{(Eqn. 1.10)}$$

These equations (1.8 to 1.10) describe the loosening and entrainment of blocks that are wedged between others on the channel bed (e.g. Fig. 1.2). However, blocks can also be removed from other locations within the channel, such as the channel banks (e.g. Hartshorn *et al.,* 2002) or from the vertical headwall of waterfalls (e.g. Lamb *et al.,* 2008b; 2014). Lamb and Dietrich (2009) developed a mechanistic model for erosion at waterfalls in

environments containing near horizontal and vertical jointing (e.g. basaltic lava columns), through the plucking and toppling of whole rock columns (Fig. 1.5). Based on the torque balance of forces acting on bedrock columns at a waterfall, such as the shear and drag of the overflowing water, the buoyancy effect of the plunge pool and the geometry of the bedrock jointing; the model provides a calculation of the stability of the rock column (Fig. 1.6; equations 1.11 – 1.15; Lamb and Dietrich, 2009).

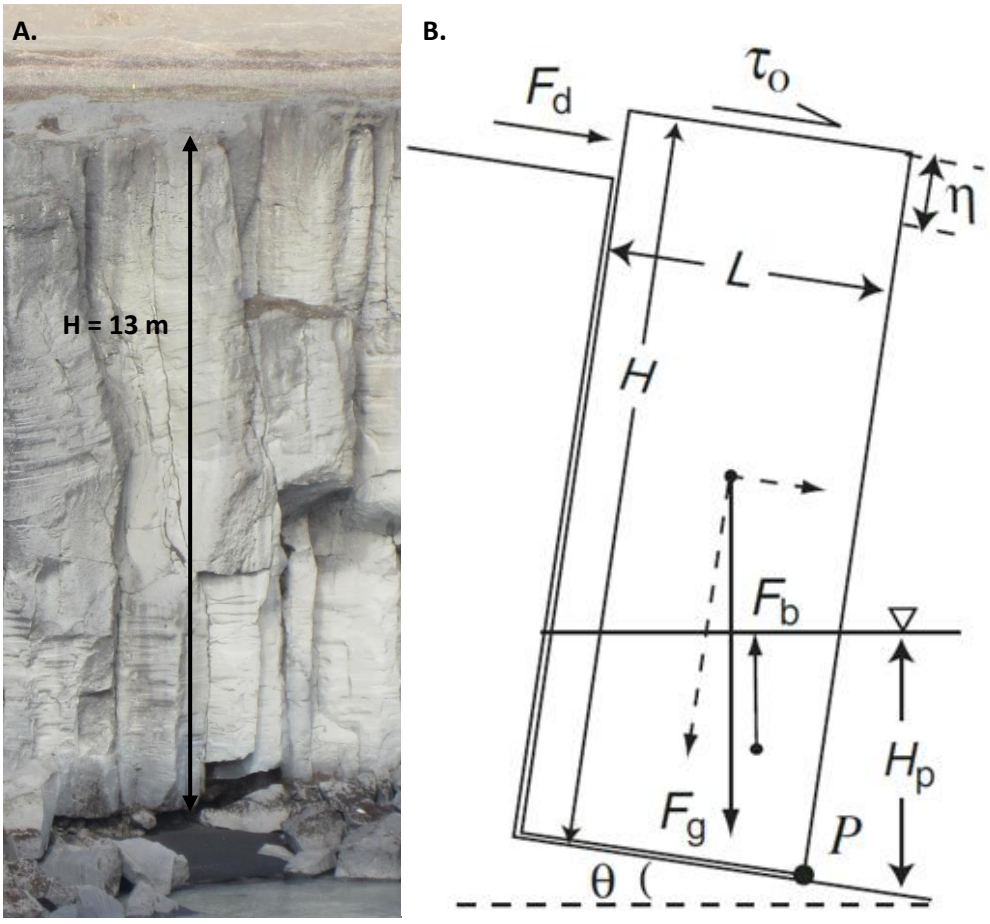

Fig. 1.5: A. Example of a rock column exposed in the canyon wall downstream of a waterfall (Selfoss, Iceland). Water flow is from left to right in the image. The height of the column is 13 m. **B.** Schematic diagram of the forces acting on a rock column at a waterfall. Water is flowing from left to right. F_d = Drag force, F_b = Buoyancy force, F_g = Force due to gravity, H = Height of block, L = Width of block, η = Distance block protrudes into the flow, H_p = Plunge pool depth, τ_o = Boundary shear stress at top of the column, P = Potential point for rotational failure, θ = Angle of block orientation. *Diagram source: Lamb and Dietrich (2009).*

The conditions for toppling of the columns are calculated using the Factor of Safety (*FS*); the ratio between the forces acting to topple the column and the resisting forces acting to keep the column standing. When the Factor of Safety is < 1, the columns are unstable and they will topple; otherwise, the columns will remain stable and erosion will not occur:

$$FS = \frac{\frac{\rho_r}{\rho} cos\theta \left(1 - \frac{HS}{L}\right) - \frac{H_p}{H}}{\frac{2\alpha^2 hS}{L}\left(1 + \frac{1}{2C_{f2}}\frac{C_d\,\eta}{L}\right)} \quad \text{(Eqn. 1.11)}$$

where ρ_r = density of the rock, ρ = density of the fluid, θ = angle of the rock from horizontal, H = total rock column height, S = channel-bed slope, L = rock column length, H_p = plunge-pool depth, α = acceleration factor, h = flow depth upstream of the waterfall, C_d = drag coefficient, C_{f2} = friction coefficient for the flow velocity average of the protrusion distance, η = protrusion length scale, α is the acceleration factor of the flow due to the waterfall and is dependent on the Froude number upstream of the waterfall (Fr). The Froude number is greater than one for supercritical flow and less than one for subcritical flow:

$$\text{For Fr} > 1: \ \alpha = 0.4\frac{C_{f1}}{S} + 1 \quad \text{(Eqn. 1.12a)}$$

$$\text{For Fr} < 1: \ \alpha = 1.4\left(\frac{C_{f1}}{S}\right)^{1/3} \quad \text{(Eqn. 1.12b)}$$

Where C_{f1} = friction coefficient for the depth averaged flow.

The plunge pool depth (H_p) can be calculated using the theory for a 2D-dimensional plane jet of water impinging on a horizontal plane at steady state (Leske, 1963; Vishcer and Hager, 1995; Chanson, 2002; Lamb and Dietrich, 2009):

$$\frac{H_p}{h} = (1 + 2(1 - cos\delta)Fr^2)^{1/2} \quad \text{(Eqn. 1.13)}$$

where δ = jet impingement angle and $cos\delta$ is dependent on the Froude number at the waterfall lip (Fr_o), the acceleration factor, the height of the plunge pool and the water depth upstream of the waterfall:

$$cos\delta = \left[\frac{2+Fr_o^2}{2+Fr_o^2+2\alpha^{2/3}\frac{H}{h}}\right]^{1/2} \quad \text{(Eqn. 1.14)}$$

In turn, the Froude number at the waterfall lip and the Froude number upstream of the waterfall can be simplified to:

$$Fr_o^2 = \alpha^3 Fr^2 = \frac{\alpha^3 S}{C_{f1}} \quad \text{(Eqn. 1.15)}$$

Through the substitution of equations 1.12-1.15 into equation 1.11, the threshold flow depth (*h*) conditions required for block toppling (when the Factor of Safety is = 1), and therefore erosion through the upstream migration of waterfalls, can be calculated using the Lamb and Dietrich (2009) model. The sensitivity of the threshold flow depth to variability in the different parameters is explored in detail in Sub-Chapter 2.3 of this thesis.

1.2.2.4 Importance of knickpoints in bedrock channel evolution

Knickpoints can be formed either at lithological boundaries between rock types of different strengths (e.g. Haviv *et al.,* 2010) or in response to an external perturbation to the river system leading to a change in the steady-state conditions (e.g. Whittaker and Boulton, 2012) such as a change in base level at the catchment outlet, an increase in rock uplift rate or relative sea level fall (e.g. Boulton *et al.*, 2014) or a sudden increase in drainage area following stream capture. Understanding the response of transient knickzones to these external perturbations is thus vitally important for the understanding of long-term landscape evolution (Flint, 1973; Bennett, 1999; Crosby and Whipple, 2006; DiBiase *et al.,* 2015). Given the long timescales that landscapes can take to adjust to external perturbations, only a few studies exist where rates of knickpoint retreat rate have been directly quantified using cosmogenic nuclide dating techniques: e.g. in Scotland

(Jansen *et al.*, 2011), Hawai`i (Mackey *et al.*, 2014) and the San Gabriel Mountains (DiBiase *et al.*, 2015). Without accurate constraints on the rates of knickpoint retreat, interpretation of base-level history based on long profile analysis using stream-power models may underestimate landscape response times if knickpoint retreat rates are actually slower than predicted or overestimate the landscape response time if the knickpoint retreat rates are actually faster than predicted (DiBiase *et al.*, 2015). Therefore, an understanding of the factors that control long term knickpoint erosion processes such as knickpoint form and retreat rate is crucial for an accurate assessment of how landscapes have evolved through time (Lamb and Dietrich, 2009; Lapotre and Lamb, 2015).

1.2.2.5 Current understanding of long term knickpoint erosion processes and controls on knickpoint retreat

The physics of waterfall formation, erosion and retreat are thought to depend on the mechanism of retreat such as plunge-pool drilling (e.g. Lamb *et al.*, 2007), undercutting (e.g. Gilbert, 1907; Stein *et al.*, 1993; Bennett, 1999; Haviv *et al.*, 2010) or column toppling (e.g. Lamb and Dietrich, 2009; Lamb *et al.*, 2014). The importance of a range of factors in controlling waterfall/knickpoint retreat have been identified by previous studies (discussed below) including discharge, rock strength, bedrock structure and knickpoint geometry, although further work is required to improve our understanding of what generates and maintains waterfalls in bedrock channels as they migrate upstream.

At a landscape scale, it has been shown that the retreat rate of knickpoints correlate with discharge (or drainage area, as a proxy for discharge) (Hayakawa and Matsukara, 2003; Bishop *et al.*, 2005; Crosby and Whipple, 2006; Berlin and Anderson, 2009; Frankl *et al.*, 2012; Rengers and Tucker, 2014; DiBiase *et al.*, 2015). In the Western San Gabriel Mountains, USA, knickpoints present in the lower reaches of the rivers (i.e. at larger drainage areas) have been retreating at rates up to two orders of magnitude higher than knickpoints located in the upper reaches of the rivers (i.e. at smaller

drainage areas); whether this is purely controlled by an increase in drainage area or differences in rock strength is currently unclear as rapid retreat rates are also present in catchments just a few square kilometres in size (DiBiase *et al.*, 2015). The mechanisms controlling the relationship between discharge and knickpoint retreat are unclear (Rengers and Tucker, 2015) although Flores-Cervantes *et al.* (2006) suggest that increased flow velocity increases the bed shear stress in the plunge pool, enhancing plunge pool erosion and knickpoint retreat.

According to the stream power model of bedrock erosion, the celerity or wave speed of a knickpoint is proportional to the drainage area when the slope exponent (n) is equal to 1 (e.g. knickpoints in the Roan Plateau, Colorado; Berlin and Anderson, 2007). For a non-linear stream power model where $n > 1$, the knickpoint retreat rate is also dependent on the channel slope, such that knickpoints will retreat faster in steeper channels (Whittaker and Boulton, 2012), which is thought to be an appropriate model for knickzone evolution in Eastern Australia (Weissel and Seidl, 1998). However, as discussed previously in Section 1.2.2.1, a weakness of the stream power model is the inherent insensitivity to stochastic flows that are prevalent in nature and the exclusion of the role of erosion thresholds. Additionally, studies that model knickpoint retreat rate using the stream power model do not take into account the complexities of erosion processes, variations in the hydraulic geometry and changes in the flow dynamics or bed cover at the knickpoints themselves (Rengers and Tucker, 2014; DiBiase *et al.*, 2015).

In addition to discharge and channel slope, other factors are also important in controlling knickpoint retreat rate such as lithological strength (Holland and Pickup, 1976; Wells *et al*., 2009), bedrock structure (Ortega *et al.,* 2013; Cook *et al.*, 2013), sediment transport and the dimensions of the knickpoint (Haviv *et al.*, 2010; Cook *et al.*, 2013), erosion thresholds coupled with stochastic forcing (Lague, 2014) and dynamic changes in the channel width (Attal *et al.*, 2011; Lague, 2014). In a series of headcut propagation experiments, knickpoints were found to retreat faster, as well as developing a

larger plunge pool, within a weaker substrate (Wells *et al.*, 2009). Hayakawa and Matsukara (2003) derived a predictive formula based on the discharge and knickpoint dimensions for the rate of knickpoint retreat using a small (nine waterfalls) field dataset from the Bono Peninsula, Japan:

$$KP_{RR} = 99.7 \left(\frac{AP}{WH}\sqrt{\frac{\rho}{S_c}}\right)^{0.73} \quad \text{Eqn. 2.5.1}$$

Where KP_{RR} = knickpoint retreat rate, A = drainage area, P = mean annual precipitation (AP is therefore a proxy for long-term discharge, as these records did not exist), W = waterfall width, H = waterfall height, ρ = fluid density and S_c = the unconfined compressive strength of the bedrock (Hayakawa and Matsukara, 2003).

Equation 2.5.1 suggests an inverse relationship between the knickpoint height and the knickpoint retreat rate, whereas an experimental modelling study (Holland and Pickup, 1976) suggests the opposite relationship exists. A numerical modelling study demonstrated that, where a vertical knickpoint has a resistant caprock overlying a less resistant subcaprock, the lateral retreat rate of the knickpoint face is equal to the downstream incision rate divided by the channel gradient, but only where the vertical face of the subcaprock is higher than a threshold height for failure in shear or by buckling (Haviv *et al.*, 2010). Thus, the height of the knickpoint, and whether these threshold conditions are met, can control the knickpoint lateral retreat rate, which is at odds with the formula (Eqn. 2.5.1) derived by Hayakawa and Matsukara (2003). In the Da`an River gorge, Taiwan, where rapid knickpoint propagation occurred between 2006 and 2008, the rate of knickpoint retreat increased when two knickpoints combined, thus creating a single, larger knickpoint, although the initial knickpoint retreat only began at the downstream limit of the gorge once bedload transport had initiated (Cook *et al.*, 2013). This increase in retreat rate from 2006 - 2008 could also potentially be linked to the bedrock structure as when the knickpoint retreat rate peaked, it was incising through a section of horizontally bedded strata of weak mud layers beneath stronger sandstone beds (Cook *et al.,* 2013). It would be expected

that the knickpoint retreat rate in a horizontally bedded strata would be faster than where the bedding planes are oriented vertically because the horizontal beds would act as pre-determined failure planes for the removal of whole blocks.

1.2.3 Flood events

High magnitude erosion events in rivers are important in controlling landscape evolution, with the majority of geomorphic work in bedrock channels occurring when flow conditions exceed threshold values, either to entrain sediment leading to erosion through abrasion (e.g. Buffington and Montgomery, 1997) or to pluck or topple blocks in jointed bedrock (e.g. Whipple *et al*., 2000; Lamb and Dietrich, 2009). This section describes some observations of erosion during flood events, and introduces the concept of 'extreme flood events', the focus of this study.

1.2.3.1 Geomorphological impact of high magnitude flood events

Numerous studies exist that document the role of high magnitude flood events leading to sediment transport (e.g. Dadson *et al.*, 2003; Lane *et al.*, 2008; Turowski *et al.,* 2013; Attal, 2015) and erosion in bedrock channels through both abrasion (e.g. Hartshorn *et al.,* 2002; Cook *et al.,* 2013; 2014) and plucking (e.g. Hartshorn *et al.*, 2002; Snyder *et al.*, 2003a). Sediment transport is important in controlling both erosion through abrasion and plucking (see Section 1.2.1) although a simple relationship does not exist between flood magnitude and sediment flux (Dunning *et al.*, 2013). According to Turowski *et al.* (2013), floods can be either be: (i) 'flood depositing'; where low-frequency, high magnitude floods supply more sediment than can be evacuated leading to net deposition within the channel through processes such as mass-wasting from hillslopes (e.g. Lane *et al.,* 2008), before the sediment being evacuated in small and moderate floods, or (ii) 'flood cleaning'; where sediment progressively builds up during small and moderate floods before being evacuated during high-magnitude low-frequency events. No channel can be solely classified as being in a 'flood-depositing' or 'flood-

cleaning' phase as the dominant behaviour can change both spatially and temporally through time, with alternating reaches present in some large basins (e.g. the Sabie River, South Africa; Heritage *et al.,* 2004; Turowski *et al.,* 2013).

Lane *et al.* (2008) showed contrasting sediment transport behaviour on the River Wharfe (Yorkshire Dales, UK). The highest magnitude floods, corresponding to low frequency storm events, could be classified as 'flood-depositing' (Turowski *et al.,* 2013) as more sediment was transferred to the River Wharfe during these events through shallow landsliding than was able to be transported by the river, leading to net aggradation (Lane *et al.*, 2008). The majority of sediment transport within the River Wharfe takes place during moderate storms that are sustained for longer time periods but do not lead to significant input of sediment from the hillslopes, indicating the relative amount of geomorphic work carried out by moderate and high magnitude flood events (Lane *et al.,* 2008), a concept first identified by Wolman and Miller (1960).

The relative efficiency of moderate flows against peak flows for sediment transport, and therefore erosion, was also explored by Hartshorn *et al.* (2002) through the significance of erosion during typhoons in the LiWu catchment in Taiwan. Erosion in bedrock channels during the 2000 wet season (highly active with typhoons) was an order of magnitude higher than the erosion rate during the dry season that followed and the following wet season (less active with typhoons) in 2001. This is thought to have been a direct result of 'supertyphoon' Bilis (return period of 20 years) in 2000, which had a peak discharge (2240 $m^3 s^{-1}$) 65 times the daily average discharge between 1960 to 2001 (36 $m^3 s^{-1}$). However, in addition to the temporal variability in the erosion rate controlled by typhoon events, the spatial pattern of erosion within the channels is also controlled by the frequency and magnitude of the high magnitude discharge events. Erosion during the 2000 wet season peaked at higher elevations (between 3 – 7 m above the mean low-flow level) than during the dry and wet seasons of 2001 (less than 3 m above mean low-

flow level) as the erosion during the typhoon events was focussed high on the channel walls rather than the channel bottom (Hartshorn *et al.,* 2002). Over the longer term, rare large magnitude floods are more important in bedrock channel widening than they are in controlling bedrock channel incision, which is dominated by relatively frequent flows of low to moderate intensity (Hartshorn *et al.,* 2002).

In addition to the effect of storm events, Hartshorn *et al.* (2002) also identified the relative importance of different erosion processes as the study reach on the LiWu River contained contrasting lithologies. The erosion rate of quartzite, which contained decimetre joint spacing, was higher than the erosion rate of unjointed schist despite the schist being four times more susceptible to abrasion (Hartshorn *et al.* 2002). Field observations suggest the higher erosion rates of the quartzite were caused by the plucking of intact blocks, which was most prominent at intermediate elevations where the erosion rates were highest (Hartshorn *et al.*, 2002). Where the bedrock structure is conducive to the removal of entire blocks, plucking is likely to be the dominant erosion mechanism leading to a higher total erosion rate, especially during high magnitude flood events.

Sediment availability within the channel system is an important factor in the ability of the rivers to erode into the bedrock, demonstrated in the Da'an River, Taiwan, by Cook *et al.* (2013). For five years following a discrete period in which 10 m of vertical uplift occurred (during the 1999 Chi-Chi Earthquake), sediment and water was ponded in a depression upstream of the uplifted channel reach. After 2004, bedload transport re-initiated and led to rapid knickpoint retreat of 620 m and up to 20 m of downcutting through abrasion by 2008; the majority of the erosion occurred during high discharge events associated with typhoons when abundant large (D_{50} > 100 mm) clasts were mobilised as bedload (Cook *et al.*, 2013). This demonstrates that rapid rates of bedrock incision can occur when there is a high availability of the tools for abrasion (e.g. coarse bedload) combined with frequent high magnitude flood events.

Falls Creek River in New York, USA, experienced a flood in 1981 with a discharge of 335 m^3 s^{-1}, the second largest event in the 75 year discharge record. The flood resulted in the significant plucking of large boulders (up to 4 m x 2 m x 0.3 m) which had not occurred in at least the 40 years previous to the flood (Snyder *et al.,* 2003a). Similarly, very large storms (return period of 5 to 15 years) significantly modified the channel morphology of the Rio Camacho, Bolivia, while smaller floods (return period of 1-7 years) did not, despite transporting a large volume of sediment (Coppus and Imeson, 2002), indicating that a threshold exists within these systems for bedrock erosion of the channels. These observations of significant bedrock erosion and sediment transport during climate-driven flood events (e.g. storms or typhoons) that occur on a timescale of 10^0 - 10^2 years (e.g. Hartshorn *et al.*, 2002; Snyder *et al.*, 2003a; Lane *et al.*, 2008; Cook *et al.*, 2013) demonstrate the importance of high (and moderate) magnitude flood events in long term landscape evolution (Turowski *et al.,* 2013). However, there exist very few studies of the impacts of flood events in geomorphological systems which occur on millennial timescales (i.e. > 10^3 years); such as floods associated with lake outbursts, large dam failures or subglacial volcanic eruptions.

1.2.3.2 Extreme flood events

1.2.3.2.1 Definition & terminology

Ice, moraine or landslide dammed lakes are ubiquitous in mountainous environments. They form when the valleys become blocked either by glacier advance, the deposition of sediment in frontal moraines or by a sudden input of hillslope sediment from a landslide that accumulates on the valley floor and blocks the river flow (Evans and Clague, 1994; Baker, 2002). Over time, glacier retreat can weaken ice-dams and the ponding of water behind unconsolidated moraine or landslide deposits can exceed the strength of the dam, potentially leading to their collapse resulting in the catastrophic drainage of large volumes of water into the landscape downstream (e.g. the Tsatichhu landslide dam, Bhutan; Dunning *et al*., 2006).

Where glaciers are located atop active volcanos, large volumes of ice can be melted by subglacial volcanic eruptions, resulting in the catastrophic release of meltwater across the landscape (e.g. the 1996 jökulhlaup at Skeiðarársandur, Iceland; Smith *et al.*, 2000). Floods of this nature tend to be characterised by the release of a large volume of water over the landscape in a short period of time, and are often rare on a human timescale (10^0-10^2 years). The occurrence of the flood events of this nature triggered by moraine, ice or landslide dam failures or subglacial volcanic activity are compiled in Table 1.1. As evident in Table 1.1, the peak discharges of these floods vary over several orders of magnitude, with the largest reconstructed floods associated with catastrophic drainage of glacial lakes during the last deglaciation, while smaller dam-break floods or jökulhlaups produced floods ranging from just $10^2 – 10^3$ m^3 s^{-1} (e.g. Clague and Evans, 1997). Baker (2009) defined a 'megaflood' as one where the peak discharge exceeds 1 x 10^6 m^3 s^{-1}. This definition rules out all but a few of the largest floods ever known to have occurred on Earth (Table 1.1), while erosion processes during smaller floods, in terms of discharge, are also capable of causing catastrophic landscape change. To avoid any possible confusion regarding the magnitude of the discharge of the floods studied in this thesis, the collective term 'extreme flood event' is used in preference to 'megaflood'. The Icelandic term 'jökulhlaup' also appears in the literature (e.g. Carrivick *et al.*, 2004; Russell *et al.*, 2010), in reference to glacial outburst floods and would be an appropriate label for the floods that are studied in Chapter 2 of this thesis. Given the broader applicability of the findings of this research related to the potential landscape change and the mechanics of the erosion processes during such events in other, non-glaciated, settings, 'jökulhlaups' are included within the umbrella term of 'extreme flood events'.

There exist several definitions of 'extreme flood events'; some that are based on the frequency of the events through time and others that are based on the 'unit stream power' (Bagnold, 1966) of the flood (e.g. Magilligan, 1992) and others that are based on the amount of geomorphic work carried out by the flood (e.g. Attal, 2015). For example, in reference to sediment transport

capacity, Attal (2015) states that an extreme flood event is one that is capable of transporting very coarse sediment in large volumes and can mobilise the entire grain population of sediment, including boulders. Magilligan (1992) and Benito (1997) refer to extreme floods as those that generate sufficient power to surpass the critical threshold within the fluvial system (Schumm, 1973) for landscape change. When the input forces of an 'extreme flood', controlled by the flood magnitude, the channel morphology and the slope, are greater than the resisting forces, controlled by the lithology, sediment and soil type, destabilisation of the fluvial system occurs which can lead to significant landscape change (Magilligan, 1992). In a study of the Columbia River gorge, formed by catastrophic drainage of Lake Missoula, Benito (1997) identified different thresholds of stream power for different landforms to be generated; 500 W m^{-2} for the production of streamlined hills and 4500 W m^{-2} to initiate processes that produce erode inner gorges within channels. In Iceland, Carrivick (2007) found that during jökulhlaups sourced from Kverkfjöll, fluvial erosion occurred where the flood power was greater than 300 W m^{-2} and carried out geomorphic work comparable to that of other late Pleistocene 'megafloods' (e.g. Lake Missoula drainage floods) despite the peak discharge being significantly smaller.

Low threshold powers are required for sediment transport than erosion, and the smaller floods listed in Table 1.1 are still capable of causing change within the fluvial system. A landslide dam failure induced flood event had a long term impact on the sediment transport dynamics in the Partnach River catchment, Germany, despite a relatively low discharge (~ 50 m^3 s^{-1}) compared to others listed in Table 1.1. In the years preceding the dam failure (2001-2005), the sediment load was dominated by the suspended sediment fraction (>86% of the total load) as coarse load transported from upstream was captured in the lake. In the years after the flood event (2005-2010), the proportion of the total sediment load that was bedload increased (over 50% between 2006-2008). This was caused by the release of more than 25,000 tonnes of sediment during the dambreak event, the reactivation/remobilisation of coarse sediment stored in the lake and the

increased local sediment supply from hillslopes due to the enhanced hillslope-channel coupling induced by the undercutting of talus slopes during the flood event (Morche and Schmidt, 2012). Smaller magnitude outburst floods also occur fairly regularly in Iceland due to subglacial volcanic activity (e.g. Russell *et al.*, 2010; Dunning *et al.*, 2013). The 2010 volcanic eruption of Eyjafjallajökull in Iceland resulted in the release of 5.7×10^7 m^3 of water during 140 jökulhlaups over a period of 30 days (Dunning *et al.*, 2013), with the peak discharge estimated at 5,000-15,000 m^3 s^{-1} (Magnússon *et al*., 2012). Despite the significantly lower discharge than the palaeo-floods triggered by the draining of Glacial Lake Missoula, the 2010 Eyjafjallajökull floods still led to significant landscape change; including the infill of the proglacial lake with 1.7×10^7 m^3 of sediment (Dunning *et al.*, 2013), but did not cause significant bedrock erosion of the landscape.

Therefore the 'extreme flood events' that are referred to in this thesis are those that produce enough power to surpass the threshold within the fluvial system for significant landscape change through erosion, rather than the magnitude of the peak discharge of the individual flood event (e.g. the definition of Baker, 2009). Floods of this nature are relatively rare on a human timescale (10^0 - 10^2 years) but relatively common on a geological timescale (> 10^3 years). In Iceland, however, due to the location of glaciers atop active volcanic centres, the recurrence interval of jökulhlaups can be much shorter (Evans and Clague, 1994) than in other environments such as steep mountain environments prone to landslide or moraine dam outburst floods (Cenderelli and Wohl, 2001).

Table 1.1: Reconstructed peak discharges during floods triggered by dam failures, glacial lake outbursts or subglacial volcanic eruptions.

Location	Flood trigger	Estimated peak discharge ($m^3 s^{-1}$)	Reference
Partnach River, Bavaria, Germany	Landslide dam failure	27 to 51	Morche *et al.* (2007)
Farrow Creek, British Columbia	Ice-dammed lake outburst	110 to 272	Clague and Evans (1997)
Kverkfjöll, Iceland (2002 Jökulhlaup)	Catastrophic drainage from geothermal lake	490	Rushmer (2002)
Malad Gorge, Idaho, USA	Erupted lava-dam induced river diversion	1250	Lamb *et al.* (2014)
Box Canyon, Idaho, USA	Erupted lava-dam induced river diversion	800 to 2800	Lamb *et al.* (2008b)
Sólheimajökull, Iceland (1999 Jökulhlaup)	Subglacial volcanic eruption, and within-event meltwater storage and release	4400	Russell *et al.* (2010)
Tsatichhu, Bhutan	Landslide dam failure	5900	Dunning *et al.* (2006)
Eyjafjallajökull, Iceland (2010 jökulhlaup)	Subglacial volcanic eruption	0.5×10^4 to 1.5×10^4	Magnússon *et al.* (2012)
Skeiðarársandur, Iceland (November 1996 Jökulhlaup)	Subglacial volcanic activity, and temporary storage in subglacial lake	$4.5\text{-}5.3 \times 10^4$	Björnsson, 2002
Big Lost River, Idaho, USA	Glacial lake drainage	6×10^4	Rathburn (1993)
Oirase River, NE Japan	Caldera lake dam failure	0.2×10^5 to 3×10^5	Kataoka (2011)

Kverkfjöll, Iceland	Subglacial volcanic eruption	0.5×10^5 to 1×10^5	Carrivick (2007)
Glacial Lake Wisconsin	Ice-dammed lake failure	1.5×10^5	Clayton and Knox (2008)
Jökulsá á Fjöllum, Iceland, (2500 yr BP)	Subglacial eruption of Bárðarbunga caldera	5×10^5	Tomasson (2002)
English Channel	-	0.2×10^6 to 1×10^6	Gupta *et al.* (2007)
Katla, Iceland (1918 Jökulhlaup)	Subglacial volcanic eruption	$0.2 – 0.3 \times 10^6$ to 1.6×10^6	Tomasson (1996), Jonsson (1982), Maizels (1993), Duller *et al.* (2008)
Aniakchak caldera, Alaska, USA	Caldera lake dam failure	0.6×10^6 to 4.8×10^6	Waythomas *et al.* (1996)
Ásbyrgi canyon, Iceland	Subglacial volcanic eruption	0.7×10^6	Waitt (2002)
Jökulsá á Fjöllum, Iceland	Subglacial volcanic eruption	0.9×10^6	Alho *et al.* (2005)
Lake Bonneville, USA	Ice-dammed lake outburst	~ 1×10^6	O'Connor (1993)
Tsangpo River, Tibet (event 1)	Ice/Moraine-dammed lake outbursts	1×10^6	Montgomery *et al.* (2004)
Tsangpo River, Tibet (event 2)	Ice/Moraine-dammed lake outbursts	5×10^6	Montgomery *et al.* (2004)
Lake Missoula, USA	Catastrophic lake drainage	1.7×10^7	O'Connor and Baker, 1992)
Altai Mountains, Siberia	Ice-dammed lake outburst	1.8×10^7	Baker *et al.* (1993)
Straits of Gibraltar	Rapid refilling of Mediterranean basin	~ 1×10^8	Garcia-Castellanos *et al.* (2008)

1.2.3.2.2 Understanding of erosion processes during 'extreme flood events'

The geomorphological impact of extreme flood events was first identified by Bretz (1923) in a study of the impact of floods following the drainage of Glacial Lake Missoula on the Channeled Scabland of northwestern USA. Since then, it has also been recognised that extreme flood events have had a significant and long-lasting effect on a range of other terrestrial environments such as the Tsangpo gorge of southeastern Tibet (Montgomery *et al*., 2004) and the Transbaikalia and Altai Mountains of Siberia (Carling *et al*., 2009a; Margold *et al*., 2011). It has also been suggested that such floods could have played a key role in the evolution of the Straits of Gibraltar (Garcia-Castellanos *et al*., 2009), the English Channel (Gupta *et al*., 2007) and in extra-terrestrial environments such as the surface of Mars (Warner *et al.,* 2010; 2013). Our current understanding of canyon formation and bedrock erosion processes during extreme flood events is limited, especially in distal areas, and is based on studies such as that of the Channeled Scabland in Washington, USA (e.g. Baker and Kale, 1998) and a small number of studies in Idaho, USA (Lamb et al., 2008b; 2014; Lamb and Dietrich, 2009), where the main motivation was to use the terrestrial landscape to infer the formation mechanisms of morphologically similar canyons on Mars.

In the Channeled Scabland of northwestern USA, the formation of large scale erosive landforms such as cataracts and anastomosing channels has been attributed to extreme floods resulting from the catastrophic drainage of Glacial Lake Missoula during the deglaciation of the Laurentide ice sheet (Bretz, 1923). Geomorphological evidence for maximum stage limits combined with step-backwater hydrological flow modelling was used by O'Connor and Baker (1992) to estimate the peak discharge of the flow following drainage of Glacial Lake Missoula to 1.7×10^7 m^3 s^{-1}.

In the Himalayas, floods associated with moraine dam failures between 1977 and 1985 in the Mount Everest region of Nepal had discharges up to 60 times greater than seasonal high flow floods (Cenderelli and Wohl, 2001) but

moraine dam breaks also generated colossal floods during the initial phases of the Pleistocene deglaciation. Around 9500 ^{14}C years ago, the failure of a moraine dam blocking the Tsangpo river in southeastern Tibet released 8.32 x 10^{11} m^3 of water down a steep narrow gorge approximately 100-200 m wide (Montgomery *et al.*, 2004). The resulting erosion potential of these floodwaters, represented by the unit stream power calculated at the head of the gorge (1 x 10^6 to 5 x 10^6 W m^{-2}), places the flood at the upper range of erosion events in the Earth's history and is likely to have caused significant downcutting and valley side widening (Montgomery *et al.*, 2004) although this has not been studied or quantified in detail.

The presence of scoured rock on the rim of Box Canyon, Idaho, and fluvially transported boulders far greater in size than the present day discharge of the spring at the base of the canyon headwall would be able to transport, support the hypothesis the canyon was cut during catastrophic flooding (minimum flood discharge of 800 – 2,800 m^3 s^{-1}) approximately 45 ka ago rather than progressively through time by groundwater seepage, as previously thought (Lamb *et al.*, 2008b). Surface exposure dating of eroded surfaces at Malad Gorge, approximately 20 km from Box Canyon, identified the timing of the erosion and also the longer term response of the landscape since the erosive flood event ~46,000 years ago (minimum flood discharge of 1250 m^3 s^{-1}, seven times the peak flow recorded (181 m^3 s^{-1}) and 40 times the largest mean annual flow (30 m^3 s^{-1}) on the river between 1916-2014; Lamb *et al.*, 2014; USGS gauging station number 13152500 - data available from waterdata.usgs.gov). The distribution of surface exposure ages and the morphology of Pointed Canyon, the sole canyon in the Malad Gorge area still containing an active channel, indicated gradual knickpoint retreat and a diffusion of the vertical canyon headwall into a series of smaller steps (Lamb *et al.*, 2014) since the erosive flood event.

Studies by Lamb *et al.* (2008b; 2014) are unique in using quantitative geomorphological techniques such as surface exposure dating using cosmogenic nuclides and topographic analysis to study the impact of a single

extreme flood event on the landscape. However, the magnitude of the floods studied by Lamb *et al.* (2008b; 2014) are of the order of 10^2 to 10^3 m^3 s^{-1}, just two orders of magnitude greater than the annual mean flow of the rivers within these canyons. There remains a lack of quantitative studies that examine bedrock erosion during extreme floods that have a discharge and erosional power towards the upper end of Table 1.1 (e.g. floods with discharge in the order of 10^4 to 10^6 m^3 s^{-1}), and their potential role in short term and long term landscape evolution. Lamb *et al*. (2008; 2014) examined the impact of, and the proceeding landscape response to, a single flood event ~45 ka ago. In order to fully assess the long term role of extreme flood events in landscape evolution, a study is required of a landscape that has experienced multiple erosive flood events over a prolonged period of time, such as the Jökulsárgljúfur canyon, Iceland, during the Holocene.

Despite widespread recognition of the potential impact of extreme flood events on landscapes, current landscape evolution models do not consider their impact in controlling bedrock landscape morphology (Carling *et al*., 2009b). Detailed quantitative studies of the impact of extreme flood events on the landscape, and of the mechanics of the erosion processes during extreme flood events, are therefore required.

1.3 Research aim & objectives

The general aim of this research is to *understand and quantify the role of extreme flood events in canyon formation and the erosion of bedrock channels.* In order for this broader research aim to be achieved, three specific research objectives have been identified and are addressed in the following chapters:

1. To quantify the impact of extreme flood events over background, longer term, bedrock erosion processes in landscape evolution.
2. To identify and improve the understanding of the mechanisms of bedrock erosion during extreme flood events.

3. To constrain the dynamics of knickpoint erosion processes during extreme flood events and during background periods of ‘normal flow’.

These research objectives and thus, the research aim, are achieved through a detailed case study of the impact of extreme flood events on the Jökulsárgljúfur canyon, Iceland (Chapter 2; addressing Objectives 1 and 2), and an experimental modelling study of knickpoint erosion processes (Chapter 3; addressing Objectives 2 and 3).

1.4 Thesis outline

The body of this thesis is organised into two main chapters, each containing separate sub-chapters. Both chapters can be read independently, but they also contribute sequentially and holistically to a greater understanding of the impact, and processes, of bedrock erosion, especially canyon formation, during extreme flood events, the aim of this study. Fig. 1.6 provides a graphical visualisation of how each Chapter and Sub-Chapter are linked to each other, and how they contribute to the achievement of the research aim.

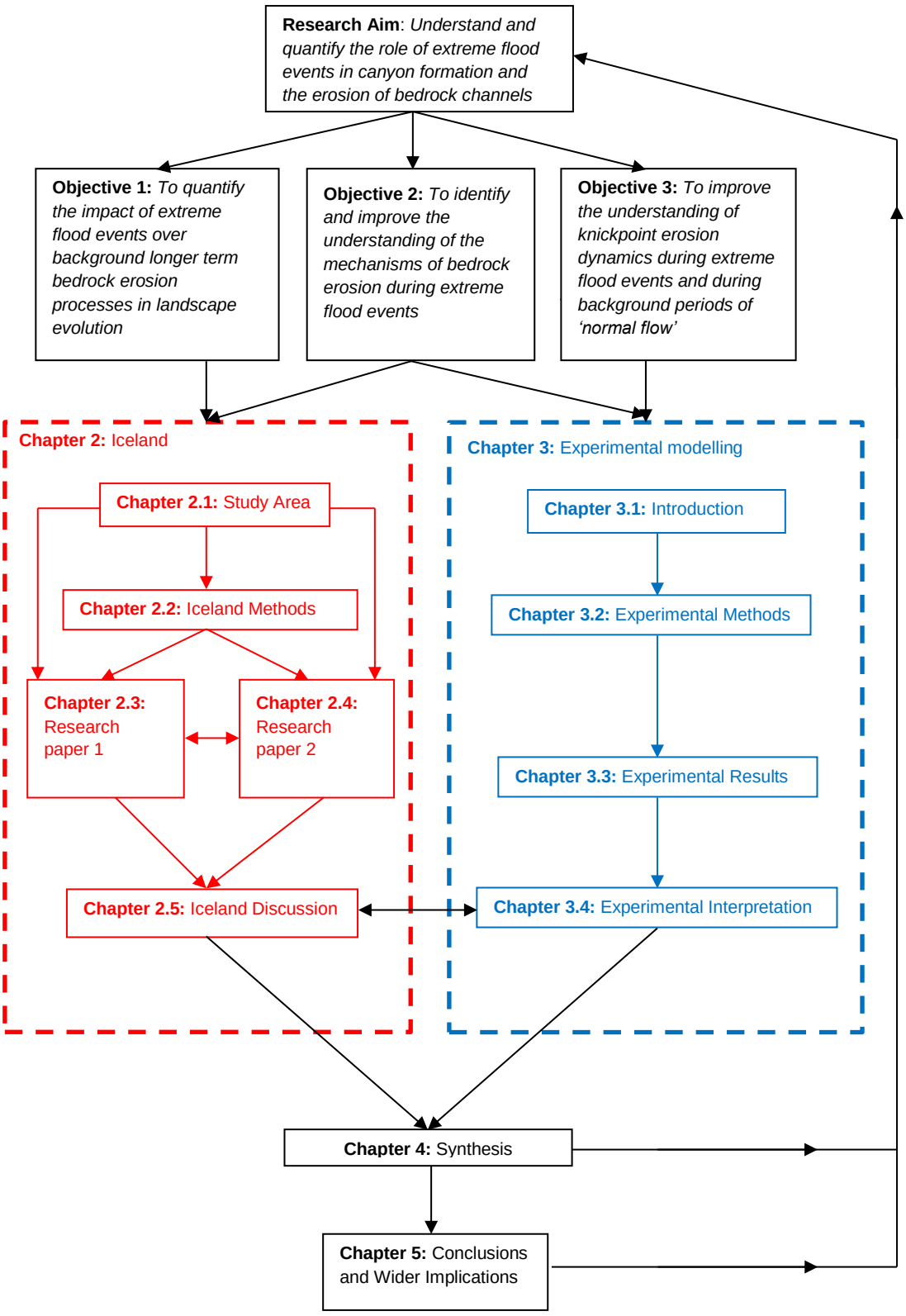

Fig. 1.6: Flow diagram of thesis structure. Sub-Chapters of Chapter 2 (Iceland) are shown in red and Sub-Chapters of Chapter 3 (Experimental modelling) are shown in blue. Arrows show linkages between Sub-Chapters. Black arrows indicates link between the Sub-Chapters and the research aim and the specific research objectives (Section 1.3).

Chapter 2 presents a detailed quantitative case study of the impact of extreme flood events on the Jökulsárgljúfur canyon and the surrounding area in North-East Iceland using a range of geomorphological, geochemical and geophysical techniques. Chapter 2 begins with a general introduction to the study area (Sub-Chapter 2.1), providing a context for extreme flood events in Iceland and the justification for why this specific landscape was selected for study. Sub-Chapter 2.2 provides a detailed description of the methods employed. The following two chapters (Sub-Chapters 2.3 and 2.4) have been written in the form of research papers and can be read as self-contained units. Sub-chapter 2.3 focuses on the surface exposure dating and topographic analysis carried out in the upper 5 km of the Jökulsárgljúfur canyon. This sub-chapter has been published in *Proceedings of the National Academy of Sciences* (Baynes *et al.* 2015; DOI: 10.1073/pnas.1415443112). Sub-Chapter 2.4 documents the impact of extreme flooding throughout the length of the Jökulsárgljúfur canyon, quantifies the volume of rock eroded from Ásbyrgi during flooding and provides a model for the evolution of the Jökulsárgljúfur canyon during the Holocene. This sub-chapter has been accepted for publication in *Geomorphology* (DOI: 10.1016/j.geomorph.2015.05.009) and is currently *in press.* Sub-Chapter 2.5 discusses the holistic nature of the findings from the Jökulsárgljúfur case study in relation to other landscapes as well as the research objectives stated in Section 1.3. It identifies the dominant erosion mechanism during extreme flood events in the study area as erosion through knickpoints propagation, which is explored further in **Chapter 3.**

Chapter 3 seeks to understand the dynamics of erosion processes at knickpoints through an experimental study of the factors that control knickpoint form and retreat rates (addressing Objective 3 above). As discussed in Section 1.2.2.4, the current understanding of knickpoint erosion processes is poor with the complexities of the erosion processes often ignored in studies of landscape evolution in favour of a simple scaling with drainage area based on the stream power incision model (Lague, 2014). It was therefore decided to carry out a series of experiments using an analogue

flume in order to improve our understanding of the dynamics of knickpoint erosion processes, as experimental models allow the isolation of possible controls on erosion processes in a controlled environment, allowing the development of new quantitative theory (e.g. Lamb *et al.*, 2015) of knickpoint erosion processes that can then be implemented into models of landscape evolution. Sub-Chapter 3.1 introduces the concept of experimental modelling and Sub-Chapter 3.2 provides a detailed description of the procedures used in the experimental data collection and subsequent data analysis. The results of the experimental modelling are documented in Sub-Chapter 3.3 and the interpretation of the findings presented in Sub-Chapter 3.4.

Finally, **Chapter 4** synthesises the findings from the preceding chapters and discusses how the combination of the study of the Jökulsárgljúfur canyon and the experimental modelling, have helped improve the understanding of bedrock erosion during extreme flood events. Outstanding questions raised by this work are addressed and possible future research outcomes based upon these are outlined.

Chapter 5 summarizes the main research conclusions of this study.

Chapter 2: Extreme flood events in the Jökulsárgljúfur canyon, northeast Iceland

Sub-Chapter 2.1: Study area

This chapter provides an introduction to the main study area for this research; the Jökulsárgljúfur canyon in northeast Iceland. The chapter begins with an overview of the wider regional context of the area in terms of glacial and relative sea level change since the Last Glacial Maximum before discussing why Iceland is a unique place to study the impact of the extreme flood events. An introduction is provided to the Jökulsárgljúfur canyon and its flooding history, which is developed in the forthcoming chapters.

2.1.1 Overview of glacial and sea level history of Iceland

2.1.1.1 Glacial history of Iceland

During the last glacial cycle, a large ice sheet developed over Iceland and extended in many places beyond the present day coastline (Fig. 2.1.1; Norðdahl, 1990; Norðdahl *et al.,* 2008; Ingolfsson *et al.*, 2010), with evidence for the maximum extent obtained from geomorphological mapping (e.g. Norðdahl and Peturrson, 2005), analysis of sedimentary deposits such as the presence of ice-rafted debris (e.g. Ólafsson *et al.*, 1993; Andrews *et al.* 2000) and numerical modelling (e.g. Hubbard *et al.,* 2006).

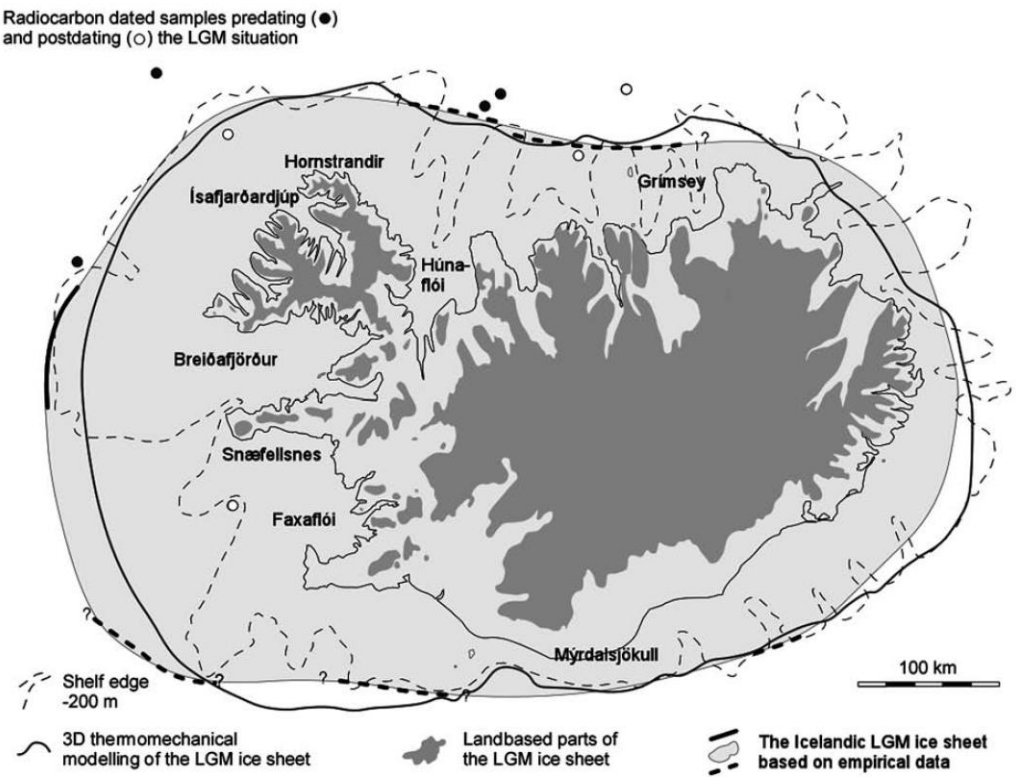

Fig. 2.1.1: Extent of Icelandic Ice Sheet at the Last Glacial Maximum (> 25 ka BP) in relation to the present day land mass and the edge of the continental shelf, including sites of dated sedimentary evidence of glacial extent both pre-LGM (black dots) and post-LGM (grey dots). *From Ingolfsson et al. (2010).*

With 81% of the Icelandic Ice Sheet grounded beneath sea level at the end of the Last Glacial Maximum (LGM; Hubbard *et al.,* 2006), deglaciation was rapid during the Bølling interstadial (15.4-13.9 ka BP) because rising eustatic sea level lead to weakening and collapse of the distal areas of the ice sheet (Ingolfsson and Norðdahl, 2001). By the end of the Bølling interstadial period, it is thought the Icelandic Ice Sheet covered ~25% of its maximum extent (Fig. 2.1.2; Ingolfsson *et al.*, 2010). The Icelandic Ice Sheet experienced re-advance during the Younger Dryas Stadial, a period of globally cooler temperatures between ~13.0-11.0 ka BP (Fig. 2.1.3). Geomorphological and sedimentological evidence suggest that during the Younger Dryas, the Icelandic Ice Sheet again covered much of the present day Icelandic land mass and in some locations, although fewer than at the LGM, extended beyond the present day coastline (Norðdahl and Petursson, 2005; Ingolfsson *et al.*, 2010).

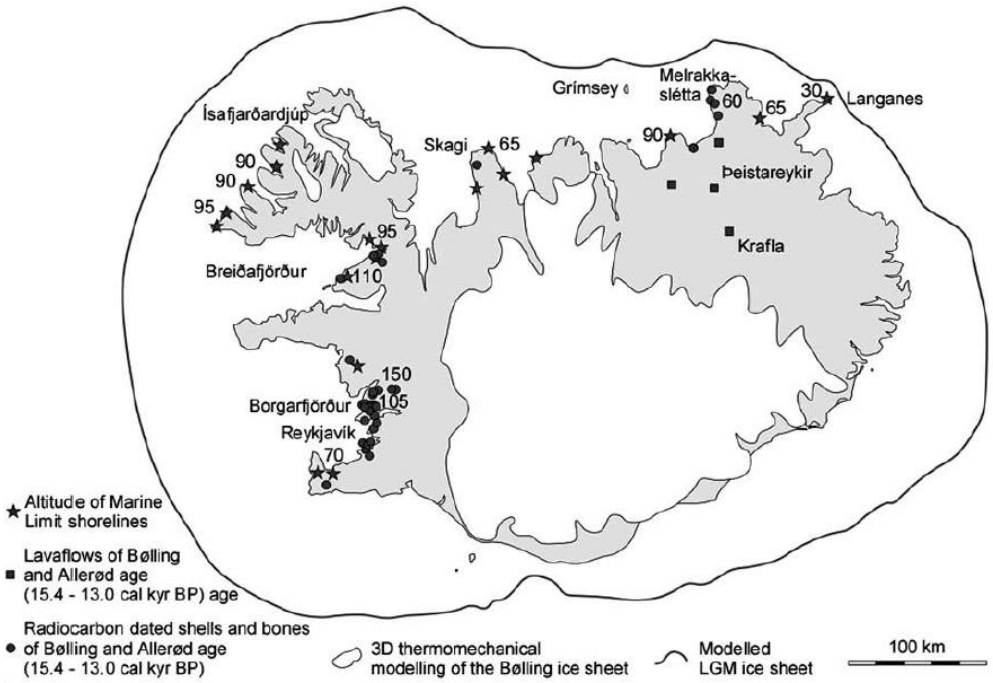

Fig. 2.1.2: Extent of Iceland Ice Sheet after Bølling deglaciation event (15.4-13.9 ka BP), compared to modelled maximum ice sheet extent. Note that the majority of North-East Iceland has been deglaciated during this period. *From Ingolfsson et al. (2010).*

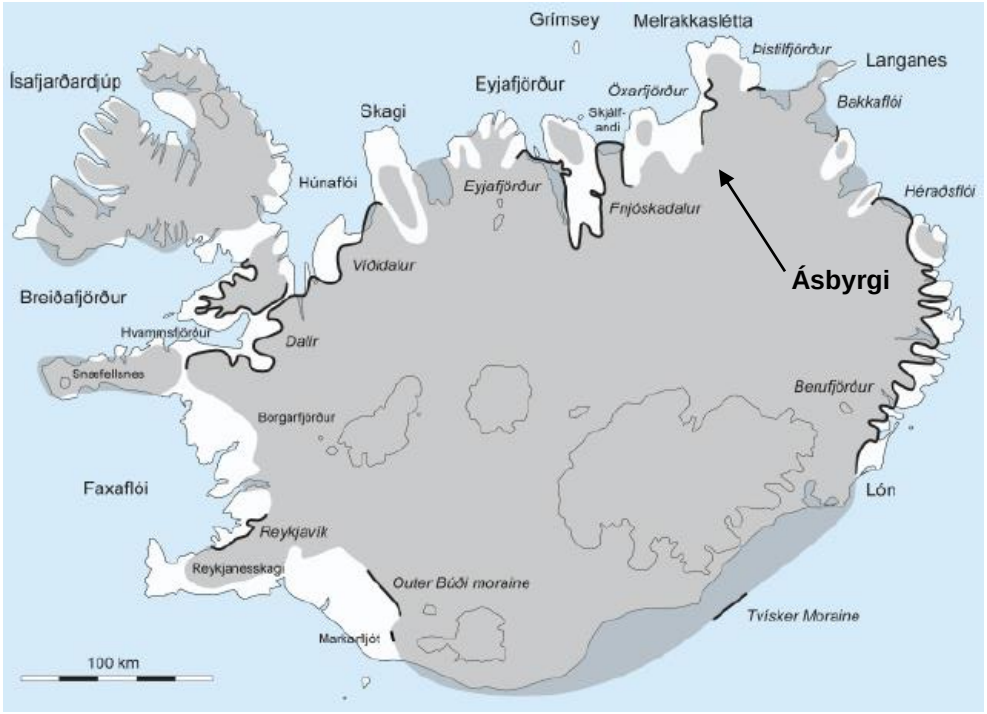

Fig. 2.1.3: Extent of the Icelandic Ice Sheet during the Younger Dryas (~10.3ka BP). Note the ice limit is in the approximate location of Ásbyrgi canyon. *From Norðdahl and Petursson (2005)*

Licciardi *et al*. (2007) explored the extent and volume of the Icelandic Ice Sheet using a geochronological technique known as surface exposure dating using cosmogenic nuclides, and the knowledge that when volcanoes erupt subglacially, they form table top mountains at the elevation of the top of the ice surface (Fig. 2.1.4). The tops of several table top volcanoes located along the length of the Jökulsá á Fjöllum river, draining from Vatnajokull to the northern coast are clustered at two periods, allowing the reconstruction of the ice surface profile at ~14 ka BP and ~10.5-11 ka BP.

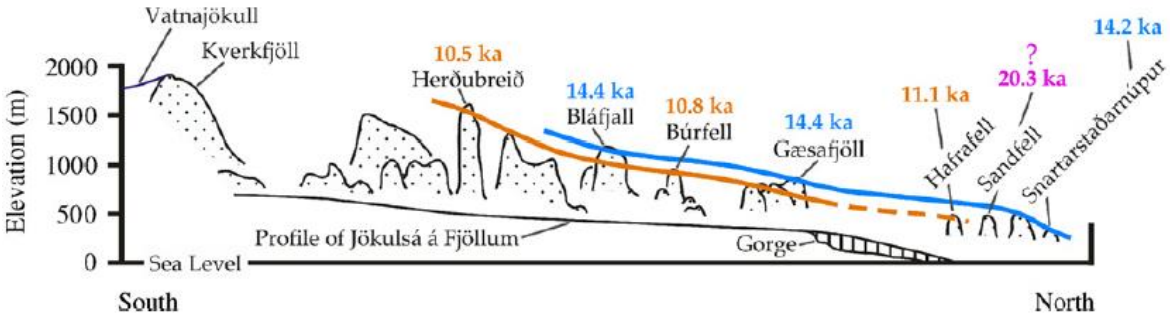

Fig. 2.1.4: Reconstructed ice surface profiles along a transect along the Jökulsá á Fjöllum river from Vatnajokull in the south to the northern coast, based on cosmogenic ^{3}He surface exposure inferred eruption ages of subglacial table-top mountains in this region (Licciardi *et al*., 2007). The inferred eruption ages fall into two clusters, with the younger cluster (10.5-11.0 ka BP, in orange) corresponding to the Younger Dryas Stadial.

These ages support the hypothesis that this reach was covered in ice during the Younger Dryas period (Fig. 2.1.3), but not the idea that glaciers had retreated across this area during the Bølling event between 15 and 14 ka BP (e.g. Ingolfsson *et al.*, 2010). A borehole drilled by the Icelandic Energy Authority (Ólafsson *et al.*, 1993) in the sediments deposited in Öxarfjörður identified the highest glacially influenced sediments (diamictite beds) at 350 m depth, thought to date to around 10,000 yr BP. Beneath these upper beds, fine grained units between further diamictite beds indicate changes in glaciation extent but it is not possible to further estimate the extent of deglaciation during these periods from a single borehole (Olafsson *et al.*, 1993). The dynamics of glacial retreat and re-advance in the early Holocene

between the LGM and the Younger Dryas therefore require further study in order to accurately determine the glacial history in this region. Following the Younger Dryas global cool period, the Icelandic Ice Sheet underwent rapid collapse, retreating to the smaller isolated ice caps present today such as Vatnajokull in southwest Iceland (Ingolfsson *et al.,* 2010). During the Holocene, fluctuations in the volumes of these smaller ice caps have been observed, with Striberger *et al.* (2012) suggesting the Vatnajokull was significantly smaller than present between 7.0 and 4.4 ka BP based on the lack of glacially derived sediments during this period in a core collected from Lake Lögurinn in eastern Iceland.

2.1.1.2 Sea level history of Iceland during the Holocene

Changes in the relative sea level (RSL) at any location on the Earth's surface is a function of several different factors, including both eustatic processes; changes in the global ocean volume, and isostatic processes; variations changes in the elevation of the continental crust through tectonics or changes in the mass balance (Fairbanks, 1989; Mitrovica *et al.,* 2001). During deglaciation, in 'near-field' environments, located close to large ice sheets, changes in RSL can be complex due to isostatic rebound of the crust following the loss of the ice mass from above. This leads to a rapid initial RSL fall as the rate of isostatic rebound exceeds the rate of eustatic sea level rise driven by the contribution of melting ice sheets to global ocean volume (Shennan *et al.,* 2012). Numerous studies in Iceland have identified the 'marine limit' from the early Holocene, the maximum elevation of postglacial RSL, far above the present day elevation of the coastline (e.g. Hjort *et al.,* 1985, Ingolfsson, 1991; Norðdahl and Petursson, 2005; Fig. 2.1.5), although the age and elevation of the marine limit in Iceland varies as a result of differences in ice thickness and the pattern, processes and timing of deglaciation (Jennings *et al.,* 2000).

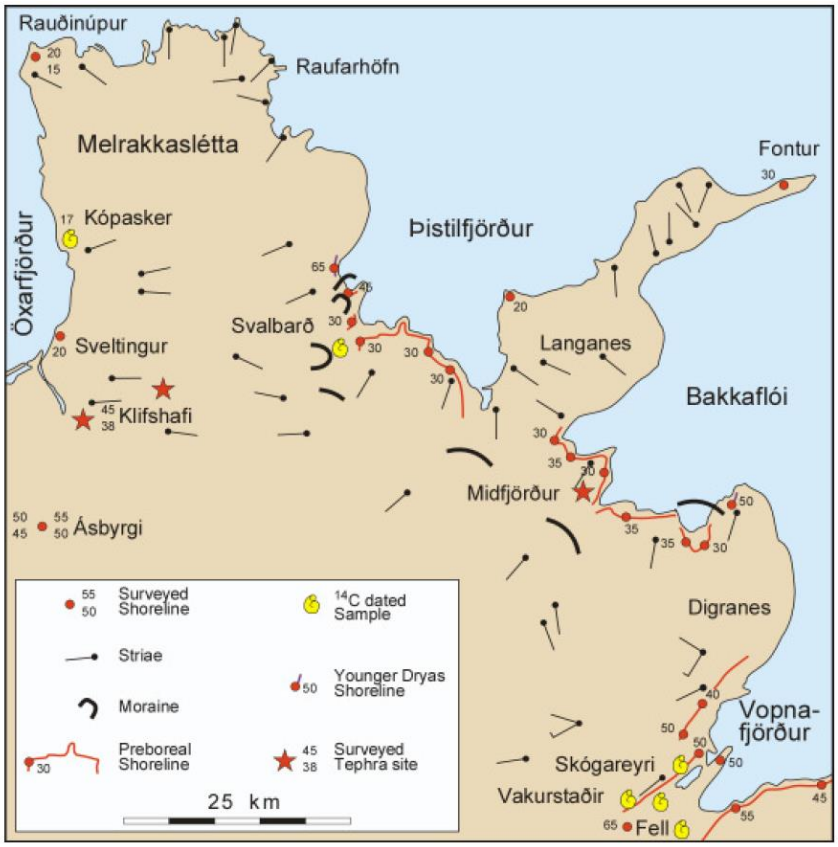

Fig. 2.1.5: Geomorphological evidence for the marine limit in northeast Iceland (e.g. moraines, raised marine terraces) during the Younger Dryas period. Numbers indicate the elevation of the features above the present day coastline, providing an estimate of the maximum RSL elevation during the Holocene. *From Norðdahl and Petursson (2005).*

The nature of lake deposits in 'isolation basins' around the Icelandic coast provide more information regarding the pattern of RSL during the Holocene, rather than simply providing an elevation and age for the timing of the maximum RSL since deglaciation (e.g. Rundgren *et al.,* 1997; Lloyd *et al.,* 2009; Brader, 2012). These studies allow the identification of a period of RSL rise during the Younger Dryas period (Fig. 2.1.6) as a result of glacio-isostatic compression of the continental crust. Glacio-isostatic rebound exceeded eustatic sea level rise during the rapid deglaciation following the Younger Dryas leading to a period of prolonged RSL fall in the early-mid Holocene (Fig. 2.1.6; Norðdahl and Petursson, 2005). The RSL fell below the present day sea-level to a lowstand in the mid-Holocene ~10-7 ka BP

depending on location around the Iceland coast (Thors and Helgadottir, 1991; Norðdahl and Petursson, 2005; Brader, 2012). Since the RSL lowstand, the rate of glacio-isostatic rebound has slowed to below the rate of eustatic sea level rise (Fig. 2.1.6), resulting in a gradual rise in RSL to the present day elevation of the coastline. Variations in RSL are important when considering studies of bedrock erosion and fluvial long profile evolution because variations in base level can result in the development of knickpoints that then propagate upstream through time (e.g. Kirby and Whipple, 2001; Section 1.2.2.4).

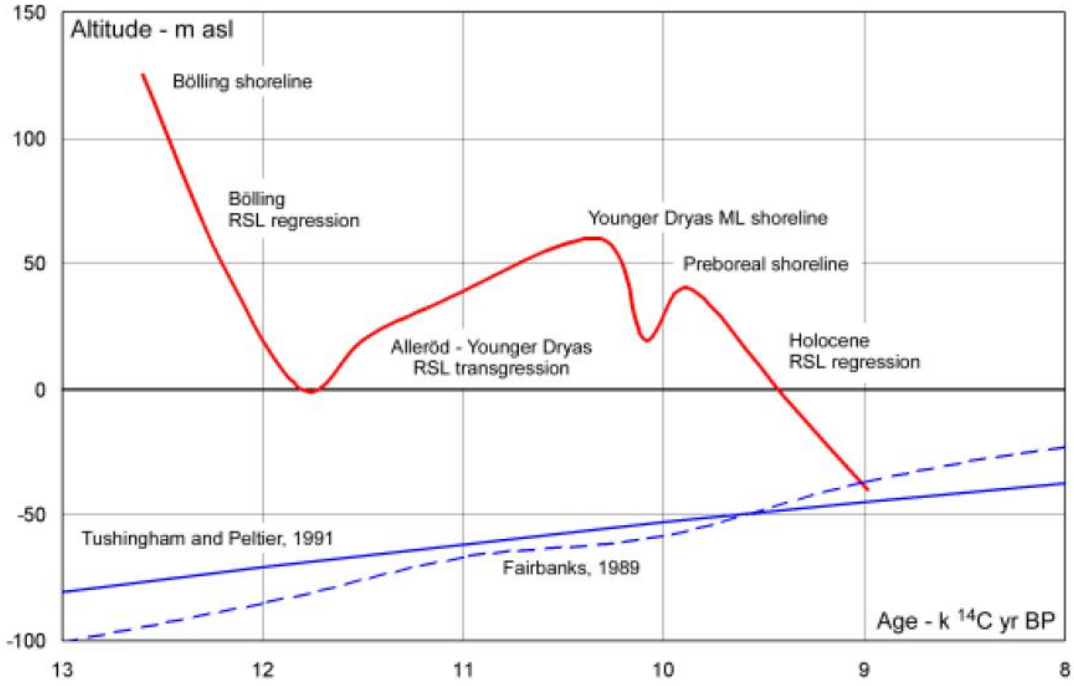

Fig. 2.1.6: Conceptual representation of relative sea-level change around Iceland during the Early Holocene. Initially there is a rapid sea level fall during the initial stages of deglaciation following the LGM during the Bølling interstadial due to glacio-isostatic rebound of the Earth's surface. There is an increase in RSL during the Younger Dryas following ice-mass loading before continual RSL fall during rapid deglaciation. RSL falls below the present day elevation of the coastline in the early-mid Holocene, with a gradual rise to present day sea level following continuing eustatic sea level rise and slowdown in glacio-isostatic rebound rates. *From Norðdahl and Petursson (2005), with eustatic sea level curves of Tushingham and Peltier (1991) and Fairbanks (1989).*

2.1.2 Volcano-Ice interactions in Iceland

Iceland is known as the ‘land of fire and ice’. The high latitude, sub-Arctic, climate of Iceland combined with its location on the Mid-Atlantic spreading ridge above a mantle plume provides a dynamic setting for investigating the contemporary interaction of glaciers and large volcanic systems (Fig. 2.1.7). High impact examples of volcano-ice interaction include the recent eruptions of Eyjafjallajökull in 2010 (Fig. 2.1.8A) and Grímsvötn in 2011 (Fig. 2.1.8B) which sent large volumes of volcanic ash into the atmosphere and disrupted airspace across northern Europe.

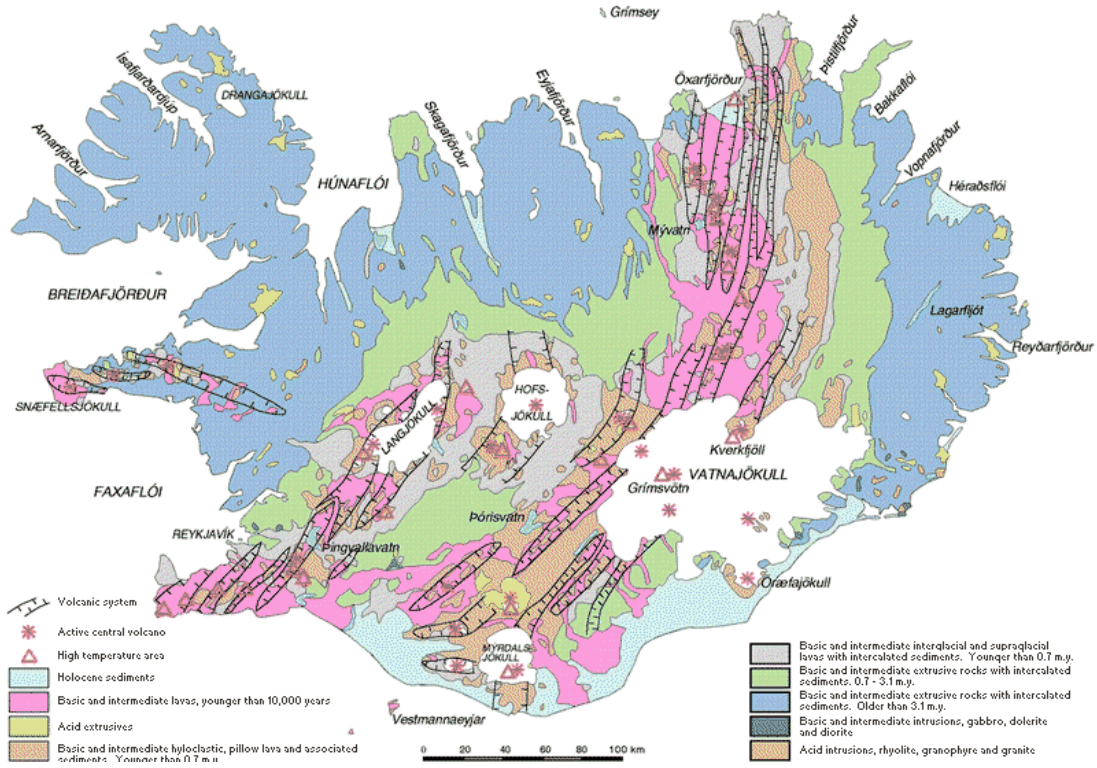

Fig. 2.1.7: Geological map of Iceland. Glaciers cover ~10% of the island, indicated in white. Also shown on the map are extensive volcanic systems, resulting in frequent volcano-ice interactions. *Image source: Jóhannesson and Sæmundsson* (*1999).*

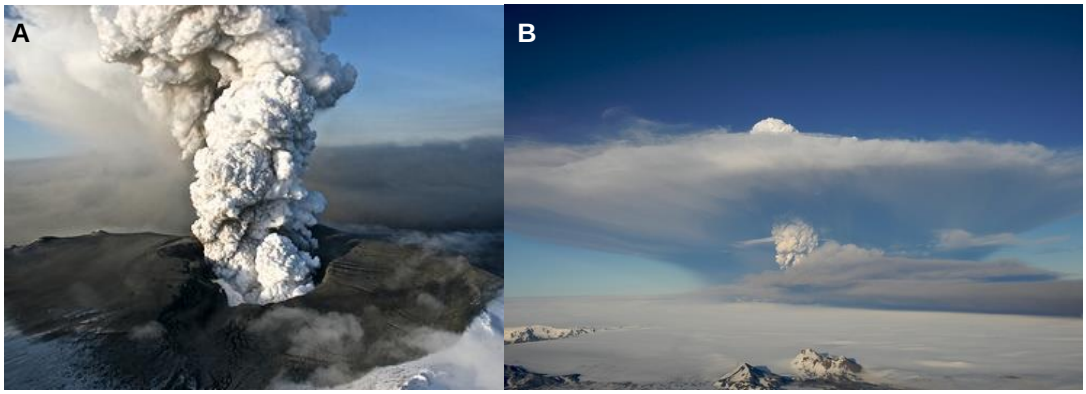

Fig. 2.1.8: Examples of recent volcano-ice interaction in Iceland. **A.** The eruption of Eyjafjallajökull in April 2010 (*Image source: http://www.geotalk.info/#!eyjafjallajkull-case-study/c1qwm*). **B.** The eruption of Grímsvötn in May, 2011 (*Image source: http://en.vedur.is/earthquakes-and-volcanism/articles/nr/2185*).

2.1.2.1 Jökulhlaups

Another consequence of the frequent volcano-ice interactions are glacial outburst floods, termed 'jökulhlaups' (e.g. Björnsson, 2002), which makes Iceland an ideal place to study the impact of extreme flood events on landscape evolution over variable timescales. Subglacial volcanic eruptions can trigger jökulhlaups either by generating meltwater directly through heat transfer or by perturbing subglacial or ice-dammed lakes that then drain catastrophically (Tweed and Russell, 1999; Russell *et al.*, 2010). The result from both processes is frequent outburst floods of varying magnitude across both mountainous landscapes and depositional plains. Previous work on Icelandic jökulhlaups include the interpretation of deposited sediments (e.g. Maizels, 1997; Duller *et al.*, 2008; Marren *et al.*, 2009; Burke *et al.,* 2010a), the reconstruction of the hydraulic conditions (e.g. Baker *et al.,* 1993; Alho *et al.,* 2005; Carrivick, 2006; 2007) and the geomorphic impact of jökulhlaups in proglacial areas close to the floodwater source (e.g. Smith *et al*., 2000; Magilligan *et al*., 2002; Carrivick *et al.*, 2004; Robinson *et al.*, 2008; Burke *et al.*, 2010b; Russell *et al.,* 2010; Dunning *et al*., 2013).

Numerous jökulhlaups have been documented in Iceland throughout the Holocene. They are a contemporary hazard for the human population across Iceland as their potential routes cross inhabited areas and infrastructure such as roads and power schemes (Clague and Evans, 1994; Gudmundsson *et al.*, 2008). Jökulhlaups can be characterised by a rapid rise to peak discharge and can have very fast (> 8 m s^{-1}) frontal velocities (Russell *et al.,* 2010) although jökulhlaups can exhibit a multitude of hydrograph shapes depending on a number of factors such as the triggering mechanism, the routing of water through the glacier (i.e. tunnelled or non-tunnelled flow) and the number of flow outlets (Tweed and Russell, 1999; Roberts, 2005). For example, the hydrograph associated with the enlargement of a single basal ice tunnel due to melting has a long rising limb followed by a rapid falling limb (Björnsson, 2002) whereas the 1996 Grímsvötn flood was characterised by a rapid rising limb followed by a long falling limb, induced by the flotation of the ice-dam by rising water levels in the Grímsvötn caldera lake generated by excess volcanically induced meltwater from the Gjalp eruption (Björnsson, 2002; 2009).

Depending on the routing of the flood, jökulhlaups can lead to either significant erosion of the submerged landscape or substantial deposition of material both in the proglacial area close to the floodwater source and in more distal areas (Magilligan *et al.,* 2002; Russell *et al.,* 2006). The majority of jökulhlaups flow over ‘sandar’ plains; large glacial outwash plains that typically contain braided rivers (Fig. 2.1.9) but some also flow through bedrock landscapes leading to erosion of the landscape (Gudmundsson *et al.,* 2008; Fig. 2.1.10). The landforms and sediments of these sandur plains are characterised by the action of jökulhlaups and each event can cause significant landscape change (e.g. Maizels, 1997; Duller *et al.*, 2014).

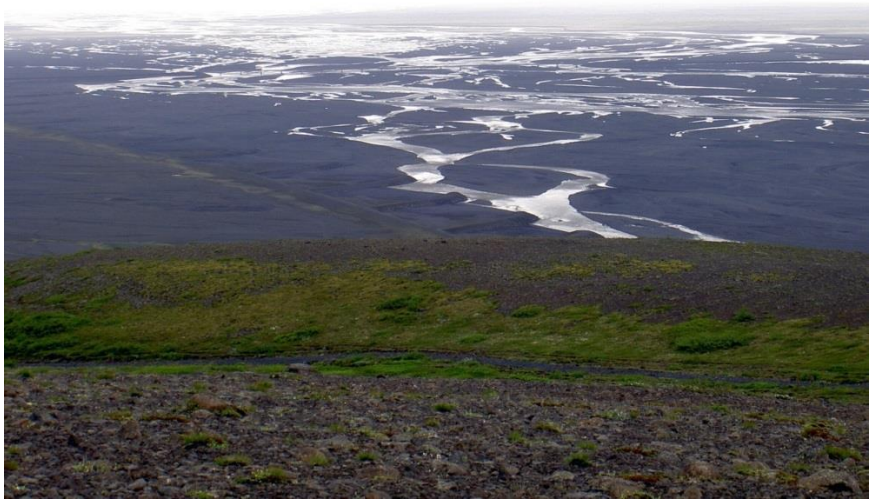

Fig. 2.1.9: Example of a typical ‘sandur’ plain at Skeiðarársandur near Skaftafell, south Iceland *(Image source: This Wikipedia and Wikimedia Commons image is from the user Chris 73 and is freely available at //commons.wikimedia.org/wiki/File:Sandur_at_Skaftafell_Iceland_2005.JPG under the creative commons cc-by-sa 3.0 license.*)

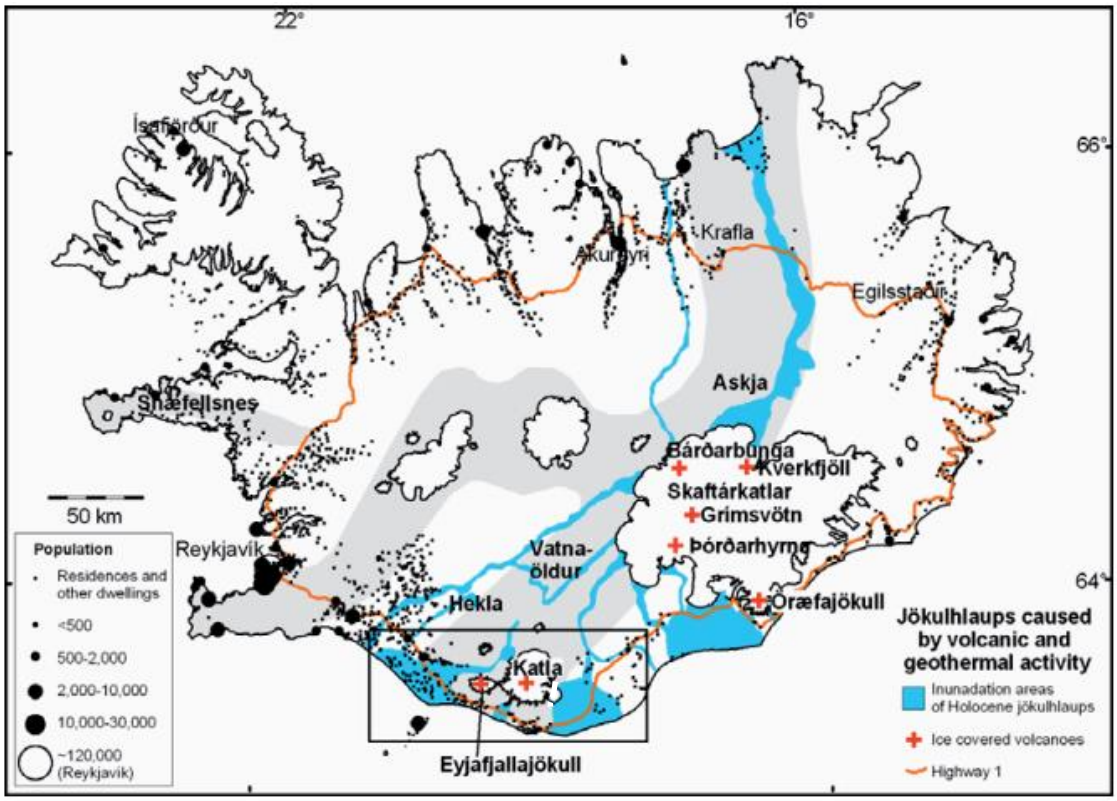

Fig. 2.1.10: Map of jökulhlaup flood routes (light blue areas) across Iceland during the Holocene. (*Image source: Gudmundsson et al., 2008*).

Maizels (1991; 1997) documented in detail the nature of sedimentary deposits associated with different jökulhlaups. Typically, 'type 1' deposits include large-scale expansion bars and dunes composed of large-scale gravel-cobble cross-bedding often capped by imbricated boulders, formed by sudden drainage of ice-dammed lakes (Maizels, 1997). 'Type 2' deposits, formed by floods triggered by subglacial volcanism are typically massive, homogenous, flood surge granules of sediment, underlain by smaller pre-surge gravels and capped by post-surge fluid bedforms representing deposition during the rising and falling stages of the flood (see Maizels, 1997 for further discussion of the nature and classification of jökulhlaup deposits).

Individual jökulhlaups can significantly alter the nature of sandur plains, such as patterns of drainage across the plain (Smith and Dugmore, 2006), significant deposition and reworking of the sediment in the plain (Smith *et al.*, 2000; Duller *et al.*, 2014), and create landforms such as eskers (Burke *et al.,* 2009) that can affect the hydrogeological system (Robinson *et al.*, 2008). The jökulhlaup across Skeiðarársandur following the 1996 eruption of Grímsvötn led to a net deposition of 13 x 10^6 m^3 of sediment across the 40 km^2 proglacial zone of Skeiðarársandur, despite a net erosion of 25 x 10^6 m^3 of sediment from the channels across the plain (Smith *et al*., 2000). The 1918 eruption of Katla, south Iceland, led to the deposition of 2 km^3 of material on the Mýrdalssandur plain, shifting the coastline seaward by several kilometres (Duller *et al.*, 2014). 80% of this material was later removed from the sandur plain by surface and subsurface water flow and coastal erosion by marine action.

Due to relatively short return period (51 ± 15 years, between 1660 and 1904; Duller *et al.*, 2014) of floods of this size compared to the landscape 'recovery time' (120 years; Duller *et al*., 2014), Mýrdalssandur has been in a dominant state of transience over the past 1000 years, leading to long-term net coastline advancement over this period (Duller *et al.*, 2014), demonstrating the importance of extreme flood events in long-term landscape evolution in depositional settings in Iceland. The nature of the 1918 Katla jökulhlaup

deposits purport to a high-energy fine-grained flow that was powerful enough to transport boulder sized material (Duller *et al*., 2008). In addition to having an impact on depositional environments, Icelandic jökulhlaups also cause significant changes in bedrock landscapes, although there has been a lack of quantitative studies that detail this impact.

2.1.2.2 Jökulhlaups along the Jökulsá á Fjöllum river

The Jökulsá á Fjöllum is one of Iceland's largest rivers, draining much of the 8,100 km^2 Vatnajökull ice cap in the south of the island and flowing 206 km north across central Iceland to the Arctic Ocean at Öxarfjörður (Fig. 2.1.11). Its typical peak summer discharge of sediment-rich glacial meltwater reaches ~500 $m^3 s^{-1}$ (Schunke, 1985, Data from Icelandic Met Office). The course of the river is characterised by a wide braided channel network upstream of the Selfoss waterfall which marks the upstream limit of the deeply incised, 28 km long Jökulsárgljúfur canyon. Downstream of this canyon, the Jökulsá á Fjöllum flows for 18 km over a large depositional sandur plain to the coast.

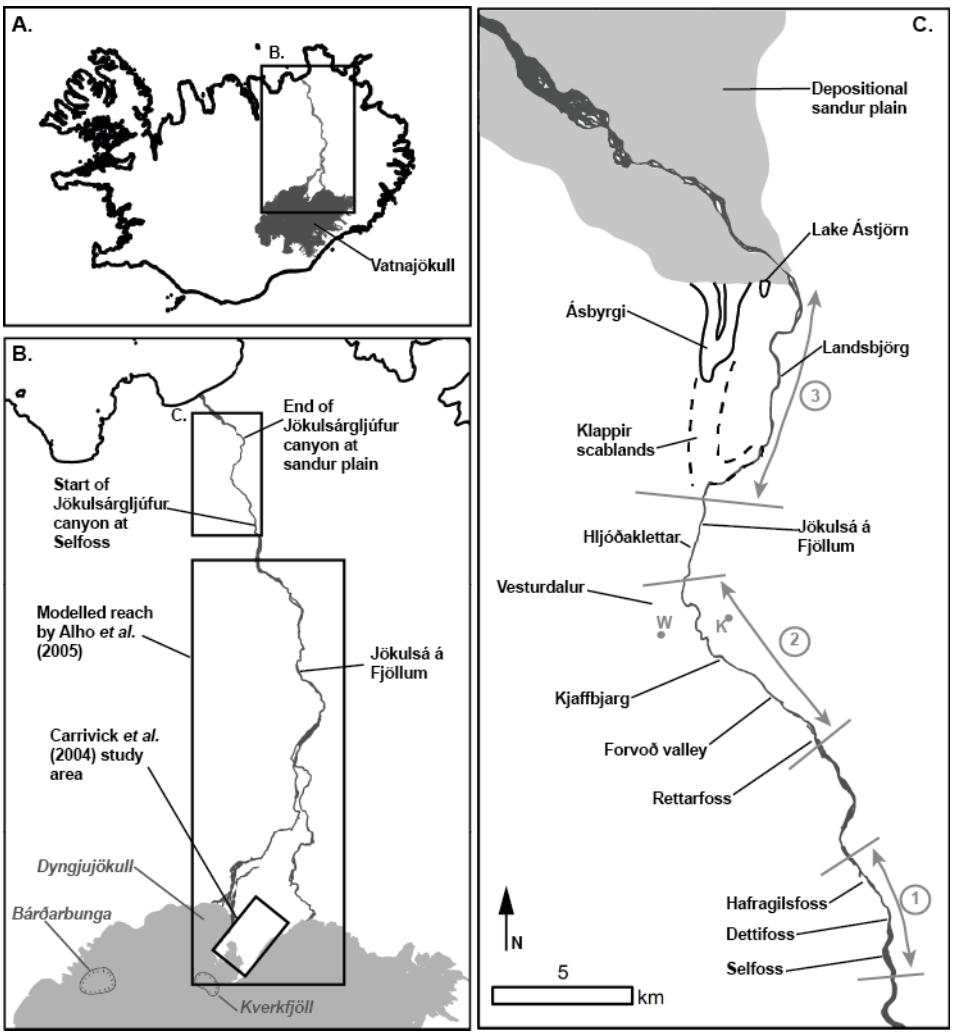

Fig. 2.1.11: A. Outline of Iceland with Vatnajökull ice cap (grey shaded area), the source of the floodwaters, and the course of the present day Jökulsá á Fjöllum draining to the North coast. **B.** Zoomed in map showing the areas studied by previous authors (Alho *et al*., 2005; Carrivick *et al*., 2004) in the upper and middle reaches of the Jökulsá á Fjöllum as well as the Jökulsárgljúfur canyon, the focus of this study. Kverkfjöll and Bárðarbunga volcanic centres are highlighted. Grímsvötn volcano is located ~25 km South of Bárðarbunga, just beyond the extent shown in the map. **C.** The Jökulsárgljúfur canyon is divided into three sections for the study: (1) The apex of the Jökulsárgljúfur canyon between Selfoss and Hafragilsfoss, discussed in detail in Sub-Chapter 2.3; (2) The Forvoð valley, containing depositional landforms; (3) The lowermost section of the Jökulsárgljúfur canyon, with the Ásbyrgi horseshoe and the Klappir scablands system, discussed in Sub-Chapter 2.4. The grey points labelled 'W' and 'K' indicate the location of the sedimentary sequences discussed in Waitt (2002) and Kirkbride *et al.* (2006), respectively.

The Jökulsá á Fjöllum has experienced multiple jökulhlaups of varying magnitude since the Last Glacial Maximum, with peak discharge for the largest flood estimated at 9×10^5 $m^3 s^{-1}$ (Table 2.1.1; Alho *et al*., 2005; Carrivick *et al.*, 2013) in the reach indicated in Fig. 2.1.11B. This estimate was determined from mapping the location and elevation of palaeo-stage indicators (PSI's) such as imbricated boulders and fluvially sculpted bedrock in the field. Step-back water modelling of the flow required to fill the wash limits using the HEC-RAS hydraulic model (US Army Corps of Engineering, 2001) indicated a peak flow discharge of 0.9×10^6 $m^3 s^{-1}$ across the area shown in Fig. 2.1.12, with power per unit area reaching 4.6×10^4 W m^{-2}. For comparison, the 'largest flood known on Earth', the late Pleistocene flood in the Altai Mountains of Siberia, had twenty times this peak discharge (1.8×10^7 $m^3 s^{-1}$) and twenty times the power per unit area produced by this flood (Baker *et al.* 1993).

Howard *et al.* (2012) estimated the discharge of the largest flood along the Jökulsá á Fjöllum to be two orders of magnitude greater than the flood modelled by Alho *et al.* (2005), at 4.5×10^7 $m^3 s^{-1}$. However, this estimate is considered 'highly unrealistic' due to a range of methodological issues, underlying assumptions made and an inconsistent interpretation of where a possible flood of this size could be sourced from (Carrivick *et al.*, 2013). Therefore, the estimate of the peak discharge of the largest flood along the Jökulsá á Fjöllum during the Holocene used for context when referring to the magnitude of jökulhlaups that have eroded the Jökulsárgljúfur canyon in the remainder of this thesis is that modelled by Alho *et al.* (2005): 0.9×10^6 $m^3 s^{-1}$. A flood of this size would require the melting of ~60-70 km^3 of ice (using the same scaling relationship of Alho *et al.,* 2007), which is ~ 2% of the total ice volume of Vatnajokull in the year 2000 (3100 km^3; Björnsson and Pálsson, 2008)

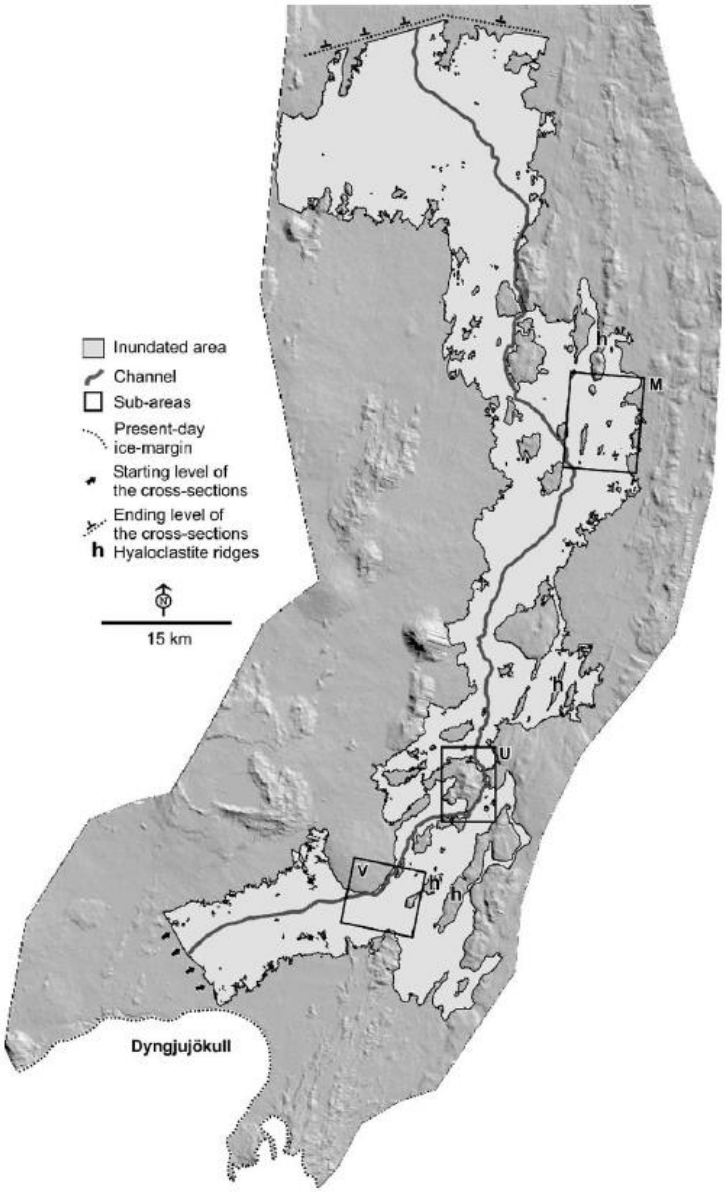

Fig. 2.1.12: Upper reaches of the Jökulsá á Fjöllum with the grey shading indicating the area inundated by a jökulhlaup with a peak discharge of 9 x 10^5 m^3 s^{-1}, modelled using the HEC-RAS hydraulic model and palaeo-stage indicators such as imbricated boulders and fluvially washed bedrock. *Figure source: Alho et al. (2005).*

While jökulhlaups of the magnitude modelled by Alho *et al*. (2005) are very rare (one occurrence since the Last Glacial Maximum, ~10^4 years ago), floods of the order of 10^4 m^3 s^{-1} occur on a millennial timescale (see Table 2.1.1) and floods with a discharge of the order of ~1.5 x 10^3 m^3 s^{-1}, three times the peak annual discharge, occur approximately twice per century (Helgason, 1987). Jökulhlaups occur along the Jökulsá á Fjöllum as a result

of either subglacial volcanism beneath Vatnajökull from one or more of the Kverkfjöll, Grímsvötn or Bárðarbunga volcanic centres (Björnsson, 2009), or the release of flood water from an ice-dammed lake to the south of Kverkfjöll (Björnsson, 2002) (Fig. 2.1.11B). The Bárðarbunga volcanic centre was last active from August 2014 to February 2015, although the fissure eruption was beyond the ice limit, thus not triggering a jökulhlaup.

Attempts have been made to identify and interpret the impact of jökulhlaups in the Jökulsá á Fjöllum that have occurred in recent history (Isaksson, 1985; Russell and Knudsen, 2002) and during the Holocene (Thórarinsson, 1950; Sæmundsson, 1973; Tomasson, 1973; Eliasson, 1974; Eliasson, 1977; Sigbjarnarson, 1996; Waitt, 2002; Carrivick *et al.*, 2004; Kirkbride *et al*., 2006). Table 2.1.1 provides a summary of the previous work on the timings and magnitude of extreme flood events along the course of the Jökulsá á Fjöllum. Fig. 2.1.13 provides a graphical visualisation of the timing and magnitude of extreme flood events proposed by the previous studies listed in Table 2.1.1.

Much of the recent work on this river has focussed on the geomorphic impact and sedimentary evidence of jökulhlaups close to the floodwater source (e.g. Carrivick *et al.*, 2004; Carrivick, 2007; Marren *et al.*, 2009) and modelling the hydraulic conditions of the floods in mid- to up-stream reaches (e.g. Alho *et al.*, 2005; Carrivick, 2006; 2007; Carrivick *et al.*, 2013). While some studies have postulated that significant bedrock erosion has occurred during extreme flood events in the downstream reaches of the Jökulsá á Fjöllum (such as inferring the role of extreme flood events in the formation of Ásbyrgi (e.g. Eliasson, 1977; Sæmundsson, 1973; Waitt, 2002), none of the previous studies have specifically tied the evolution of the bedrock landscape within the Jökulsárgljúfur canyon to extreme flood events, or explored the mechanics of the erosion processes at work during such events. Thus, this research fills an important gap in the understanding of the role of extreme flood events in the evolution of the Jökulsá á Fjöllum and surrounding landscape.

Table 2.1.1: Summary of previous work into the timing and magnitude of extreme floods along the Jökulsá á Fjöllum. *Adapted from Carrivick et al. (2013)*.

Study	Timing of floods	Estimated peak discharge ($m^3 s^{-1}$)	Source/triggering mechanism	Evidence	Methods
			Historic floods (in years AD)		
Thórarinsson (1950)	1490, 1655, 1684, 1711, 1712, 1716, 1717		Dyngjujökull	Historical witness accounts from Axarfjordur and Keldhuverfi	Field visit, 1946 to Kverkfjöll
Thórarinsson (1959)	1655, 1684, 1711, 1712, 1776, 1717, 1729		Subglacial volcanic bursts from Kverkfjöll and/or Dyngjujökull	Historical witness accounts from Axarfjordur and Keldhuverfi	
			Holocene floods (in years BP)		
Sæmundsson (1973)	1 earliest post-glacial Less than 2900	-	-	Lava striations relative to maximum glacial extent moraines	Geomorphological mapping
Tomasson (1973, 2002)	2500	$0.4 – 0.5 \times 10^6$	1973 study; Kverkfjöll caldera or Grímsvötn by subglacial melting, but most likely ice-dammed lake south of	'H3' Tephra layer (3000-3100 years BP; Larsen and Eiríksson, 2008)	Aerial photograph interpretation and field visits. Manning equation, flood-filled canyon and measurement of present-day topography

			Kverkfjöll.		
			2002 study; Bárðarbunga caldera		
Helgason (1987)	7100, 4600, 3000, 2000	4×10^5	'Volcanism' or an Ice-dammed lake	-	-
	Approx. 2 per century	1.5×10^3	Rapid spring thaw or other 'special circumstances'		
Waitt (1998)	9000-8000, 2000	1×10^6	-	'H5' tephra layer (~ 7100 years BP; Larsen and Eiríksson, 2008)	-
Waitt (2002)	1 flood between 9000-8000, 16 floods between 8000-4000, 1 flood between 2500-2000	Flood between 2500-2000 years = 7×10^5	Kverkfjöll caldera	Stratigraphy and tephra (H5). See Fig. 1 for location of study	Field visits in 1986 and 2000 Geomorphological mapping, Sedimentology and Step-backwater modelling
Alho *et al.* (2005)	-	0.9×10^6	Bárðarbunga caldera	Palaeo Stage Indicators: e.g. imbricated boulders and washed bedrock (i.e. bedrock with exotic well-rounded clasts)	Step-backwater modelling
Kirkbride *et al.* (2006)	5020, 4610	$> 7 \times 10^5$	Kverkfjöll or Grímsvötn	^{14}C AMS dates from Betula macrofossils within peat layers in stratigraphy – see Fig. 1 for location of study	Field visit, Sedimentology and Geochemical analysis

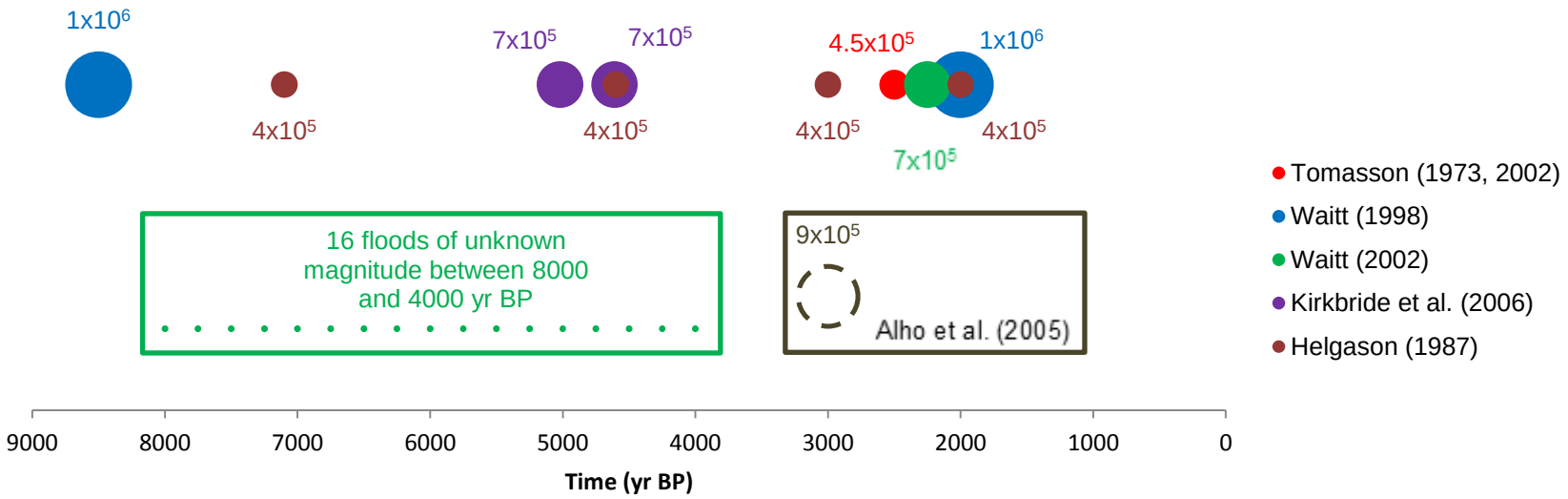

Fig 2.1.13: Graphical representation of the estimates of palaeo-flood discharge along the Jökulsá á Fjöllum during the Holocene that are listed in Table 2.1.1. Area of circle is proportional to the flood discharge, indicated by the labels. Colours represent different published studies. The estimate of peak discharge by Alho *et al.* (2005) does not have a time estimate associated with it, but is included in the grey inset to allow comparison with other studies. Waitt (2002) suggested 16 floods occurred between 8000 and 4000 yr BP, although a corresponding estimate of the magnitude of each of these floods is not provided, but they are plotted within the green inset box assuming a regular time period between each flood event. The historical floods identified by Thórarinsson (1950; 1959) are not included in this figure, as the flood magnitude is not known and the 14 floods would all be clustered within 200 years at the right hand side of the graph.

2.1.3 Jökulsárgljúfur canyon

The principal study area for this work is the Jökulsárgljúfur canyon in the downstream reaches of the Jökulsá á Fjöllum (Fig. 2.1.11C), selected for study because evidence for bedrock erosion and canyon formation during extreme flood events has long been recognised in previous literature (e.g. Sæmundsson, 1973; Eliasson, 1977). Additional evidence for the action of extreme events has been documented upstream (e.g. Carrivick *et al.*, 2004) and the hydraulics of the largest flood has been modelled with the peak discharge estimated at 0.9×10^6 $m^3 s^{-1}$ (Alho *et al.,* 2005). Despite this previous work, there exists no research on the Jökulsárgljúfur canyon that has specifically studied the impact of the extreme flood events on the erosion of the canyon, nor tied the formation of different areas of the canyon to specific events.

Within the Jökulsárgljúfur canyon are three distinct reaches, each exhibiting evidence for extreme flood events, discussed in detail subsequently in Sub-Chapter 2.4 (Fig. 2.1.1C). The geological history of the area is complex (see geological maps below; Fig. 2.2.16, 2.2.17, 2.2.19), with active volcanic activity erupting lava onto the surface in this area through the Quaternary period and into the Holocene (Saemundsson *et al.,* 2012). All of the lava flows within the eroded Jökulsárgljúfur canyon are less than 800,000 years old with some Holocene lava flows produced by the eruption of volcanic fissures across the area. The most significant contributor of lava to the area comes from Storaviti, producing lava that covers the area to the south and west of Ásbyrgi (Saemundsson *et al.,* 2012). The main rock type in the study area is freshly erupted lavas that contain olivine and pyroxene minerals within the basalt matrix. This rock type is suitable for the surface exposure dating using cosmogenic ^{3}He geochronological technique applied in this study, allowing an accurate interpretation of the time evolution of the canyon as it has been eroded using this method.

Downstream of the Jökulsárgljúfur canyon, the Jökulsá á Fjöllum flows across a sandur plain that flows into Öxarfjörður, the youngest of the

depositional basins located on the North coast of Iceland, and formed as a result of the tectonic evolution of the Tjornes Fracture Zone (TFZ) (Ólafsson *et al.*, 1993). Over the past 10 million years, uplifted or drilled Tertiary and Quaternary sediments indicated the coastline in Öxarfjörður has not deviated significantly during this time despite prominent subsidence within the basin, with shallow marine sediments alternating with terrestrial sediments and material of volcanic origin (Ólafsson *et al.,* 1993). A borehole drilled by the Icelandic Energy Authority close to the present day coastline revealed that large volumes of sediment have been deposited on the Öxarfjörður sandur plain in the last 10,000 years, with the first evidence of glacial influence (e.g. diamictite) located at 350 m depth (Ólafsson *et al.*, 1993). The sediments above the glacial units indicate evidence of sea level transgression followed by regression as the Jökulsá á Fjöllum outwash delta built northwards into Öxarfjörður.

Above the glacial units, between 140 and 350 m depth, fine consolidated mud and silt layers are present, thought to have been transported along the sea floor by turbidity currents and between 140 and 65 m depth, fine consolidated sandy layers containing some marine fossils are considered to have been deposited in deep water (Olafsson *et al.,* 1993). A shell fragment at 70-80 m depth was dated to 3000^{14}C yr BP (Georgsson *et al.,* 1998 Importantly for this study of the impact of extreme flood events, the upper 65 m of sediment are unconsolidated layers of coarse sand and conglomerates deposited by the outwash of the Jökulsá á Fjöllum river flowing into Öxarfjörður and building up a delta from the south through time.

At the head of the canyon, the Jökulsá á Fjöllum becomes deeply incised into the surrounding terrain (Fig. 2.1.14), with three large waterfalls over a 5 km long reach: Selfoss (13 m high), Dettifoss (54 m high; Fig. 2.1.15) and Hafragilsfoss (20 m high). Within this reach, the impact of extreme flood events on the bedrock landscape, and the dominant erosion mechanisms, are documented in Sub-Chapter 2.3, based on topographic analysis and surface exposure dating using cosmogenic ^{3}He. The geology of the area is

characterised by young (< 0.8 Ma) basalt lava flows stacked on top of each other, ranging in structure from regular near vertical columns with metre-scale joint spacing to blocky rubbly lavas with centimetre to decimetre scale jointing (Fig. 2.1.115).

Fig. 2.1.13: The upper reaches of the Jökulsárgljúfur canyon, NE Iceland, where the Jökulsá á Fjöllum becomes deeply incised into the surrounding terrain. The canyon is approximately 500 m wide and 100 m deep. The surrounding terrain is draped in glacial sediment, deposited in the last glacial period. The study of the impact of extreme flood events on the bedrock landscape, and the dominant erosion mechanisms, in this section of the Jökulsárgljúfur canyon are documented in Sub-Chapter 2.3.

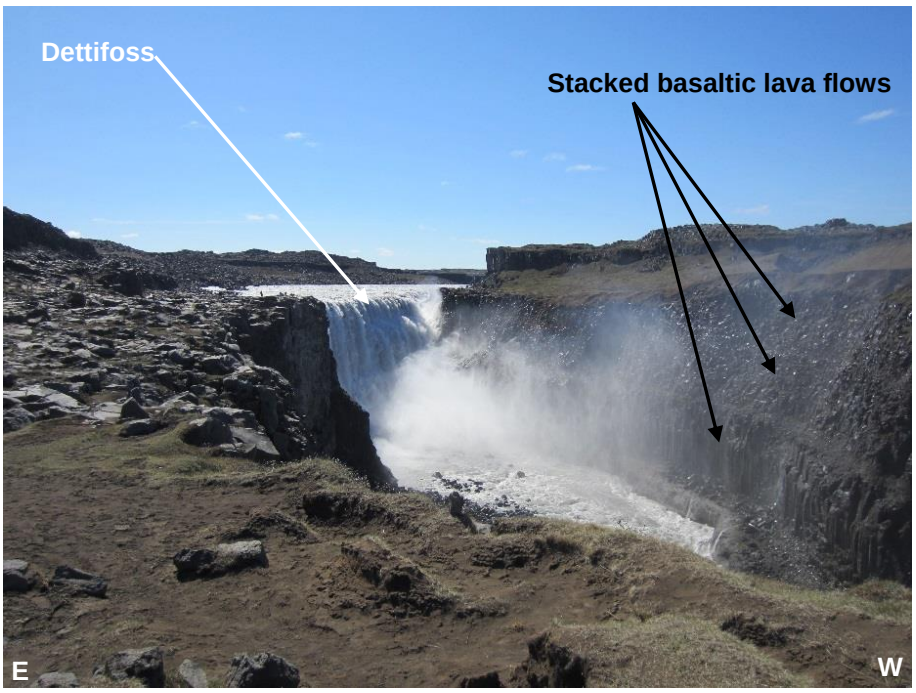

Fig. 2.1.15: Looking upstream towards Dettifoss (54 m high) at the head of the Jökulsárgljúfur canyon, NE Iceland. Clearly visible in the canyon walls downstream of Dettifoss are the basaltic lava flows stacked on top of each other, ranging in structure from regular near vertical columns with metre-scale joint spacing to blocky rubbly lavas with centimetre to decimetre scale jointing.

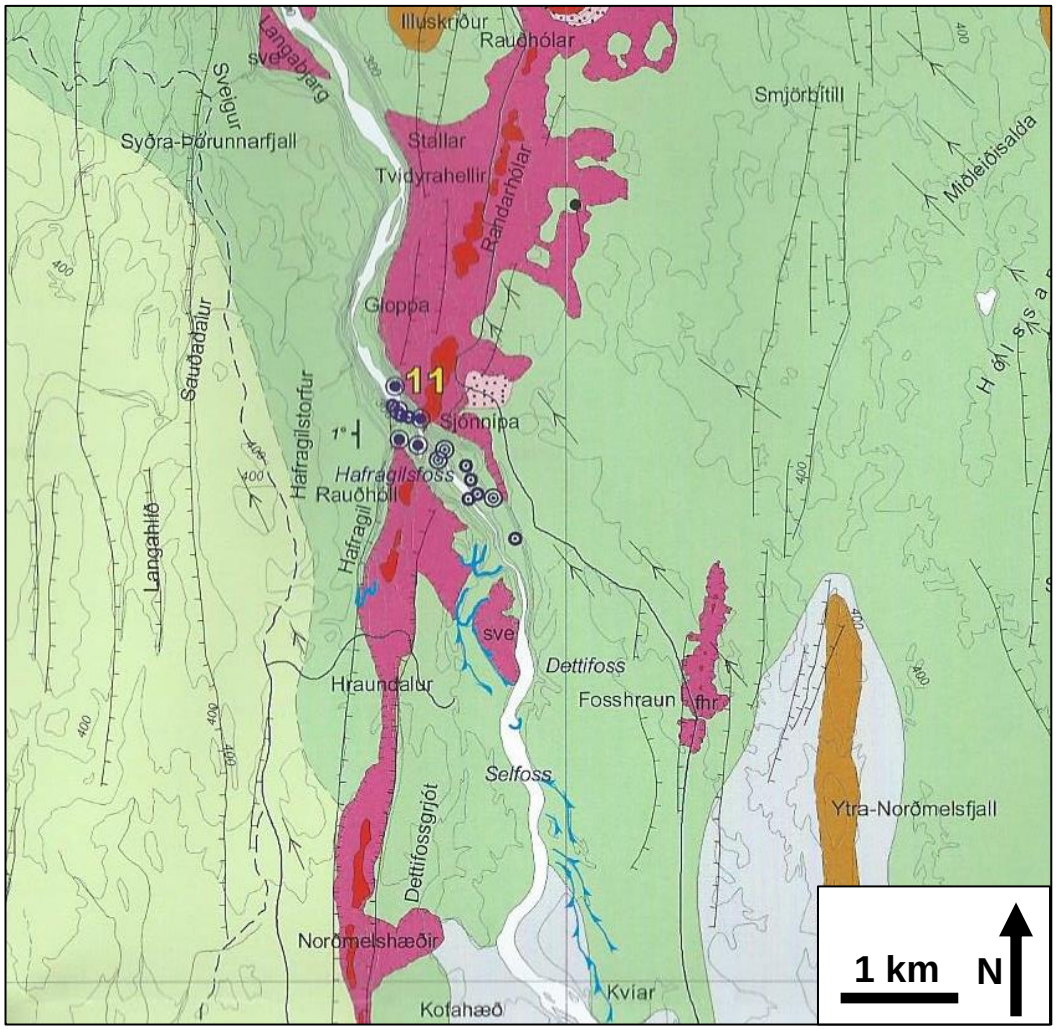

Fig. 2.1.16: Detailed geological map of the upper 5 km of the Jökulsárgljúfur canyon at Dettifoss. The key to the colours is provided in Fig. 2.1.17. Important features of note include the red areas that indicate the location of scoria cones from a fissure eruption, with the purple area indicating the extent of the lava flow corresponding to this eruption (> 6100 years old). The green shading indicates lava flows that erupted during the Quaternary (< 800k years old). Blue lines indicate dry erosion channels. The Jökulsárgljúfur canyon has eroded through the lava erupted from the fissure, giving an independent constraint on the timing of erosion within the canyon (*Source: scanned from: Saemundsson et al., 2012, scale bar and north arrow added).*

Fig. 2.1.17: Key for geological maps (Figs. 2.1.16, 2.1.18, 2.1.20), *scanned from: Saemundsson et al. (2012).*

Midway along the Jökulsárgljúfur canyon is the Forvoð valley (Fig. 2.1.11C; Fig. 2.1.18; 2.1.19), where widespread evidence for deposition of large

volumes of sediment during extreme floods is present (Eliasson, 1977); this evidence is documented in Sub-Chapter 2.4.

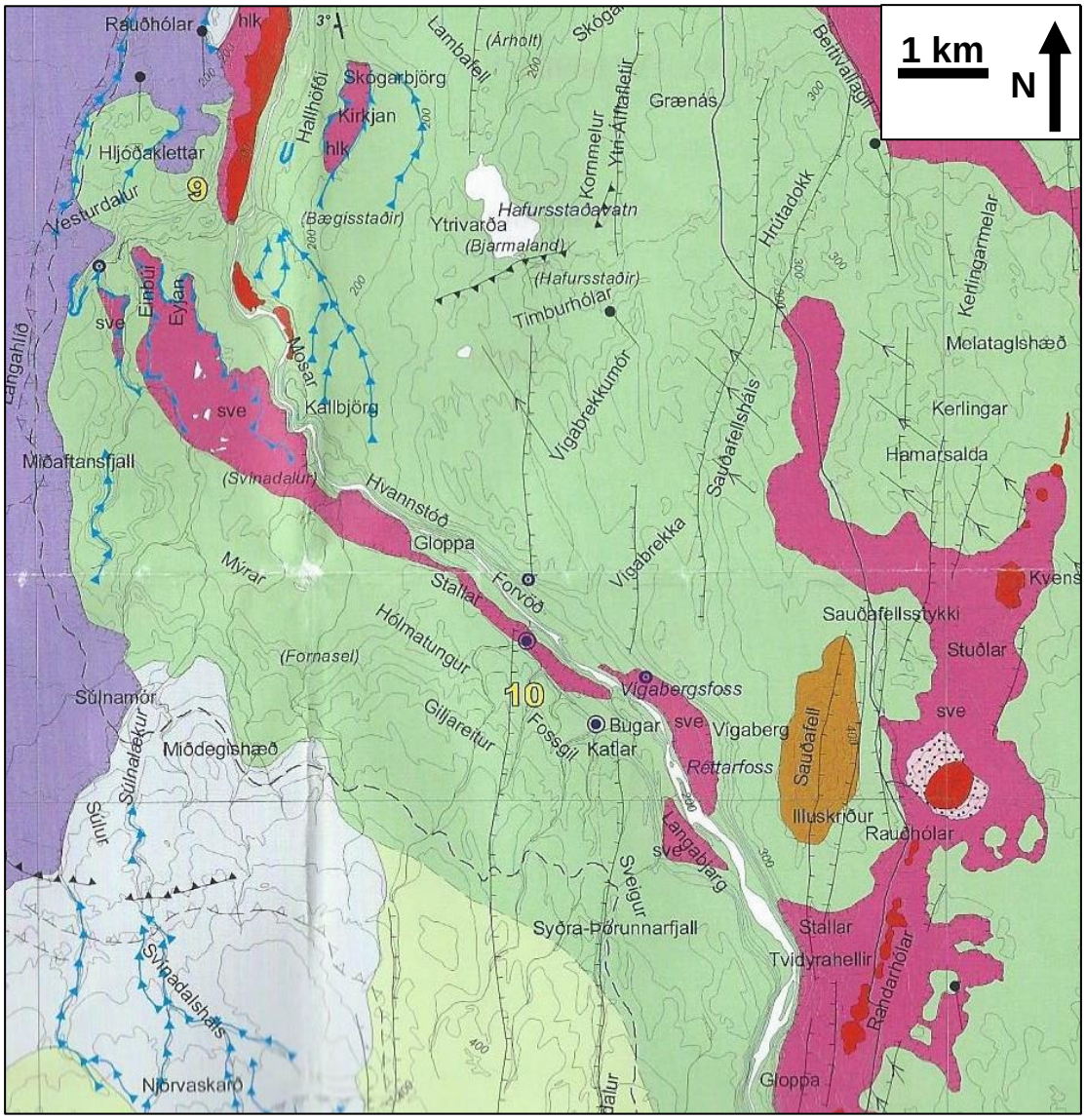

Fig. 2.1.18: Detailed geological map of the Forvoð valley in the middle reaches of the Jökulsárgljúfur canyon – there is some overlap between the areas shown in Fig. 2.1.16 and 2.1.20. The key to the colours is provided in Fig. 2.1.17. The dark purple shading in the west indicates an area of lava shield that is > 7000 years old, thought to have erupted from the Storaviti, one of the largest lava shields in Iceland. Blue lines indicate dry erosion channels. (*Source: scanned from: Saemundsson et al., 2012, scale bar and north arrow added).*

Fig. 2.1.19: Looking into the Forvoð valley, in the mid-reaches of the Jökulsárgljúfur canyon. The evidence for extreme flood events in this reach of the canyon are documented and mapped in Sub-Chapter 2.4

At the lower end of the Jökulsárgljúfur canyon is additional evidence for the erosive impact of extreme flood events, with the Klappir scablands area and Ásbyrgi canyon (Sæmundsson, 1973); the latter is a large dry cataract now disconnected from the current course of the Jökulsá á Fjöllum (Fig. 2.1.11C; Fig. 2.1.21).

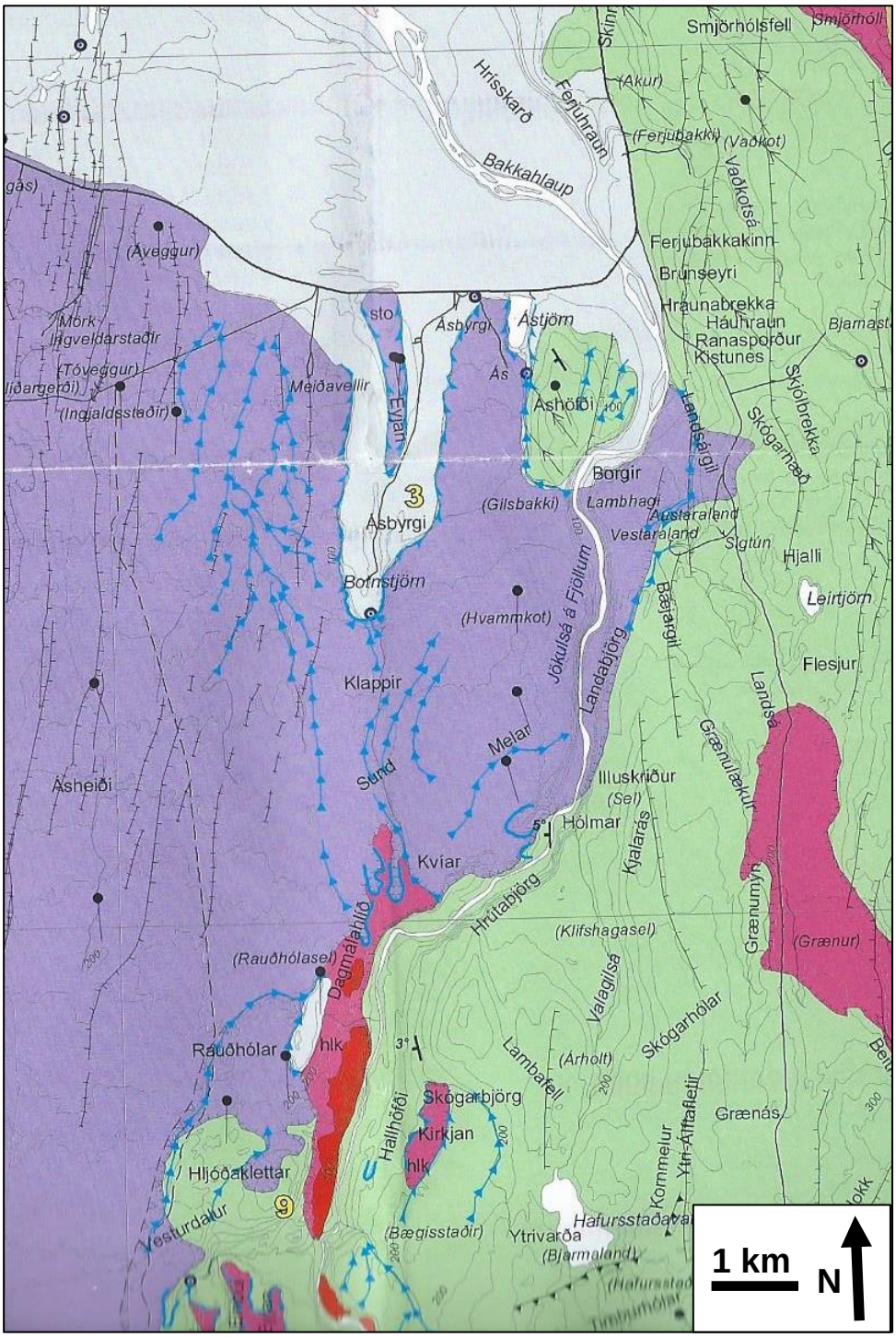

Fig. 2.1.20: Detailed geological map of the Ásbyrgi, Klappir and Vesturdalur area of the Jökulsárgljúfur canyon – there is some overlap between the area shown in Fig. 2.1.18. The key to the colours is provided in Fig. 2.1.17. The red area indicates the crater row that erupted at Hljodaklettar in the early Holocene and the light purple areas indicating the extent of recent lava flows (> 6100 years old) produced during this eruption. The dark purple shading, including Ásbyrgi canyon itself, indicates an area of lava shield that is > 7000 years

old, thought to have erupted from the Storaviti, one of the largest lava shields in Iceland. Blue lines indicate dry erosion channels. Within Ásbyrgi, and stretching across the sandur plain to the north are 'undefined surface deposits' of loose unconsolidated sedimentary material (*Source: scanned from: Saemundsson et al., 2012, scale bar and north arrow added).*

This area contains outstanding preservation of large-scale fluvial landforms which have not undergone any erosion since their formation and have remained clearly exposed at the surface without deep soils or vegetation. Therefore this area offers an excellent opportunity to quantify the impact of extreme floods. As a result, the analysis in this research was carried out using geomorphological mapping, surface exposure age dating, topographical analysis and geophysical surveys of deposited sediment (methods described in Sub-Chapter 2.2 and results presented in Sub-Chapters 2.3 and 2.4). The interpretation, within the context of previous work (e.g. Sæmundsson, 1973; Eliasson, 1977; Waitt, 2002), of how extreme flood events have affected the evolution of the Jökulsárgljúfur canyon, and how the quantitative study of this landscape has benefitted the understanding of the erosion processes during extreme events, is discussed in Sub-Chapter 2.5.

Fig. 2.1.21: Looking north into the 3 km long, up to 100 m deep, Ásbyrgi from the canyon rim. Sub- Chapter 2.4 documents and maps the evidence for extreme flood events in this landscape and also the impact of extreme floods is quantified through the calculation of the volume of rock eroded.

Sub-Chapter 2.2 Methods

In order to successfully quantify the impact and improve the understanding of the role of extreme flood events in the evolution of the Jökulsárgljúfur canyon a range of methods from across the fields of geomorphology, geochronology and geophysics were utilised, described in detail in this Sub-Chapter.

2.2.1 Assessment of evidence for extreme flood events in the landscape

Carrivick *et al.* (2004) created a list of key criteria to identify the occurrence of extreme floods in bedrock channels, from macro-scale landforms such as cataracts and anastomosing channels to microforms such as potholes and flutes (Table 2.2.1). It should be noted that many of the landforms listed in Table 2.2.1 are not exclusive to the action of extreme flood events, and the presence of these landforms within a landscape should not necessarily lead to the conclusion that an extreme flood event has taken place (Carrivick *et al.*, 2013). However, considering the landscape as a whole and the relationship between multiple landforms across a range of spatial scales can give an insight into the magnitude of the events that formed them (Carling *et al.*, 2009c). The criteria in Table 2.2.1 was used to document and map erosional and depositional landforms in the study landscape using field observations and aerial photography which allows the interpretation of the impact of extreme flood events that have occurred in the Jökulsárgljúfur canyon. Geomorphological maps of each of the main study areas, highlighting the key landforms and the interpretation of such landforms for the action of extreme floods, are presented in Section 2.4.1.3.

Table 2.2.1: Table of geomorphological evidence used for identifying the impact of extreme flood events in bedrock channels (adapted from Carrivick *et al*., 2004). Modifications include the addition of boulder terraces in 'macroscale landforms' and recent studies; e.g. Lamb *et al.* (2008b, 2014).

Scale	Geomorphological feature for distinguishing bedrock-channelled jökulhlaups	Selected references
Macroforms	- Anastomosing channel pattern of valley-wide palaeo-channels (or strath terraces) eroded into bedrock, indicating the location of palaeo-flows	Kehew and Lord, 1986; Rudoy, 2002; Waitt, 2002; Gupta *et al.*, 2007;
	- Deep trench-shaped valleys	Kehew and Lord, 1986; Lamb *et al.*, 2008b, 2014
	- Cataracts (abandoned amphitheatre-shaped dry waterfall eroded into bedrock, convex amphitheatre shape indicates palaeo-flow direction)	Baker, 1973; Kehew and Lord, 1986; Rudoy, 2002; Lamb *et al.*, 2008b, 2014;
	- Flow overspilling previous drainage divides (evidence for overflow of valley beyond present day valley configuration, such as eroded or scoured surfaces across ridgetops)	Shakesby, 1985; Kehew and Lord, 1986
	- Scoured surface (exhibiting evidence for fluvial flow that washes away/erodes material from the top of the bedrock surface)	Kehew and Lord, 1986; Lamb *et al.*, 2008b, 2014
	- Boulder terraces (depositional terraces made up of large boulders that extend over large spatial scales: > 500 m in length, > 10 m in height)	Baker, 1973; O'Connor, 1993
Mesoforms	- Streamlined residuals of sediment (streamlined landforms that are oriented longitudinally in the direction of the palaeo-flow)	Baker, 1988, Komar, 1984; Wiedmer *et al*., 2010
	- Obstacle and ice block marks	Baker, 1973; Fay, 2002
	- Wash limits (evidence for the	Maizels, 1995

		maximum elevation of palaeo-flow stages, such as upper limit of scoured valley sides or surfaces)	
	-	Boulder surfaces and boulder bars	Baker, 1973; O'Connor, 1993
	-	Dunes (depositional sedimentary features in the shape of a mound or a ridge, oriented longitudinally in the direction of the palaeo-flow)	Baker, 1973; Maizels, 1995; Carling, 1996; Wiedmer *et al.*, 2010
	-	Bars (elevated region of deposited sediment, gravel or boulder, that has been deposited by the flow)	Carling *et al*., 2002
	-	Slackwater deposits (layered sedimentary deposits formed by stationary water where the flow is unstressed, can be used to identify number of inundation events, and the elevation of inundation)	Baker, 1973; Baker and Bunker, 1985
Microforms	-	Potholes, flutes, furrows, obstacle marks, and grooves (small-scale erosional features in bedrock surfaces; typically smoothed by abrasion due to the impact of transport sediment)	Hancock *et al*., 1998; Whipple *et al.*, 2000; Richardson and Carling, 2005; Wilson and Lavé, 2014

2.2.2 Field measurements to reconstruct flow conditions during extreme floods

2.2.2.1 Boulder surveys

Many studies (e.g. Costa, 1983; Clarke, 1996; Lamb *et al.,* 2008b; Stokes *et al.*, 2012) use the size of boulders that have been transported by a flood to reconstruct the discharge of the flood event. Boulder size can be used to estimate the flow discharge required to transport the boulders; giving a minimum bound of the magnitude of the palaeo-flood that transported them.

Caution should be employed when using such a method as different equations can give different estimates of flood discharge and there are issues with both the collection of the boulder size data and the interpretation of the resulting estimates (see discussion in Stokes *et al.*, 2012). Within these caveats, the method of Clarke (1996; equations 2.2.1 – 2.2.11), described by Stokes *et al.* (2012), was used to calculate a rough estimate of the minimum flood discharge that would be required to transport the largest boulders in the two canyons of Ásbyrgi (Fig. 2.2.1; 2.2.2). The width of each corresponding canyon was used with the flow width and the bed slope extracted from a high resolution (1 m) digital elevation model. A full sensitivity analysis of the discharge estimate depending on variability of the input parameters is provided in Appendix B. The technique described below is covered in detail in Stokes *et al.* (2012).

Fig. 2.2.1: Looking south into the western canyon of Ásbyrgi, with the deposited boulder field in the foreground.

Fig. 2.2.2: An example of a boulder deposited in the eastern canyon of Ásbyrgi. The three axes of the boulders were measured using a tape measure for 27 boulders in the western canyon and 55 boulders in the eastern canyon.

The boulder axes measured in the field (*A, B, C*) is used to determine the nominal diameter (in metres) of the boulder (*D*):

$$D = (ABC)^{\frac{1}{3}} \qquad \text{Eqn. 2.2.1}$$

The nominal diameter of the boulder is then used to calculate the mass (in kg) of a cubic boulder and a spherical boulder of this size (M_{Bc} *and* M_{Bs} respectively):

$$M_{Bc} = \sigma D^3 \qquad \text{Eqn. 2.2.2a}$$

$$M_{Bs} = \sigma\left(\left(\frac{\pi}{6}\right)D^3\right) \qquad \text{Eqn. 2.2.2b}$$

where σ is the density of the boulder (in kg m^{-3}). The mass of the boulder is used to calculate the 'resisting force' (F_R, in Newtons) of the both a cubic boulder (F_{Rc}) and a spherical boulder (F_{Rs}):

$$F_{Rc} = M_{Bc}\left(\frac{(\sigma-\rho)}{\sigma}\right) g\left(\left((cos\beta)\mu_c\right) - (sin\beta)\right) \quad \text{Eqn. 2.2.3a}$$

$$F_{Rs} = M_{Bs}\left(\frac{(\sigma-\rho)}{\sigma}\right) g\left(\left((cos\beta)\mu_s\right) - (sin\beta)\right) \quad \text{Eqn. 2.2.3b}$$

where ρ is the fluid density (in kg m^{-3}), g is the acceleration due to gravity (9.81 m s^{-2}), β is the bed slope angle (in radians) measured in the field, μ_c is the coefficient of sliding for a cubic boulder and μ_s is the coefficient of sliding for a spherical boulder. For calculating the discharge at the onset of boulder movement, the drag force (F_D, in Newtons) of both a cubic boulder (F_{Dc}) and a spherical boulder (F_{Ds}) is calculated after setting F_R to equal F_C:

$$F_{Dc} = \frac{(C_{Dc}F_{Cc})}{(C_{Lc}+ C_{Dc})} \quad \text{Eqn. 2.2.4a}$$

$$F_{Ds} = \frac{(C_{Ds}F_{Cs})}{(C_{Ls}+ C_{Ds})} \quad \text{Eqn. 2.2.4b}$$

where C_{Dc} is the drag coefficient for a cubic boulder, C_{Ds} is the drag coefficient for a spherical boulder, C_{Lc} is the lift coefficient of a cubic boulder and $C_{Ls}$is the lift coefficient of a spherical boulder. The critical velocity (V_c in m s^{-1}) is equivalent to the competent bottom velocity at the height of about 1/3 of a particle diameter above the bed at the condition of incipient motion and is calculated using the following set of equations:

$$A_{Bc} = D^2 \quad \text{Eqn. 2.2.5a}$$

$$A_{Bs} = \pi\frac{D^2}{2} \quad \text{Eqn. 2.2.5b}$$

$$V_{Cc} = \left(\frac{2\left(\frac{\left(\frac{F_{Dc}}{C_{Dc}}\right)}{\rho}\right)}{A_{Bc}}\right)^{\frac{1}{2}} \quad \text{Eqn. 2.2.6a}$$

$$V_{Cs} = \left(\frac{2\left(\frac{\left(\frac{F_{Ds}}{C_{Ds}}\right)}{\rho}\right)}{A_{Bs}} \right)^{\frac{1}{2}}$$ Eqn. 2.2.6b

where A_{Bc} is the cross-sectional area of a cubic boulder and A_{Bs} is the cross-sectional area of a spherical boulder. The critical velocity of a cubic boulder and the critical velocity of a spherical boulder are then averaged to give a critical velocity used in subsequent calculations:

$$V_C = \frac{V_{Cs} + V_{Cc}}{2}$$ Eqn. 2.2.7

From the critical velocity, it is possible to calculate the average velocity of the flow (V_{avg} in m s^{-1}):

$$V_{avg} = 1.2\, V_C$$ Eqn. 2.2.8

Using Manning's roughness coefficient '*n*', the mean flow depth *d* (m) is calculated:

$$n = 0.295\, tan\beta^{0.377}$$ Eqn. 2.2.9

$$d = \left(\left(\frac{V_{avg} n}{tan\beta^{\frac{1}{2}}} \right)^{\frac{1}{2}} \right)^{3}$$ Eqn. 2.2.10

Discharge (Q, in m^3 s^{-1}) can then be calculated using the channel width (w, in metres) measured in the field:

$$Q = w\, d\, V_{avg}$$ Eqn. 2.2.11

2.2.2.2 Bedrock structure joint spacing measurements

The Lamb and Dietrich (2009) model for block toppling at knickpoints was discussed in the introduction (Section 1.2.2.3). A key input parameter for calculating the threshold flow depth required for knickpoint retreat through block toppling is the joint spacing of the columnar basalt. In order to use the Lamb and Dietrich (2009) model, the joint spacing of the columnar basalt was measured in the field using a tape measure. A limitation of the Lamb and Dietrich (2009) model is that the calculations are made assuming each column is free-standing and of equal size; however, there is some variability in the joint spacing of the columns within the Jökulsárgljúfur canyon (Fig. 2.2.3). Therefore, multiple measurements were made of the bedrock joint spacing and the average value was used in the calculations; a sensitivity analysis of the threshold flow depth depending on different values of joint spacing, as well as column tilt angle and channel slope was performed (see Appendix A), showing that threshold flow depth is very sensitive to column width while variations in tilt angle and channel slope have less of an impact.

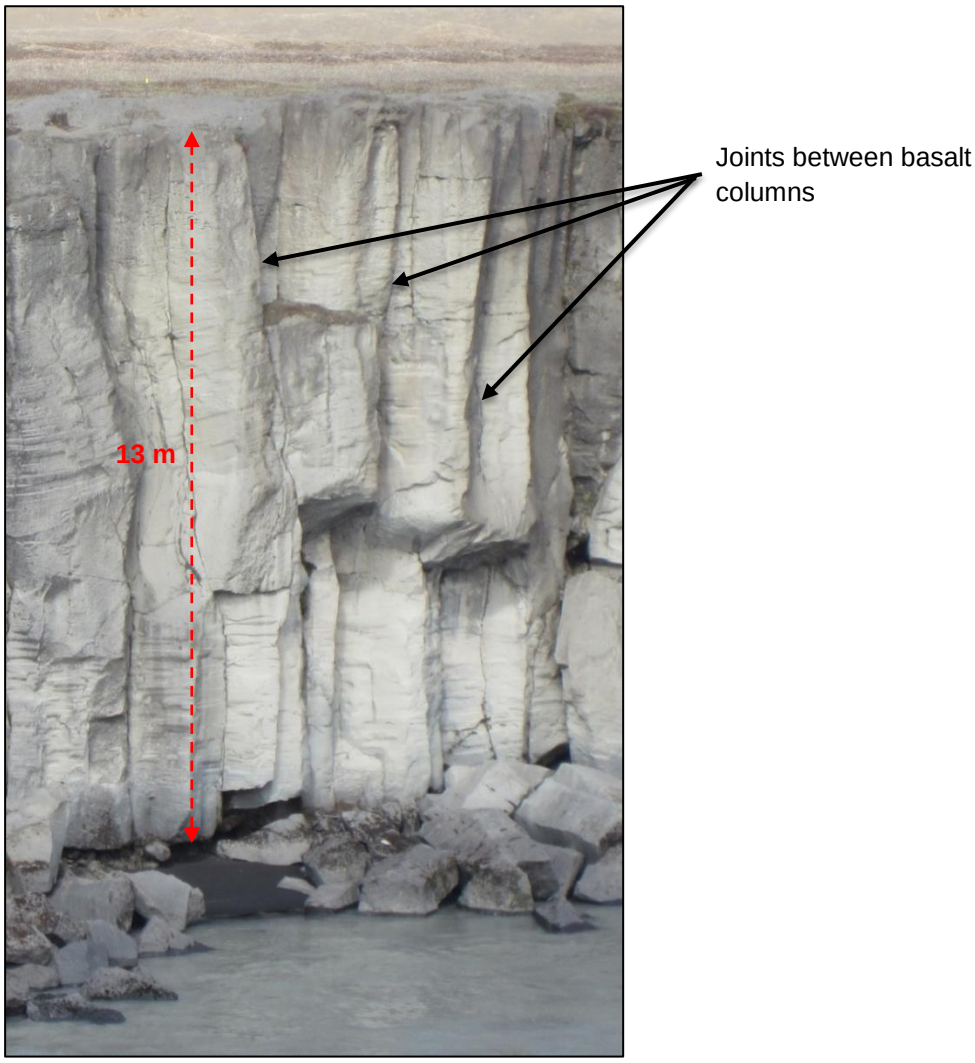

Fig. 2.2.3: The columnar basalt unit associated with Selfoss waterfall (see Appendix A for calculations using Lamb and Dietrich, 2009).

2.2.3 Topographic analysis

A requirement for a detailed assessment of the impact of extreme flood events on the landscape is an accurate quantification of landscape change during such events (e.g. Dunning *et al.*, 2013). Here, we used a range of techniques from topographic surveying (Section 2.2.3.1) and DEM analysis (Section 2.2.3.2) to geophysical surveys of deposited sediment (Section 2.2.4) to explore the impact of extreme flood events in the evolution of the Jökulsárgljúfur canyon.

2.2.3.1 Topographic surveying

High resolution (sub-centimetre) topographic surveys of the landscape morphology were carried out using a Total Station (Fig 2.2.4). Near the Jökulsárgljúfur canyon apex at Dettifoss, two Total Station surveys were carried out from the western canyon wall of features such as strath terrace (palaeo river bed locations) heights and the outline of the cataracts within the overspill channel. At Ásbyrgi, Total Station surveys were carried out to characterise the morphology of the canyon rim and canyon floor of Ásbyrgi.

Fig. 2.2.4: Total Station survey location above Hafragilsfoss waterfall on the western wall of the Jökulsárgljúfur canyon. The Total Station surveys were carried out to provide highly accurate estimates of the heights and locations of strath terrace surfaces within the canyon. Photo taken looking east; for scale, Hafragilsfoss is 25 m in height.

In some locations, it was not practical to use a Total Station due to the distance covered and the line-of-sight requirement from the Total Station location to the survey point. An alternative method was employed in these situations using a Laser Range Finder, which provides the horizontal and

vertical distance to the target location at 0.1 m accuracy. While not as accurate as a Total Station, the Laser Range Finder technique allows reconstruction of the gorge morphology over distances > 2 km in a short period of time.

2.2.3.2 Digital Elevation Model analysis

At Ásbyrgi, the volume of the canyon was quantified using a high resolution (1 m) Digital Elevation Model (DEM) (*Source: TanDEM-X collected on 02/09/2012*). DEMs are used regularly to accurately calculate the volume of erosion through comparison of surfaces pre-erosion and surfaces post-erosion (e.g. Ferrier *et al.*, 2013). This technique was used to evaluate the volume of material eroded from Ásbyrgi since formation, by creating a 'pre-erosion' surface through the interpolation of elevation values from around the outer rim of the canyon and the Island. This surface was then subtracted from the 'present day' DEM using the 'Raster Calculator' tool in ArcGIS (Fig. 2.2.5).

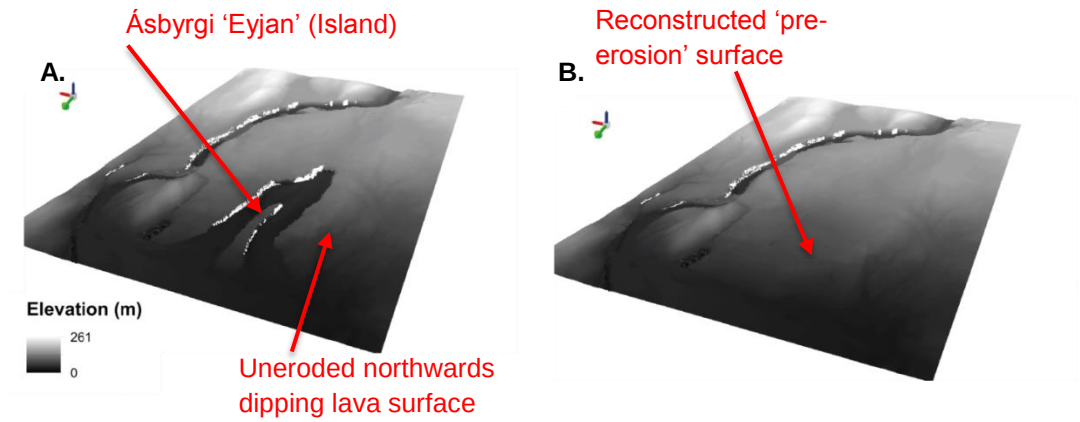

Fig. 2.2.5: Oblique view, looking southeast, of the Digital Elevation Model at Ásbyrgi with **(A)** showing the 'present-day' post erosion surface, with the horseshoe shaped canyon clearly visible and **(B)** showing the 'pre-erosion' surface, interpolated from elevation data from the outer rim and the top of the Island. The difference between the two surfaces allows an estimate of the volume of rock eroded from Ásbyrgi since formation.

2.2.4 Geophysical survey of deposited sediments

While the DEM analysis in section 2.2.3.2 allows an accurate quantification of the volume of material eroded through analysis of the modern day canyon and a pre-flood surface at Ásbyrgi, this assumes that the modern day canyon surface represents the configuration of the canyon at the end of the bedrock erosion during the flood event. This is not a valid assumption for Ásbyrgi as sediment has been deposited across the canyon floor. Therefore, in order to accurately assess the volume of bedrock eroded from Ásbyrgi, an assessment of the sediment depth is required. This was carried out using a near-surface geophysical technique; Electrical Resistivity Tomography (ERT). ERT surveys are non-destructive and provide great spatial coverage when multiple profiles are collected. ERT is an established method for imaging the near subsurface and has been used for a wide-range of applications, including detecting the bedrock-sediment interface (Hsu *et al.*, 2010; Chambers *et al.,* 2012), aquifer characterisation (Doetsch *et al.*, 2012), detection of subsurface cavities (Martinez-Lopez *et al.*, 2013), rockwall retreat rates (Siewert *et al.*, 2012) and permafrost depth and structure (You *et al*., 2013).

2.2.4.1 Electrical Resistivity Tomography data collection

The ERT surveys were carried out using a Wenner array (Fig. 2.2.6A) across transects A-L shown in Fig. 2.2.7, with 25 electrodes at 5 m spacing (Fig. 2.2.6B), allowing measurements using electrode spacings ranging from 5 to 40 m. By increasing the spacing between the electrodes, the current penetrates deeper, building up a data section that can be interpreted in terms of lateral and depth variations in electrical resistivity. Some of the transects were built up from multiple surveys in order to cover a longer distance than the 120 m possible in a single 25 electrode survey, such as the long transect along the middle of the eastern canyon (Transect G, 680 m long; Fig 2.2.7).

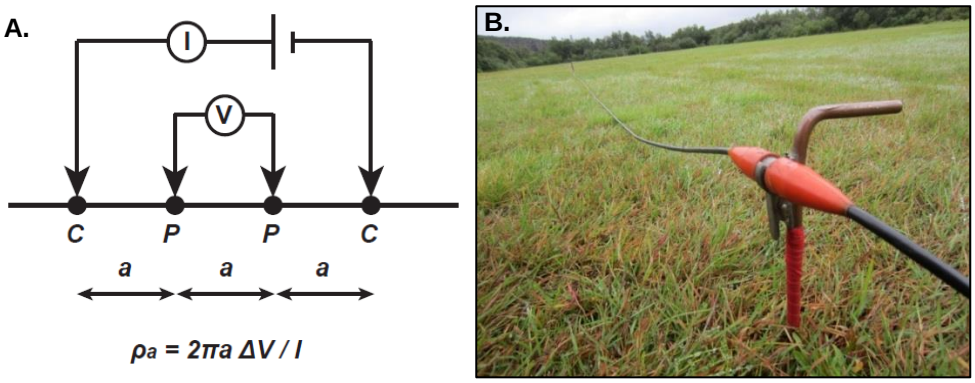

Fig.: 2.2.6A: Diagrammatic representation of the Wenner electrode array used in the ERT surveys. During a measurement, current is sent through the two current electrodes (*C*) and then measured at the two potential electrodes (*P*), at equal electrode spacing (*a*). The apparent resistivity (ρ_a) for each measurement is determined using the equation shown. **B.** One of the electrodes placed into the ground during a survey within Ásbyrgi.

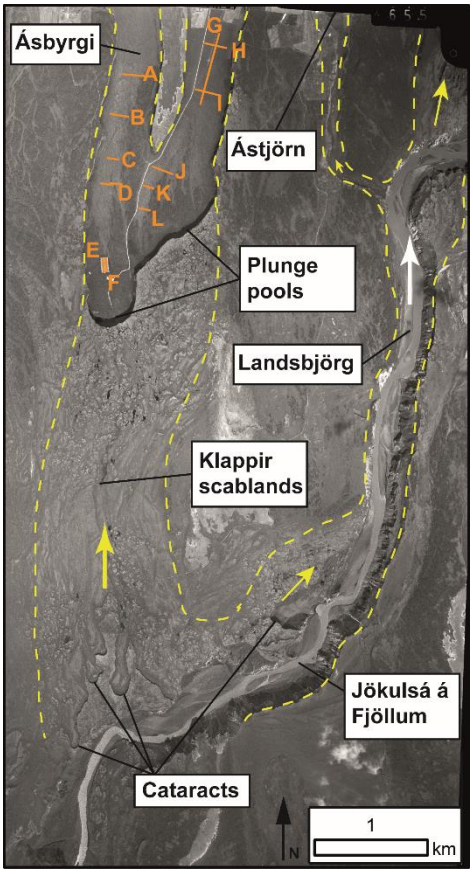

Fig. 2.2.7: Aerial photograph of the Klappir scablands and Ásbyrgi canyon. The present day course of the Jökulsá á Fjöllum is within the deeply incised main Jökulsárgljúfur canyon which flows to the east at Landsbjörg. Ásbyrgi is a large (3 km long, 1 km wide) horseshoe

shaped canyon cut into a northwards dipping lava succession with an island preserved between the two main channels. The yellow dashed lines indicate the areas which have been inundated by floodwaters, with the Klappir area of scabland topography with bedrock ridges and pools clearly visible. At the upstream limit of the scablands, there are four dry cataracts providing additional evidence for erosion during an extreme flood event in this area. The location of the plunge pools at the apex of the western and eastern Ásbyrgi canyons are shown. The orange lines within Ásbyrgi indicate the location of the Electrical Resistivity Tomography (ERT) surveys in the canyon floor. Aerial photograph source: Landmælingar Íslands.

2.2.4.2 Electrical Resistivity Tomography data processing

Different inversion methods are available in the 'res2Dinv' software (res2Dinv version 3.4; Geotomo, 2001) used to process the ERT data. The conventional least squares method minimises the square of the difference between the measured and the calculated apparent resistivity values and produces a model with smooth resistivity variations (Loke *et al.*, 2003). However, the technique is not perfectly appropriate when the subsurface contains sharp boundaries between resistivity interfaces as the smoothing of the boundaries between layers makes their localisation difficult. We therefore employed a 'robust iterative inversion' to model our survey data, whereby the absolute changes in the resistivity values are minimised (Claerbout and Muir, 1973). This approach produces models of the subsurface with sharp interfaces between different subsurface structures which have different resistivity values (Loke *et al.,* 2003), and was deemed most appropriate because we expect to see a sharp boundary between the sediment deposits and the basalt bedrock beneath. The model iterations were stopped when the percentage misfit between the measured and the calculated apparent resistivity was less than 5% or no further improvement to the fit was possible with further iterations. In the case of Transect E, there was no further improvement to the fit after five iterations, when RMS error was 5.9%.

Broadly, sedimentary deposits have the lowest resistivity and igneous rocks the highest (Telford *et al.*, 1990). We therefore expect the bedrock-sediment interface in each of our profiles to be shown by a sharp horizontal downward

transition from regions of low to high resistivities. The typical range of resistivity for basalt is large: 10^1 – 1.3 x 10^7 Ωm (Telford *et al.*, 1990) due to a number of factors including the water content in fractures and pore space. The resistivity of dry (0% water content) basalt is 1.3 x 10^7 Ωm whereas basalt with 0.95% water content typically has a much lower resistivity of 4 x 10^4 Ωm (Telford *et al.*, 1990). The results from the ERT surveys are presented in Section 2.4.1.4).

2.2.5 Historical aerial photography

In heavily jointed basaltic bedrock, significant erosion and canyon formation can occur through the upstream migration of knickpoints due to the toppling and transportation of lava columns once a threshold flow depth is exceeded (Lamb and Dietrich, 2009; Lamb *et al.*, 2014). Understanding of the background retreat rate of the knickpoints within the Jökulsárgljúfur canyon is therefore important when attempting to interpret the relative impact of extreme flood events in landscape evolution through time. This was carried out through the comparison of georeferenced historical aerial photos of Dettifoss in 1955 and 1998. The position of Dettifoss in each year was digitised in ArcGIS and the distance between these positions, divided by the time between the images (43 years) provides the longer term background knickpoint retreat rate. Ideally, the 'background' retreat rate would be measured over a longer time period, but the earliest historical aerial photographs suitable for analysis were obtained in 1955.

2.2.6 Surface exposure dating using cosmic ray produced ^{3}He

2.2.6.1 Introduction and applications

Surface exposure dating using cosmogenic nuclides is a geochronological technique that has become widely used recently in geomorphology as it is a quantitative technique that assesses the time that rocks have been exposed

on the Earth's surface (Gosse and Phillips, 2001; Niedermann, 2002). Surface exposure dating has been used in fluvial geomorphology since the late 1990's with some studies using the exposure ages of abandoned bedrock strath terraces to calculate fluvial incision rates. Examples of such studies include the Indus River in the Himalayas (Burbank *et al.,* 1996), the Braldu River in the Karakorum (Seong *et al.,* 2008), the New River in Virginia (Ward *et al.,* 2005) and the Fremont River in Utah (Repka *et al.*, 1997), while Lavé and Avouac (2000) used exposure ages of terraces to infer rock uplift rates across the Main Frontal Thrust of the Himalayas. Lamb *et al.* (2008b) used exposure ages of boulders within Box Canyon as well as the exposure age of scoured rock at the rim of the canyon to infer that the canyon had been formed during an extreme flood event rather than the original hypothesis of formation through seepage erosion. Other studies have used surface exposure dating to determine the processes and rates of knickpoint retreat (e.g. in western Scotland; Jansen *et al.*, 2011 and on the volcanic island of Kaua`i, Hawai`i; Mackey *et al.*, 2014). In this study, surface exposure ages of fluvial surfaces are also used to determine the processes and rates of knickpoint retreat, as well as the number and timing of extreme flood events.

Large canyons can be formed during extreme flood events through the toppling and removal of blocks in heavily jointed basaltic bedrock (Lamb *et al.*, 2008b; 2014), once a threshold flow depth has been exceeded (Lamb and Dietrich, 2009). Bedrock erosion during extreme floods in such settings is therefore dominated by plucking rather than abrasion, resulting in the formation and upstream propagation of large vertical knickpoints (e.g. Box Canyon and Stubby Canyon, Idaho; Lamb *et al.*, 2008b; 2014). As the knickpoints propagate upstream, rock is removed typically over the thickness of one or more lava flows (> 10 m), exposing pristine fluvially eroded bedrock surfaces to cosmic rays and initiating the accumulation of cosmogenic nuclides. We therefore assume that the age derived from the cosmogenic nuclide concentrations reflects the age of formation of a given fluvially eroded bedrock surface and the distribution of samples within a landscape can be

used to infer how it has evolved through time (Fig. 2.2.8), assuming no further erosion of the surface. The surface exposure ages therefore represent a minima, as erosion after exposure would reduce the concentration of cosmogenic nuclides and the true exposure age would actually be greater than calculated. If a knickpoint is retreating steadily through time, as would be expected if associated with a normal flow regime, the exposure age of samples from fluvial bedrock surfaces would become progressively younger with decreasing distance from the modern knickpoint location (Seidl *et al.*, 1997; Jansen *et al.*, 2011; Mackey *et al.*, 2014). If, on the other hand, a knickpoint retreated a large distance in a short period of time, such as during an extreme flood event, the exposure ages would be expected to cluster around the time of that significant erosion event (Lamb *et al.*, 2014). Recognition of the canyon morphology and the measurement of precise exposure ages are therefore key to distinguishing between models of canyon formation.

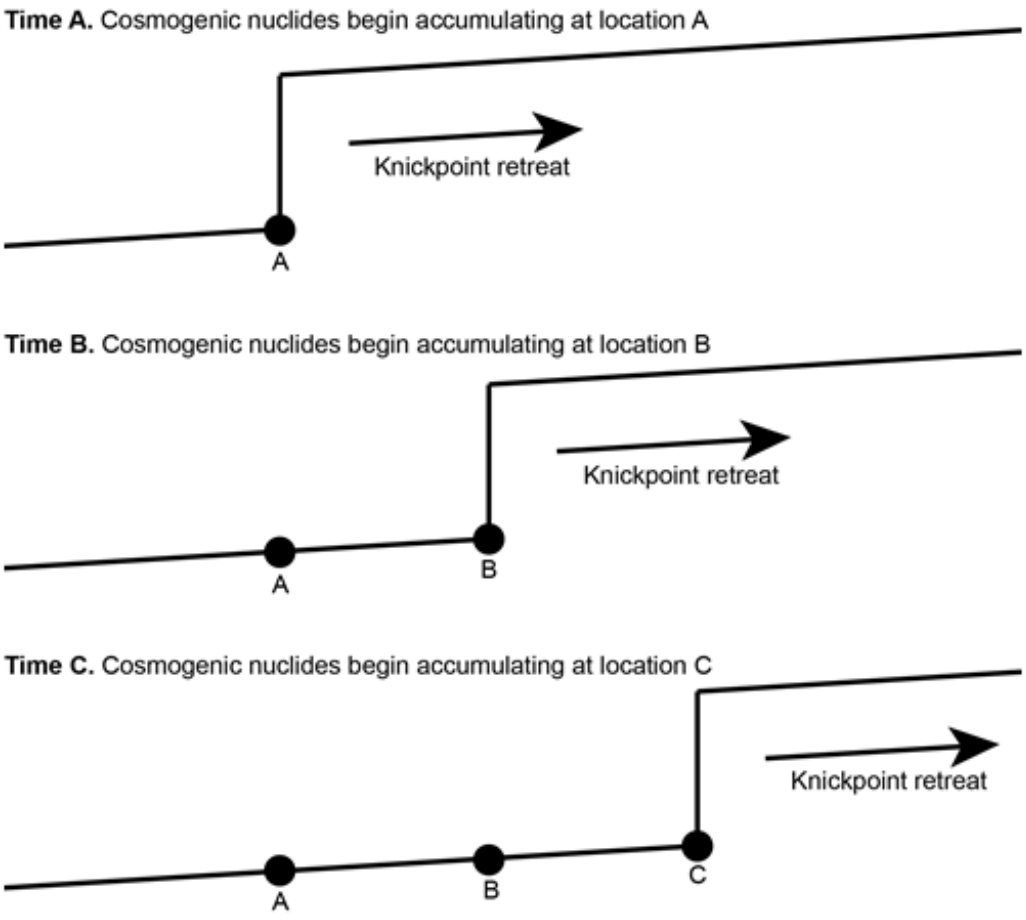

1. If the knickpoint is retreating progressively through time:

   Exposure Age A > Exposure Age B > Exposure Age C

2. If the knickpoint retreats suddenly:

   Exposure Age A = Exposure Age B = Exposure Age C

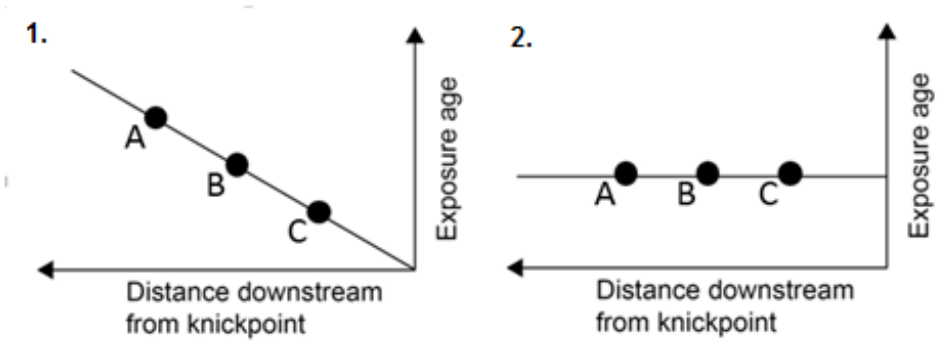

Fig. 2.2.8: Conceptual model of how surface exposure ages can be used to distinguish between models of progressive (scenario 1) or sudden (scenario 2) knickpoint retreat.

2.2.6.2 Theory

The technique is based on the fact that the Earth's atmosphere is constantly bombarded by cosmic rays with very high energies (up to ~10^{20} eV) made up mostly of protons and α particles (Lal, 1988; Gosse and Phillips, 2001; Dunai, 2010; Niedermann, 2002). As these particles move through the atmosphere, a secondary cascade of particles is produced which has a higher proportion of neutrons. When these particles reach the Earth's surface they can produce cosmogenic isotopes such as ^{3}He and ^{21}Ne through spallation (Gosse and Phillips, 2001), whereby a lighter nucleus is produced due to the loss of a few protons or neutrons following the reaction of a nucleus with a high-energy, fast-moving particle (see Niedermann, 2002, for compilation of the different chemical reactions between cosmic rays and target elements that produce a host of different cosmogenic nuclides). These reactions are mineral dependent so in basaltic environments, such as Iceland, these reactions occur in olivine and pyroxene minerals. He and Ne are stable and, unlike cosmogenic radionuclides such as ^{10}Be, do not decay once they are produced, allowing the easier calculation of the surface exposure age as corrections regarding the half-life do not need to be taken into account.

Helium present in minerals located on the Earth's surface can be sourced from three different origins: (i) reactions with cosmic rays, producing cosmogenic ^{3}He (hereafter referred to as $^{3}He_c$) in the fluid inclusions of the minerals (ii) ^{4}He produced through radioactive decay of uranium, thorium and lithium (e.g. alpha particles, hereafter referred to as $^{4}He_r$) or (iii) magmatic ^{3}He and ^{4}He present in the crystal lattice and fluid inclusions of the minerals since the rocks were initially erupted onto the Earth's surface (hereafter referred to as He_m). These different helium components occupy different sites within the mineral structure and can be released by different extraction methods. ^{3}He held within the melt inclusions of the minerals (magmatic in origin) is released during the crushing experiments and ^{3}He held within the crystal lattice (magmatic and cosmogenic in origin) is released during the

melt extraction experiments (see Section 2.2.6.3 below for details of procedures).

Determining the exposure age of rocks requires the measurement of the concentration of ^{3}He held in both the crystal lattice and the melt inclusions, the production rates of $^{3}He_c$ and $^{4}He_r$ and the time since the rocks were erupted (i.e. the time since $^{4}He_r$ started accumulating). Where the eruption age of the rocks in not known, the exposure age can be calculated using two end member scenarios: (i) assuming all ^{4}He present in the mineral is radiogenic in origin and (ii) assuming that none of the ^{4}He present in the mineral is radiogenic in origin. Assuming no radiogenic ^{4}He is present, the lower limit on the surface exposure age range is calculated by subtracting the $(^{3}He/^{4}He)_{Crushed}$ ratio from the $(^{3}He/^{4}He)_{Melt}$ ratio in order to determine the $(^{3}He_{Cosmogenic}/^{4}He)$ ratio (e.g. Niedermann, 2002). Assuming all the ^{4}He is radiogenic in origin, the upper limit on the surface exposure age range is calculated assuming all of the ^{3}He in the melt measurement is cosmogenic in origin. Once the concentration of $^{3}He_c$ has been determined, the exposure age is calculated by dividing the $^{3}He_c$ concentration by the local cosmogenic production rate (See Sub-Chapter 2.3 and Appendix A for full details of the isotope concentrations and exposure age calculations in this study).

The production of cosmogenic isotopes is a slow process with the limited penetration of cosmic rays into the rock. The penetration depth follows an exponential decay curve within the very top of the Earth's surface (Niedermann, 2002; Licciardi *et al.,* 2006) and the rate of production of cosmogenic isotopes is varied across the Earth, with the highest production rates at high elevations and high latitudes, because all of the energy spectrum enters the atmosphere parallel to the geomagnetic field lines at the poles, rather than at an angle at lower latitudes (Niedermann, 2002). Different scaling methods exist for the calculation of the local production rate for any location on the Earth's surface (Fig. 2.2.9), with the different models (e.g., Lal, 1991; Dunai, 2000) providing slightly different estimates of local production rate with the greatest differences occurring at low latitude high

altitude locations. The scaling method of Dunai (2000) is adopted in this study, which is based on using variations in the geomagnetic field inclination across the Earth's surface. The magnitude of the production rate at the Earth's surface is estimated at calibration sites (e.g. Tabernacle Hill, Utah, USA; Goehring *et al.*, 2010) where the age since exposure to cosmic rays is accurately known through other techniques such as radiocarbon ages. These rates are then scaled to a reference production rate for high latitude locations at sea level (SLHL) using a scaling method discussed previously (e.g. Dunai, 2000). The scaling method is then used to scale the reference SLHL production rates to calculate the local production rate at the sample locations based the latitude and altitude of the sample

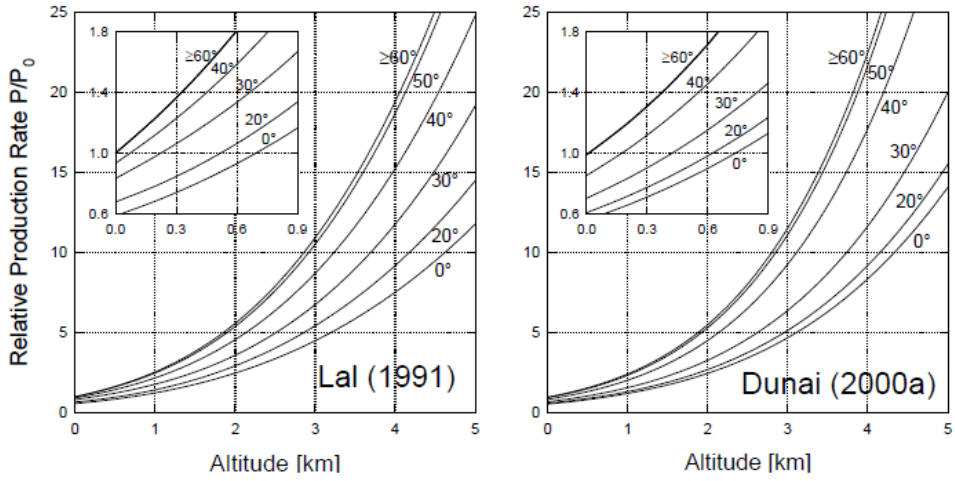

Fig. 2.2.9: The cosmogenic production rates at varying altitude and latitude derived from the Lal (1991) and Dunai (2000) scaling methods. At any given location on the Earth's surface, these curves can be used to calculate the *in situ* production rate of cosmogenic nuclides which can then be used to calculate the time since the rock has been exposed on the Earth's surface. The greatest differences between scaling models exist in low latitude, high altitude locations while there is little difference in high latitude areas such as Iceland. *From Niedermann (2002).*

The dip of the surface can influence the production rate of cosmogenic nuclides as if it is inclined, part of the cosmic ray flux will be blocked resulting in a lower production rate (Fig. 2.2.10A; Gosse and Phillips, 2001; Niedermann, 2002). In order to mitigate this effect, samples were selected

such that they were as horizontal as possible, and the dip of the surface was measured using a clinometer so that a correction could be applied where appropriate. Similarly, the production rate of cosmogenic nuclides can be reduced if large obstacles are located on the horizon, such as large mountains or valley walls which 'shield' the sampled surface from cosmic rays (Fig. 2.2.10B; Gosse and Phillips, 2001; Niedermann, 2002). The distance and angle of large obstacles on the horizon was measured for each sample so a correction factor could be applied if required (see Appendix A for details of surface dip and topographic shielding measurements for the samples).

A.

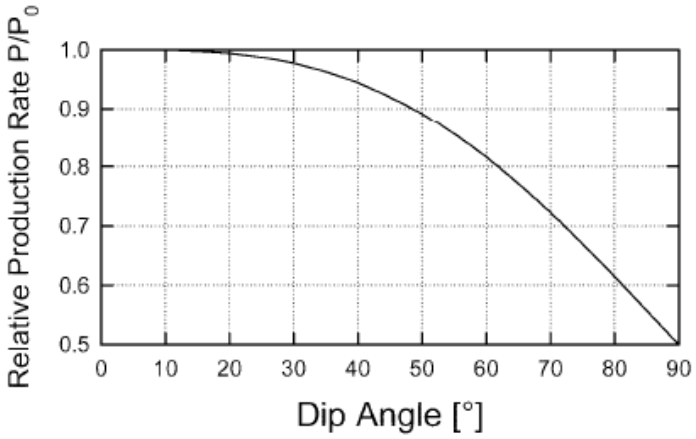

B.

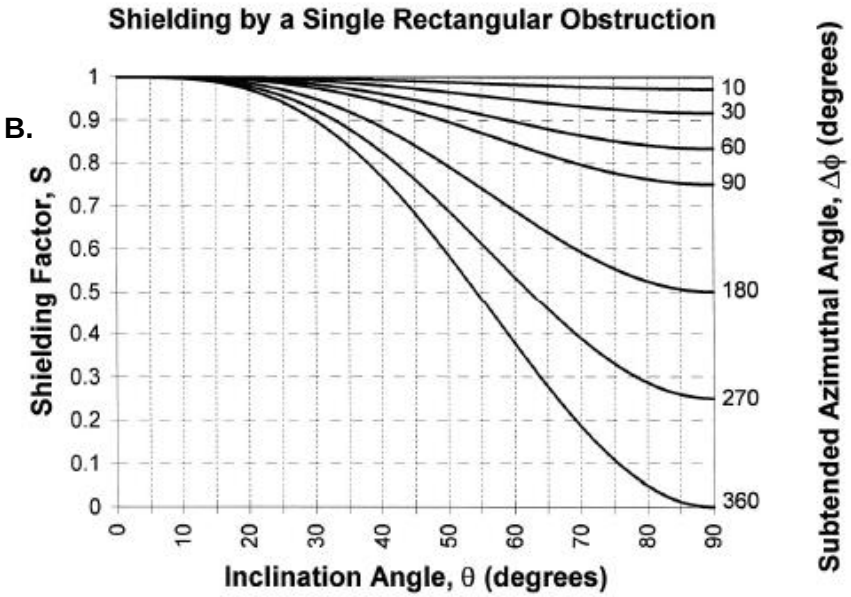

Fig. 2.2.10: A. The influence of the dip angle on the cosmogenic nuclide production rate (*P*) relative to the production rate on a flat surface (P_0). The greater the dip of the surface, the lower the production rate (*P*) will be in the surface as the flux of cosmic rays penetrating the surface is reduced. **B.** The shielding effect on the production rate of cosmogenic nuclides from a single rectangular obstruction reaching up to an inclination angle (θ) and extending over a subtended azimuth angle (Δφ). The shielding factor is applied to the production rate, so rectangular blocks that have low inclination values (up ~20 degrees) have little to no impact on the production rate of cosmogenic nuclides. *From Niedermann (2002); see Gosse and Phillips (2001) for discussion of equations that can be used for shielding/dip corrections.*

Additional local shielding of samples from sources such as covering by vegetation, soil and/or snow could also affect the local production rate of cosmogenic nuclides at the sample locations (Gosse and Phillips, 2001; Zweck *et al*. 2013). The impact of vegetation/soil cover on the production rate is assumed to be negligible due to location of the samples within the canyon and the lack of soil/vegetation presence in close proximity to the sample locations (See photos of sample locations in Appendix A). The duration and depth of annual snow cover in the study area is unknown, so a correction factor was not calculated for the samples processed in this study. Therefore, the calculated surface exposure ages represent the minima, due to the assumption of both negligible subsequent erosion of the surface (see Section 2.2.6.1) and negligible shielding by vegetation, soil and/or snow.

2.2.6.3 Method for surface exposure dating using ^{3}He

There are four main stages in the process of obtaining an exposure age from a bedrock surface (Fig. 2.2.11); this section describes each of these stages in detail.

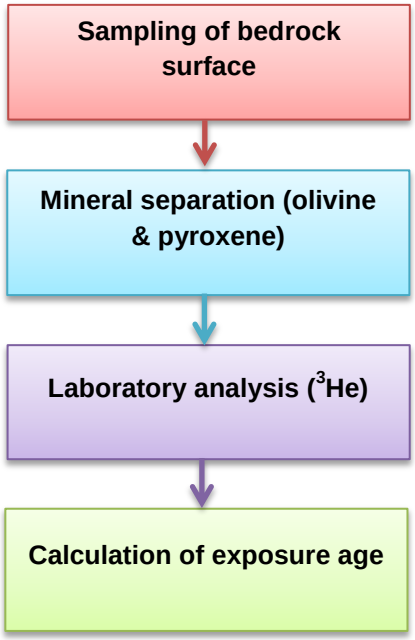

Fig. 2.2.11: The four stages of terrestrial cosmogenic nuclide dating process. First, samples are collected in the field. Olivine and pyroxene are then extracted before being analysed for their cosmogenic ^{3}He nuclide content. These are used to calculate the exposure age of the bedrock surface (see details in Sub-Chapter 2.3 and Appendix A).

2.2.6.3.1 Sampling

Nine samples were collected and analysed for cosmogenic ^{3}He surface exposure dating from the Jökulsárgljúfur canyon (orange stars in Fig. 2.2.12); eight of these samples were collected from upper 5 km of the main Jökulsárgljúfur canyon (Fig. 2.2.12A), and one sample collected from an eroded notch (> 2 m local relief) at the scoured rim of Ásbyrgi canyon (Fig. 2.2.12B). Additional samples were also collected from the rim of Ásbyrgi, Ásbyrgi island and across the Klappir scablands (blue samples in Fig. 2.2.12B), but were not analysed due to cost and time constraints. Assuming no subsequent erosion of the canyon rim of Ásbyrgi (which is inferred based

on the lack of overland flow into the canyon and perfect preservation of features in the Klappir scablands), the exposure age obtained from this sample (AR1) will tell us when erosion last occurred at the canyon rim, and therefore the timing of the last extreme flood event that contributed to the erosion of Ásbyrgi.

Samples were collected from strategic locations that would allow the temporal evolution of bedrock erosion within the canyon to be determined. Therefore, samples were collected different locations longitudinally along the canyon, both within the overspill channel and the main canyon (Fig. 2.2.12) so that the timing of the upstream migration of knickpoints can be identified. As the different strath terrace levels indicate different palaeo-locations of the river bed through time, multiple samples were collected from each of the terraces so the timing of different knickpoints could be identified. From the initial samples collected in the field, it was decided that the majority of the samples that would be processed would be located in the Dettifoss area (Fig. 2.2.12A) with a single sample processed from the rim of Ásbyrgi (Fig. 2.2.12B). This was because, in order to develop a high resolution model of how the upper reaches of the Jökulsárgljúfur canyon has evolved, as many samples as possible from the length of this section of the canyon should be examined. A single sample was processed from Ásbyrgi to determine whether the erosion in this location occurred before, or was coincident with, the erosion that has taken place 28 km further upstream at the apex of the canyon. All samples were collected from bedrock surfaces that had clearly been eroded by fluvial activity, with no obvious signs of weathering or burial by vegetation or soil that may affect the local production of cosmogenic nuclides at each of the sample locations (Gosse and Phillips, 2001). Photographs of all sampling locations are provided in Appendix A.

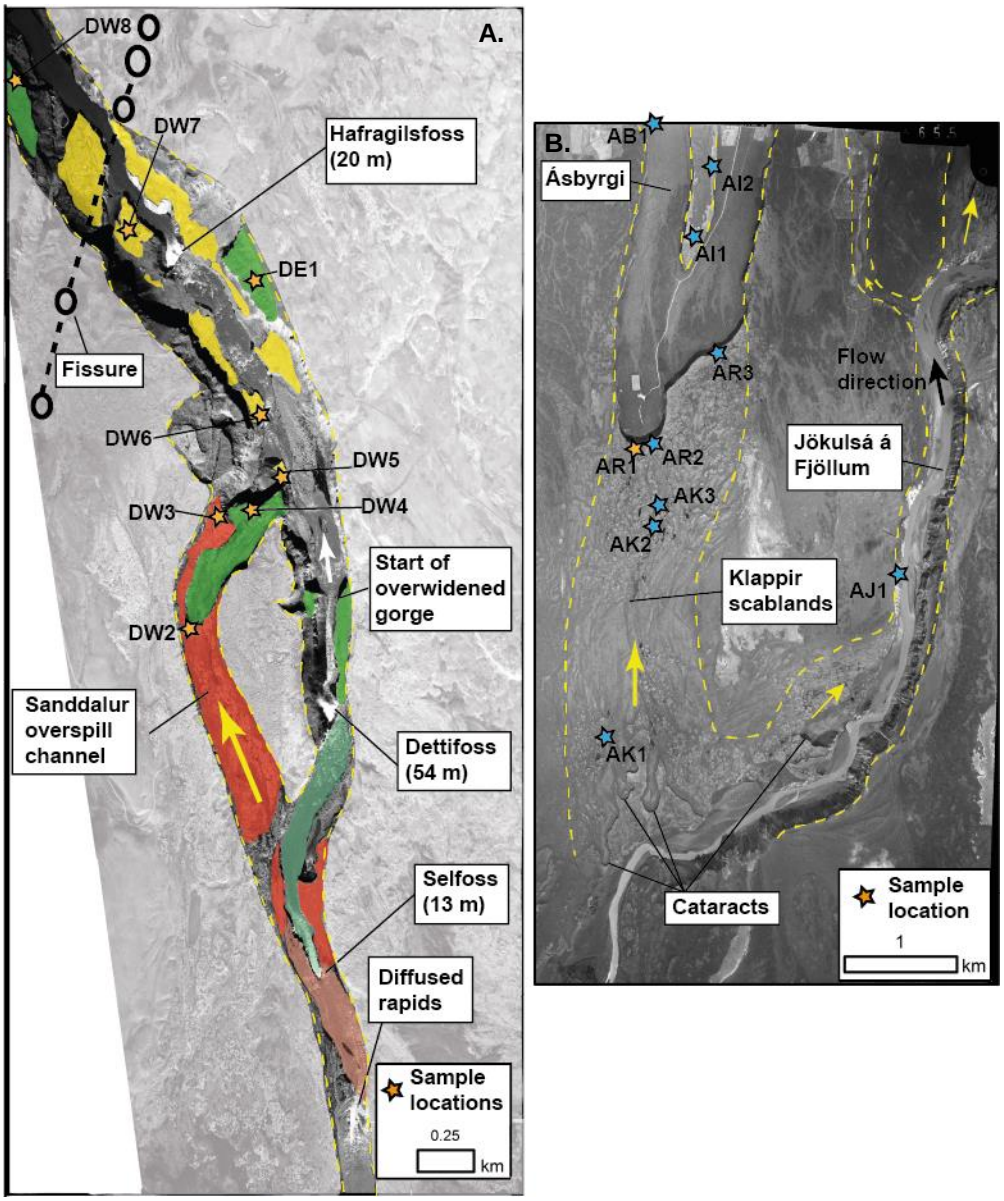

Fig. 2.2.12: A. Aerial photograph from 1998 of the 5 km study reach at the head of Jökulsárgljúfur canyon. Yellow dashed lines delineate the areas where clear evidence for fluvial erosion is present (landscape outside these areas is shaded to improve clarity. The three large knickpoints are highlighted: Selfoss, Dettifoss and Hafragilsfoss (height in brackets), as well as the Sanddalur overspill channel which contains two cataracts. The volcanic fissure that erupted 8.5 ka ago (black circles show volcanoes) provides an independent constraint on the maximum age of the canyon. Orange stars indicate the locations of the samples collected for surface exposure dating using cosmogenic ^{3}He. The location of the upper, middle and lower terraces is shown in red, green and yellow, respectively; active fluvial surfaces associated with upper and middle terraces are shown in transparent red and green upstream of Dettifoss. **B**. Ásbyrgi canyon and the Klappir scabland area immediately upstream. This landscape exhibits perfectly preserved landforms

that were formed during an extreme flood event, with the Jökulsá á Fjöllum now flowing in a deeply incised canyon to the east. Orange star indicates the location of the sample collected and analysed from the rim of Ásbyrgi. Blue stars indicate samples collected but not analysed due to time and cost constraints.

It is important that the surfaces that are sampled produce an age that truly reflects the time since the corresponding surface was exposed to cosmic rays. If the surface of the rock has been weathered significantly (i.e. greater than a few centimetres lost from the surface; Niedermann, 2002), the age obtained from the analysis of the concentration of the cosmogenic ^{3}He could be significantly younger than the true age of exposure because of the exponential decay of production rate with depth. Cosmogenic nuclides only accumulate in the top few centimetres of the Earth's surface which, if removed by weathering, can lead to a concentration of cosmogenic ^{3}He in a surface sample that is lower than the concentration that will give the true representation of the exposure age. In order to negate this impact, the samples collected for analysis in this study were from surfaces that were clearly formed by fluvial action, exhibiting evidence such as fluting, without any evidence for subsequent weathering. Due to the field area being located within a National Park, permission was granted that samples only be taken from loose blocks that were already detached from the bedrock (Fig. 2.2.13). However, samples were only taken from loose *in situ* blocks that had not been transported a large distance from their initial location since they became detached from the surface (less than 1 cm horizontal movement). It is also possible that the concentration of cosmogenic nuclides measured may not reflect the true time since exposure if the samples contained cosmogenic nuclides inherited from another source. For example, after a basalt lava flow has been erupted, the top surface of the lava flow will be exposed to cosmic rays and cosmogenic nuclides will start accumulating. In this study, it is assumed all of the cosmogenic ^{3}He measured in the laboratory analyses has accumulated since exposure by erosion, rather than inherited from exposure during the period between lava flow eruption and subsequent burial under

younger flows above. The polished rock surfaces on all terraces are made of non-vesiculated, compact lava (see photos of sample locations in Appendix A). This indicates removal of the very top of the lava flows (either rubbly aa or vesiculated pahoehoe) where inherited cosmogenic ^{3}He concentrations would have been the greatest, either through erosion by water or emplacement of subsequent flows

Fig. 2.2.13: Photograph showing an example of *an in situ* plucked block that has clearly not been transported far since detachment from the bedrock surface. Such a block is suitable for sampling. Sample: AI2 (Fig. 2.2.12)

Masarik and Reedy (1995) showed that the boundary effect of the air-surface interface on the total cosmic ray neutron flux (that produces ^{3}He) means that, despite the exponential decay in the production of cosmogenic nuclides with depth, the production is uniform in the upper few centimetres of the Earth surface (Fig. 2.2.14). Therefore only the top 5 cm of the samples were kept for the analysis, with the part of the rock below this depth sawed off back in Edinburgh.

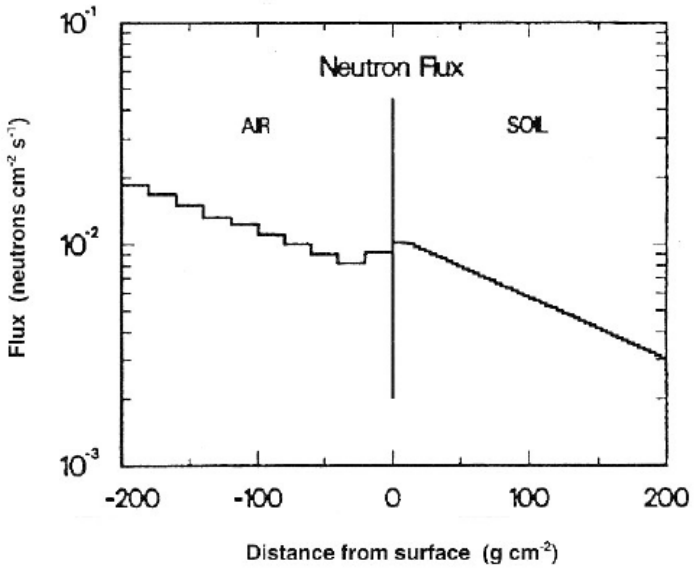

Fig. 2.2.14: Effect of air-surface interface on the cosmic ray neutron flux, calculated by Masarik and Reedy (1995). Despite the exponential decay in neutron flux (and cosmogenic nuclide production rate) with depth, the effect of the air-surface interface leads to a uniform production rate in the upper few centimetres on the Earth's surface. The samples were therefore trimmed to 5 cm before proceeding with mineral separation. Distance is measured in this plot using g cm^{-2}, due to the differing gravitational force with varying distance from the centre of the Earth. *Diagram source: Niedermann (2002).*

2.2.6.3.2 Mineral Separation

Cosmogenic ^{3}He is produced in olivine and pyroxene crystals within the basalt as a result of the interaction between the atoms in minerals and cosmic rays. These minerals therefore need to be extracted from the basalt samples collected in the field before analysis. The standard mineral separation process (Fig. 2.2.15) was carried out in four stages: sample crushing, separation of magnetic and non-magnetic minerals, separation of dense minerals using a heavy liquid and the subsequent hand picking of the target minerals (olivine and pyroxene) under a microscope (Gosse and Phillips, 2001; Licciardi *et al*., 2007; Lamb *et al.*, 2014).

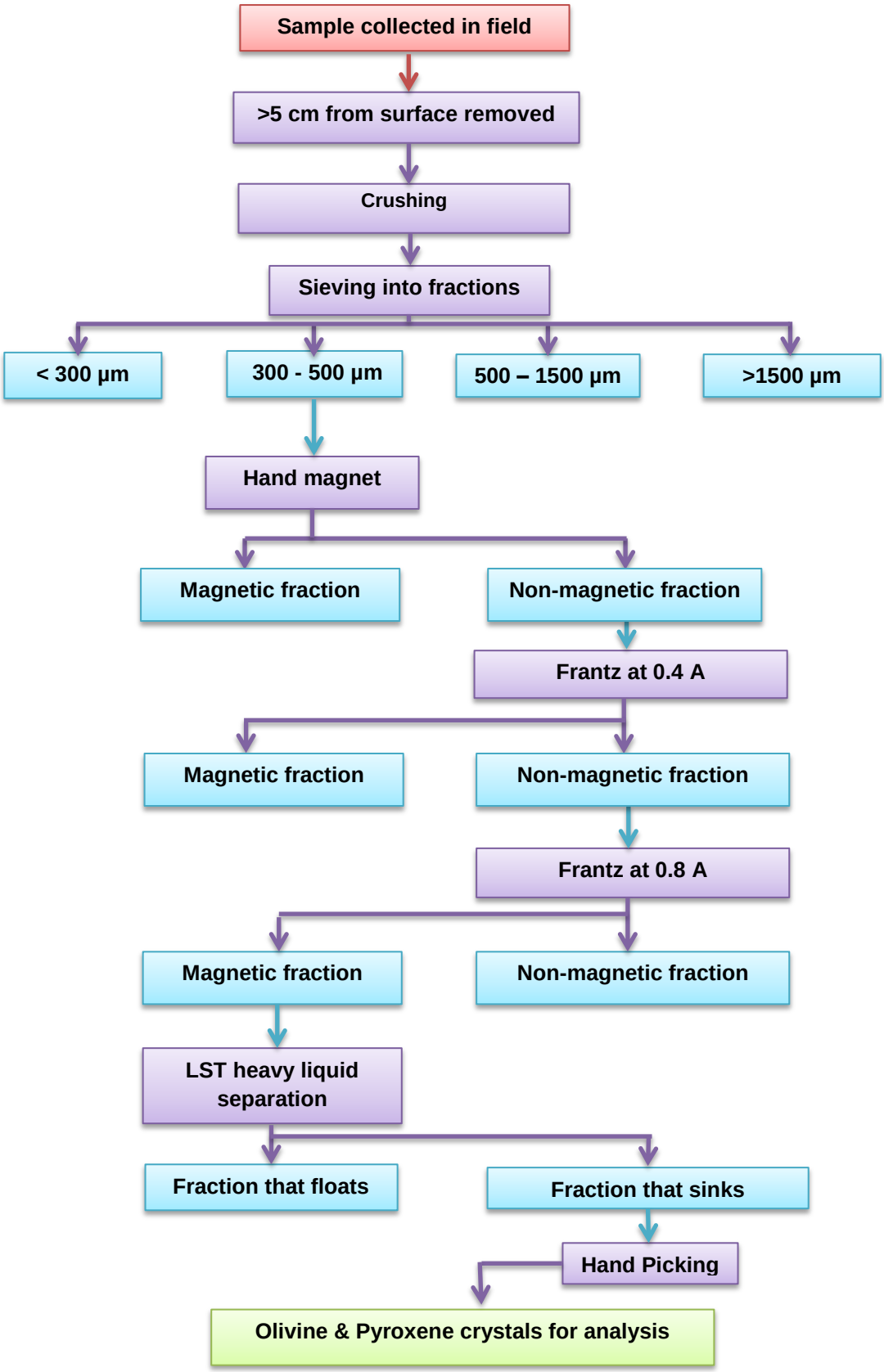
Sample collected in field
>5 cm from surface removed
Crushing
Sieving into fractions
< 300 µm
300 - 500 µm
500 – 1500 µm
>1500 µm
Hand magnet
Magnetic fraction
Non-magnetic fraction
Frantz at 0.4 A
Magnetic fraction
Non-magnetic fraction
Frantz at 0.8 A
Magnetic fraction
Non-magnetic fraction
LST heavy liquid separation
Fraction that floats
Fraction that sinks
Hand Picking
Olivine & Pyroxene crystals for analysis

Overleaf: Fig. 2.2.15: Flow chart showing the different stages of the mineral separation process. Purple boxes represent separation techniques. Blue boxes represent the product of each of these stages.

The samples were crushed using a jaw crusher and sieved into four separate fractions: < 300 µm, 300 – 500 µm, 500 – 1500 µm and > 1500 µm. The majority of the olivine and pyroxene minerals in the rock samples were contained within the 300 – 500 µm fraction after crushing, although some were also identified in the 500 – 1500 µm fraction during hand picking. However, the rock samples also contained a lot of other minerals, such as feldspar, so magnetic separation was carried out in order to reduce the volume of material that the olivine/pyroxene was hand-picked from.

Magnetic separation was a two-stage process, firstly using a hand-magnet to remove magnetite followed by the use of a Frantz magnetic separator (Fig. 2.2.16; Oberteuffer, 1974). The Frantz incorporates an electromagnet where the current can be varied according to requirement. The sample is fed into a funnel at the top of an angled vibrating shelf and the minerals that are magnetic move towards the side of the shelf where the magnetic flux is greater. The minerals move along down the vibrating shelf (set at 25° slope with a tilt of 20°) into two collection buckets.

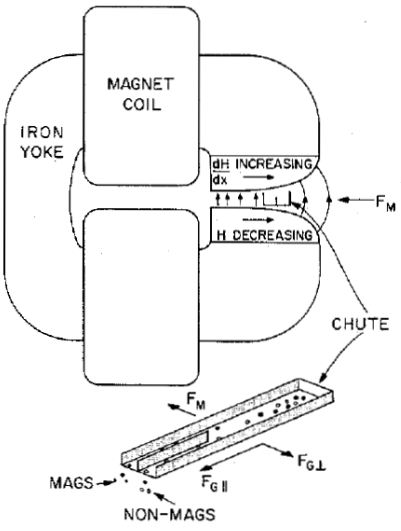

Fig. 2.2.16: Diagrammatic representation of the Frantz magnetic separator. *From Oberteuffer (1974).*

Olivine is magnetic at relatively low amperage so the samples were run through the Frantz twice to remove as many other minerals as possible. Firstly, the samples were fed through the Frantz at 0.4 A with the olivine grains separated in the non-magnetic fraction. The amperage was then increased to 0.8 A with olivine being separated into the magnetic fraction. However, this does not completely separate the olivine from all other minerals so an additional stage was carried out using the heavy liquid LST (solution of 80-85% lithium heteropolytungstates mixed with water). LST is a heavy liquid that has a density of 2.85 g cm^{-3}; minerals that are denser than the LST sink to the bottom of the flask whereas the lighter minerals float. Olivine has a density of 3.32 g cm^{-3} and therefore is part of the 'sink' fraction after the sample has been through the LST. The final stage of separation requires the identification and hand picking of individual olivine and pyroxene grains using a binocular microscope. This process is carried out until enough material has been collected (~ 1 gram required per sample). The hand picking technique is also useful as it allows a quality control check on the mineral grains to be carried out, so that grains which have large melt inclusions, and thus potentially a high radiogenic source of ^{3}He, can be removed before the laboratory analysis.

2.2.6.3.3 Laboratory analyses

As discussed in section 2.2.6.2, the exposure age of the surface is determined through the analysis of the abundance of the cosmogenic ^{3}He. In order to distinguish between the magmatic $^{3}He_{m}$ and cosmogenic $^{3}He_{c}$ components, gas was initially extracted from the fluid inclusions by *in vacuo* crushing of the sample. Gases containing the cosmogenic component are then released from the crystal lattice through melting of the sample in a furnace at 1400 $^{\circ}C$. After each of these extractions, the same procedure is used for gas purification and analysis in a mass spectrometer. The geochemical analysis was carried out in the Nobel Gas laboratory at GFZ Potsdam and is summarised by the flow chart in Fig. 2.2.17. The following sections describe the process, with more detail in Niedermann *et al.* (1997).

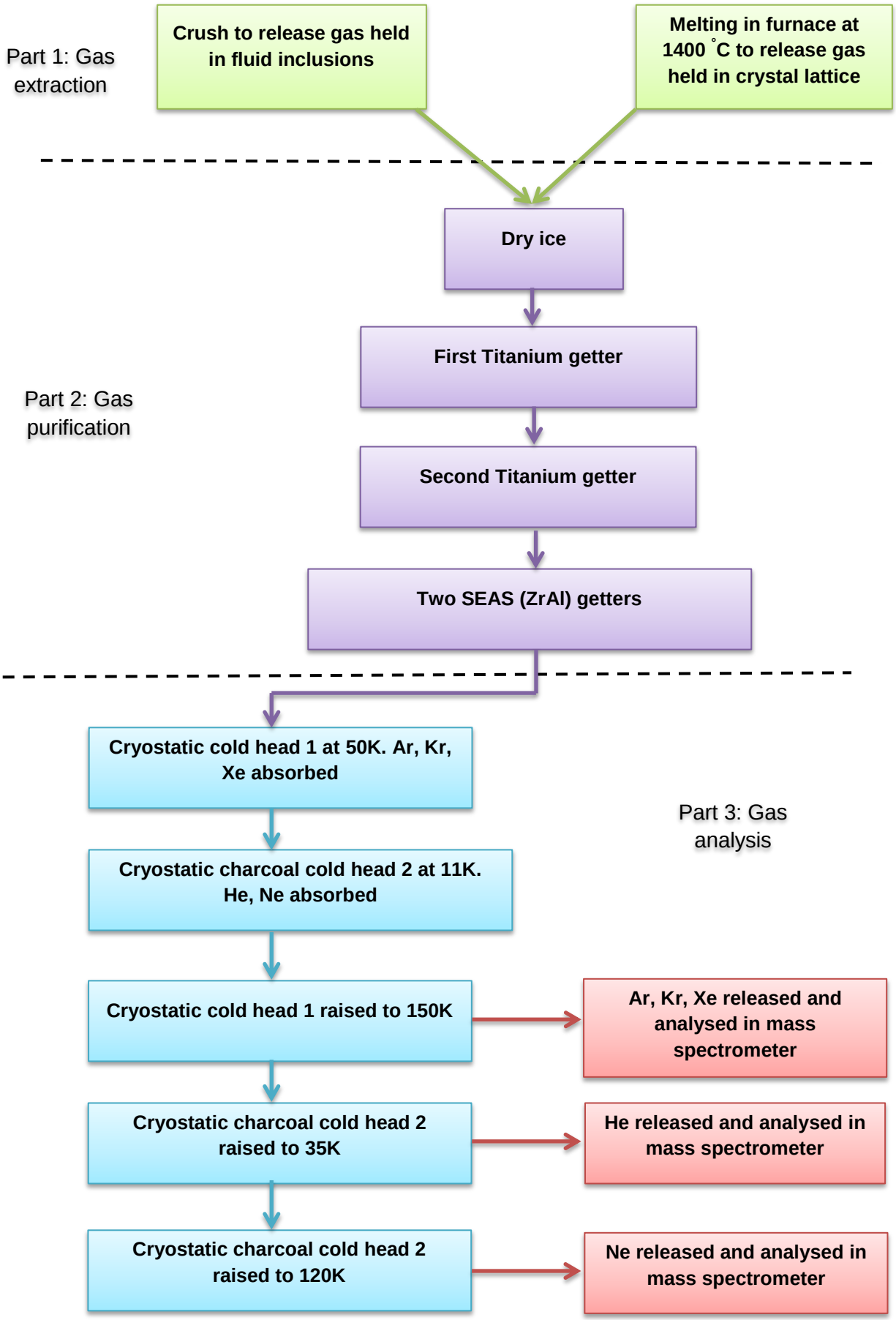
Part 1: Gas extraction
Crush to release gas held in fluid inclusions
Melting in furnace at 1400 °C to release gas held in crystal lattice
Dry ice
Part 2: Gas purification
First Titanium getter
Second Titanium getter
Two SEAS (ZrAl) getters
Part 3: Gas analysis
Cryostatic cold head 1 at 50K. Ar, Kr, Xe absorbed
Cryostatic charcoal cold head 2 at 11K. He, Ne absorbed
Cryostatic cold head 1 raised to 150K
Ar, Kr, Xe released and analysed in mass spectrometer
Cryostatic charcoal cold head 2 raised to 35K
He released and analysed in mass spectrometer
Cryostatic charcoal cold head 2 raised to 120K
Ne released and analysed in mass spectrometer

Preceding page, Fig. 2.2.17: Summary flow chart showing the different stages of the analysis procedure in the laboratory. The gas is extracted either through crushing (for the magmatic ^{3}He component) or melting in the furnace (for the cosmogenic ^{3}He component). Once extracted, the gas is purified (part 2) and then the gases are separated in the two cryostatic cold heads (part 3). Each gas is then analysed in the mass spectrometer in turn.

The first stage of the laboratory analyses is to measure the gases stored within the fluid inclusions in the sample, which are from a magmatic source rather than produced by interaction with cosmic rays and released by crushing (Fig. 2.2.18). The minerals are repeatedly crushed for 10 minutes and the gas produced is then released into the purification part of the gas line before being measured. Once the samples have been crushed, the powder is collected and wrapped in aluminium foil before being placed in the sample carousel in preparation for the melt extraction experiment. Gas stored within the crystal lattice of the olivine and pyroxene minerals is released by melting the minerals in a furnace at $1400^{o}C$ (Fig. 2.2.19). At the start of each melt extraction experiment, the carousel is rotated and the sample dropped into a titanium lined crucible in the furnace below (Fig. 2.2.20).

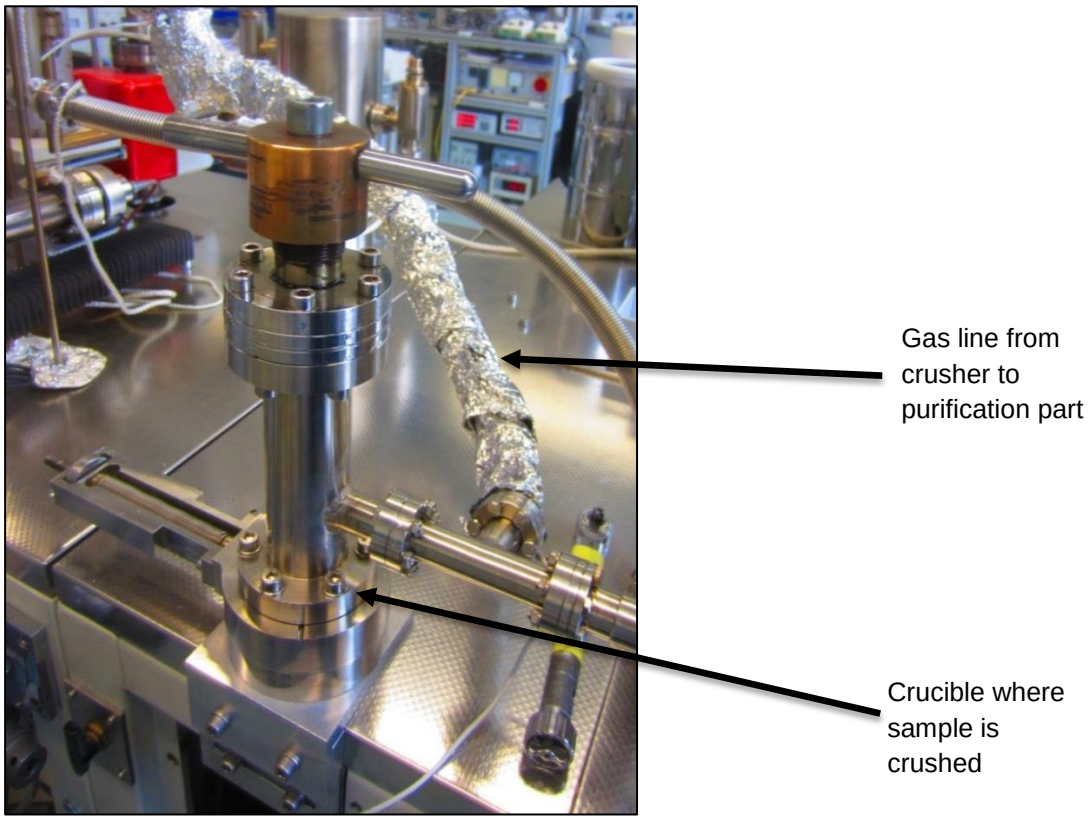

Fig. 2.2.18: The crusher used to extract the gas from the melt inclusions of the olivine and pyroxene minerals. The crushing takes place in a vacuum, and is input into the gas purification part along the line indicated.

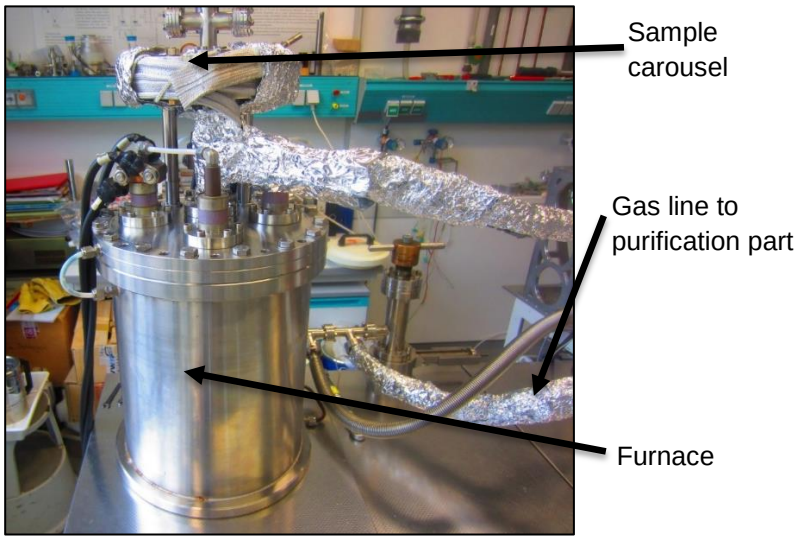

Fig. 2.2.19: The sample carousel, furnace and gas line to the purification part. The crusher can also be seen in the background.

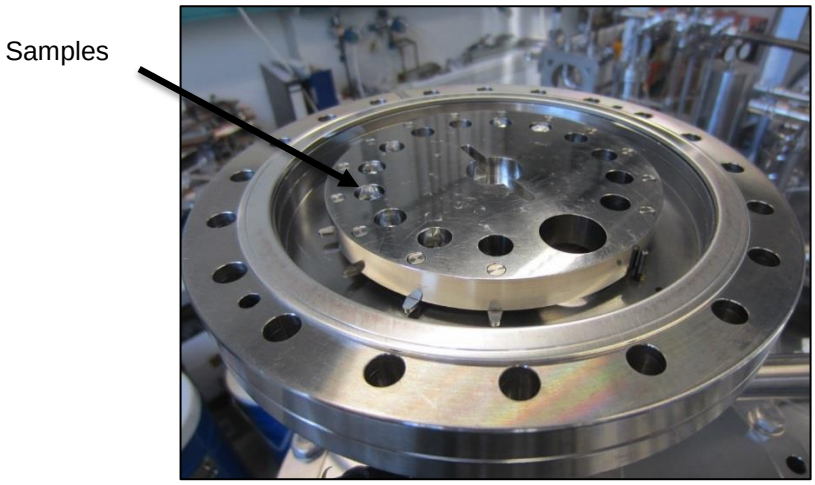

Fig. 2.2.20: Sample carousel containing the samples waiting to be dropped into the furnace. Each sample is wrapped in aluminium foil which melts during the heating process. The carousel holds up to 14 samples.

The samples are heated to 1400 °C over the course of 20 minutes in the furnace and then the temperature is maintained at 1400 °C for a further 20 minutes. The gases produced through the melting of the minerals are then released into the gas purification section through a gas line.

Once the gas has been released from the sample, either through crushing or melting, it is cleaned to remove potential interferences particularly by volatiles including H_2O and CO_2 before it is analysed in the mass spectrometer. There are three main stages which remove impurities and reduce the background levels of the gases that are not analysed. Initially, the gas is cleaned for ten minutes in a section of pipe that is immersed in dry ice. The gas is then pumped into a titanium sponge getter heated at 400 °C for ten minutes before being pumped into a second Ti-Getter also at 400 °C for a further ten minutes (Fig. 2.2.21). The final stage of gas purification is to clean the gas in two SAES (ZrAl) getters for ten minutes (Fig.2.2.22). The gas is then pumped into the analysis part of the system, containing two cryostatic cold-heads and the mass spectrometer.

Ti sponge getters

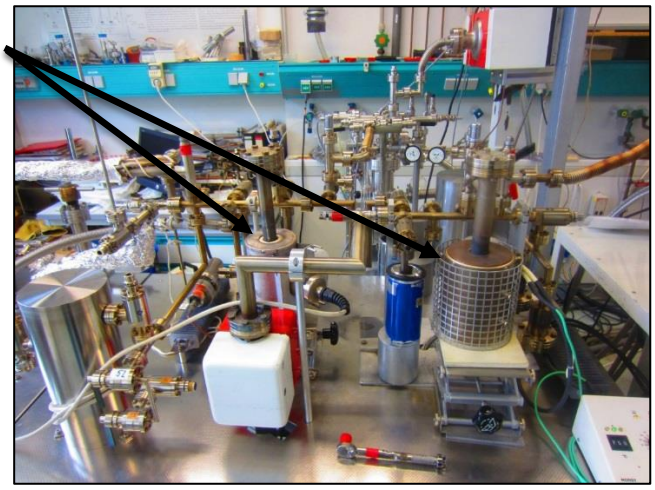

Fig 2.2.21: Part two: gas purification. After the gas has been extracted in either the crusher or the furnace, it is purified using dry ice, two titanium sponge getters and two SEAS (ZrAl) getters

Fig. 2.2.22: The two SEAS (ZrAl) getters used to purify the gas before analysis. They absorb all the remaining active gases from within the vacuum, leaving the noble gases Argon, Krypton, Xenon, Helium and Neon for analysis.

The mass spectrometer is used to measure the abundance of the five noble gases of interest: Helium (He), Neon (Ne), Argon (Ar), Krypton (Kr) and Xenon (Xe). Helium and Neon are analysed separately and Argon, Krypton and Xenon are analysed together. These gases are separated through the differential freezing temperatures of the gases in the cryostatic cold heads (Fig. 2.2.23). Initially, the purified gas is pumped into the first cryostatic cold head set at 50K. Argon, Krypton and Xenon are absorbed at this temperature and the remaining Helium and Neon is then pumped into a second cryostatic cold head set at 11K containing activated charcoal. Once the Helium and Neon have been absorbed in the second cryostatic cold head, the temperature in the first cryostatic cold head is raised to 150K which releases the Argon, Krypton and Xenon. These gases are then pumped into the VG5400 noble gas mass spectrometer which measures the concentration of each of these gases (Fig. 2.2.24). Absorbed Helium is then released by raising the temperature of the second cryostatic cold head to 35K, ensuring the Neon in the second cryostatic cold head remains absorbed. The Helium is then pumped into the VG5400 noble gas mass spectrometer and the concentration of the different isotopes (^{3}He and ^{4}He) measured. Finally, the temperature in the second cryostatic cold head is raised to 120K, releasing the stored Neon which is then measured in the VG5400 noble gas mass spectrometer. There are two detectors in the mass spectrometer; an axial electron multiplier and a Faraday cup (Fig. 2.2.25), located on the high mass side of the multiplier. The trap current is set to 400 µA for the Helium and Neon measurements and 200µA for the Argon, Krypton and Xenon measurements.

‘Blank’ measurements were routinely run between each of the sample measurements (both crusher and melt extractions) to ensure the gas concentration levels were back down to a suitable level. Between each melt extraction, the furnace was heated to 1400 $^{\circ}$C for a duration of three hours to ensure that the previous sample was fully degassed before the next ‘blank’ measurement was undertaken. To calibrate the mass spectrometer, ‘standard’ measurements of gas were routinely run through the line;

containing an artificial gas mix of 0.1030 cm^3 containing 12.4 x 10^{-8} cm^3 at standard temperature and pressure (STP) of ^4He, 11.0 x 10^{-8} cm^3 STP of ^{20}Ne, 12.3 x 10^{-8} cm^3 STP of ^{40}Ar, 883 x 10^{-12} cm^3 STP of ^{84}Kr and 404 x 10^{-12} cm^3 STP of ^{132}Xe.

Once the concentrations of ^3He and ^4He had been measured from each of the crushed and melt extraction experiments, they were used to determine the exposure age of each of the samples (see Sub-Chapter 2.3 and Appendix A for these calculations).

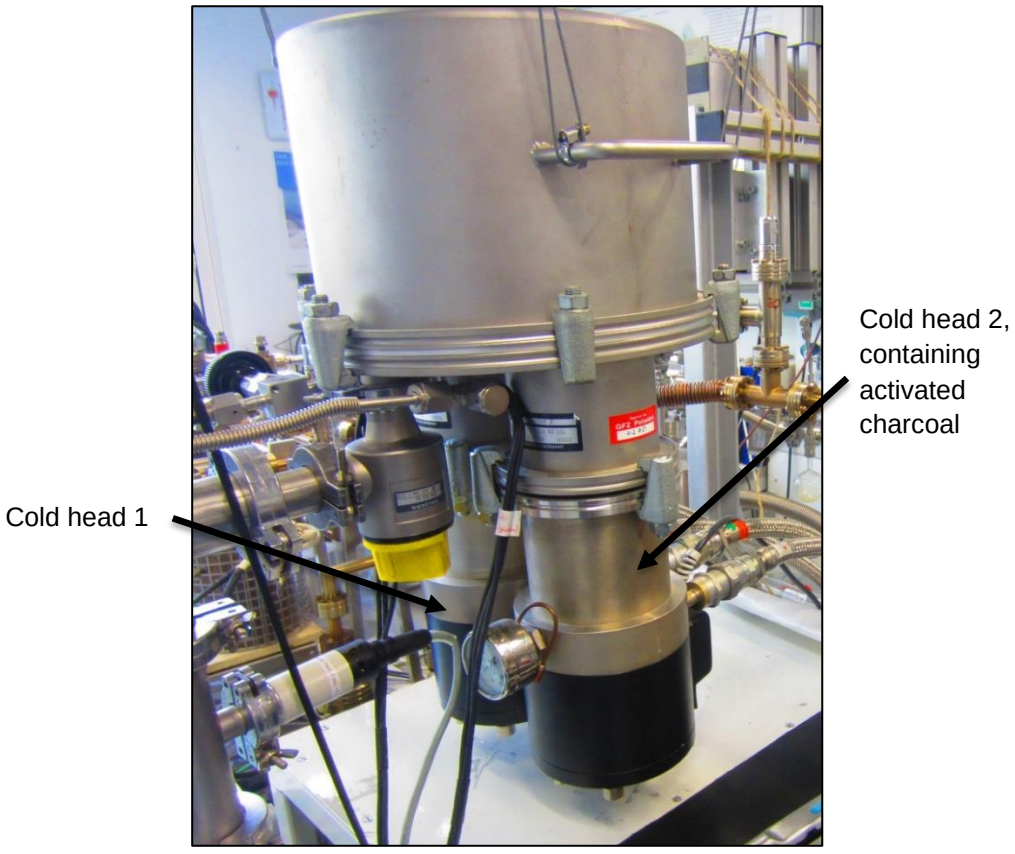

Fig. 2.2.23: The two cryostatic cold heads used to separate the Noble gases. Ar, Kr and Xu are absorbed at 50K in cold head 1 and He and Ne are absorbed by the charcoal at 11K in cold head 2. The gases are released by the heating of the cold heads (see Figure)

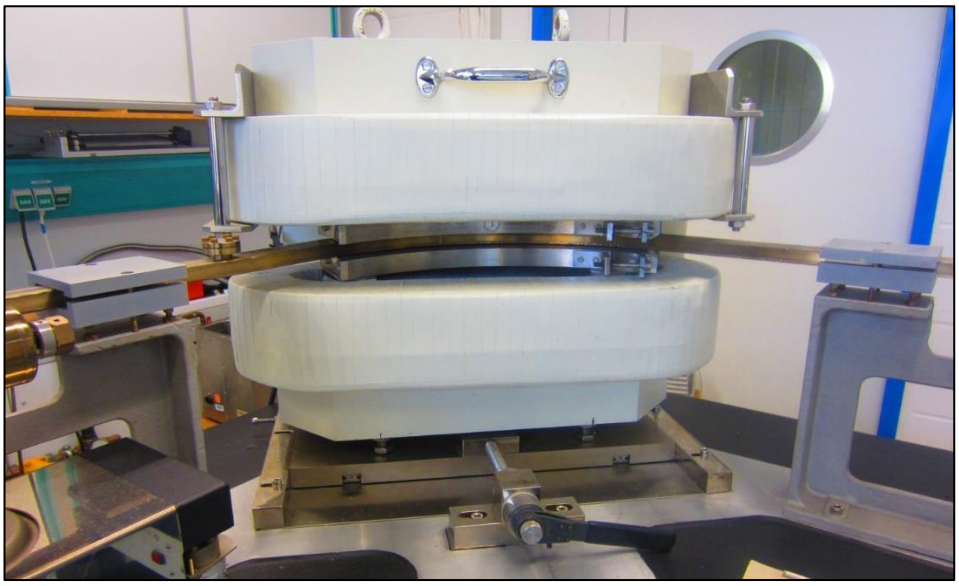

Fig. 2.2.24: VG5400 noble gas mass spectrometer at GFZ Potsdam

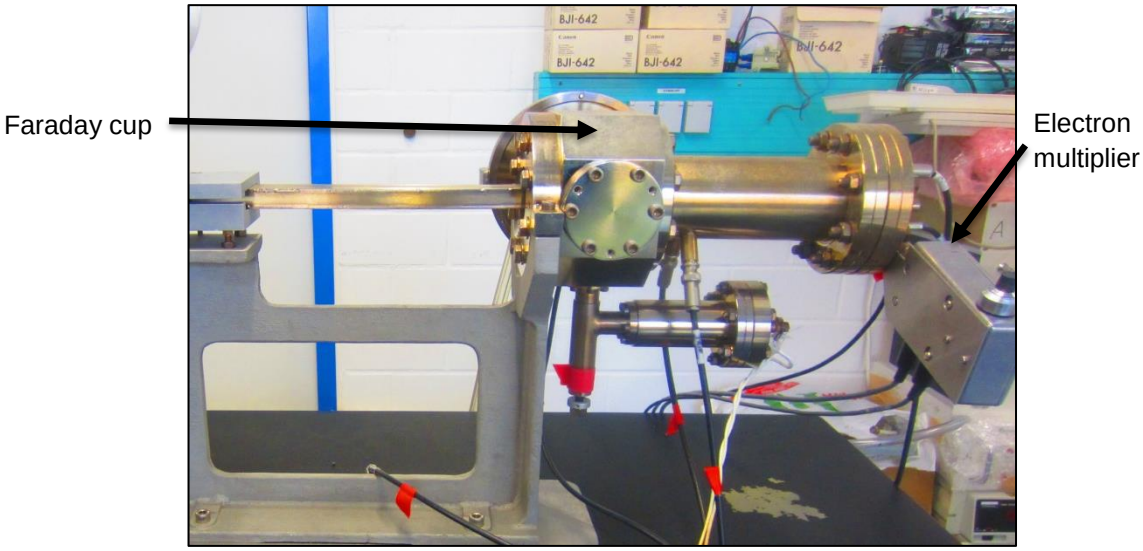

Fig. 2.2.25: The Faraday cup and electron multiplier detectors, for measuring the volumes of different gases.

2.2.6.3.4 Exposure age and ^{3}He production rate calculation

Appendix A provides all of the detailed information relevant for the calculations of the surface exposure age ranges. Table A1 shows general sample information (e.g. location, elevation), He isotope data measured during the laboratory analyses (both the crushed and melt experiments) and

the calculated exposure age ranges. Table A2 provides information used for the estimate of radiogenic ^{4}He production from the decay of uranium and thorium. The eruption age of the basalt lava flows from which the samples were collected is not known other than “younger than 800 ka” (Sæmundsson, 2012); however based on radiogenic ^{4}He production rates, the total amount of ^{4}He measured in the samples could have been produced within ~30-150 ka (Table A2), which means we cannot exclude that up to 100% of total ^{4}He may be radiogenic in origin. If the basalt eruption age is higher than 30-150 ka, then an unknown fraction of radiogenic ^{4}He would have been lost from the samples. Nevertheless, the crushing extractions show that magmatic He is present as well and has certainly not been completely degassed prior to the melting extractions. Therefore, the ^{4}He measured in the samples may be anything between purely magmatic and purely radiogenic in origin. Therefore the maximum range in which the true surface exposure age may lie is given, using a 0% and 100% fraction of radiogenic ^{4}He to total ^{4}He, respectively, as the lower and upper limit.

Assuming no radiogenic ^{4}He, the lower limit on the surface exposure age range is calculated by subtracting the $(^{3}He/^{4}He)_{Crushed}$ ratio from the $(^{3}He/^{4}He)_{Melt}$ ratio in order to determine the $(^{3}He_{Cosmogenic}/^{4}He)$ ratio (Kurz, 1986; Gosse and Phillips, 2001; Niedermann, 2002). Assuming all the ^{4}He is radiogenic in origin, the upper limit on the surface exposure age range is calculated assuming all of the ^{3}He in the melt measurement is cosmogenic. The production rate of ^{3}He was calculated using a reference sea-level high-latitude (SLHL) production rate of 124 at g^{-1} yr^{-1}, scaled using the Dunai (2000) scaling scheme from the calculated production rate in olivine and pyroxene at the Tabernacle Hill, calibration site of Goehring *et al.* (2010) in Utah, USA. The SLHL production rate was then scaled to each individual sample location using the Dunai (2000) scaling scheme based on the elevation and latitude of the sample, given in Table A1.

The true exposure age for each sample lies between the upper and lower limits calculated using the different assumptions of radiogenic ^{4}He content,

with the exception of DW8 where only a maximum age limit is possible due a contamination of the sample with basalt matrix (as evidenced by $(^3He/^4He)_{Melt} < (^3He/^4He)_{Crushed}$).

Table A3 provides all the information regarding the dip measurements of all the samples, as well as the topographic shielding measurements. As all measurements of dip and shielding are low, there is a negligible correction required for the production rate of cosmogenic ^3He. This is due to the cosmic ray flux being greatest from directly above the sample location as there is less atmosphere to pass through so shielding blocks/topography located at a low angle on the horizon have a very small impact on the overall production rate (see Fig. 2.2.10).

Sub-Chapter 2.3: Erosion during extreme flood events dominates Holocene canyon evolution in northeast Iceland

Baynes ERC, Attal M, Niedermann S, Kirstein LA, Dugmore AJ, Naylor M (2015) Erosion during extreme flood events dominates Holocene canyon evolution in northeast Iceland. *Proceedings of the National Academy of Sciences* 112 (8), 2355-2360. DOI: 10.1073/pnas.1415443112

2.3.0 Sub-Chapter outline

This sub-chapter has been published in *Proceedings of the National Academy of Sciences*, in collaboration with my co-authors. The paper is freely available for download (fully open access) from the PNAS website. My contribution to this work is substantial as I carried out every stage of the work from research design, data analysis and paper writing. I designed the initial research plan with my supervisors in Edinburgh; Mikaël Attal, Andrew Dugmore and Linda Kirstein. Mikaël and I carried out the topographic surveys and collected the samples. Linda showed me the method for mineral separation which I carried out alone in Edinburgh. I travelled to Potsdam, Germany, to process my samples for surface exposure dating in the Nobel Gas laboratory at GFZ, under the supervision of Samuel Niedermann. Samuel also contributed to the interpretation of the surface exposure ages. Mark Naylor contributed to some of the data analysis in the Supplementary Information (Appendix A.3). I wrote the paper and designed all of the figures herein.

The anatomy of a *PNAS* article contains both an abstract and a ‘significance statement’; a short (< 120 word) lay summary of the importance of the research. Both are included at the start of this chapter (Section 2.3.0.1 and 2.3.0.2). The main bulk of the chapter (Section 2.3.1) can be read as a

standalone unit, although references are made to extra information and analyses presented in Appendix A at the end of this thesis.

2.3.0.1 Abstract

Extreme flood events have the potential to cause catastrophic landscape change in short periods of time (10^0 – 10^3 hours). However, their impacts are rarely considered in studies of long-term landscape evolution (> 10^3 years), because the mechanisms of erosion during such floods are poorly constrained. Here we use topographic analysis and cosmogenic ^{3}He surface exposure dating of fluvially sculpted surfaces to determine the impact of extreme flood events within the Jökulsárgljúfur canyon (northeast Iceland) and to constrain the mechanisms of bedrock erosion during these events. Surface exposure ages allow identification of three periods of intense canyon cutting about 9, 5 and 2 ka ago during which multiple large knickpoints retreated large distances (> 2 km). During these events, a threshold flow depth was exceeded, leading to the toppling and transportation of basalt lava columns. Despite continuing and comparatively large scale (500 m^3 s^{-1}) discharge of sediment-rich glacial meltwater, there is no evidence for a transition to an abrasion-dominated erosion regime since the last erosive event because the vertical knickpoints have not diffused over time. We provide a model for the evolution of the Jökulsárgljúfur canyon through the reconstruction of the river profile and canyon morphology at different stages over the last 9 ka and highlight the dominant role played by extreme flood events in the shaping of this landscape during the Holocene.

2.3.0.2 Significance statement

The importance of high-magnitude, short-lived events in controlling the evolution of landscapes is not well understood. This matters because during such events, erosion processes can surpass thresholds and cause abrupt landscape changes that have a long lasting legacy on landscape morphology. We show that extreme flood events, during which the flow depth exceeds the threshold for erosion through plucking rather than abrasion, are

the dominant control on the evolution of a large bedrock canyon in Iceland. The erosive signature of these events is maintained within a dynamic landscape over millennial timescales, emphasizing the importance of episodic extreme events in shaping landscapes.

2.3.1 Introduction

Extreme floods in both terrestrial and extra-terrestrial environments can cause abrupt landscape change that can have long-term consequences (Bretz, 1923; Baker and Kale, 1998; Garcia-Castellanos *et al.*, 2009; Gupta *et al*., 2007; Warner *et al.*, 2013), especially when a geomorphic threshold is exceeded (Schumm, 1979). The timescale over which this change is visible is controlled by the ability and efficiency of background processes to re-shape the landscape. As a result, progress in understanding both short term and long term landscape evolution requires better knowledge of bedrock channel erosion processes and thresholds over the different scales at which geomorphological processes operate (Howard *et al.,* 1994; Whipple *et al.*, 2000; Sklar and Dietrich, 2001).

The majority of research into extreme flood events has focused on the interpretation of deposited sediments (e.g., Duller *et al.*, 2008; Carling, 2013) and the reconstruction of the hydraulic conditions prevailing during such events (e.g., Baker *et al*., 1993; Alho *et al.*, 2005; Carrivick, 2007). Further work has defined the geomorphic impact of extreme flood events in proglacial areas close to the source of the flood water (e.g., Carrivick *et al.*, 2004; Dunning *et al.*, 2013). Studies that examine the processes of bedrock erosion, especially large canyon formation, during extreme flood events, can help establish a diagnostic link between formation processes and morphology in canyons in both terrestrial and extra-terrestrial settings, but they remain scarce (e.g., Lamb *et al.*, 2008; 2014; Lamb and Fonstad, 2010). Here, evidence for bedrock landscape change during extreme floods along the course of the Jökulsá á Fjöllum River (northeast Iceland) is used to test

whether the contemporary landscape morphology reflects erosion during rare extreme events, or longer term ‘background’ erosional processes.

The Jökulsá á Fjöllum has experienced multiple glacial outburst floods (jökulhlaups) since the Last Glacial Maximum, with peak discharge for the largest flood estimated to be in the order of 0.9×10^6 m^3s^{-1} (Alho *et al.*, 2005; Carrivick *et al.*, 2013). The landscape contains many characteristic landforms associated with extreme flood events, including boulder bars and terraces, dry cataracts such as Ásbyrgi, numerous flood overspill channels and the Jökulsárgljúfur canyon (Fig. 2.3.1) (e.g. Thórarinsson, 1950; Tomasson, 1973; Waitt, 2002; Carrivick *et al.*, 2004; Kirkbride *et al.,* 2006). The canyon has been carved through a volcanic system which was active 8.5 ka BP (Eliasson, 1974) ~4 km downstream of its head. As the canyon is cut directly through the fissure and associated lava flows and there is no evidence of lava from the fissure flowing into the canyon, the eruption age provides an independent constraint on the maximum age for the formation of the canyon upstream of the fissure (Fig. 2.3.1). The impact of the largest flood events has never been tied to the evolution of the bedrock landscape within the Jökulsárgljúfur canyon, as previous studies have focused on sedimentary deposits (e.g. Waitt, 2002; Kirkbride *et al.*, 2006). This study uses topographic analysis and cosmogenic ^{3}He surface exposure dating of fluvial surfaces to determine the erosive impact of extreme flood events and assess the importance, and legacy, of high-magnitude low-frequency events in landscape evolution over multi-millennial timescales.

2.3.2 Conceptual model of canyon formation

Large canyons can be formed during extreme flood events through the toppling and removal of blocks in heavily jointed basaltic bedrock (Lamb *et al.*, 2008; 2014), once a threshold flow depth has been exceeded (Lamb and Dietrich, 2009). Bedrock erosion during extreme floods in such settings is therefore dominated by plucking rather than abrasion, resulting in the

formation and upstream propagation of large vertical knickpoints (e.g. Box Canyon and Stubby Canyon, Idaho, Lamb *et al.*, 2008; 2014). As the knickpoints propagate upstream, rock is removed typically over the thickness of one or more lava flows, exposing pristine rock surfaces to cosmic rays and initiating the accumulation of cosmogenic nuclides. The surface can subsequently become abandoned through the retreat of a knickpoint at a lower level, leaving strath terraces above the active channel. If a knickpoint is retreating steadily through time, as would be expected if associated with a normal flow regime, the exposure age of samples from fluvial surfaces would become progressively younger with decreasing distance from the modern knickpoint location (Jansen *et al.*, 2011; Seidl *et al.*, 1997; Mackey *et al.,* 2014). If, on the other hand, a knickpoint retreated a large distance in a short period of time, such as during an extreme flood event, the exposure ages would be expected to cluster around the time of that significant erosion event (Lamb *et al.*, 2014). Recognition of the canyon morphology and the measurement of precise exposure ages are therefore key to distinguishing between models of canyon formation.

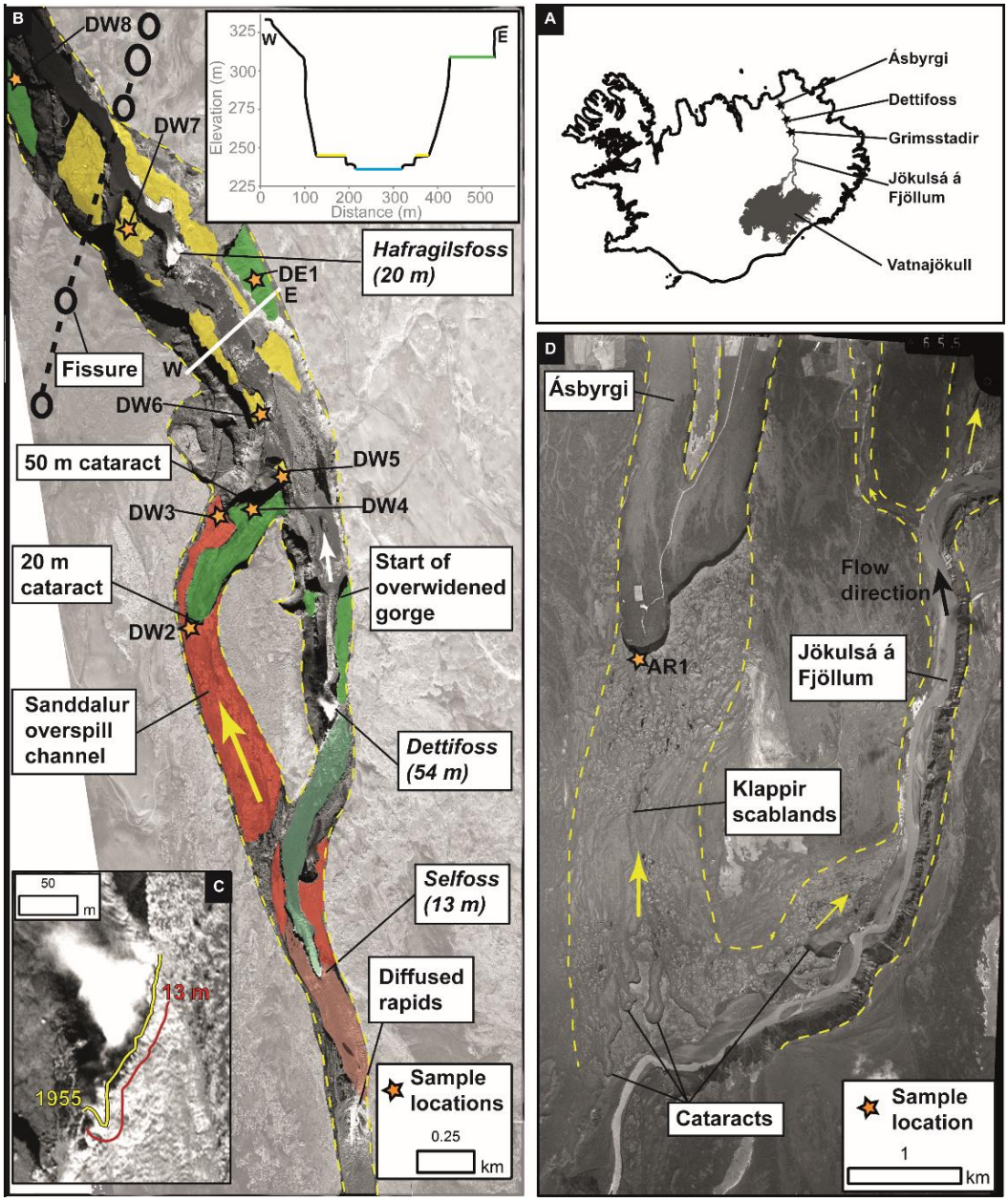

Fig. 2.3.1: A. Location map of Iceland showing the Vatnajökull ice cap, the source of the floodwaters, and the course of the Jökulsá á Fjöllum. The locations of the two study sites - the upper 5 km of Jökulsárgljúfur canyon at Dettifoss and Ásbyrgi, 25 km further downstream, are shown with black stars. The location of the gauging station at Grimsstadir used for hydrological calculations is also shown. **B.** Aerial photograph from 1998 of the 5 km study reach at the head of Jökulsárgljúfur canyon. Yellow dashed lines delineate the areas where clear evidence for fluvial erosion is present (landscape outside these areas is shaded to improve clarity). The three large knickpoints are highlighted: Selfoss, Dettifoss and Hafragilsfoss (height in brackets), as well as the Sanddalur overspill channel which contains two cataracts. The volcanic fissure that erupted 8.5 ka ago (black circles show volcanoes) provides an independent constraint on the maximum age of the canyon. Orange stars

indicate the locations of the samples collected for surface exposure dating. The upper, middle and lower terraces are shown in red, green and yellow, respectively; active fluvial surfaces associated with upper and middle terraces are shown in transparent red and green upstream of Dettifoss. A cross-section of the gorge across the line from W to E is inset. **Inset C.** A zoomed in image of Dettifoss from 1998, with the yellow line showing the digitised position of the waterfall in 1955. Dettifoss has been mostly stable during the 43 year period between the images, with only a small retreat (max 5 m) evident on the western side of the channel. If the Jökulsárgljúfur canyon was formed by the progressive retreat of Dettifoss following the fissure eruption (2500 m in 8.5 ka, equivalent to a rate of 0.3 m/yr), we would expect to see a minimum of 13 m of retreat between 1955 and 1998, shown with the red line. **D.** Ásbyrgi canyon and the Klappir scabland area immediately upstream. This landscape exhibits perfectly preserved landforms that were formed during an extreme flood event, with the Jökulsá á Fjöllum now flowing in a deeply incised canyon to the east.

2.3.3 Canyon morphology

At the head of the Jökulsárgljúfur canyon, the Jökulsá á Fjöllum becomes deeply incised into the surrounding terrain, with the drop in elevation occurring at three large vertical waterfalls, all within the five kilometre-long study reach: Selfoss (13 m-high), Dettifoss (54 m-high), and Hafragilsfoss (20 m-high) (Fig. 2.3.1). The underlying bedrock is columnar basalt, with multiple sub-horizontal lava flows stacked on top of each other (Fig. 2.3.2). The structural control exerted by these lava flows is strong: the river cascades from the top of one lava flow to the top of the flow beneath at the Hafragilsfoss and Selfoss knickpoints and it drops the height of three lava flows at Dettifoss (Fig. 2.3.2). Crucially, the canyon floor is always found to coincide with the top of a lava flow and there is no evidence for active vertical incision into the lava flows other than the knickpoints themselves (Fig. 2.3.1, 2.3.2). This implies that vertical incision through abrasion is limited and that knickpoint propagation due to the toppling of basalt columns is the dominant mode of erosion in the canyon. This is corroborated by the high width-to-depth ratio exhibited by the Jökulsá á Fjöllum, with the flow depth at Selfoss rarely reaching 3 m during peak summer discharge (Appendix A.2.1). The Jökulsá á Fjöllum is 150 m wide at Selfoss, which gives a width-to-depth ratio

of 50, similar to large alluvial rivers (e.g., ratio of ~59 for alluvial reaches of the Yellowstone River, USA; Finnegan *et al.,* 2005) rather than actively incising bedrock rivers (e.g., ratio of ~5 for a range of bedrock rivers incising into high-grade metamorphic or granitic rocks; compilation in Finnegan *et al.,* 2005).

Three strath terrace surfaces are found at different elevations throughout the canyon (Fig. 2.3.2, 2.3.3A), indicating the position of palaeo-river beds. They too are strongly controlled by the bedrock structure, as each surface corresponds to the top of a lava flow. These terraces have been sculpted by fluvial abrasion, exhibiting bedforms such as flutes and polished surfaces (Fig. 2.3.2D). The formation of two of the three terraces can be directly associated with the upstream propagation of knickpoints within the present day canyon: the upper and middle terraces have been abandoned by the retreat of Selfoss and Dettifoss, respectively (Fig. 2.3.2A, 2.3.2B). The lower terrace is ~10 m above the active river channel between Dettifoss and Hafragilsfoss (Fig. 2.3.2C). The 200 m wide Sanddalur flood overspill channel to the West of Dettifoss contains both the upper and middle terraces, with a 20 m vertical cataract at the transition between the surfaces and a 50 m vertical cataract where it re-joins the main canyon (Fig. 2.3.1).

Fig. 2.3.2: Photographs of the three large waterfalls within the gorge in the study reach: **A.** Selfoss (13 m), **B.** Dettifoss (54 m) and **C.** Hafragilsfoss (20 m). Highlighted on the photographs are the three strath terraces: the upper, middle and lower terraces are highlighted in red, green and yellow, respectively. Evidence for fluvial action on the strath terraces includes small-scale flutes, shown in **D.** The strath terraces correspond to the tops of different lava flows, which can be seen exposed in the canyon walls on each of the photos.

2.3.4 Surface exposure ages and chronology of flood events

Samples for surface exposure dating were collected from fluvially-polished bedrock surfaces on the strath terraces, both along the modern river and in the overspill channel (Fig. 2.3.1, 2.3.3A). We assume that the exposure age represents the time at which a given location on the river bed was exposed to cosmic rays due to the removal of overlying rock by the upstream migration of a knickpoint. We assume that there is negligible subsequent surface erosion and a negligible shielding effect from water in the channel which could reduce the concentration of cosmogenic nuclides; to minimise these potential effects, samples were taken as far away as possible from the centre of the channel where water depth and erosion are expected to peak. We also assume that all of the cosmogenic ^{3}He has accumulated since exposure by erosion, rather than during the period between lava flow eruption and subsequent burial under younger flows. We note that the polished rock surfaces on all terraces are made of non-vesiculated, compact lava (Fig. 2.3.2D). This indicates removal of the very top of the lava flows (either rubbly aa or vesiculated pahoehoe) where inherited cosmogenic ^{3}He concentrations would have been the greatest, either through erosion by water or emplacement of subsequent flows. This therefore limits the potential contribution from inherited cosmogenic ^{3}He from exposure before burial. We acknowledge, however, that there may still be an unquantifiable amount of inherited cosmogenic helium in the samples that may lead to an overestimation of the surface exposure ages.

The surface exposure ages fall into two distinct clusters; the total age ranges of three samples overlap between 5.4 and 4.8 ka and those of five samples between 2.3 and 1.4 ka (Fig. 2.3.3B). The uncertainty in the geochemical measurements for sample DE1 is large but the maximum exposure age is constrained by sample DW8 on the same terrace level further downstream. Due to upstream migration of knickpoints, DE1 cannot have been exposed earlier than DW8, giving a maximum exposure age of 5.4 ka. An analysis of the distribution of ages (Appendix A.3) indicates that, even under the

assumption of a progressive migration of knickpoints, large variations in knickpoint retreat rates (from < 0.25 to > 2 m/yr) would be required to produce such an age distribution over the last 8.5 ka. These variations, combined with the overlap of surface exposure ages across multiple terraces (Fig. 2.3.B) and limited retreat of the waterfalls over historical times (Fig. 2.3.1C), lead us to interpret the surface exposure age clusters as indicators of rapid upstream propagation of knickpoints during two periods of intense canyon cutting ~5 and ~2 ka ago (Appendix A.3). Importantly, the ages show that sections of the lower terrace and the overspill channel were exposed simultaneously 2 ka ago, indicating that multiple knickpoints were actively migrating at different elevations at this time. The Sanddalur overspill channel contains samples that have ages in both clusters, which is evidence for erosion in this channel during both the identified canyon cutting periods.

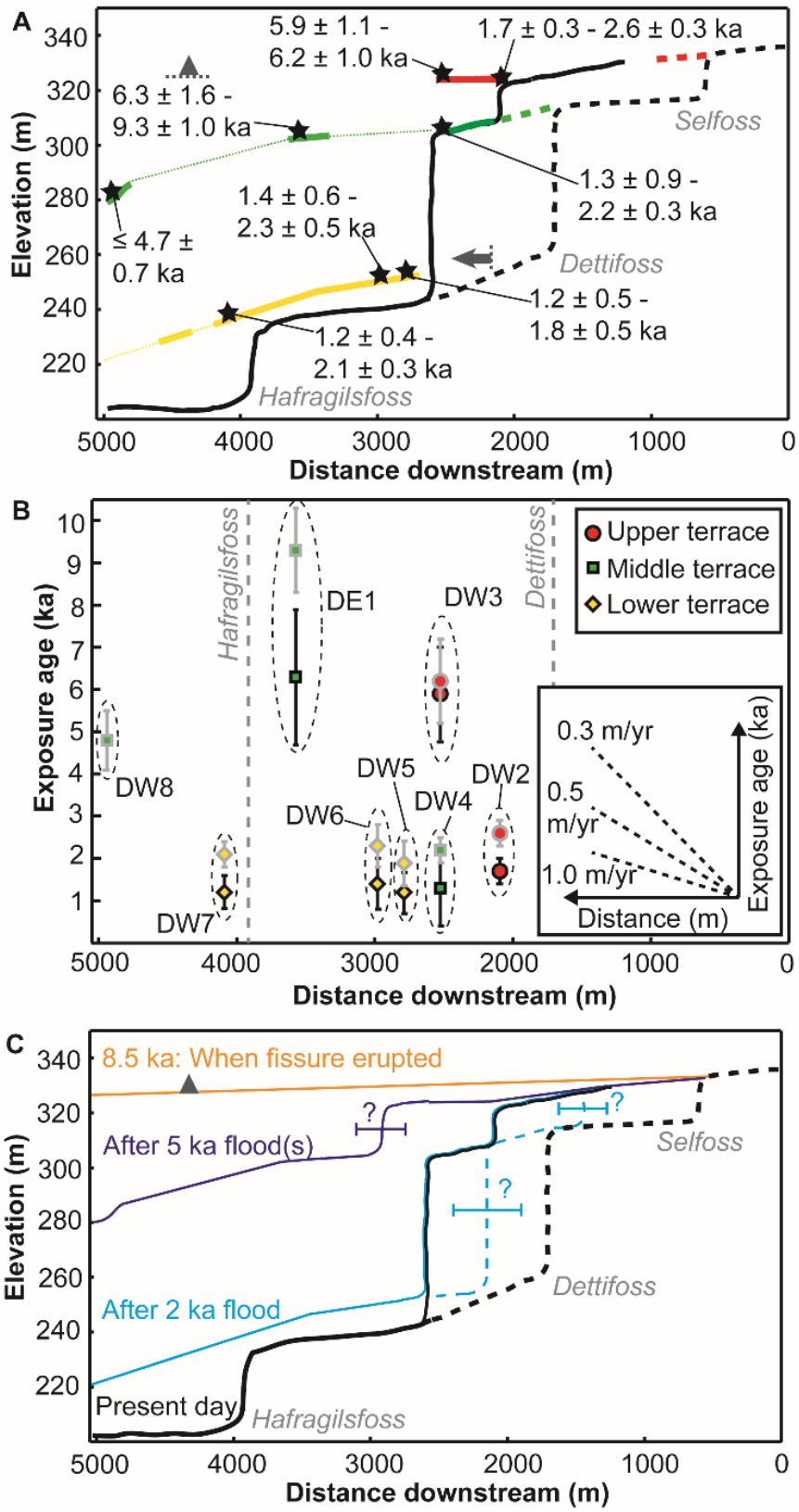

Fig. 2.3.3: Surface exposure ages and model of canyon evolution during the Holocene **A.** Long profile of the Jökulsá á Fjöllum through the study reach shown in black and locations

and elevations of the strath terraces shown in red, green and yellow (same colours as Figs. 2.3.1 and 2.3.2). Upstream of the confluence between the overspill channel and the main channel, the dashed lines indicate the topography within the main channel and the solid line indicates the topography within the overspill channel (*idem* in C). Exposure age ranges are provided for each sample, with the younger age calculated assuming there is no radiogenic ^{4}He in the sample and the older age calculated assuming all ^{4}He is radiogenic in origin (see Appendix A.1). The triangle marks the elevation and the location of the volcanic fissure that erupted 8.5 ka ago. Bold arrow marks the beginning of the over-widened gorge within the main channel. **B.** Surface exposure age ranges of the samples plotted against distance downstream (min. age in black and max. age in grey). Error bars represent the analytic error (2σ) for each sample (Table A1). The ages fit clearly into two clusters from 5.4 to 4.8 ka and from 2.3 to 1.4 ka, demonstrating that large stretches of the terraces were exposed at the same time, interpreted to result from the upstream propagation of knickpoints during extreme flood events during these periods. Inset shows lines of age = *f* (distance) corresponding to different knickpoint retreat rates (0.3, 0.5 and 1.0 m/yr), with 0.3 m/yr representing the rate at which Dettifoss would have retreated if retreat were steady since 8.5 ka. Inset plotted at the same scale as the main graph, so slope of lines can be directly compared to the distribution of exposure ages **C.** Proposed evolution of the canyon during the Holocene. The strath terraces and exposure ages have been used to reconstruct the long profile of the Jökulsá á Fjöllum when the fissure erupted (in orange), after the 5 ka flood event(s) (in dark blue) and after the 2 ka flood event (in light blue). There has been no subsequent erosion since the 2 ka extreme flood event within the overspill channel. Bars with question marks indicate uncertainty on the position of knickpoints (palaeo-Dettifoss at 2 ka ago is likely to be where the gorge over-widens).

Ásbyrgi, located 25 km downstream of the study reach (Fig. 2.3.1), has a very similar morphology to canyons in Idaho, with an amphitheatre shaped canyon head and a vertical headwall, typical of formation during an extreme flood event (Lamb *et al.*, 2008; 2014). There is no current overland flow or spring flow into the canyon capable of eroding or transporting the large boulders (size typically ranging between 0.5 and 3 metres) found in the canyon. Furthermore, the Klappir area immediately upstream of the canyon rim exhibits clear scabland morphology reminiscent of other landscapes that have experienced extreme flood events (e.g., Bretz, 1923) (Fig. 2.3.1). A sample collected from scoured bedrock in an eroded notch at the rim of

Ásbyrgi gives a range for the exposure age of 8.8 ± 1.6 ka to 11.0 ± 1.5 ka (see Appendix A.1 for explanation of upper and lower age limits on each sample), much earlier than either of the age clusters from the samples further upstream. Therefore, we infer that there was an erosive flood event along the Jökulsá á Fjöllum in the early Holocene. The absence of fluvial reworking and the outstanding preservation of the geomorphological features in the Klappir area indicate that the Jökulsá á Fjöllum never reoccupied the Klappir area following this flood event that likely carved the Ásbyrgi canyon. The floodwaters of the subsequent extreme flood events must therefore have been funnelled through the modern Jökulsá á Fjöllum canyon further east, though overspilling with minimal erosive impact over the Klappir area cannot be ruled out.

2.3.5 Discussion

This study has identified three periods of intense canyon cutting in two reaches of the Jökulsá á Fjöllum throughout the Holocene. Our exposure ages alone do not allow us to distinguish between the impact of a single flood or a series of flood events during the periods of rapid canyon cutting identified, due to levels of uncertainty. However, previous work has identified one extreme flood event in the early-Holocene and one in the late-Holocene by dating sedimentary deposits (Waitt, 2002); we tie the evolution of the bedrock landscape at Ásbyrgi and at Dettifoss to these early Holocene (~9 ka ago) and late Holocene (1.5-2 ka ago) flood events, respectively. Around 15 km downstream of Dettifoss, a sedimentary sequence containing up to 16 flood layers is believed to record events since 8 ka (Waitt, 2002). The youngest two events in this sequence have been dated to 5.0 and 4.6 ka (Kirkbride *et al.*, 2006), consistent with our cluster of exposure ages at ~5 ka. We therefore hypothesise that the knickpoint retreat identified at ~5 ka is the result of one or both of these floods; the older floods identified in the sequence would have contributed to the migration of knickpoints between Ásbyrgi and Dettifoss. We believe the possible influence of inherited cosmogenic ^{3}He is minimal. Firstly, it is unlikely that all ^{3}He is inherited

because samples with different exposure ages are found on a single terrace. Secondly, exposure ages on different terrace levels overlap in two clusters that fit with the timing of floods identified in the stratigraphic record. We acknowledge that all ages are similar on the lower terrace, which could reflect inheritance (the real exposure age of the surface may be much younger); however, because these ages overlap with other ages on the middle and upper terrace (Fig. 2.3.3B), we privilege a scenario where inheritance is minimal and the ages reflect the true exposure age.

It is known that there was no incised gorge in the early Holocene when the volcanic fissure erupted onto the surface (Fig. 2.3.3C), but there was an extreme flood event around this time which carved Ásbyrgi further downstream. The clustering of ages from the middle terrace and the overspill channel shows that there was a second period of intense canyon cutting between 5.4 and 4.8 ka which led to ~40 m of vertical incision at the apex of the fissure and the formation of a knickpoint between the upper and middle terraces (Fig. 2.3.3C). Our exposure ages show that the entire length of the lower terrace within the study reach (> 2.5 km) was exposed during another period of intense canyon cutting ~2 ka ago, associated with the retreat of the ~50 m high knickpoint that makes up Dettifoss. It is hypothesised that this knickpoint retreated to where the canyon is no longer over-widened (where the contemporary river fills the whole width of the canyon; Fig. 2.3.1, 2.3.3C), with Dettifoss migrating a further ~500 m to its current location since the last extreme flood event (at an average rate of ~0.3 m/yr). There has also been some erosion since the last extreme flood event further downstream, with the lower terrace becoming abandoned, and we suggest that this has occurred during a series of small flood events, although we do not have direct evidence for this from our surface exposure ages as it was impossible to collect samples from the bottom of the canyon. We suggest the knickpoints themselves were generated at the coast in the early stages of the Holocene, possibly during the RSL lowstand (Section 2.1.1), exploiting weaknesses in the lava flows due to the plucking of large blocks. Once the knickpoints were generated over the height of one or more lava flows, the vertical headwall of

the knickpoints was maintained as they propagated upstream through the toppling and transportation of the lava columns.

Calculations based on the model described in Lamb and Dietrich (2009) indicate that a minimum water depth of 8.1 m would be required to initiate toppling of the basalt columns in the study area, corresponding to a minimum discharge of 3250 m^3/s at Selfoss (Appendix A.2.2). Such discharge is six times higher than the maximum peak discharge recorded between 1973 and 1979 in this region (Schunke, 1985, Data from Icelandic Met Office) and twice the discharge associated with floods that occur approximately twice per century (Helgason, 1987).

It is thought that the extreme flood events last for a period of days rather than months or years (Björnsson, 2002). The rates of knickpoint retreat during the short-lived Jökulsárgljúfur floods (hundreds of meters in days) are far greater than the highest documented long term knickpoint retreat rates in other rivers of a similar scale, such as the ~1.5 m/yr retreat rate of the Horseshoe Falls at Niagara between 1842 and 1905 (Gilbert, 1907). The cumulative effect of the two periods of intense canyon cutting in the mid- and late-Holocene, inferred to represent the effect of two or three extreme flood events, is 100 m of vertical incision at the downstream extent of the study reach over the last 8.5 ka, equivalent to an average of ~12 mm/yr; this rate is similar to some of the most rapidly eroding rivers in tectonically active settings, such as the Nanga Parbat in the NW Himalayas (Burbank *et al.*, 1996).

Vertical stepped knickpoints generated during extreme flood events can be diffused over time through abrasion and plucking of small blocks (Lamb *et al.*, 2014). This is exemplified by the incised slot gorge at Malad Gorge, Idaho: following an extreme flood event ~46 ka that formed a ~50-m-high waterfall, the Pointed Canyon knickpoint has been retreating at 0.025 m/yr for at least the last 33 ka while also diffusing the vertical headwall into a series of smaller steps (Lamb *et al.*, 2014). We do not find evidence for diffusion of the vertical headwalls of Selfoss, Dettifoss or Hafragilsfoss since the last erosive extreme flood event 2 ka ago, suggesting that the river has not made the

transition from the plucking-dominated erosive regime during the floods to an abrasion-dominated erosive regime during ‘background’ non-flood periods. Potential explanations for this observation include:

Firstly, bedload impact is the main driver of erosion and knickpoint retreat by abrasion (Cook *et al.,* 2013); the persistence of plucking-dominated morphology may therefore be attributed to a combination of high resistance to abrasion of the fresh basalt with limited transport of coarse bedload over the last 2 ka, supported by qualitative field observation of lack of coarse sediment (i.e., coarser than pebble size) upstream of the gorge. Secondly, expected flow depths in a bedrock constriction during the extreme floods would be far greater than the 8.1 m threshold value (modelled flow depths are up to 59 m in constrictions further upstream of our study area; Alho *et al.*, 2005), which supports the assertion that the dominant erosion mechanism during the flood events is through column toppling and transportation. Nine small outburst floods inundated the depositional sandur plain downstream of the Jökulsárgljúfur canyon between 1655 and 1730 (Ísakkson, 1985): they may have acted to maintain the vertical headwall of the larger knickpoints, while also contributing to the ~500 m retreat of Dettifoss, the retreat of Hafragilsfoss and the abandonment of the lower terrace, possibly through the diffusion of small steps into rapids between Dettifoss and Hafragilsfoss. The recent spatial stability of Dettifoss despite an ~5 m retreat of the western part between 1953 and 1998 is demonstrated by analysing historical aerial photographs (Fig. 2.3.1C), suggesting that a flow depth that exceeds the block toppling threshold has not occurred during this time period. Finally, a key part of the model of knickpoint retreat through block toppling (Lamb and Dietrich, 2009) is the destabilising effect of buoyancy forces acting in the plunge pool at the base of the headwall. There is a small set of rapids upstream of Selfoss, which possibly formed after a small vertical step (in the order of a couple of metres) was diffused through abrasion (Fig. 2.3.1B). We suggest that the larger plunge pools at the larger knickpoints may act to support the maintenance of a vertical headwall by promoting the collapse of basalt columns. Where knickpoints are not of sufficient size to generate a

plunge pool, abrasion will act to diffuse the knickpoint into a series of rapids over time. In our study area, the threshold knickpoint height would be between 2 and 13 m.

2.3.6 Conclusions

Our work demonstrates the importance of thresholds in landscape evolution, with significant landscape change occurring during extreme floods when a flow depth threshold has been surpassed. Two periods of intense canyon cutting in the mid and late Holocene are identified at the apex of the Jökulsárgljúfur canyon, thought to have been the result of discrete erosive flood events during these periods. The erosive impact of an additional flood in the early Holocene is also identified further downstream at Ásbyrgi. The effects of these floods have dominated the long term (multi-millennial) evolution of the system, with the resulting landscape morphology containing a legacy of extreme floods that can be maintained over millennial timescales, despite the occurrence of many other floods of lesser magnitude. Erosion is primarily through the upstream migration of knickpoints associated with the toppling and removal of basalt columns. During each period, up to three >13 m-high knickpoints retreated over distances that could exceed 2 km. The cumulative effect of the extreme floods at the apex of the canyon is up to 100 m of vertical erosion over the last 8.5 ka, equivalent to an average vertical incision rate of ~12 mm/yr, two orders of magnitude higher than average erosion rates in East and South Iceland (Geirsdottir *et al.,* 2007). This highlights the importance of high-magnitude, low-frequency flood events in shaping landscapes and the need to consider them when analysing or forecasting the evolution of landscapes, especially those that are prone to flooding through landslide, moraine or ice-dam failures or subglacial lake outbursts. In landscapes dominated by stacked basaltic lava flows, erosion through the toppling of columns generates a clear morphological signature characterised by vertical knickpoints. Limited bed load sediment transport and plunge pools at the base of high knickpoints may be responsible for the persistence of these features over long periods of time (> 2 ka).

Sub-Chapter 2.4: Catastrophic impact of extreme flood events on the morphology and evolution of the lower Jökulsá á Fjöllum (northeast Iceland) during the Holocene

Baynes ERC, Attal M, Dugmore AJ, Kirstein LA, Whaler KA (2015) Catastrophic impact of extreme flood events on the morphology and evolution of the lower Jökulsá á Fjöllum (northeast Iceland) during the Holocene. *Geomorphology.* DOI: 10.1016/j.geomorph.2015.05.009

2.4.0 Sub-Chapter outline

This sub-chapter has been accepted for publication in *Geomorphology* and is currently *in press*. My contribution to this work is substantial as I carried out every stage of the work from research design, data analysis and paper writing. I designed the initial research plan with my supervisors in Edinburgh; Mikaël Attal, Andrew Dugmore and Linda Kirstein. Mikaël and I carried out the topographic surveys and mapped the field evidence for extreme flood events in the field. I carried out the analysis using the remotely sensed data (aerial imagery and DEM). Kathy Whaler introduced me to the Electrical Resistivity Tomography geophysics technique; I collected this data in the field. Kathy then guided me through the subsequent data processing and interpretation but I carried out all of the analysis and produced the figures myself. I collectively brought all the different aspects of this paper together and developed the discussion and model of the evolution of the canyon.

The main bulk of the sub-chapter (Section 2.4.1) can be read as a standalone unit, although the detail of the method employed for the palaeo-discharge estimate from the boulder size is given in Appendix B. Some of the content may appear to be a repeat of earlier sub-chapters (e.g. 2.1 and 2.2), but this is to ensure this sub-chapter can be read as a standalone unit suitable for publication.

2.4.0.1 Abstract

The impact of extreme flood events is rarely considered in studies of long-term landscape evolution, despite the potential for catastrophic landscape change in a short period of time. Here, we use an integrated approach of geomorphological mapping, topographic analysis and geophysical surveys to identify and quantify the impact of extreme flood events (jökulhlaups) along the Jökulsá á Fjöllum, Iceland, where evidence for the action of such floods is widespread on microspatial to macrospatial scales. The apex of the 28-km-long Jökulsárgljúfur canyon is characterised by a complex network of palaeo-flood channels and large vertical knickpoints such as Dettifoss (54 m high) and Hafragilsfoss (20 m high). Downstream, the Forvoð valley contains large terraces of boulder-rich deposits (50 m thick, > 3 km long). Near the outlet of the canyon is Ásbyrgi, a dry canyon (3 km long, 1 km wide, up to 90 m deep) with eroded cataracts and scabland morphology immediately upstream and ~90 m above the current river channel. Topographic analysis and electrical resistivity tomography surveys show that 0.144 km^3 of rock was eroded from Ásbyrgi during its formation ~10,000 years ago, and just 4% of this eroded volume is currently filled with sediment deposits, up to 5 m thick. Deposited boulders across the canyon floor of Ásbyrgi demonstrate that the discharge of the jökulhlaup that formed the canyon was at least 39,000 $m^3 s^{-1}$. We present a model for the evolution of the lower Jökulsá á Fjöllum and the Jökulsárgljúfur canyon during various stages of an extreme flood event. Reconstruction of the early Holocene flood event includes the initiation and development of different canyons before the capture of all floodwater within one canyon at the end. We tie the evolution of the lower Jökulsárgljúfur canyon to established chronology of flood events during the Holocene further upstream and highlight the dominant impact of extreme flood events over background processes in this landscape.

2.4.1 Introduction

Extreme flood events are characterised by the release of a large volume of water over the landscape in a short period of time. Such events occur in a range of environments and can be triggered by glacial lake outbursts (e.g. Baker *et al.*, 1993), landslide or moraine dam failures (e.g. Dunning *et al.,* 2006), or by subglacial volcanic eruptions (e.g. Björnsson, 2009; Dunning *et al.,* 2013). Extreme flood events are common over geological timescales, and the potential for geomorphic change during such events is great owing to high peak discharges, potentially over 10^6 m^3 s^{-1} (Baker, 2002). Previous work has identified the impact of extreme flood events in the evolution of a range of terrestrial environments such as the Channeled Scabland of northwestern USA following the draining of Glacial Lake Missoula (Bretz, 1923), the Tsangpo gorge of southeastern Tibet (Montgomery *et al.*, 2004), and the Transbaikalia and Altai Mountains of Siberia (Carling *et al.*, 2009a; Margold *et al.*, 2011); it has also been suggested that such floods could have played a key role in the evolution of the Straits of Gibraltar (Garcia-Castellanos *et al.*, 2009), the English Channel (Gupta *et al.,* 2007), and the surface of Mars (Warner *et al.*, 2010; 2013). Despite this, current landscape evolution models do not consider the impact of extreme flood events in controlling bedrock landscape morphology (Carling *et al.,* 2009b). Detailed quantitative studies of the impact of extreme flood events on the landscape are therefore required.

Glacial outburst floods, termed ‘jökulhlaups’, occur regularly in Iceland owing to the location of large ice caps atop active volcanoes (e.g. Björnsson, 2002), which makes Iceland a globally important place to study the impact of extreme flood events. Previous work on Icelandic jökulhlaups include the interpretation of deposited sediments (e.g. Maizels, 1997; Duller *et al.*, 2008; Marren *et al.*, 2009), the reconstruction of the hydraulic conditions (e.g. Baker *et al.,* 1993; Alho *et al.,* 2005; 2010; Carrivick, 2006; 2007) and the geomorphic impact of jökulhlaups in proglacial areas close to the floodwater source (e.g. Magilligan *et al.*, 2002; Carrivick *et al.*, 2004; Dunning *et al.*,

2013). Our current understanding of canyon formation and bedrock erosion processes during extreme flood events is limited, especially in distal areas, and is based on studies such as that of the Channeled Scabland in Washington, USA (e.g. Baker and Kale, 1998) and a small number of studies in Idaho, USA (Lamb *et al.,* 2008; 2014; Lamb and Dietrich, 2009) where the main motivation was to use the terrestrial landscape to infer the formation mechanisms of morphologically similar canyons on Mars. Building on recent work in the upper reaches of the Jökulsárgljúfur canyon, Iceland (Sub-Chapter 2.3 - Baynes *et al.*, 2015), the aim of this study is to reconstruct the bedrock landscape evolution of the lower Jökulsá á Fjöllum, in particular the impact of extreme flood events that are known to have occurred since deglaciation (Thórarinsson, 1950; Sæmundsson, 1973; Tomasson, 1973; Eliasson, 1974; 1977; Sigbjarnarson, 1996; Waitt, 2002; Kirkbride *et al.*, 2006; Sub-Chapter 2.3 - Baynes *et al.*, 2015). This objective is achieved through documenting an inventory of landscape features within the Jökulsá á Fjöllum that are characteristic of the work of extreme floods, establishment of the chronology of floods, and assessment of the geomorphic impact of these extreme flood events during the Holocene using topographic analysis and electrical resistivity tomography (ERT) surveys.

2.4.2 Study area

The Jökulsá á Fjöllum is one of Iceland's largest rivers, draining much of the 8,100 km^2 Vatnajökull ice cap in the south of the island and flowing 206 km north across central Iceland to the Arctic Ocean (Fig. 2.4.1A). The Jökulsá á Fjöllum has experienced multiple jökulhlaups of varying magnitude since the Last Glacial Maximum, with peak discharge for the largest flood estimated at 0.9×10^6 $m^3 s^{-1}$ (Alho *et al.*, 2005; Carrivick *et al.*, 2013). Jökulhlaups occur along the Jökulsá á Fjöllum as a result of either subglacial volcanism beneath Vatnajökull from one or more of the Kverkfjöll, Grímsvötn, or Bárðarbunga volcanic centres (Björnsson, 2009) or the release of floodwater from an ice-dammed lake to the south of Kverkfjöll (Björnsson, 2002) (Fig. 2.4.1B).

Attempts have been made to identify and interpret the impact of jökulhlaups in the Jökulsá á Fjöllum in recent history (Isaksson, 1985; Russell and Knudsen, 2002) and during the Holocene (Thórarinsson, 1950; Sæmundsson, 1973; Tómasson, 1973; Eliasson, 1974; 1977; Sigbjarnarson, 1996; Waitt, 2002; Carrivick *et al.*, 2004; Kirkbride *et al.*, 2006; Sub-Chapter 2.3 - Baynes *et al.*, 2015). Much of the recent work on this river has focussed on the geomorphic impact and sedimentary evidence of jökulhlaups close to the floodwater source (e.g. Carrivick *et al.,* 2004; Carrivick, 2007; Marren *et al.*, 2009) and on modelling the hydraulic conditions of the floods in mid-stream to upstream reaches (e.g. Alho *et al.,* 2005; Carrivick, 2006; 2007; Carrivick *et al.*, 2013). Chapter 2.3 (Baynes *et al.,* 2015) identified evidence for large-scale, rapid canyon cutting within the Jökulsárgljúfur canyon during three erosive periods in the Holocene, using cosmogenic nuclides concentrations to date the exposure of fluvially sculpted bedrock surfaces.

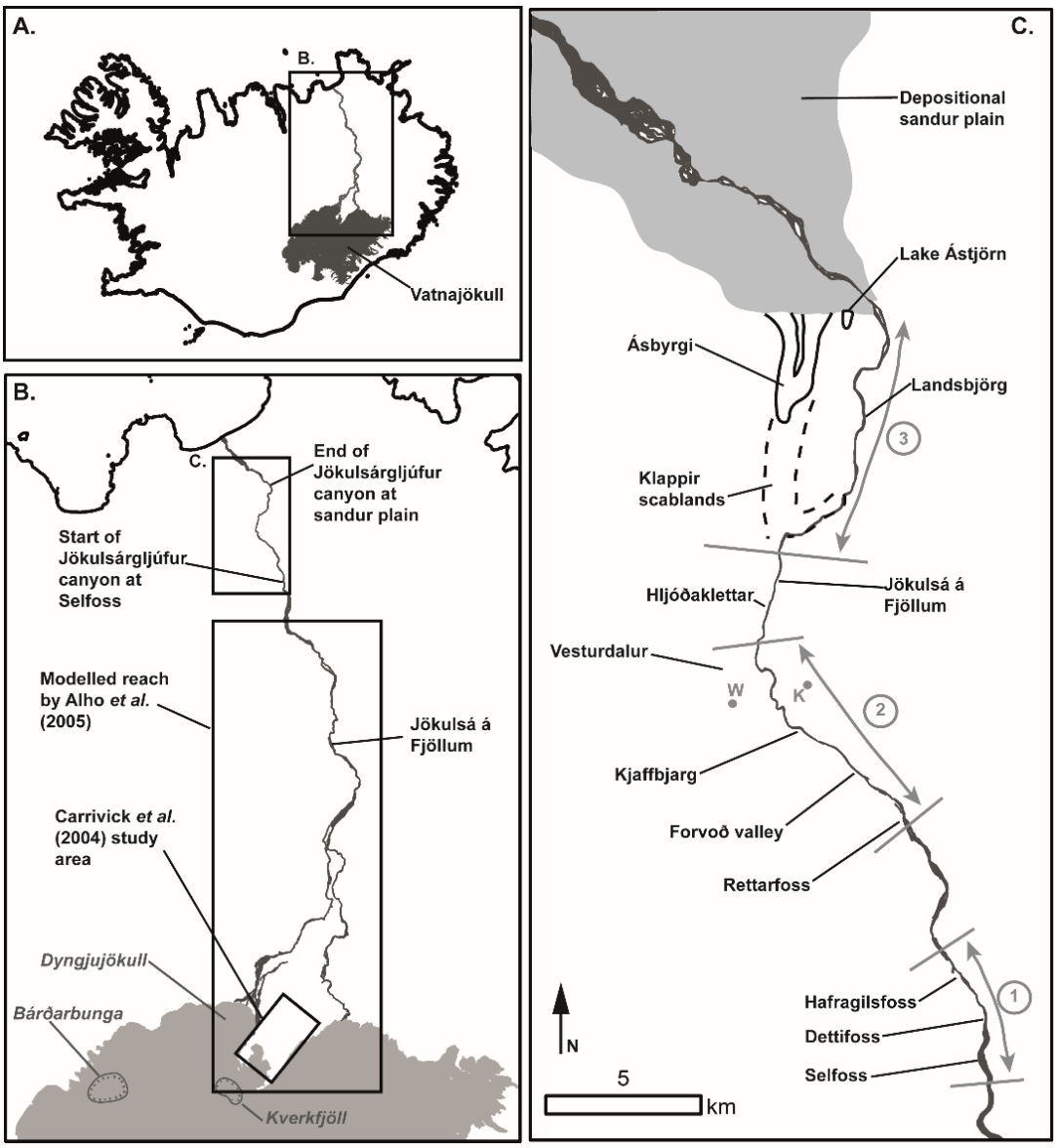

Fig. 2.4.1: A. Outline of Iceland with Vatnajökull ice cap (grey-shaded area), the source of the floodwaters, and the course of the present day Jökulsá á Fjöllum draining to the north coast. **B.** Zoomed in map showing the areas studied by previous authors (Carrivick *et al.*, 2004; Alho *et al.*, 2005) in the upper and middle reaches of the Jökulsá á Fjöllum as well as the Jökulsárgljúfur canyon, the focus of this study. Kverkfjöll and Bárðarbunga volcanic centres are highlighted. Grímsvötn volcano is located ~25 km south of Bárðarbunga, just beyond the extent shown in the map. **C.** The Jökulsárgljúfur canyon is divided into three sections for the study: (1) the apex of the Jökulsárgljúfur canyon between Selfoss and Hafragilsfoss; (2) the Forvoð valley, containing depositional landforms; and (3) the lowermost section of the Jökulsárgljúfur canyon, with the Ásbyrgi horseshoe and the Klappir scablands system. The grey points labelled 'W' and 'K' indicate the location of the sedimentary sequences discussed in Waitt (2002) and Kirkbride *et al.* (2006), respectively.

Three distinct reaches are identified within the Jökulsárgljúfur canyon, each exhibiting evidence for extreme flood events (Fig. 2.4.1C). The first reach is the main study area of Sub-Chapter 2.3 (Baynes *et al.*, 2015) at the head of the canyon. There, the Jökulsá á Fjöllum becomes deeply incised into the surrounding terrain, with three large waterfalls over a 5-km-long reach: these are Selfoss (13 m high), Dettifoss (54 m high), and Hafragilsfoss (20 m high); the canyon was carved through the retreat of these waterfalls during extreme floods. Downstream of this reach is the Forvoð valley, where widespread evidence for deposition of large volumes of sediment during extreme floods is present. At the lower end of the Jökulsárgljúfur canyon, additional evidence for the erosive impact of extreme flood events with the Klappir scablands area and Ásbyrgi canyon, a large dry cataract now disconnected from the current course of the Jökulsá á Fjöllum. This area contains outstanding preservation of large-scale fluvial landforms that have not undergone any alteration since their formation and therefore offer an excellent opportunity to quantify the impact of extreme floods. Downstream of this reach, the Jökulsá á Fjöllum flows for 18 km over a large depositional sandur plain to the coast. The geology of the area is characterised by young (< 0.8 Ma) basalt lava flows stacked on top of each other, ranging in structure from regular, near-vertical columns with metre-scale joint spacing to blocky, rubbly lavas with centimetre to decimetre scale jointing. The ages of abandoned bedrock surfaces show significant canyon formation occurred at Ásbyrgi ~10,000 years ago and at the head of the Jökulsárgljúfur canyon ~5,000 and ~1,500 years ago through the upstream migration of large knickpoints such as Dettifoss and Selfoss (Sub-Chapter 2.3 - Baynes *et al.*, 2015).

2.4.3 Morphological and sedimentological evidence for extreme floods along the Jökulsá a Fjöllum downstream of Selfoss

Carrivick *et al.* (2004) created a list of key criteria to identify the occurrence of extreme floods in bedrock channels, from macroscale landforms such as cataracts and anastomosing channels to microforms such as potholes and

flutes (Table 2.2.1 in Sub-Chapter 2.2). Notably, many of the landforms listed in Table 2.2.1 are not exclusive to the action of extreme flood events, and the presence of these landforms within a landscape should not necessarily lead to the conclusion that an extreme flood event has taken place (Carrivick *et al.*, 2013). However, considering the landscape as a whole and how multiple landforms are 'associated' to each other across a range of spatial scales can give an insight into the magnitude of the events that formed them (Carling *et al.*, 2009c). We use the criteria in Table 2.2.1 to document erosional and depositional landforms in the study landscape using field observations and aerial photographs. The following sections describe this evidence in each of the three study reaches (Fig. 2.4.1C): (i) Selfoss to Hafragilsfoss, (ii) the Forvoð valley, and (iii) Ásbyrgi and the Klappir scablands.

2.4.3.1 Selfoss to Hafragilsfoss

From the apex of the Jökulsárgljúfur canyon at Selfoss to ~5 km further downstream, the Jökulsá á Fjöllum becomes deeply incised into the surrounding terrain (Fig. 2.4.2). Exposed in the canyon wall ~4 km downstream of its head is a volcanic conduit that brought lava to the surface in a fissure eruption about 8.5 ka BP (Eliasson, 1974). This event provides an independent constraint on the maximum age for the formation of the canyon upstream of the fissure and indicates that at least 4 km of the canyon was cut in the last 8.5 ka. In this section, a clear pattern of multiple palaeo-channels has been cut into bedrock, including the Sanddalur overspill channel (200 m wide) that contains a 20-m-high cataract, a dry vertical waterfall characteristic of erosion during jökulhlaups (Carrivick *et al.*, 2004; Lamb *et al.*, 2008; 2014) (Fig. 2.4.3A), and a 50 m high cataract where the channel re-joins the western wall of the main canyon. The vertical headwalls of the three waterfalls in the active channel are also characteristic of the migration of knickpoints in columnar basalt environments during large floods (Lamb and Dietrich, 2009; Sub-Chapter 2.3 - Baynes *et al.*, 2015) (Fig. 2.4.3B). Further macroscale evidence for the action of extreme flooding is the relative size of the contemporary river compared to the size of the canyon. With the

exception of the 500-m reach immediately downstream of Dettifoss, the Jökulsá á Fjöllum does not fill the canyon floor, even during regular annual spate stages (peak annual discharge from 1973-1979 was ~500 $m^3 s^{-1}$ at Grimsstadir, 25 km upstream of Selfoss; Schunke, 1985, Data from Icelandic Met Office) (Fig. 2.4.3C). This underfit suggests that the canyon was formed when the flow in the river was significantly greater. Three distinct strath terrace levels are present within the canyon, indicating the palaeo-location of the river bed (Sub-Chapter 2.3 - Baynes *et al.,* 2015). All of these terraces, and the contemporary river bed, correspond to the top of lava flows. Despite small-scale fluting (on the scale of tens of centimetres) and sub-meter scale scouring on the strath terraces, evidence is limited for widespread vertical incision of the channel into the lava flows through abrasion. This fact demonstrates that the dominant mechanism of canyon erosion is the upstream propagation of knickpoints through the toppling and subsequent transportation of bedrock columns, once the flow depth has surpassed a threshold value (Sub-Chapter 2.3 - Baynes *et al.*, 2015).

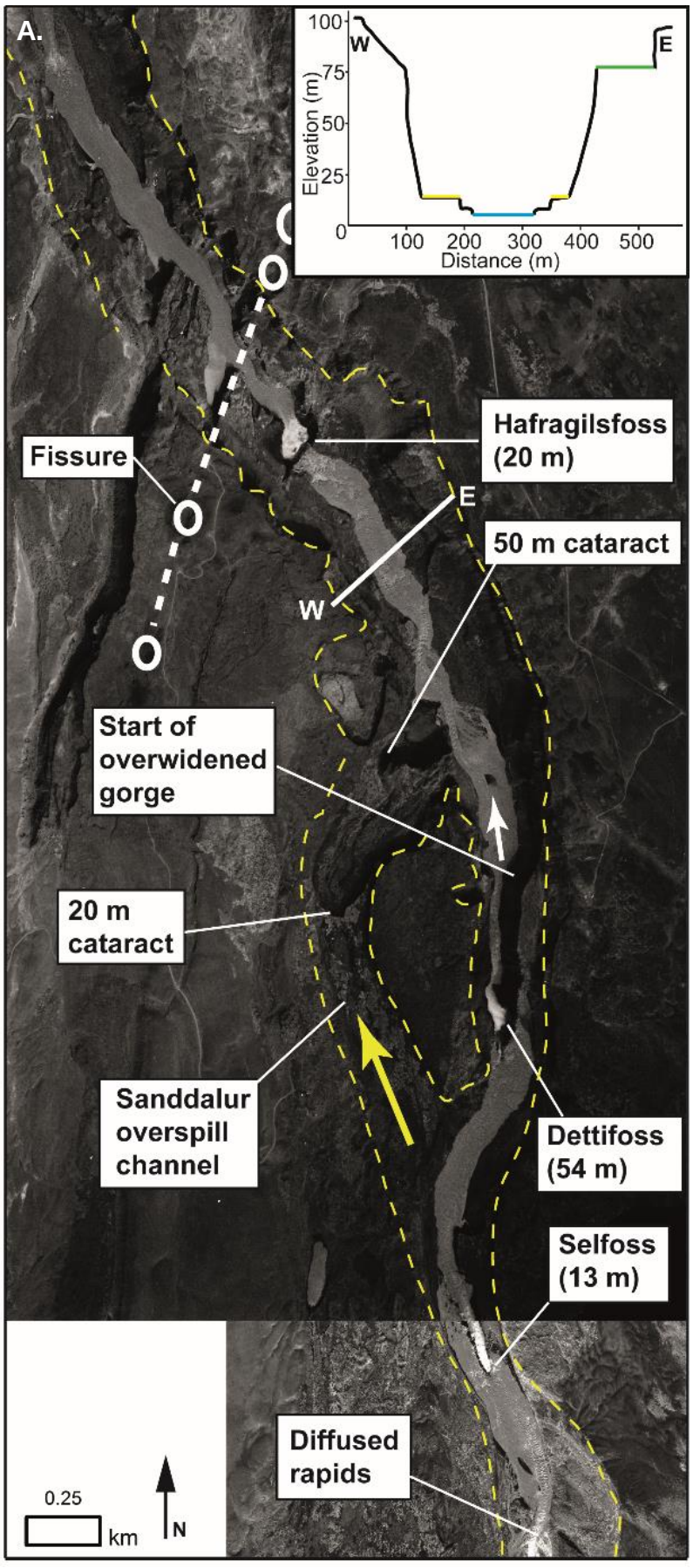
A.
100
75
50
25
0
Elevation (m)
W
E
100
200
300
400
500
Distance (m)
Hafragilsfoss
(20 m)
Fissure
E
W
50 m cataract
Start of
overwidened
gorge
20 m
cataract
Sanddalur
overspill
channel
Dettifoss
(54 m)
Selfoss
(13 m)
Diffused
rapids
0.25
km
N

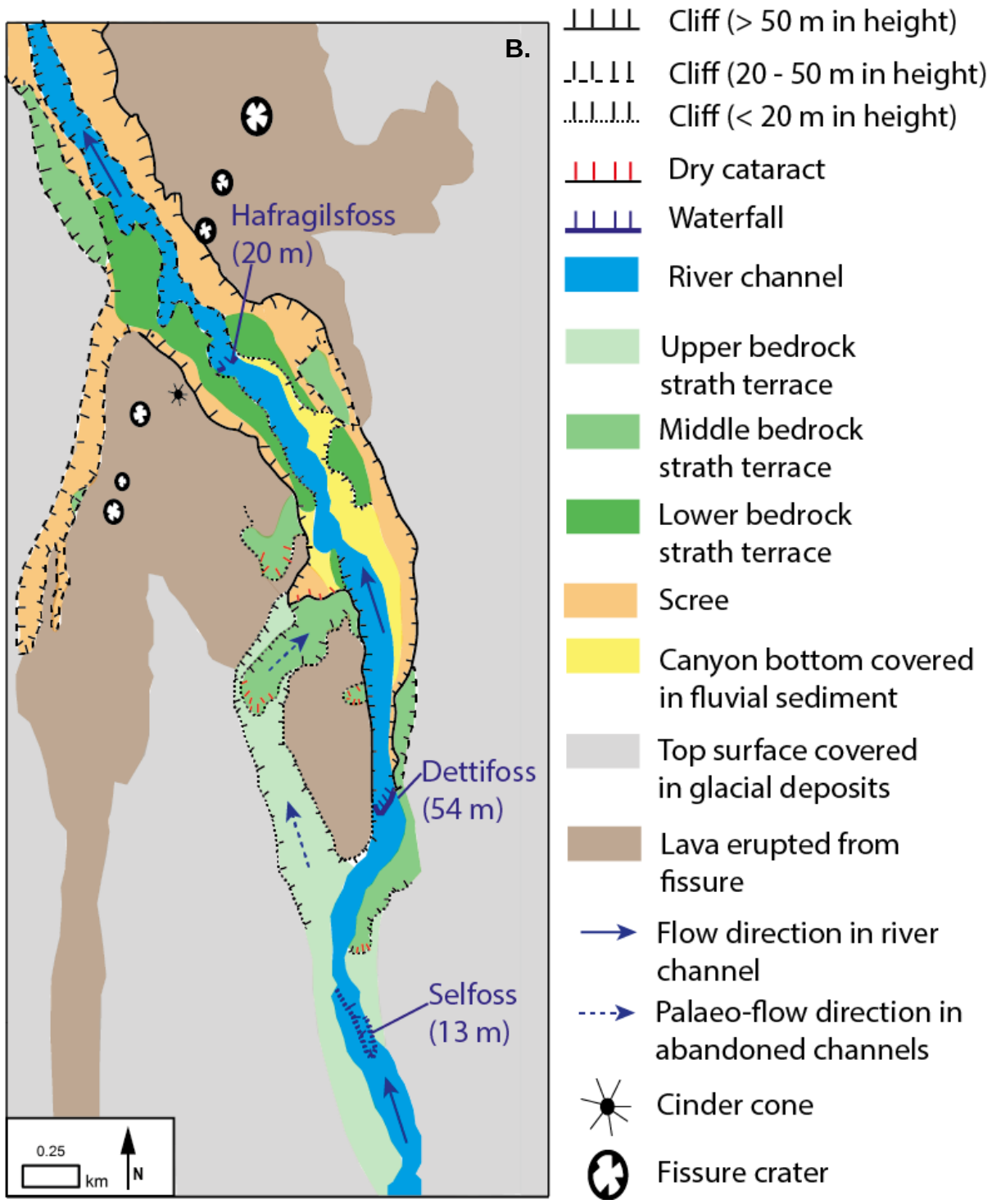

Fig. 2.4.2: Aerial photograph **(A)** and geomorphological map **(B)** showing the upper 5 km of the Jökulsárgljúfur canyon where the Jökulsá á Fjöllum is deeply incised with three vertical waterfalls; Selfoss (13 m in height), Dettifoss (54 m in height), and Hafragilsfoss (20 m in height) (adapted from Chapter 2.3 - Baynes *et al.,* 2015). The dashed yellow lines in A indicate the areas where evidence for erosion during extreme flood events is clear. The 200-m-wide Sanddalur overspill channel contains a 20-m vertical cataract and a 50-m vertical

cataract where it rejoins the main canyon. The fissure that erupted 8.5 ka ago (Eliasson, 1974) is highlighted with white circles in A and the cinder cones marked in B. A cross section of the gorge across the line from W to E is inset. With the exception of the 500 m of canyon immediately downstream of Dettifoss, the Jökulsá á Fjöllum does not fill the canyon, suggesting that the flow was much greater when the canyon was formed. Aerial photograph source: Landmælingar Íslands.

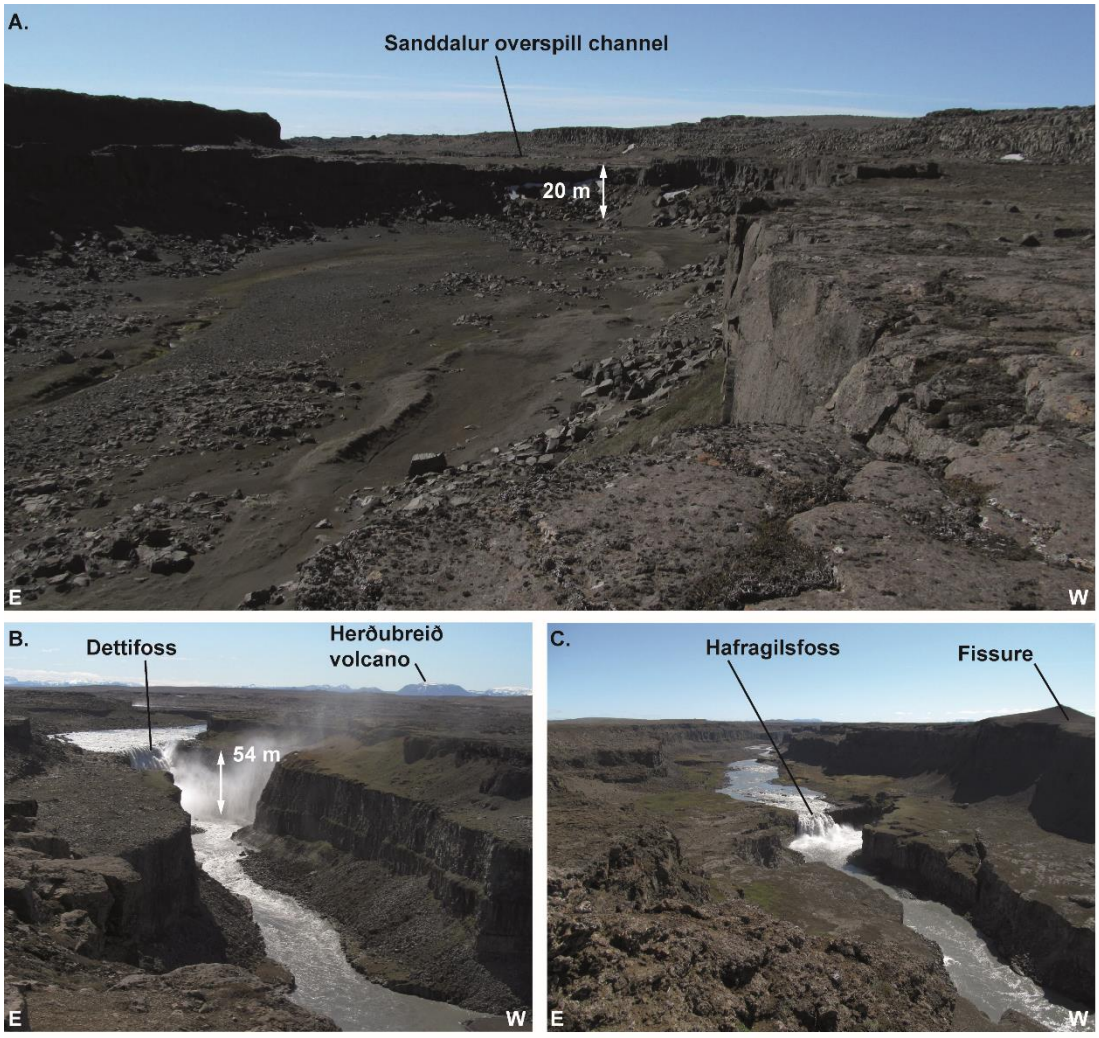

Fig. 2.4.3: Evidence for the impact of extreme flood events in the upper reach of the Jökulsárgljúfur canyon. **A.** Looking upstream (south): the Sanddalur overspill channel contains clear fluvially sculpted surfaces and a 20-m dry cataract. **B.** Looking upstream toward Dettifoss (54 m in height): the Jökulsárgljúfur canyon contains three large vertical waterfalls formed by the upstream retreat of knickpoints through the toppling of basalt

columns. **C.** Looking upstream toward Hafragilsfoss (25 m in height) from the location of the fissure that erupted 8.5 ka ago (Eliasson, 1974): the canyon cuts through the fissure, providing an independent constraint on the age of the canyon as all of the erosion has occurred since the fissure erupted. Strath terraces, indicating the palaeo-location of the river bed, can be seen on the edges of the canyon. Long stretches of these terraces have been exposed at the same time, including the Sanddalur overspill channel (Sub-Chapter 2.3 - Baynes *et al.*, 2015).

2.4.3.2 Forvoð valley to Vesturdalur

Nine kilometres downstream of the apex of the Jökulsárgljúfur canyon is the Forvoð valley, which contains landforms that testify to the action of extreme flood events in erosional and depositional contexts (Fig. 2.4.4A, B). Downstream of the Rettarfoss waterfall, the river is incised in a relatively narrow valley (20 m wide); 48 m above the current river channel on the eastern side of the valley is an extensive, heavily scoured bedrock surface with relief of up to a few metres (Fig. 2.4.4C); this surface was likely formed and then abandoned during an extreme flood (Waitt, 2002), and the high amplitude relief may be the result of efficient plucking promoted by the small size of the basaltic columns and intense fracturing, making blocks with size rarely exceeding 30 cm available for transport. Downstream of the slot canyon, the valley widens and landforms associated with deposition rather than erosion is evident. Boulder surfaces and boulder bars are defined by Carrivick *et al.* (2004) as ‘mesoform’ evidence for the action of extreme floods (Table 2.4.1), although they should also be considered on the macroscale here as they extend on both sides of the Forvoð valley for > 3 km and some of the deposits are up to 50 m thick (Fig. 2.4.5). On the western side of the river, boulder-rich deposits up to 47 m thick (some blocks > 1 m in diameter) are found above the current river level; and are two clear boulder-rich terraces are located on the eastern side of the valley, 5 m and 21 m above the river bed, respectively (Fig. 2.4.5). Such extensive, thick, and coarse deposits are likely associated with extreme palaeo-flow conditions (Wohl, 1992). We suggest that the boulder-rich sediment deposited in the

Forvoð valley is a result of floodwaters losing energy as they pond behind the forced narrowing caused by the bedrock constriction at Kjaffbjarg (Fig. 2.4.4A). Subsequent stages of the flood, or subsequent floods, have reworked the boulder-rich deposits in the valley, incising through them but preserving the terrace surfaces high on the valley sides.

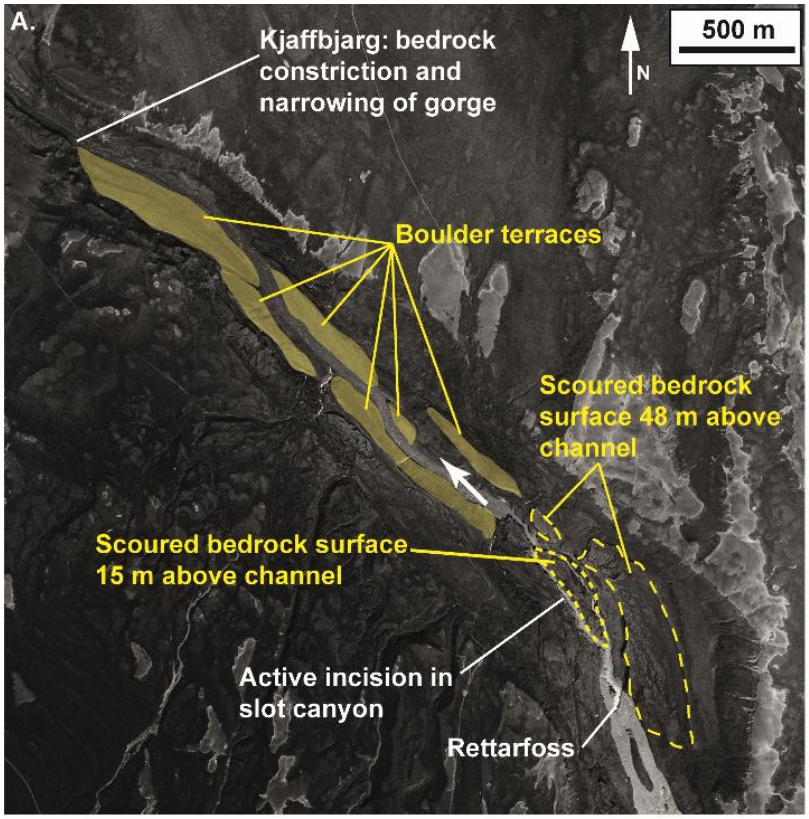

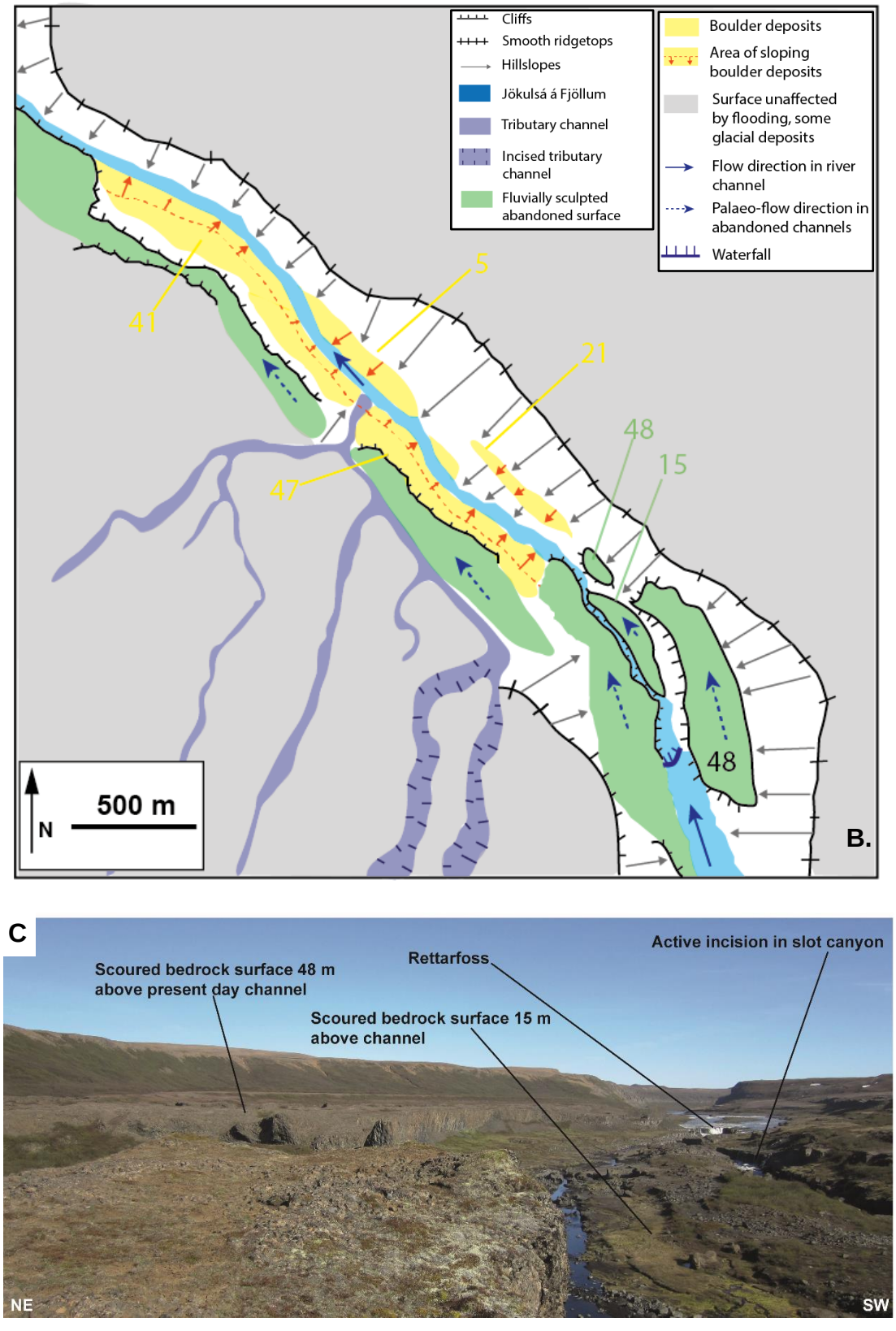

Fig. 2.4.4: Aerial photograph **(A.)** and geomorphological map **(B.)** of the Forvoð valley. Rettarfoss, the waterfall in the upstream part of a narrow, actively incising slot canyon, is

highlighted. The dashed yellow lines in A. indicate the heavily scoured bedrock surface 48 m above the current river channel and a lower bedrock terrace abandoned in the 1950s (Vatnajökulsþjóðgarður National Park Tourist Information). The yellow-shaded areas identify the large boulder terraces, thought to have been deposited during an extreme flood event, possibly owing to a backwater effect as a result of water ponding up behind the narrow bedrock constriction at Kjaffbjarg (also highlighted). Numbers in B are the elevation of the indicated surface above the present day river channel. Aerial photograph source: Landmælingar Íslands. **C.** Looking upstream toward Rettarfoss waterfall, showing the upper part of the Forvoð valley and the strath terraces identified in **A**. The surface is heavily scoured due to the rubbly nature of the bedrock. The columns are thin, not well developed, and fractured such that joint spacing between blocks rarely exceed 30 cm, making blocks easily plucked and transported.

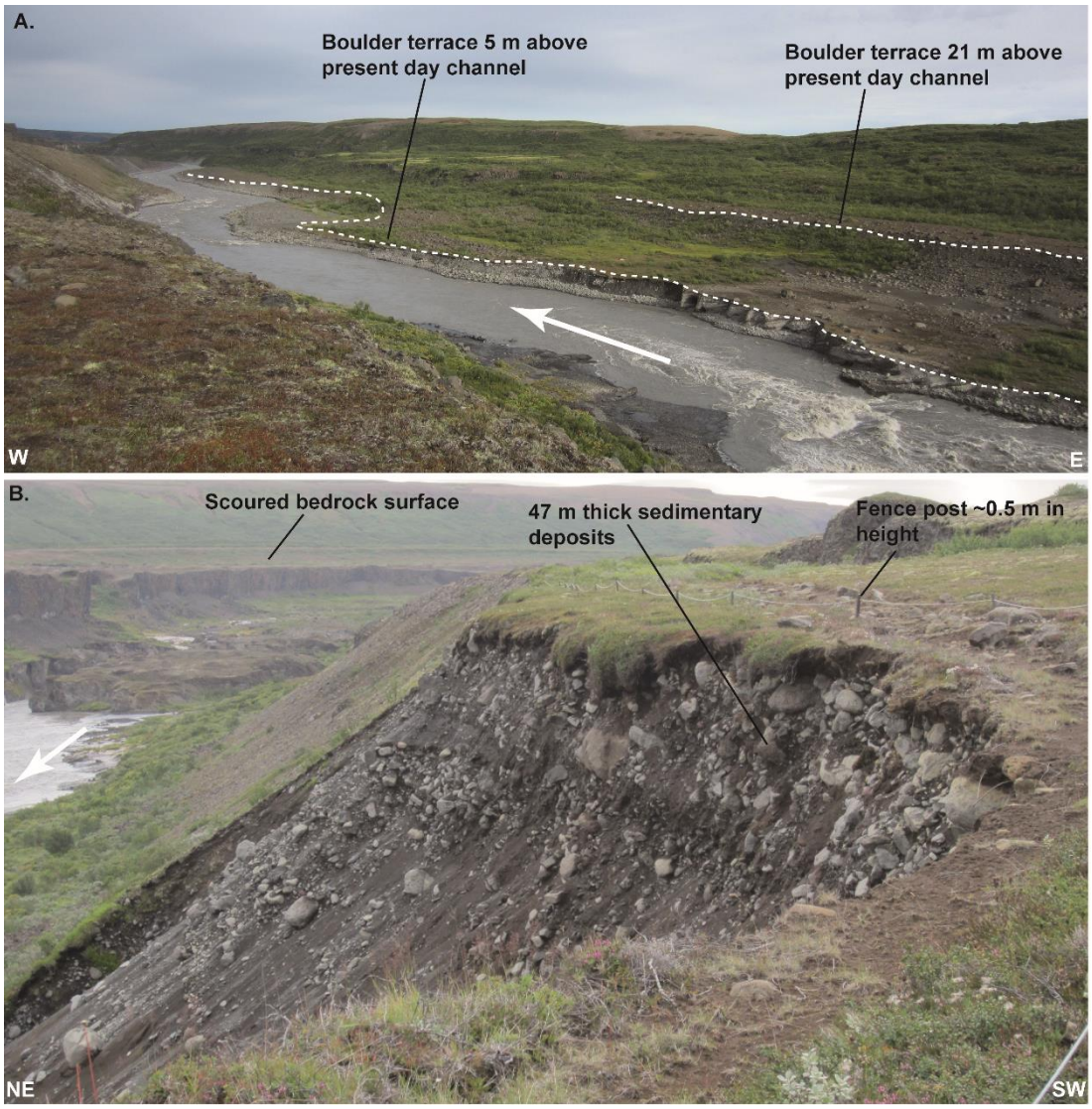

Fig. 2.4.5: Within the Forvoð valley, large boulder-rich terraces are exposed on both sides of the valley. On the eastern side of the valley, two terraces made up of sediment containing abundant large boulders are located 5 and 21 m above the current river level as seen in **A.** The white arrow indicates the direction of flow of the river. On the western side of the valley, one large fill terrace is present that is 47 m thick and contains boulders with diameter > 1 m, shown in picture **B** (taken looking upstream); the scoured bedrock terrace from Fig. 2.4.4 is shown in the background of the photograph. For scale, the fence posts on the top of the deposits are ~0.5 m high.

Downstream of the Kjaffbjarg bedrock constriction, the Jökulsá á Fjöllum flows within a deeply incised scabland area at Vesturdalur (Fig. 2.4.1C) before flowing along the eastern edge of another post-glacial volcanic fissure at Hljóðaklettar (Eliasson, 1974; Waitt, 2002). Vesturdalur is a key location of previous studies that have identified extreme flood events along the Jökulsá a Fjöllum. Waitt (2002) and Kirkbride *et al.* (2006) identified sedimentary sequences containing sandy flood deposits from this location (Fig. 2.4.1C). Waitt (2002) identified up to 16 sandy flood layers high above the west side of the Jökulsá á Fjöllum thought to have been laid down between 8,000 and 4,000 years ago, constrained by the presence of H4 and H3 tephra layers in the sequence that were deposited following eruptions of Hekla volcano ~3,800 yr BP and ~2,900 yr BP, respectively (Kirkbride *et al.*, 2006). Two flood layers in a sequence on the eastern side of the valley, corresponding to the layers at the top of the sequence identified by Waitt (2002), were dated by Kirkbride *et al.* (2006) to 5,020 and 4,610 cal. yr BP. This sedimentary evidence suggests that multiple large flood events affected this part of the canyon during the mid-Holocene.

2.4.3.3 Ásbyrgi and Klappir scablands

Perhaps the most striking evidence for erosion during extreme floods along the Jökulsá á Fjöllum can be found at Ásbyrgi canyon and the Klappir scablands. Ásbyrgi is a horseshoe-shaped canyon (3 km long, 1 km wide, up to 90 m deep), which is disconnected from the current river that now flows in

a deeply incised canyon at Landsbjörg to the east (Figs. 2.4.1C, 2.4.6). Between Ásbyrgi and the main Jökulsárgljúfur canyon is Lake Ástjörn, a small cataract now filled with water, that exhibits the same amphitheatre shape as Ásbyrgi albeit on a smaller scale (250 m wide). Upstream of Ástjörn is a narrow scabland tract leading from the main Jökulsárgljúfur canyon but hanging ~60 m above the modern river. Ásbyrgi has been cut into a succession of lava flows with a northward dipping surface (slope: 0.025). The Klappir scablands are a flood-scoured area of bedrock ridges and pools that clearly mark out the route of the floodwaters into the head of Ásbyrgi (Figs. 2.4.6/2.4.7B). At the 'upstream' (southern) end of the area are four smaller (100 m wide, 10 m high) amphitheatre-shaped cataracts that also open toward the north (indicating flow direction from the south), which are located high (~90 m) above the current course of the river (Fig. 2.4.7). These cataracts include plunge pools at the base of the headwall featuring sediment ridges that could be interpreted as push-bars (Carling *et al.*, 2009c); these bars show no obvious reworking since their formation (Fig. 2.4.7A). At the rim of Ásbyrgi, large-scale potholes (up to 10 m in depth) and flutes are clearly visible (Fig. 2.4.7C), and several notches (3-5 m in height) have been cut into the rim of the vertical headwall of the canyon (Fig. 2.4.8A). The exposure age of bedrock in one of these notches has been put at between 7.2 and 12.5 ka, indicating that Ásbyrgi and the Klappir scablands were formed during an extreme flood event in the early Holocene, shortly after deglaciation (Sub-Chapter 2.3 - Baynes *et al.*, 2015).

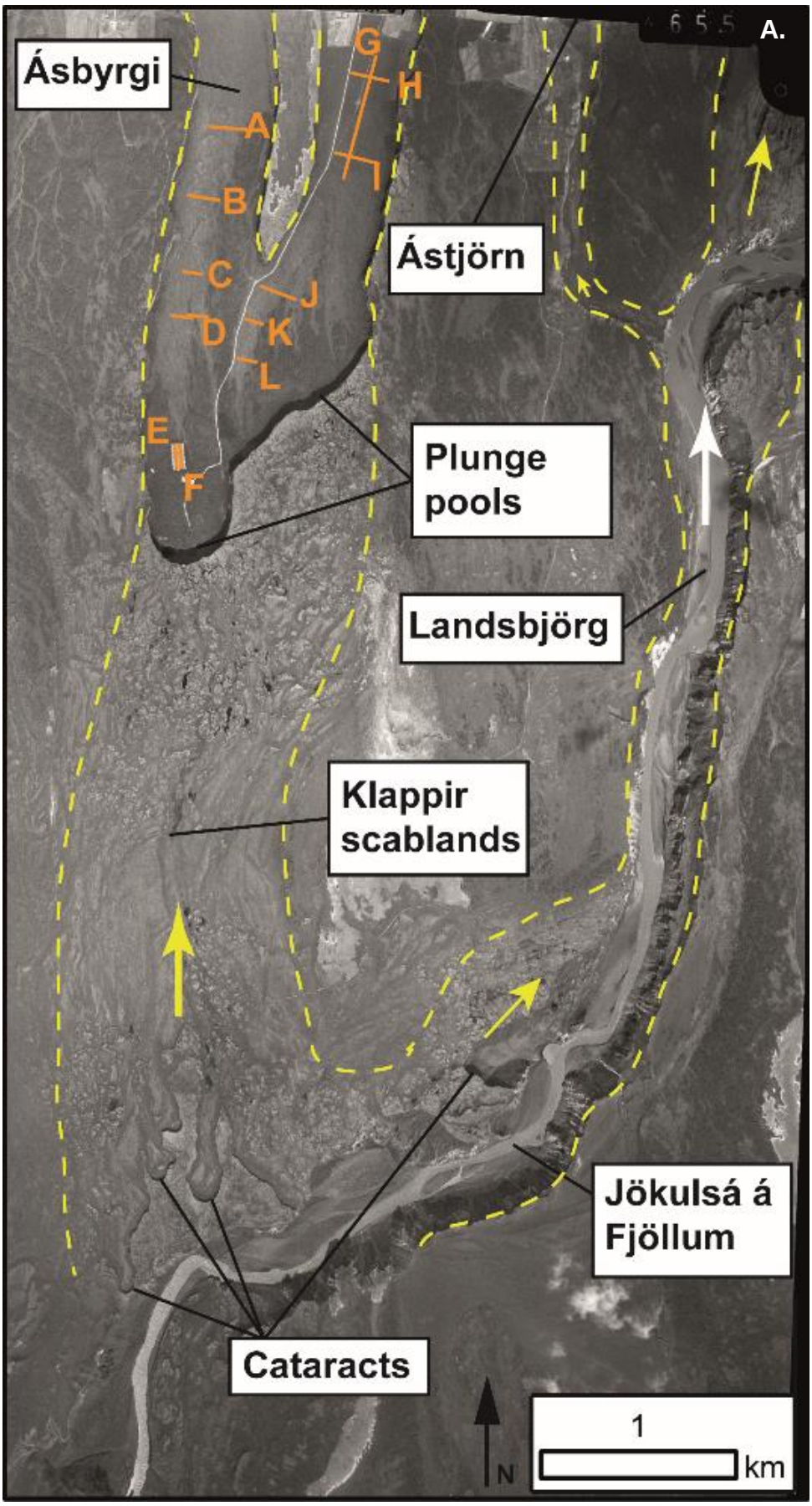
A.
Ásbyrgi
A
B
C
D
E
F
G
H
I
J
K
L
Ástjörn
Plunge pools
Landsbjörg
Klappir scablands
Jökulsá á Fjöllum
Cataracts
N
1
km

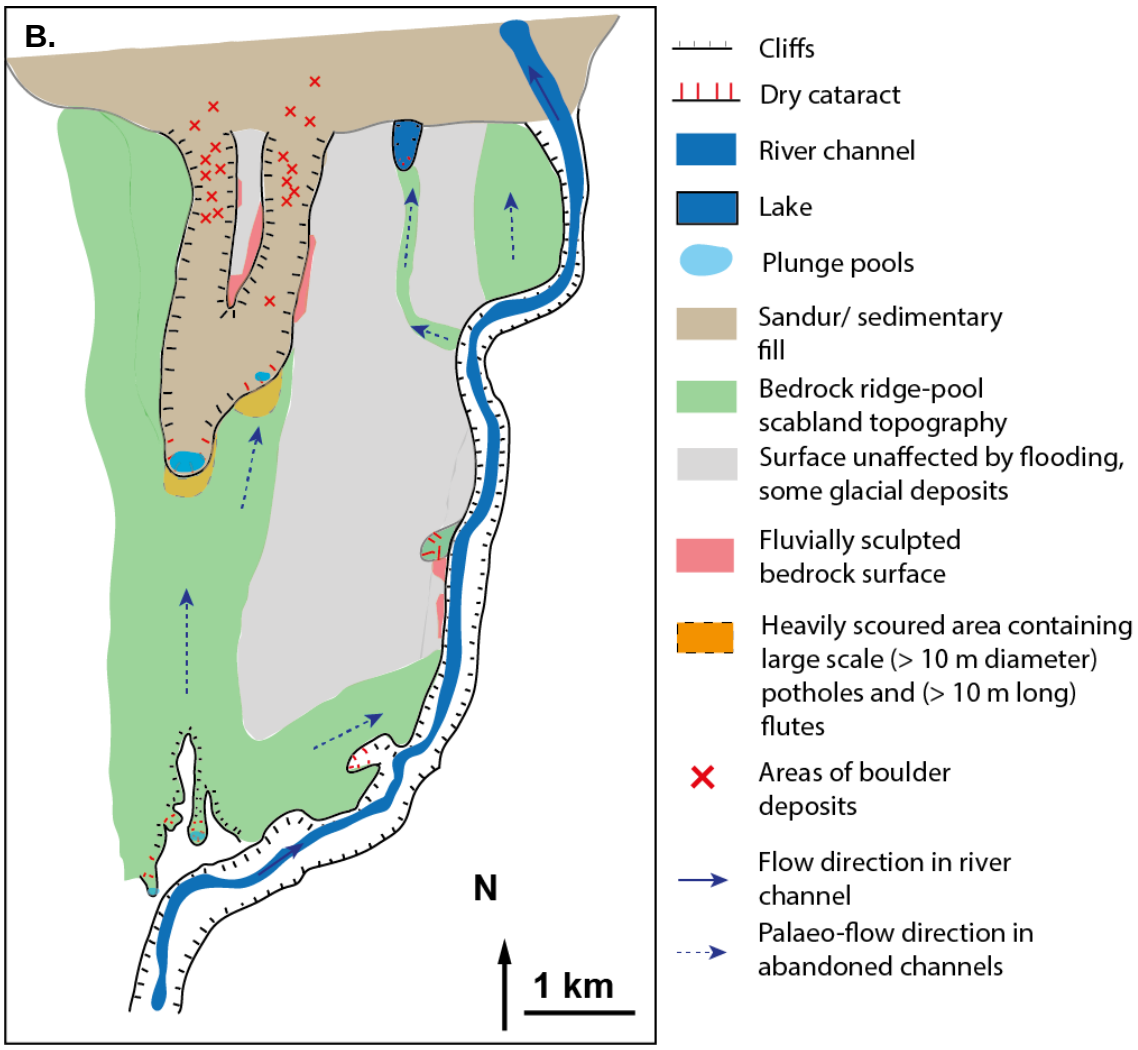

Fig. 2.4.6: Aerial photograph **(A)** and geomorphological map **(B)** of the Klappir scablands and Ásbyrgi canyon. The present day course of the Jökulsá á Fjöllum is within the deeply incised main Jökulsárgljúfur canyon that flows to the east at Landsbjörg. Ásbyrgi is a large (3-km-long, 1-km-wide) horseshoe-shaped canyon cut into a northward-dipping lava succession with an island preserved between the two main channels. The yellow dashed lines indicate the areas in A and the green areas in B that have been inundated by floodwaters, with the Klappir area of scabland topography with bedrock ridges and pools clearly visible. At the upstream limit of the scablands, four dry cataracts provide additional evidence for erosion during an extreme flood event in this area. The locations of the plunge pools at the apex of the western and eastern Ásbyrgi canyons are shown, and the area of large scale erosional landforms (Fig. 2.4.7) is marked in B. The red areas in B correspond to areas of fluvially sculpted bedrock shown in Fig. 2.4.9. The orange lines in A within Ásbyrgi indicate the location of the electrical resistivity tomography (ERT) surveys in the canyon floor, with letters corresponding to the profiles in Fig. 2.4.11. Aerial photograph source: Landmælingar Íslands (A. Adapted from Sub-Chapter 2.3 - Baynes *et al.*, 2015).

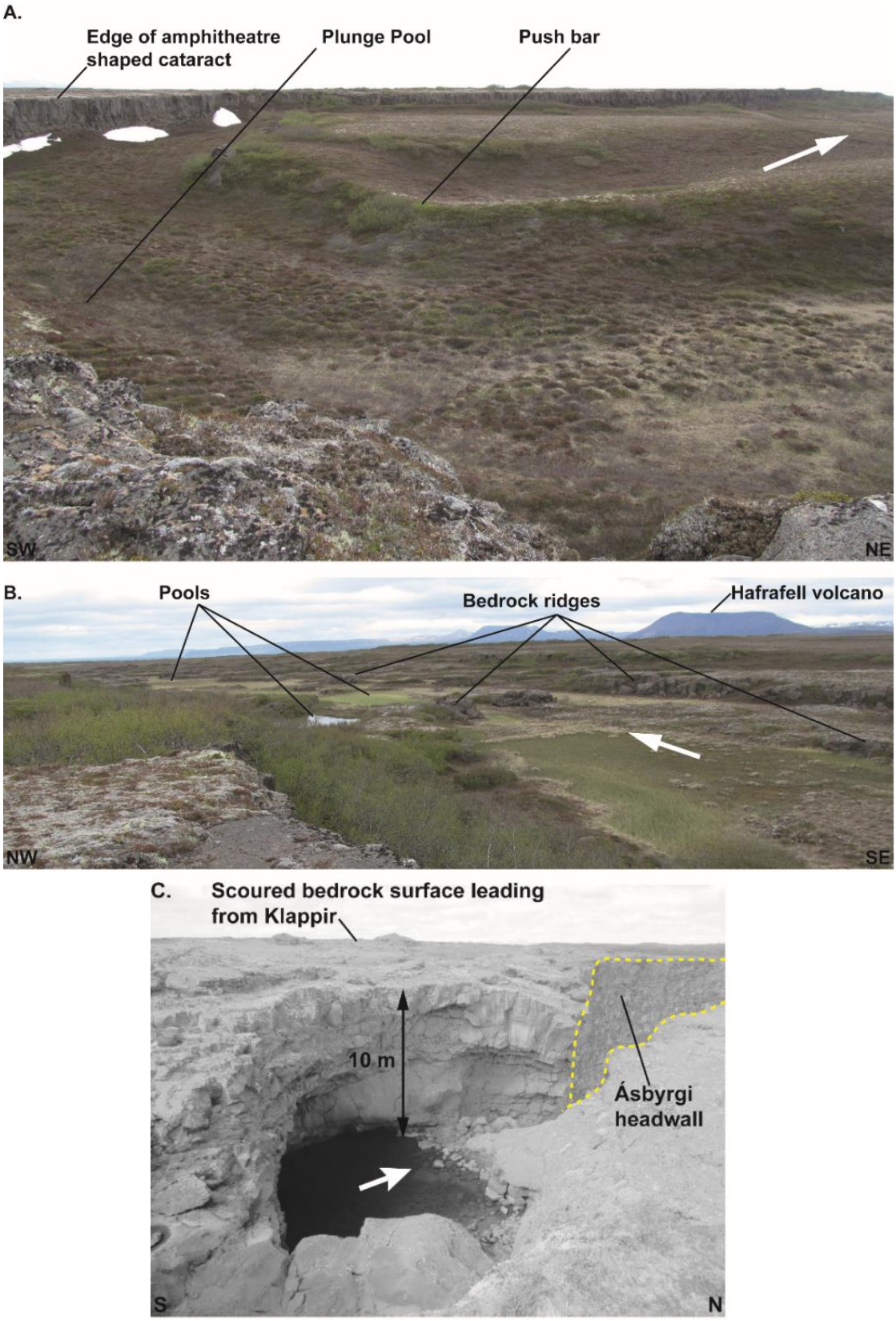

Fig. 2.4.7: Landforms in the Klappir scabland area suggest the action of powerful flows. In the south are three dry cataracts ~100 m wide with a 5-10 m vertical cliff at their head (**A.**).

Within the cataracts are arcuate sediment ridges that could be interpreted as push-bars preserved in pristine condition, showing no evidence for subsequent fluvial reworking. Downstream of the cataracts is an area with distinctive scabland morphology (**B.**). Characterised by a series of bedrock ridges and pools (local relief ~5 m), this area clearly marks the route of the flood waters, as can also be seen in the aerial photograph (Fig. 2.4.6). White arrows indicate the direction of the floodwaters. Hafrafell, a nearby table-top volcano that erupted subglacially, is shown. The eruption age of Hafrafell has been dated to 11,100 ± 2,200 years, thought to coincide with deglaciation in this area (Licciardi *et al.*, 2007). **C.** Megascale fluvial bedrock erosion landforms at the scoured rim of Ásbyrgi. Looking west into a 10-m-deep pothole within one of the eroded notches identified in Fig. 2.4.8, with flow direction to the north (white arrow). In the background of the photograph is the 90-m-high vertical headwall of Ásbyrgi (edge of rim highlighted in yellow).

The horseshoe of Ásbyrgi is made up of two parallel channels that have eroded back and coalesced (Fig. 2.4.6). Between the two parallel channels is 'Eyjan', or 'Island', a bedrock outcrop rising to the same elevation as the lava surface around the main rim of Ásbyrgi. The western canyon retreated further south, and its headwall marks the location of the highest cliffs (90 m) in Ásbyrgi. At the base of the headwalls of the western and eastern canyons are large relict plunge pools (Fig. 2.4.8B). The floor of Ásbyrgi is covered in sediment, with many large boulders (some > 3 m in diameter) found on the surface of the deposits (Fig. 2.4.8B). The maximum measured boulder size can be used to calculate the minimum discharge of the palaeo-flood that transported them (e.g., Costa, 1983; Clarke, 1996; Stokes *et al.*, 2012). Caution should be employed when using such a method as different equations can give different estimates of flood discharge, and there are issues with the collection of the boulder size data and the interpretation of the resulting estimates (see discussion in Stokes *et al.*, 2012). Within these caveats, we used the method described by Stokes *et al.* (2012) to calculate a rough estimate of the minimum flood discharge that would be required to transport the largest boulders in Ásbyrgi. The largest measured boulder in the eastern Ásbyrgi channel (diameter = 1.49 m) gives a minimum palaeo-discharge estimate of 12,000 $m^3 s^{-1}$. In the western channel, where the diameter of the largest measured boulder is 3.75 m, the minimum discharge

estimate is 39,000 $m^3 s^{-1}$ (see Appendix B for sensitivity analysis and full list of parameters used).

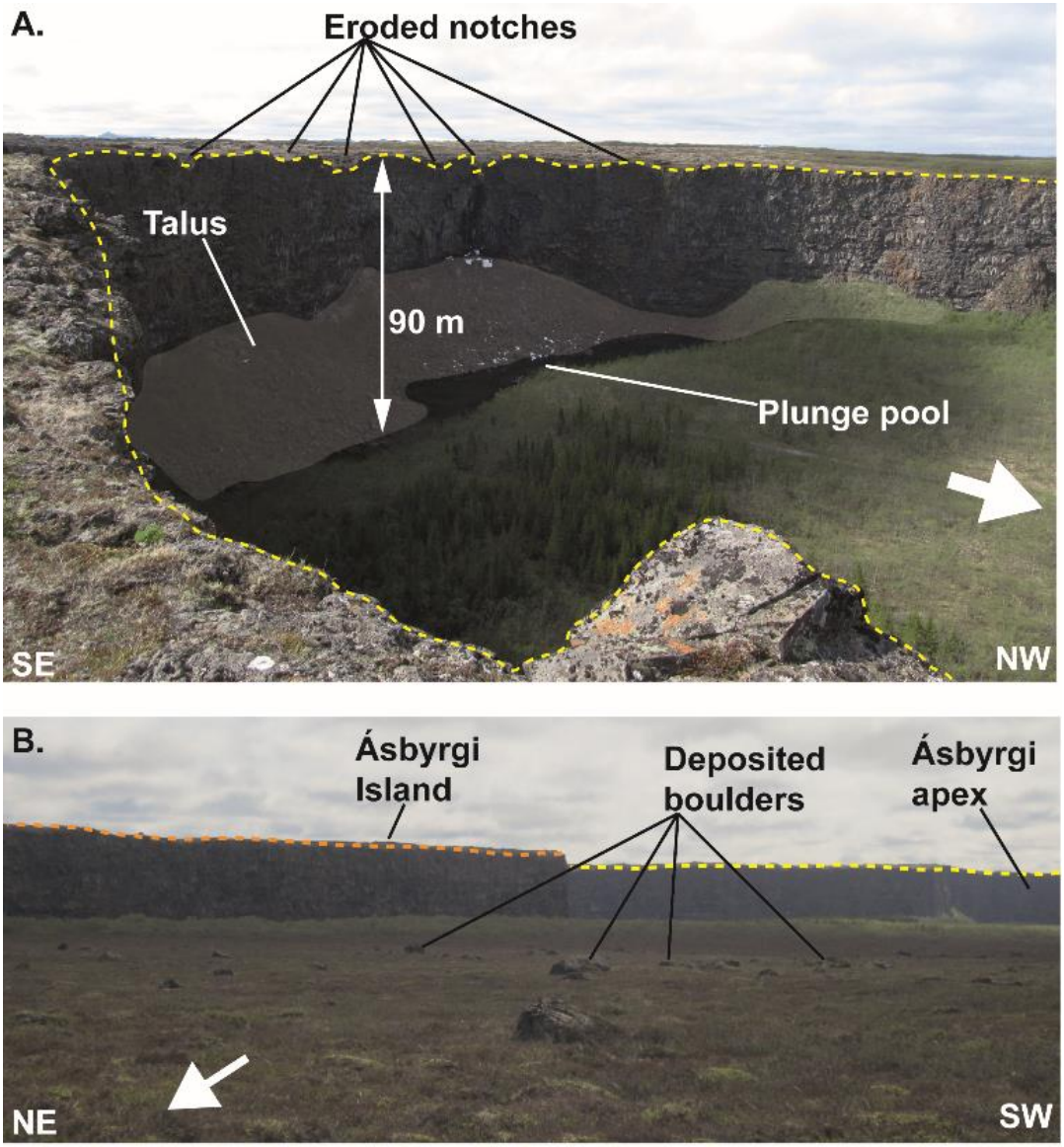

Fig. 2.4.8: Ásbyrgi canyon is a horseshoe-shaped cataract cut into a northward-dipping lava succession. The vertical headwall at the apex of Ásbyrgi is 90 m high with a large plunge pool at the base and a pile of sediment deposited immediately downstream (**A.**). Several eroded notches are present along the rim of the canyon (canyon edge highlighted with yellow dashed line). At the base of the headwall, talus deposits resulting from rockfalls and there is no evidence for reworking by overland flow. **B.** Looking into the western canyon of Ásbyrgi from near the canyon outlet. The rim of the main canyon is highlighted in yellow and the rim of the Ásbyrgi Island is shown in orange. The floor of Ásbyrgi is covered in sediment including large boulders (some > 3 m in diameter). There is no evidence for recent flow within the canyon so it is hypothesised that these boulders were deposited following

transportation during an extreme flow. The source of the boulders is impossible to determine, but we suggest that they were initially part of the lava succession into which Ásbyrgi has been cut rather than transported from further upstream. From this we propose that the floodwaters that formed Ásbyrgi were powerful enough to transport boulders of 3 m in diameter. White blocky arrows indicate palaeo-flow direction (to the north).

Small-scale fluvially sculpted bedforms on the top surface of the Island between the two eroded channels that make up the Ásbyrgi 'horseshoe' provide evidence that, pre-flood, the river flowed over the lava surface into which Ásbyrgi has been eroded (Fig. 2.4.9). Surveys from across the Island indicate a palaeo-flow direction that is consistently from the south (Fig. 2.4.9). These surfaces were formed before Ásbyrgi was eroded as the canyon walls cut straight across some of the landforms (Fig. 2.4.9B) and we propose that they were not formed during the flood as they are substantially smaller in scale (relief in the order of a few tens of centimetres) than the flutes, furrows, and potholes found at the rim of Ásbyrgi (relief in the order of a few metres, up to 10 m; Fig. 2.4.7C; Richardson and Carling, 2005). Similar-scale fluvial surfaces to those found on the Island are found on the eastern rim of Ásbyrgi and on the western rim of the modern canyon to the east (Fig. 2.4.6). During the last glacial period, the Icelandic ice sheet extended beyond the north coast of Iceland, covering the area containing Ásbyrgi and the Jökulsárgljúfur canyon (Norðdahl, 1990; Hubbard *et al.,* 2006; Licciardi *et al.*, 2007). During the retreat of the ice sheet across the central highlands, the discharge of the proto-Jökulsá á Fjöllum was likely greater owing to enhanced glacial ablation during deglaciation. Upstream of the Jökulsárgljúfur canyon, the Jökulsá á Fjöllum is at present a large braided river system (sometimes > 1 km in width) flowing on a bedrock substratum; it is possible that the river developed such morphology all the way to the coast before the canyons were eroded. The fluvial surfaces on Ásbyrgi Island, on the eastern rim of Ásbyrgi and the western rim of the main canyon, indicate the palaeo-course of this system. Fluvial sediment is lacking on these surfaces, possibly because the sediment would have been entrained and transported during the early stages of the

jökulhlaup before the surfaces were abandoned by the upstream propagation of the canyon headwalls.

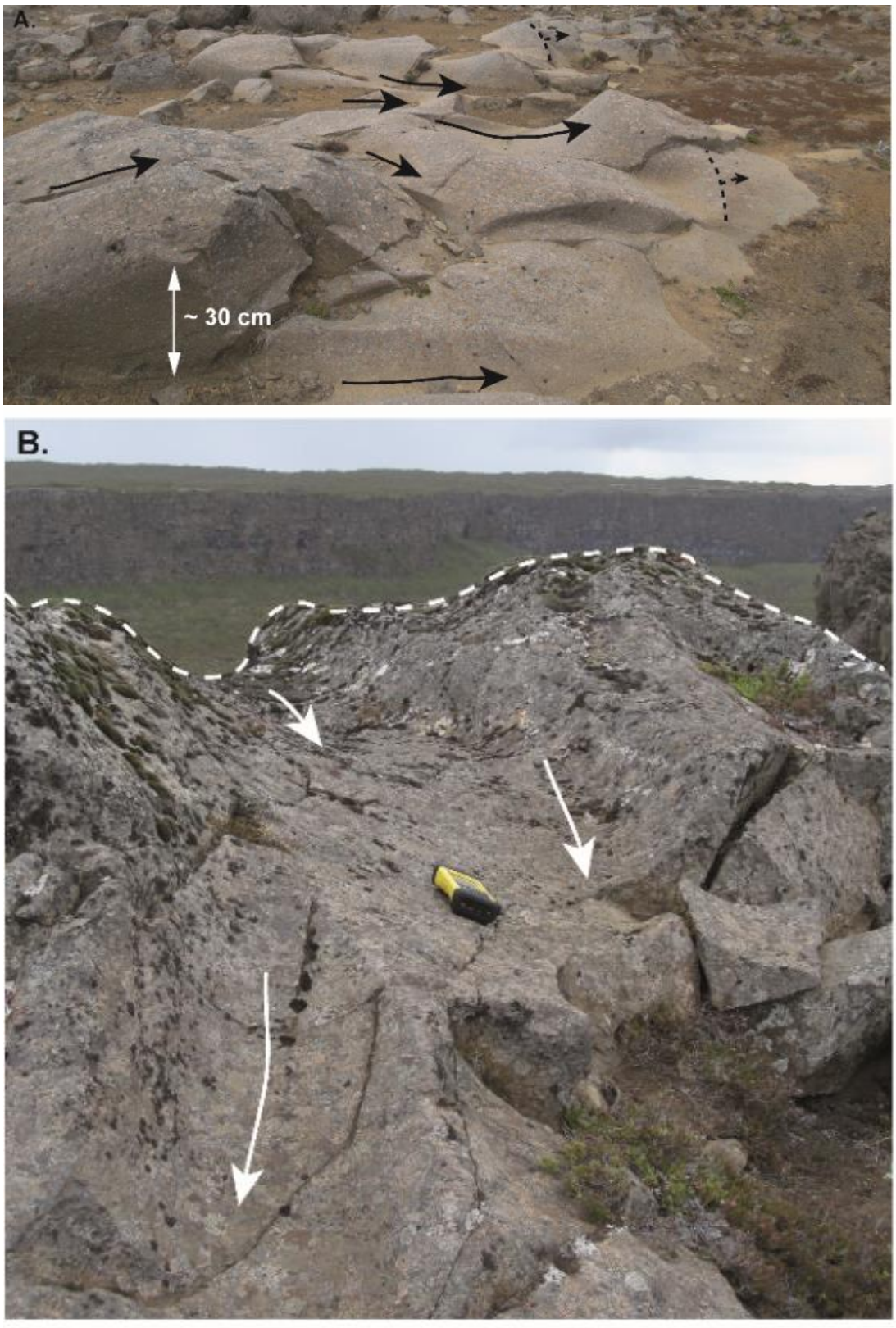

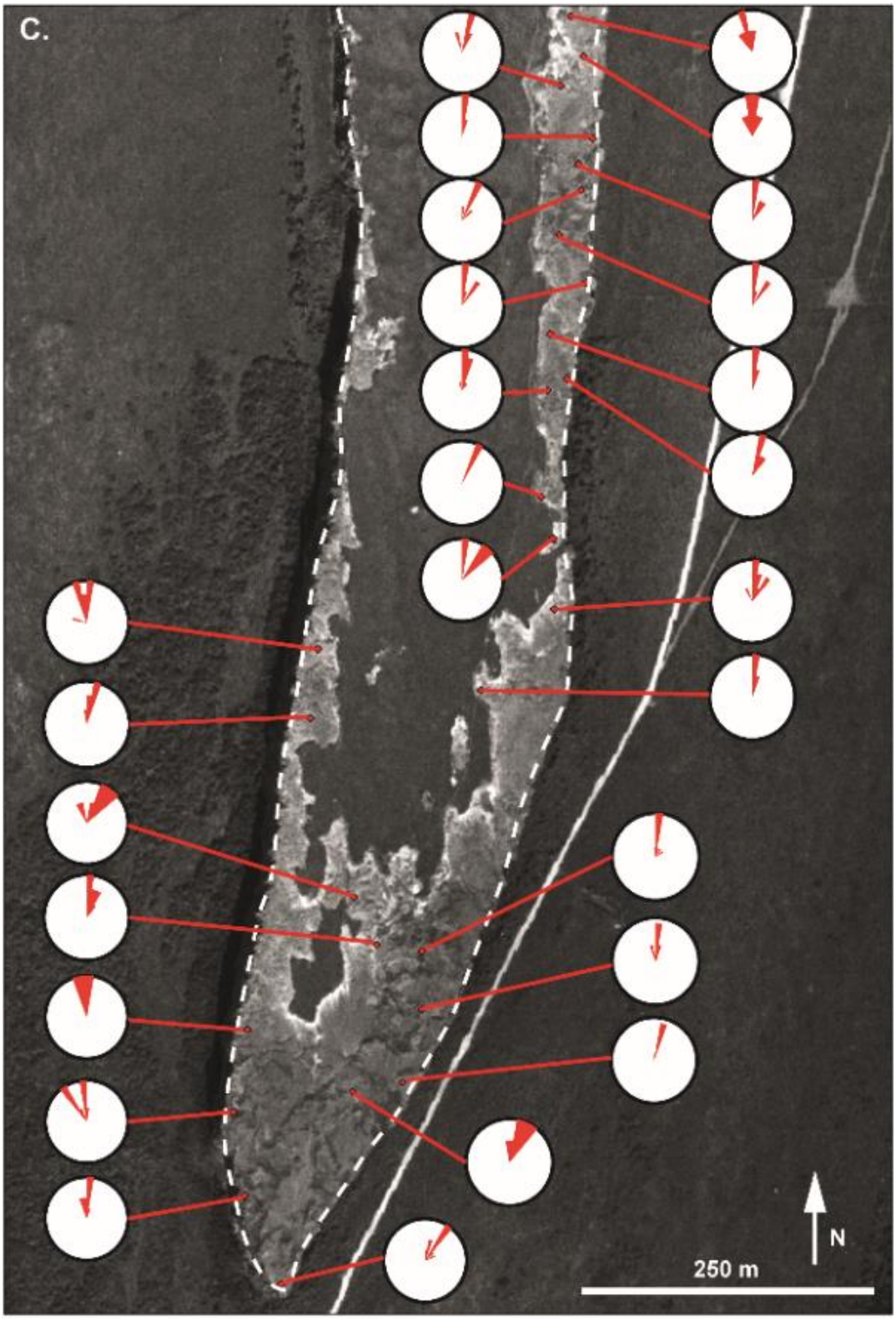

Fig. 2.4.9: Evidence for palaeo-flow on Ásbyrgi Island. **A.** The morphology of the flutes and furrows allows the identification of the flow direction of the palaeo-river that formed them. Flutes and furrows (solid black lines) are parallel to the flow direction; dashed lines represent the crests of upstream-facing convex surfaces that are perpendicular to the palaeo-flow

(Wilson and Lavé, 2014). Flow-direction is to the north. Local relief of bedrock surface is ~30 cm. **B.** The landforms atop the Island between the two Ásbyrgi canyons were formed before the canyon was carved, because the flutes and furrows lead right to the edge of the vertical walls (white dashed line). Photograph looking southeast on eastern edge of the Island. For scale, dimensions of GPS unit are 17 x 9 x 4 cm. **C.** Aerial photograph (source: Landmælingar Íslands) of the apex of Ásbyrgi Island (outline shown by dashed white line) showing the palaeo-flow direction of the fluvially sculpted bedrock features from 27 survey locations (total measurements = 182). All of the sites indicate a palaeo-flow direction broadly to the north.

2.4.4 Volume of rock eroded from Ásbyrgi and sediment depth

As demonstrated in section 2.4.3.3, the evidence for extreme flood events at Ásbyrgi and the Klappir scabland area immediately upstream is clear. The landscape is disconnected from the course of the present day Jökulsá á Fjöllum, which now flows in a deeply incised canyon to the east at Landsbjörg (Fig. 2.4.6). The Klappir scablands and Ásbyrgi contain landforms preserved in pristine condition, unburied and with no evidence for fluvial modification through erosion since their formation, suggesting abandonment following the event that carved Ásbyrgi. Klappir and Ásbyrgi therefore provide an unusually good opportunity to examine the impact of a single extreme flood event in eroding bedrock and then in depositing sediment. Combined topographic analysis and near-surface geophysics surveys were used to evaluate the volume of bedrock eroded from Ásbyrgi and the thickness of sediment deposited during the waning stages of the flood.

The volume of rock eroded from Ásbyrgi was quantified using high-resolution topographic data based on a total station survey and a 1.8-m resolution digital elevation model (*DEM source: TanDEM-X collected on 02/09/2012*). A ‘pre-flood’ surface was constructed by interpolating the elevation values from around the outer rim and the Island surface across the top of the canyon. An initial estimate of the rock eroded from Ásbyrgi during formation was made through the subtraction of the ‘pre-flood’ surface from the ‘present day’ DEM (Fig. 2.4.10A), giving a total of 0.139 km^3. However, this is an underestimate of the true amount of rock eroded from Ásbyrgi as the floor of the canyon is

completely covered with sediment. An assessment of the sedimentary thickness was carried out using electrical resistivity tomography (ERT) surveys across the canyon floor. The ERT surveys are non-destructive and provide greater spatial coverage than point measurements when multiple profiles are collected. The ERT is an established method for imaging the near subsurface and has been used for a wide range of applications, including detecting the bedrock-sediment interface (Hsu *et al.*, 2010; Chambers *et al.,* 2012), aquifer characterisation (Doetsch *et al.*, 2012), detection of subsurface cavities (Martinez-Lopez *et al.*, 2013), rockwall retreat rates (Siewert *et al.,* 2012), and permafrost depth and structure (You *et al.*, 2013). The ERT surveys were carried out across transects A-L shown in Fig. 2.4.6, with 25 electrodes at 5-m spacing, allowing electrode spacings ranging from 5 to 40 m. By increasing the spacing between the electrodes, the current penetrates deeper, building up a data section that can be interpreted in terms of lateral and depth variations in electrical resistivity. Some of the transects were built up from multiple surveys in order to cover a longer distance than the 120 m possible in a single 25-electrode survey, such as the long transect along the middle of the eastern canyon (transect G, 680 m long; Fig 2.4.6).

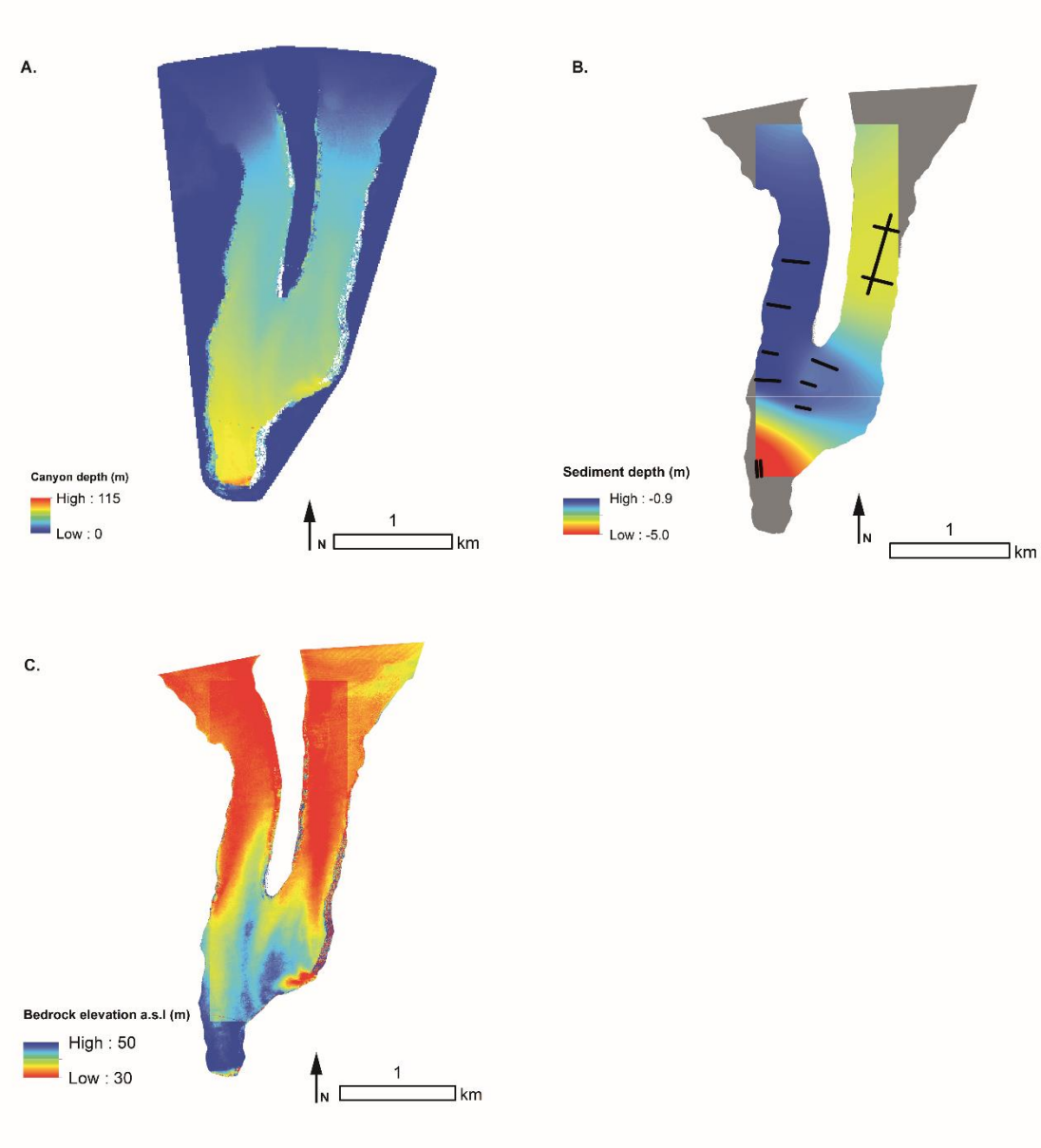

Fig. 2.4.10: A. Depth of Ásbyrgi canyon calculated by subtracting the DEM of the 'pre-flood' top surface interpolated from elevation values around the outer rim and the Island and the DEM of the present day canyon. The total volume of rock eroded between the two DEMs, without accounting for the deposited sediment in the floor of Ásbyrgi, is 0.139 km^3. **B.** Interpolated sediment depth to the floor of Ásbyrgi from the ERT data using the 'spline with barriers' function in ArcGIS. This surface is used to calculate a minimum estimate of the sediment deposited within Ásbyrgi through a comparison with the DEM of the canyon floor (0.005 km^3). The areas at the exit of the canyon are not considered owing to the spatial coverage of the ERT surveys (black lines) and the processing extent of the interpolation algorithm. **C.** Elevation of bedrock above sea level. Beyond the processing extent of the interpolation algorithm, the bedrock elevation is represented by the DEM of the canyon floor.

Different inversion methods are available in the 'res2Dinv' software (res2Dinv version 3.4; Geotomo, 2001). The conventional least squares method minimises the square of the difference between the measured and the calculated apparent resistivity values and produces a model with smooth resistivity variations (Loke *et al.*, 2003). However, the technique is not perfectly appropriate when the subsurface contains sharp boundaries between resistivity interfaces as the smoothing of the boundaries between layers makes their localisation difficult. We therefore employed a 'robust iterative inversion' to model our survey data, whereby the absolute changes in the resistivity values are minimised (Claerbout and Muir, 1973). This approach produces models of the subsurface with sharp interfaces between different subsurface structures that have different resistivity values (Loke *et al.,* 2003) and was deemed most appropriate because we expect to see a sharp boundary between the sediment deposits and the basalt bedrock beneath; all images presented here have been produced using this method (Fig. 2.4.11). The model iterations were stopped when the percentage misfit between the measured and the calculated apparent resistivity was < 5% or no further improvement to the fit was possible with further iterations. In the case of transect E, no further improvement occurred to the fit after five iterations, when RMS error was 5.9%.

Broadly, sedimentary deposits have the lowest resistivity and igneous rocks the highest (Telford *et al.,* 1990). We therefore interpret the bedrock-sediment interface in each of our profiles as the sharp horizontal downward transition from regions of low to high resistivities (Fig. 2.4.11). The typical range of resistivity for basalt is large: 10^1 – 1.3 x 10^7 Ωm (Telford *et al.*, 1990) because of a number of factors, including the water content in fractures and pore space. The resistivity of dry (0% water content) basalt is 1.3 x 10^7 Ωm whereas basalt with 0.95% water content typically has a much lower resistivity of 4 x 10^4 Ωm (Telford *et al.*, 1990). The peak resistivity in each of our surveys is up to 3.7 x 10^3 Ωm, which implies that the basalt in our study area has a water content > 1%. This is to be expected as the rocks are located in a coastal region with a wet climate. We are confident that the

transition to high resistivity found a few metres below the surface is the top of bedrock (Fig. 2.4.11). The layer of lower resistivity at the base of each of the surveys is interpreted to represent the water table owing to its broadly consistent depth at ~15 m across all surveys.

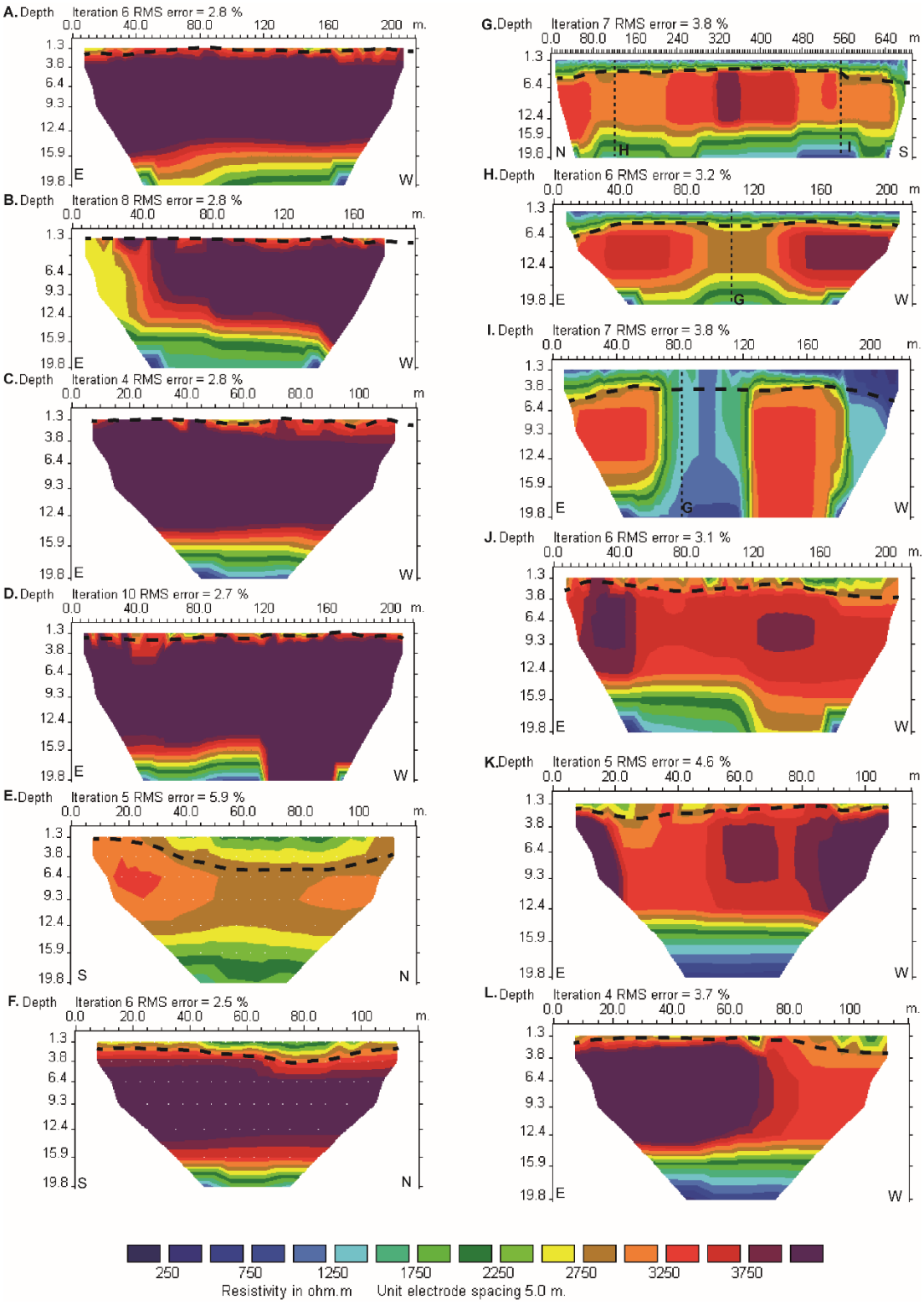

Fig. 2.4.11: Electrical resistivity tomography imaging of the subsurface. Labels **A-L** refer to the location of each transect shown in Fig. 2.4.6. Surveys A-D are from the western canyon; they show a depth to the bedrock-sediment interface of ~1 m. Surveys E and F are parallel to each other from the field close to the apex of Ásbyrgi; they show a sediment thickness of

~5 m. Survey G is a longitudinal survey along the middle of the eastern canyon with surveys H and I also from the eastern canyon, each showing a uniform sediment thickness of ~3 m. Surveys J-L are from the region between the two main canyons and have a sediment depth of ~1.5 m. The letters at the edges of each profile (bottom) indicate the orientation of the transects. Vertical dashed lines and corresponding labels on **G**, **H**, and **I** indicate the location where the transects cross each other.

The ERT surveys show that the sediment is ~1 m thick across the floor of the western gorge (Figs. 2.4.11A-D) and 3 m thick in the eastern gorge (Figs. 2.4.11G-I). Owing to forest cover, only two surveys were carried out in a field near the apex of the western gorge, but these show that the sediment in this region of the canyon is ~5 m thick (Fig. 2.4.11E-F). We hypothesise that this is because of the survey location on top of the pile of sediment immediately downstream of the plunge pool. These surveys were parallel to each other and have produced a similar subsurface morphology despite a slight difference in the peak resistivity values, indicating reproducibility of the results. The three surveys undertaken in the region between the two main channels indicate a sediment depth of ~1.5 m in this region (Figs. 2.4.11J-L).

Sediment depths were interpolated across the canyon floor using the 'Spline with Barriers' function in ArcGIS (Fig. 2.4.10B). Owing to the limits on the spatial coverage of the ERT surveys, the interpolated surface does not cover the canyon floor in the apex of the western channel of Ásbyrgi or in some of the areas at the exit of the western and eastern canyons. The volume of sediment within Ásbyrgi was estimated by subtracting the interpolated surface from the DEM of the canyon floor topography, giving a volume of 0.005 km^3, making up < 4% of the total volume of rock eroded from Ásbyrgi at 0.144 km^3. This is a minimum estimate as the interpolated surface does not cover the entire floor of Ásbyrgi, although the additional sediment located beyond the interpolated surface is unlikely to cause a significant increase in the estimate of total rock eroded. Figure 2.4.10C shows the bedrock surface elevation above sea level, created by subtracting the interpolated sediment depth (Fig. 2.4.10B) from the DEM of the canyon floor. The area close to the

apex of Ásbyrgi is affected by the presence of trees that are picked up by the DEM (the highest elevation areas in blue) but further north, near to the outlet of the two canyons, the elevation of the bedrock surface above sea level is very similar. This observation suggests that when the two canyons were retreating, before they coalesced, the vertical knickpoints at the headwall of the canyon were the same height.

2.4.5 Discussion

Some of the features described in Section 2.4.3, such as boulder erratics, are not exclusive to the action of extreme flood events and individually should not be used as evidence for the action of extreme flood events (Carling *et al.,* 2009c; Carrivick *et al.*, 2013). However, as multiple different landforms across all scales of the Carrivick *et al.* (2004) criteria are found in three distinct and very different reaches of the Jökulsárgljúfur canyon, we suggest that the evidence for extreme flood events is unequivocal in this landscape. Combining this with the identification of three significant periods of canyon cutting in Sub-Chapter 2.3 (Baynes *et al.,* 2015) at ~10,000, ~5,000 and ~2,000 years ago, the following sections reconstruct the landscape evolution of the lower Jökulsá á Fjöllum during the Holocene.

2.4.5.1 Model of formation of Ásbyrgi and Klappir during a flood ~10,000 years ago

The presence of fluvially sculpted surfaces on the top of Ásbyrgi Island as well as strath terraces above the Jökulsárgljúfur canyon to the east suggests that during the retreat of the last Icelandic ice sheet, a major river flowed from the south over the northward-dipping lava surface into which the canyons have been eroded. The timing of the jökulhlaup is important as it provides an independent constrain on the minimum age at which the lower reaches of the Jökulsá á Fjöllum must have been deglaciated. As shown in Section 2.1.1, the region was thought to have been glaciated during the Younger Dryas period (13.0-11.5 ka BP), and the timing of the jökulhlaup ~10 ka BP

suggests that the ice must have retreated from area rapidly after the Younger Dryas period. This proto-Jökulsá á Fjöllum may have been substantially wider than the modern river channel as the discharge may have been higher because of increased meltwater generated during a major period of deglaciation. It possibly generated a large braided river system with multiple active channels on the lava substrate similar to the present day Jökulsá á Fjöllum upstream of Selfoss. This palaeo-river system could have simultaneously occupied, and fluvially sculpted, the surface at the top of Ásbyrgi Island and the surface close to the present day main canyon (Fig. 2.4.12A). Alternatively, the palaeo-river system could have been similar in size to the present day Jökulsá á Fjöllum and could have migrated the 2.5 km across the lava surface, sculpting the two bedrock surfaces at different times (Fig 2.4.12A). It is possible that at this time, the relative sea level was lower than the present day elevation (see Section 2.1.1 for detailed variations in RSL around the Icelandic coast), possibly generating sea-cliffs at the downstream edge of the lava flow into which Ásbyrgi and the main Jökulsárgljúfur canyon have been eroded. The sandur plain downstream of the Jökulsárgljúfur canyon has been built by the northwards propagation of the river flowing into the Öxarfjörður depositional basin, with 65 m of sediment deposited in the last 10,000 years (Ólafsson *et al.,* 1993), suggesting that at the time of the early-Holocene jökulhlaup the sandur plain may not have been present possibly exposing sea cliffs at the lava flow edge and triggering an upstream incision wave.

During the initial phases of the early Holocene jökulhlaup, the floodwaters spread across the Klappir area and the area to the east, over what would become the course of the modern day river. The eastern floodwaters split, and two canyons (the origins of the main Jökulsárgljúfur canyon at Landsbjörg and Lake Ástjörn) began to be incised through the plucking and toppling of large basalt blocks and columns at the lava flow front (Fig. 2.4.12B). The floodwaters in the Klappir area also began incising at the lava flow front with two canyons forming close to each other (the beginnings of the modern Ásbyrgi canyon) (Fig. 2.4.12B). Upstream of these four main

canyons, the Klappir area began to be sculpted into the ridge and pool scabland morphology seen today, with the smaller cataracts starting to be formed under a similar process to the main canyons to the north.

Figure 2.4.12C shows the proposed locations of the canyons midway through the jökulhlaup, with the floodwaters flowing into the Ástjörn canyon captured owing to the upstream migration of the head of the main Jökulsárgljúfur canyon further east. We propose that the jökulhlaup had no further impact on the scabland tract leading to Lake Ástjörn, which is now exposed ~60 m above the modern channel (Fig. 2.4.12C). The two canyons of Ásbyrgi were also still retreating at the mid flood stage (Fig. 2.4.12C); and at some point during the latter stages of the flood, the two canyons coalesced to form the horseshoe-shaped canyon seen today (Fig. 2.4.12D). Based on the maximum size of boulders deposited across the canyon floor, calculations suggest that the discharge of the jökulhlaup that eroded Ásbyrgi was at least 39,000 m^3 s^{-1}, although it may have been greater than this magnitude. The perfect preservation of landforms in the Klappir scablands and the maintained vertical headwall of Ásbyrgi suggest that the floodwaters were diverted from this area at the end of the flood and we propose that this occurred through the capture of the waters because of the retreat of the headwall of the main Jökulsárgljúfur canyon to the east (Fig. 2.4.12D). The ERT profiles reveal that the sediment in the canyon floor is just a thin veneer only a few metres thick over the bedrock surface, filling < 4% of the total volume. We propose that this sediment was deposited across the canyon floor of Ásbyrgi during the latter stages of the flood when the waning floodwaters were no longer powerful enough to transport the sediment load (Fig. 2.4.12D).

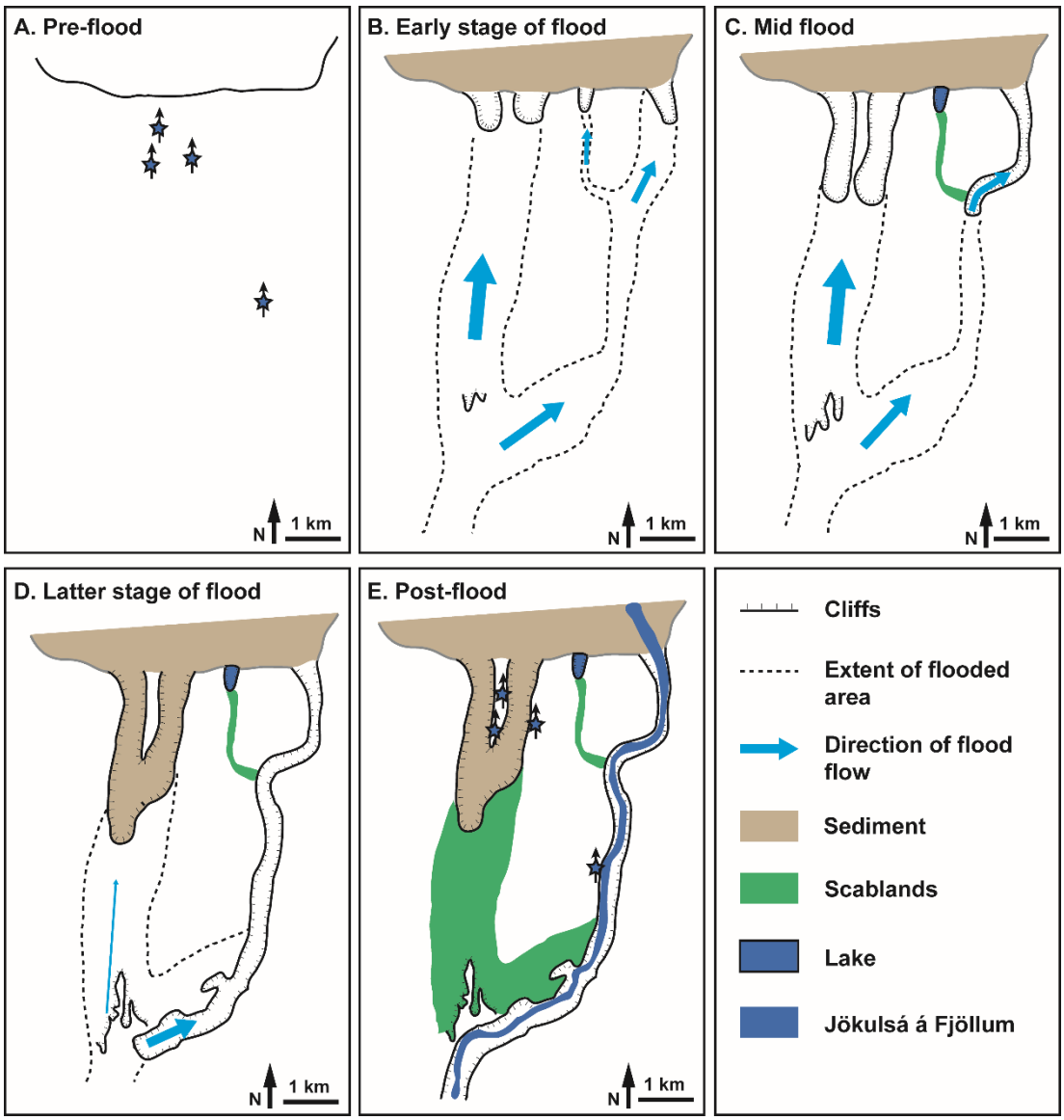

Fig. 2.4.12: Proposed macroform evolution of the lower Jökulsárgljúfur canyon during an extreme flood event in the early Holocene. **A.** Before the flood, the precise course of the Jökulsá á Fjöllum is impossible to determine; but fluvially sculpted surfaces on the top of Ásbyrgi Island, the eastern rim of Ásbyrgi and the western rim of the main canyon at Landsbjörg indicate that a river once flowed here before the canyons were formed. The locations of the fluvially sculpted surfaces are shown by the blue stars (also shown in E for comparison), with direction of palaeo-flow shown by the black lines. **B.** In the early stages of the flood, the floodwaters follow the course of the pre-flood river and also spread to the east. At the northern limit of the lava surface, four canyons begin to be incised. Through time, the floodwaters flowing into the canyon that currently contains Lake Ástjörn are captured by the faster retreat of the canyon to the east **(C.)** while the two Ásbyrgi canyons continue to retreat until they coalesce. The western canyon of Ásbyrgi continues to retreat and, eventually, the large canyon to the east retreats far enough to also capture the floodwaters flowing across

the Klappir scablands into Ásbyrgi. During the waning flow, a thin layer of sediment is deposited in the bottom of Ásbyrgi **(D.)**. The headwall in the main canyon continues to retreat, disconnecting Ásbyrgi and Klappir from the course of the Jökulsá á Fjöllum leading to the outstanding preservation of the landforms **(E.)**. Subsequent floods along the Jökulsá á Fjöllum are channelled in the main canyon, although some potential minor reoccupation of Klappir may have occurred, which stripped some of the soils (Waitt, 2002). The main canyon at Landsbjörg is drawn here assuming that all the erosion in this main canyon occurred during the early Holocene flood, although additional reworking of the canyon morphology during later floods cannot be ruled out.

Waitt (2002) proposed that the eroded scabland area immediately upstream of Ásbyrgi was reoccupied during the late Holocene flood ~1,500 years ago as the soil in this area lacks the H3 (~2,900 yr BP), H4 (~3,800 yr BP) and H5 (~6,000 yr BP) tephra layers, while the soil beyond the scabland limits do contain them. This observation suggests that the soils in the scabland area were washed away after the deposition of the H3 layer, most likely during the late Holocene flood. However, the exposure age from the eroded notch at the rim of Ásbyrgi (9,850 ± 2,650 yr from sample in a notch a couple of metres under the original surface of the lava flow; Sub-Chapter 2.3 - Baynes *et al.,* 2015) suggests that any flow through here during the mid- and late Holocene was not powerful enough to cause any significant bedrock erosion (i.e. not enough to 'reset' the concentration of cosmogenic nuclides). Thus, we can be confident that the carving of Ásbyrgi represents the impact of an early Holocene flood event. The effect of any mid- or late Holocene floodwaters that overtopped the scablands and flowed into Ásbyrgi on the sediments deposited across the canyon floor is unknown, but the presence of the eroded boulders (from the early Holocene flood) and the thin layer of canyon floor deposits suggest that at least some of the material was preserved. The loss of additional material through aeolian processes is unlikely because of the morphology of the canyon and the vegetation cover.

Over time, overland flow into a canyon with a vertical headwall should act to diffuse the knickpoint through abrasion and plucking of small blocks (Lamb *et*

al., 2014). As the Ásbyrgi headwall is vertical and contains no evidence for diffusion since its formation, we propose that the Klappir scablands and Ásbyrgi were formed during a single extreme flood event. The floodwaters were diverted at the end of the flood preventing further fluvial activity that could have diffused the canyon headwall or reworked the landforms present on the Klappir scablands. Figure 2.4.12E shows the state of the landscape at the present day, which is likely to be very similar to that of the immediate aftermath of the early Holocene flood, although the morphology of the main canyon at Landsbjörg may have been altered after the early Holocene flood owing to subsequent modification during moderate and large floods in the mid- and late Holocene.

2.4.5.2 Evolution of lower Jökulsá á Fjöllum during mid-late Holocene floods

While we hypothesise that the knickpoint at the head of the main Jökulsárgljúfur canyon retreated at least as far as to capture the floodwaters flowing into Ásbyrgi, we have no evidence to suggest the exact position of the knickpoint at the end of the early Holocene flood. Waitt (2002) stated that the canyon already existed before the eruption of a fissure at Hljodaklettar ~9,000 years ago, as some of the cinder cones lie within the canyon (Fig. 2.4.1C). This chronology supports the theory that an early-Holocene flood, pre-fissure eruption, initiated formation of the Jökulsárgljúfur canyon and that erosion through headwall retreat proceeded at least as far as Hljodaklettar. We suggest that the 16 floods identified by Waitt (2002) and Kirkbride *et al.* (2006) at Vesturdalur have contributed to the upstream propagation of the knickpoint(s) from Hljodaklettar to the current apex of the Jökulsárgljúfur canyon. The two youngest floods dated by Kirkbride *et al.* (2006), as well as a late Holocene extreme flood that several authors agree has taken place (Sæmundsson, 1973; Tómasson, 1973; Helgason, 1987; Waitt, 2002), led to significant erosion within the upper 5 km of the canyon (Sub-Chapter 2.3 - Baynes *et al.*, 2015). Additional erosion of the downstream reach of the main canyon during the mid- and late Holocene floods cannot be ruled out but we

believe this is minimal because of the absence of active, or relict, knickpoints within this part of the canyon. An abandoned terrace on the east side of the canyon at Landsbjörg represents a historical position of the river bed (Fig. 2.4.6), but the age of formation and abandonment of this terrace is not currently known. The occurrence of extreme flood events in the mid-Holocene that were powerful to cause significant erosion within the Jökulsárgljúfur canyon is important for implications regarding the evolution of the Vatnajokull ice cap during the Holocene. As the source of the floodwaters, there must have been a large volume of ice located above the volcanic centres of Bárðarbunga, Kverkfjöll or Grímsvötn at ~5000 years ago. This is different to the findings of Striberger *et al.* (2012) who suggest, using lake sediments that, Vatnajokull was substantially smaller than present between 9000 and 4400 years ago.

2.4.6 Conclusions

Our work documents widespread evidence for bedrock erosion during extreme flood events in the lower Jökulsá á Fjöllum in northern Iceland. Multiple discrete phases of extreme flooding have occurred during the Holocene, leaving a lasting legacy on the landscape morphology in three distinct reaches. Evidence for erosion during extreme floods is clear at Dettifoss and Ásbyrgi, while evidence for deposition is found in the Forvoð valley. Ásbyrgi, unaltered since formation, contains a thin veneer of sediment in the floor of the canyon documented using an ERT survey; sediment fills < 4% of the total 0.14 km^3 volume of material that was eroded during an early Holocene extreme flood event, with reconstructed discharge of at least 39,000 m^3 s^{-1}. During this flood, coincident erosion was occurring in what is now the main Jökulsárgljúfur canyon through upstream migration of the canyon headwall. The canyon head retreated far enough to capture the floodwaters flowing across the Klappir scablands into Ásbyrgi; all future flow of the Jökulsá á Fjöllum and all subsequent floods were channelled within the main canyon at Landsbjörg to the east and caused significant erosion further

upstream, although a small-scale overtopping over Klappir during later floods cannot be ruled out. The overall contribution of extreme flooding along the Jökulsá á Fjöllum during the Holocene has been the formation of a 28-km-long, up to 100-m-deep canyon in < 10 ka. This highlights the importance of extreme flood events in the erosion of bedrock landscapes, with discrete high-magnitude events having the potential to cause catastrophic landscape change that can be preserved over millennial timescales.

Sub-Chapter 2.5: Discussion

2.5.1 Impact of extreme flood events on the evolution of the Jökulsárgljúfur canyon

Despite numerous previous studies on the impact of jökulhlaups within the Jökulsárgljúfur canyon (Table 2.1.1), most (e.g. Sæmundsson, 1973; Eliasson, 1977) have focussed on specific locations such as Ásbyrgi. Sections 2.3 and 2.4 of this research are the first to consider the collective impacts in the whole of the Jökulsárgljúfur canyon, exploring the impacts of jökulhlaups in specific locations (e.g. volume of rock eroded from Ásbyrgi in Section 2.4.4) as well as the evolution of the whole canyon through time during discrete events. The first research objective was to quantify the impact of extreme flood events in landscape evolution, which Sections 2.3 and 2.4 achieve through the detailed quantitative study of the Jökulsárgljúfur canyon, including the calculation of 0.144 km^3 of rock eroded from Ásbyrgi and the identification of rapid knickpoint retreat over distances of hundreds of metres (exceeding 2.5 km in one instance) at the apex of the canyon during discrete events.

The timing of the periods of canyon cutting identified within the Jökulsárgljúfur canyon (Section 2.3.4) is consistent with the stratigraphic work of Waitt (2002) and Kirkbride *et al.* (2006) in the Vesturdalur area of the Jökulsárgljúfur canyon, although the model proposed for the evolution of the bedrock canyon during extreme flood events (Section 2.4.5.1) differs from previous interpretations. Eliasson (1977) suggested that Ásbyrgi was carved in three events; 4.6, 3.0 and 2.0 ka ago, while Sæmundsson (1973) argued that Ásbyrgi was formed during an event in the early Holocene before being lengthened and narrowed during a late Holocene event 2.9 ka ago. Sæmundsson (1973) does, however, acknowledge that the preservation of soil older than 7.1 ka (i.e. containing the H5 tephra layer) on the rim of Ásbyrgi is incompatible with the erosion occurring during the late Holocene. The surface exposure age from the upstream rim of Ásbyrgi (Section 2.3.4) has helped constrain the timing and the number of flood events that eroded

the canyon, with the early Holocene age supporting the hypothesis of Ásbyrgi being carved during a single extreme flood event shortly after deglaciation.

The early-Holocene formation age of Ásbyrgi, given its location in the lower reaches of the Jökulsárgljúfur canyon, is also consistent with the concept of an ‘upstream incision wave’ whereby the erosive signal travels upstream in a bedrock channel through knickpoint retreat, with the upper reaches of the canyon being eroded must recently (see Fig. 2.2.10). Additional surface exposure ages from the rim of Ásbyrgi, as well as the top of the Ásbyrgi Island, would help confirm the timing of the formation of Ásbyrgi, although it is expected that these samples would also give surface exposure ages in the early Holocene (~9-10 ka ago). Waitt (2002) did not find any of the H3, H4 and H5 tephra layers preserved in the soil in the scabland tract immediately upstream of Ásbyrgi, suggesting that the late Holocene flood scoured this area, although we suggest that this floodwater would not have been powerful enough to ‘reset’ the surface exposure age of the bedrock at the rim of Ásbyrgi through erosion, with the majority of flow focussed in the main canyon to the east.

The upper reaches of the Jökulsárgljúfur canyon have been eroded most recently, during a period that matches the age of flood deposits in the Vesturdalur area of the canyon (Kirkbride *et al.*, 2006) in the mid-Holocene (~ 5 ka ago) as well as a flood event during the late-Holocene (~1.5-2 ka ago). Due to the uncertainty associated with the surface exposure ages (Sub-Chapter 2.3), they alone do not allow the identification of individual flood events, rather the timing of periods of rapid canyon cutting that span a few hundred years. However, the consistency of these age clusters with estimates of flood timings from sedimentary deposits (Waitt, 2002; Kirkbride *et al.*, 2006) allow us to suggest that the upper reaches of the Jökulsárgljúfur canyon have been eroded during one or two flood events in the mid-Holocene and a single large flood event in the late Holocene.

When considering the Jökulsárgljúfur canyon as a whole, Sub-Chapter 2.3 and 2.4 demonstrate that just a few discrete high magnitude flood events in

the last ~12 ka have been responsible for the formation of the 28 km long canyon. While no direct measurements of the peak discharge of the erosive flood events have been carried out in this study, the minimum estimates of the flow required from transported boulders at Ásbyrgi (> 3.9 x 10^4 m^3 s^{-1}) and the threshold conditions for block toppling at the waterfalls in the upper reaches of the canyon (> 3 x 10^3 m^3s^{-1}) are both possible within the estimates of the largest flood events that occurred along the course of the Jökulsá á Fjöllum during the Holocene (9 x 10^5 m^3 s^{-1}; Alho *et al.*, 2005).

2.5.2 Landscape morphology and concept of landscape 'state'

A geomorphic system can be defined either as being in a state of dynamic equilibrium or considered as in a cycle of erosion, depending on the timescale over which landscape change is considered (Schumm and Lichty, 1965). Therefore, it is important to consider the impact of extreme events on landscape evolution over both short (i.e. the duration of the flood) and long (i.e. over millennia) timescales. Wolman and Miller (1960) assessed the relative importance of high magnitude, low frequency events and the proportion of 'geomorphic work' they do in the formation of landscape features. Developing this concept further, Wolman and Gerson (1978) considered the effectiveness of such high magnitude events in terms of the time taken for the landscape to recover back to its original form following the perturbation during the high magnitude event. If the landscape recovers to its original form quickly following the extreme perturbation, then the high magnitude event is deemed to have been less 'effective' than an event where the landscape takes much longer to 'recover' (Wolman and Gerson, 1978).

This can be quantified using the 'transient-form ratio', whereby at any moment in time the state of a landscape can be classified as either 'transient' or 'steady' (Brunsden and Thornes, 1979). If the time elapsed since the last major, 'geomorphologically effective', event is less than the characteristic 'landscape recovery' timescale; the landscape can be defined as in a

‘transient’ state. On the other hand, if the time elapsed since the last major, geomorphologically effective, event is greater than the characteristic landscape recovery timescale, evidence for the extreme event should no longer be visible within the landscape morphology and it can be defined as in a ‘steady state’ (Brunsden and Thornes, 1979). Anderson and Calver (1977) suggested that the timescale and frequency of effective events is important for understanding the landscape form and its appearance. The landscape form is dependent on the overall effect of past events and their magnitude-frequency distribution, setting the time that the landscape has to ‘recover’ from the effects of the formative event (Anderson and Calver, 1977). Additionally, the time elapsed since the last formative event is important as their degree of degradation, or ‘recovery’, sets the appearance of the landscape morphology (Anderson and Calver, 1977).

A common example of a ‘transient’ landscape response to a perturbation is the propagation of a knickpoint up a bedrock channel following a base level fall, an increase in uplift rate or a change in climatic conditions (Whipple, 2001; Crosby and Whipple, 2006; DiBiase *et al.*, 2015). The time taken for the transient signal of the knickpoint to reach the upper reaches of the channel can be defined as the ‘recovery time’ (Whipple, 2001; Allen, 2008). While the knickpoint is migrating through the system, the time since the last geomorphologically effective event is less than the recovery time and thus the landscape is in a ‘transient’ state. Once the signal of the perturbation has migrated throughout the length of the system, the landscape is in ‘steady state’ until the next perturbation to the steady state conditions (Allen, 2008). Thus, the effectiveness, and the legacy, of the perturbation in forming landscape features is a function of the recurrence interval of the event and the time required for the landscape to recover the form existing prior to the event (Wolman and Gerson, 1978). Whipple (2001) suggest that due to the rapid changes in climatic conditions during the Quaternary, it is impossible for actively uplifting orogens, such as Taiwan, to reach ‘steady-state’ due to the regularity of variations in external boundary conditions and the long timescale of landscape response.

The regularity of jökulhlaups in Iceland have been shown to lead to a dominant state of 'transience' of the depositional Mýrdalssandur plain, which experiences extreme flood events due to volcanic activity of Katla, located beneath the Mýrdalsjökull ice cap (Duller *et al.*, 2014). Over the last 1000 years, the forcing frequency of the floods (51 ± 15 years, with the most recent in 1918; Duller *et al.*, 2014), which transport and deposit massive volumes of sediment, has been less than the time taken for the landscape to 'recover' (estimated at ~120 years), thus leading to long-term land surface growth through net advance of the coastline (Duller *et al.*, 2014).

In an erosive environment containing basaltic lava columns, 'geomorphologically effective events' can be defined as periods when the flow conditions surpass the threshold for a transition to an erosion regime dominated by the toppling and transportation of the basalt lava columns, which manifests itself in the landscape morphology in the form of knickpoints with vertical headwalls. Over time, the background flow conditions should act to gradually diffuse the vertical headwall into a series of smaller steps (e.g. Pointed Canyon, Idaho; Lamb *et al.*, 2014) and eventually the landscape should 'recover' to its original form; a smooth river profile. Since formation of a vertical amphitheatre shaped headwall during an extreme flood event ~ 45 ka ago, the knickpoint at the apex of Pointed Canyon, Idaho, has been slowly retreating at the rate of 2.5 cm a^{-1}, while also diffusing into a series of vertical steps (Lamb *et al.*, 2014). This process can be defined as the 'recovery phase' of the landscape following the highly 'effective' extreme flood event that initially formed the canyon with a vertical headwall. Due to the very slow nature of the erosion by abrasion or plucking of individual blocks rather than by toppling of whole columns, the timescale for 'landscape recovery' in an erosive environment such as Pointed Canyon (> 10^4 years) is much longer than in the depositional setting of Mýrdalssandur (~10^2 years; Duller *et al.* 2014).

Given the similarity in the nature of the bedrock (columnar basalt) and the landscape morphology (column toppling during high flow conditions leading

to knickpoints with vertical headwalls) between Pointed Canyon, Idaho, and the Jökulsárgljúfur canyon, the same concept of landscape 'state' and 'recovery' can be applied in each landscape. Therefore, it would be expected that the vertical headwalls of the knickpoints within the Jökulsárgljúfur canyon would eventually 'recover' through time, possibly over a similar timescale as Pointed Canyon (> 10^4 years).

The threshold discharge for column toppling at the knickpoints in the Jökulsárgljúfur canyon was > 3250 $m^3 s^{-1}$, approximately six times the peak annual discharge (Schunke, 1985, Data from Icelandic Met Office) and twice the discharge of floods that occur on centennial timescales (Helgason, 1987). Catastrophic erosion and significant knickpoint retreat occurred during periods of rapid canyon cutting ~ 5 and ~ 2 ka, which also acted to 'reset' the vertical headwalls of the knickpoints that are characteristic of a column toppling dominated erosion regime. Thus, the recurrence interval of the 'geomorphologically effective events' is of the order of 10^3 years, far shorter than the time required for the landscape to 'recover' (>10^4 years, if we assume a similar recovery timescale as Pointed Canyon). Therefore the Jökulsárgljúfur canyon can be defined as having been in a 'transient state' throughout the Holocene (Wolman and Gerson, 1978; Brunsden and Thornes, 1979; Allen, 2008; Duller *et al.*, 2014), with the extreme flood events acting to maintain the legacy of their action (the vertical headwalls of knickpoints) during this period.

2.5.3 Erosion processes during extreme flood events and implications for landscape evolution and landscape 'state'

Within the framework of Brunsden and Thornes (1979), the Jökulsárgljúfur canyon is very unusual, if not unique, in its perpetual 'transient' landscape state, due to the frequency of extreme flood events triggered by subglacial volcanism beneath Vatnajökull and the relatively low threshold above 'normal' flow conditions for a transition to a column toppling erosion regime

leading to a small recurrence interval of geomorphologically effective events. Additionally, the low rates of erosion through abrasion due to the lack of coarse (bigger than pebble size) sediment transported as bedload leads to a long ‘landscape recovery’ timescale, ensuring the Jökulsárgljúfur canyon never reaches a ‘steady state’.

The complexities of the erosion processes that emerge during transient, or spatially/temporally non-uniform forcing through time, are poorly constrained but are critical for quantitative evaluations of past landscape evolution (DiBiase *et al.*, 2015). Section 2.3.5 identified that erosion by the upstream migration of waterfalls through the toppling and transportation of lava columns is the dominant mechanism of erosion during extreme flood events within the Jökulsárgljúfur canyon, achieving the second specific research objectives of this study.

However, the influence of waterfalls on long-term bedrock channel evolution remains poorly understood (DiBiase *et al.*, 2015) despite the fact they can make up significant portions of elevation change in river long-profiles (Ortega *et al.*, 2013). In the Jökulsárgljúfur canyon, erosion during extreme flood events has led to the ‘transient’ landscape state through the generation and upstream migration of waterfalls with vertical headwalls, but additional work is required to understand the factors that lead to waterfall generation and how they evolve through time, in terms of both knickpoint form and retreat rate.

Other than a simple comparison with Pointed Canyon, Idaho, the factors controlling the timescale of the ‘landscape recovery’ through gradual knickpoint diffusion and retreat in the Jökulsárgljúfur canyon are unclear. The Jökulsárgljúfur canyon differs from Pointed Canyon in several important ways, most notably the magnitude of the discharge of the river that flows within it. Between 1916 and 2005, the average discharge of the Malad River at a gauging station 15 km upstream of Pointed Canyon was just 8.1 $m^3 s^{-1}$ (USGS, 2005), two orders of magnitude lower than the average discharge of the Jökulsá á Fjöllum at Grimmstadir (Schunke, 1985, Data from Icelandic

Met Office). Therefore, it could be expected that the 'landscape recovery' time following column toppling during an extreme flood event would be different in the Jökulsárgljúfur canyon compared to Pointed Canyon, Idaho. A study of the controls of knickpoint erosion during the background 'landscape recovery' period is therefore required in order to further constrain the factors controlling the timescale of landscape recovery in the Jökulsárgljúfur canyon.

2.5.4 Summary of outstanding questions regarding knickpoint retreat mechanisms and motivation for experimental study

Understanding mechanisms of knickpoint retreat is important for both landscape evolution over long timescales (e.g. Berlin and Anderson, 2007; DiBiase *et al.*, 2015) and short timescales, such as those related to erosion in the Jökulsárgljúfur canyon during extreme flood events and during background 'landscape recovery' periods between extreme flood events.

The results from Sub-chapters 2.3 and 2.4 suggest that the structure of the bedrock is an important control on both the form, and retreat rates, of the knickpoints within the Jökulsárgljúfur canyon. However, given the current uncertainty in the wider understanding of knickpoint erosion processes and in the relative importance of factors such as discharge and knickpoint size (as discussed in Section 1.2.2.4), this was explored further in Chapter 3 in order to achieve Objective 3 of this study and to achieve the wider research aim.

Chapter 3: Physical modelling of knickpoint erosion processes

3.1 Introduction

Experimental modelling of geomorphic systems can allow the study of geomorphic processes in a controlled environment, where the role of important variables can be isolated and quantified, which can be very hard to achieve in the natural environment (Turowski *et al.*, 2006; Lamb *et al.,* 2015). However, being able to apply the findings to natural systems is a fundamentally important consideration in any experimental study of geomorphic systems (Turowski *et al.*, 2006; Malverti *et al.*, 2008). Two different approaches have been applied in previous experimental modelling studies to achieve representative findings: (i) an attempt to maintain a strict scaling relationship between the experimental and natural landscapes for a single process (e.g. Paola *et al.*, 1992; Whipple *et al.*, 1998; Roering *et al.*, 2001) and (ii) an experimental approach that produces landforms that are qualitatively similar to natural landscapes and systems regardless of the dominant erosion process at work (e.g. Hasbargen and Paola, 2000; Lague *et al.*, 2003; Turowski *et al.* 2006; Bonnet, 2009). The second approach has been applied here, which has been successful in the past in studies that use silica paste as an experimental bedrock substrate. For example, Bonnet (2009) highlighted the potential importance of drainage divide migration in long term landscape evolution while Turowski *et al.* (2006) examined the response of experimental channels to variations in tectonic uplift rate, despite the complexities in the erosion processes not being accounted for in the models.

This chapter begins by introducing the key objectives of this experimental modelling study, before discussing the set-up of the box flume and the methods used for data extraction and data analysis (Section 3.2). The results are presented in Section 3.3 and are interpreted in Section 3.4.

3.1.1 Experimental modelling research objectives

The research aim of this experimental study is to achieve Objective 3 of the wider research study: *to constrain the dynamics of knickpoint erosion*

processes during extreme flood events and during background periods of 'normal flow'. Chapter 2 identified the key role of large knickpoint retreat during extreme flood events in controlling landscape evolution over millennial timescales in Iceland but an understanding of the role of knickpoints in the long term evolution of bedrock river channels, an understanding of the dynamics of knickpoint erosion processes during background 'non-flood' periods is also required.

Two sets of experiments were designed to help understand the dynamics of knickpoint erosion processes (Objective 3) which is then related to the wider research aim and the other two objectives in Chapter 4. Given the proposed importance of knickpoint dimensions (e.g. Hayakawa and Matsukara, 2003; Haviv *et al.,* 2010) and the often assumed dependence on discharge (e.g. Berlin and Anderson, 2007) in controlling knickpoint form, propagation rate and decay (see Section 1.2.2.4 for further references), the two sets of experiments presented here will answer the following two questions:

1. What is the effect of knickpoint geometry on knickpoint form and retreat rate?
2. What is the effect of discharge on knickpoint form and retreat rate?

In order to answer the first research question, a series of experiments (highlighted in red in Table 3.1.1 and Fig. 3.1.1) were carried out where the discharge was held constant at 1 litre per minute and the initial base level drop varied between 0.5 and 4 cm. The channel width under a constant discharge of 1 l/min was ~7 cm, and the range of base level drops (0.5 – 4 cm) therefore represents knickpoints that have a height/width ratio ranging from 0.07 to 0.57, covering a range of knickpoint geometries that are present in nature (e.g. Dettifoss has a height/width ratio of 54/150 = 0.36).

The second research question was explored using two further sets of experiments; (i) total discharge for each experiment varied 0.1 and 2 l/min while the initial base level drop was kept constant at 2 cm (highlighted in blue

in Table 3.1.1 and Fig. 3.1.1) and (ii) the effect of temporal variability in the hydrograph was tested using a ‘tipping bucket’ (Fig. 3.1.2) where the mean discharge was 1 l/min, delivered in five pulses of 200 ml over the course of 60 seconds. The initial base level drop was varied between 0.5 and 4 cm in these experiments (highlighted in orange in Table 3.1.1 and Fig. 3.1.1), the same as the experiments where discharge was kept constant, allowing the impact of discharge variability on knickpoint retreat to be isolated from background processes. A summary diagram of how these experiments help achieve the wider research aim of the experimental study is provided in Fig. 3.1.1.

Table 3.1.1: List of parameters for each of the experiments carried out. Experiments listed in red test the role of knickpoint height in controlling knickpoint retreat (research question 1), experiments in blue and orange test the role of discharge magnitude and variability respectively (research question 2) and experiments in purple are those at the start of each day to explore channelization into a flat surface (Fig. 3.1.3). Expt 16 is listed in red and blue as the data from this experiment can be used to answer both research question 1 and 2.

Expt no.	Discharge C = Constant V – Variable (tipping bucket)	Initial slope (degrees)	Channel initially channelised (C) or Unchannelised (UC)	Initial base level drop (cm)
1	1 l/min C	1	UC	1.5
2	1 l/min C	1	UC	4
3	1 l/min C	-	C	4.5
4	1 l/min C (0.82l/min to start)	5	UC	1.5
5	1 l/min C	-	C	4
6	1 l/min C	-	C	1
7	1 l/min C	3.3	UC	2
8	1 l/min C	-	C	4
9	1 l/min C	-	C	1.5
10	1 l/min C	3.8	UC	2
11	1 l/min C	-	C	4
12	1 l/min C	-	C	1.5
13	1 l/min C	1.9	UC	2
14	1 l/min C	-	C	0.5
15	1 l/min C	-	C	0.5
16	1 l/min C	-	C	2
17	1.5 l/min C	3.6	UC	2
18	0.5 l/min C	-	C	2
19	0.2 l/min C	-	C	2
20	0.1 l/min C	-	C	2
21	1 l/min V	3.1	UC	2
22	1 l/min V	-	C	4
23	1 l/min V	-	C	1.5
24	1 l/min V	-	C	0.5
25	1 l/min V	-	C	2
26	1 l/min V	3.9	UC	2
27	1 l/min V	-	C	3
28	1 l/min V	-	C	1
29	1 l/min V	-	UC	2
30	2 l/min C	4.1	UC	0
31	2 l/min C	-	C	2
32	1 l/min V	-	C	0.5
33	1 l/min V	-	C	0.5
34	1 l/min V	-	C	1
35	1 l/min C	-	C	1
36	1 l/min C	-	C	3

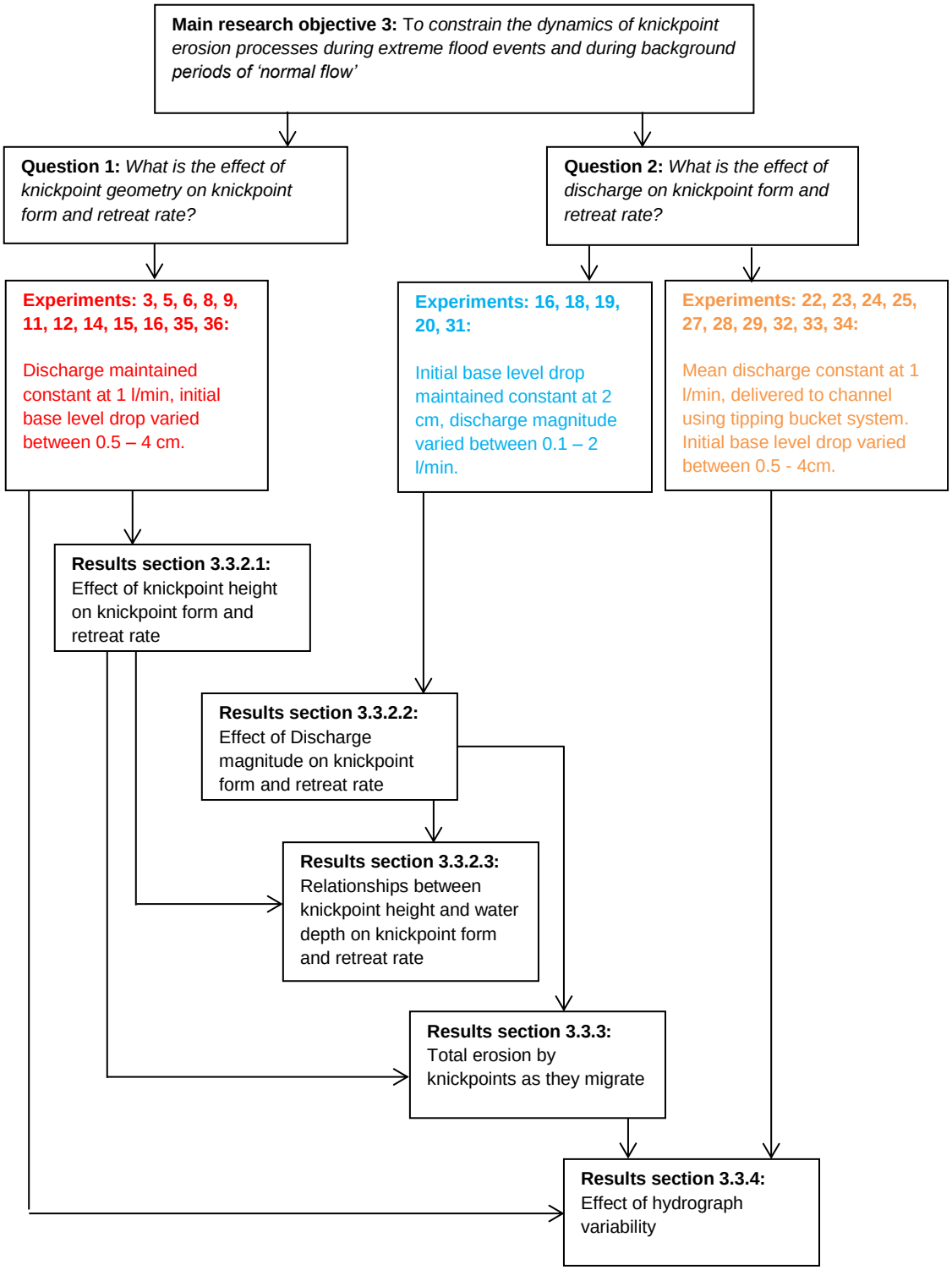

Fig. 3.1.1: Flow diagram of how each of the sets of experiments (Table 3.1.1) help achieve the wider aim of the experimental modelling study. Also shown are the links between each of the results sections (3.3) and how the understanding of knickpoint erosion processes is developed through this chapter. The interpretation of these results is presented in Section 3.4.

Fig. 3.1.2: The 'tipping bucket' (volume = 0.2 l) used to simulate pulses of water to the channel. Total discharge for these experiments was 1 l/min, which was delivered to the channel five times per minute, every 12 seconds. Variations in discharge delivery may produce different patterns (faster or slower) of knickpoint retreat compared to knickpoints undergoing a constant discharge.

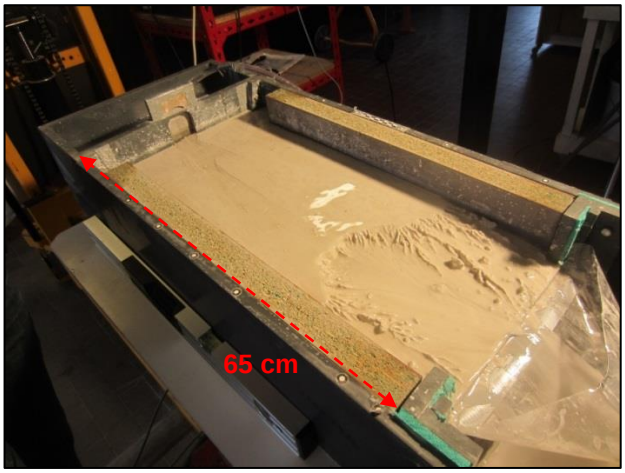

Fig. 3.1.3: Example of an experiment exploring the development of a channel across a flat surface. The initial slope of the channel was changed, resulting in either channel incision or escarpment retreat across the width of the flume. The evolution of the topography was monitored until a channel had formed and the slope of the channel had reached equilibrium (~0.05).

3.1.2 Flume set-up

The experiments were carried out in a flume at the Université de Rennes 1, France, developed over recent years by Jean-Jacques Kermarrec (lead engineer, Université de Rennes), Dimitri Lague (Université de Rennes) Jens

Turowski (during his PhD at University of Cambridge, UK), Alzeena Batta (University of Cambridge Masters student) and Christophe Caillarec (Université de Rennes Masters student). The flume is 0.65 m long and 0.3 m wide, containing a homogenous substrate of silica cement. The flow of water into the channel was controlled using a reservoir upstream of the channel inlet, to dampen pump related turbulence. At the downstream end of the channel, the outlet could be lowered to represent an instantaneous base level fall. This creates a knickpoint at the downstream end of channel that can be monitored as it retreats upstream (Fig. 3.1.4).

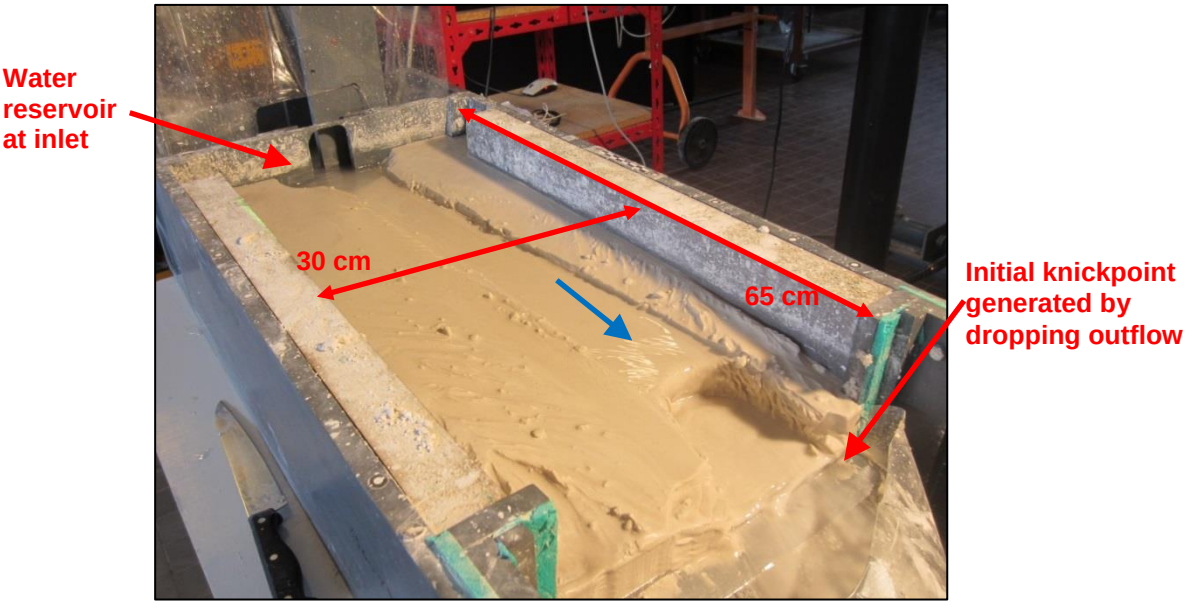

Fig. 3.1.4: Experimental set up. Blue arrow indicates the flow direction of the water.

The homogenous substrate was created through the mixing of 25 kg of granular silica (D_{50} = 40 µm) with 12.5 kg of spherical silica beads (D_{50} = 40 µm) and 8.23 litres of water in a cement mixer. The resulting paste was then transferred into the box flume and re-homogenised using a high frequency concrete vibrator to re-liquefy the paste and remove any air trapped during the mixing process. At the end of the mixing process, silica paste is cohesive and behaves in a similar way to bedrock in a natural river channel (Turowski *et al.,* 2006; Bonnet, 2009).

3.1.3 Relevance of experimental channel to natural rivers

Similar to Turowski *et al.* (2006) and Bonnet (2009), the erosion of the silica paste in these experiments is through grain detachment when the bed shear stress is greater than the critical shear stress to detach material from the channel bed, rather than abrasion. The Froude number in the experiments varies between sub and supercritical which is typical of natural mountain rivers but the Reynold's number is generally lower, leading to flow that is more laminar than fully turbulent (except in the plunge pools); flow in natural mountain rivers is typically fully turbulent. This has an advantage in that the experimental flume dimensions, and therefore the experimental run-time, can be reduced (Malverti *et al.*, 2008). Malverti *et al.* (2008) demonstrated that the evolution of the longitudinal bed profiles of turbulent and laminar rivers are governed by identical dimensionless equations and therefore follow the same dynamics, allowing the extrapolation from the experimental scale where flow is more laminar to the field scale of steep mountain rivers where flow is typically more turbulent. Despite the simplifications in the erosion processes and flow hydraulics within the experimental channel, the sediment transport behaviour is similar to natural rivers as material is transported both in suspension and as bedload, testified to by the observation of bedload sheets migrating downstream. Therefore, the results and understanding of knickpoint erosion processes developed in these experiments are relevant for the understanding of the knickpoint erosion processes in natural river settings.

3.2 Methods

3.2.1 Data collection

While the experiments were ongoing, data were collected using three complementary techniques: a Leica ScanStation 2 Terrestrial Laser Scanner (TLS) system, a mounted time lapse camera and visual observations. The TLS was used to collect high spatial resolution (millimetre scale) point clouds of the topography of the experimental channel at 60 second intervals throughout the duration of the experiments (Fig. 3.2.1). This high spatial and temporal resolution data allow the evolution of the channel topography, and therefore the knickpoint location, to be monitored accurately through time. The Leica ScanStation 2 TLS uses a green laser with a wavelength that can penetrate water, a capability beyond other TLS systems that use a Near-Infra Red wavelength, allowing the mapping of the channel bed. The spot size of the laser is ~ 3 mm and the typical ranging noise on the experiment surface is 1.5 mm (1 standard deviation). In some cases, bank undercutting took place through the lateral erosion of the channel creating overhanging banks that prevented the laser scanner from recording returns from the whole width of the channel. To prevent this, the overhanging banks were removed manually during the experiment using a knife to restore line-of-sight access to the whole of the channel.

A time lapse camera was mounted directly above the experimental channel and was programmed to collect a photograph every 60 seconds (Fig. 3.2.2), allowing the retreat of the knickpoint to be monitored through time as well as the identification of other features such as terrace formation downstream. Additionally, visual observations were made by the observer throughout the experiments to complement the mounted camera imagery and the point clouds. The hydrograph for the ‘tipping bucket’ experiments was determined using a mass balance located at the outflow of the channel. As water flowed into a bucket, the balance monitored the increase in mass every second, which was then used to infer the discharge and its variability. While the water

did contain some suspended sediment, its proportion to water volume was negligible so unlikely to significantly affect the mass balance readings.

Fig. 3.2.1: The Leica ScanStation 2 Terrestrial Laser Scanner system used to collect the high resolution topographic data of the experimental channel every 60 seconds.

Fig. 3.2.2: Example of one of the images collected using the mounted time lapse camera. Flow is from right to left in this image. Also visible at the top edge of the flume, at the boundary between the paste and the wooden board is the green laser beam from the laser scanner.

3.2.2 Data processing

Data were extracted from the laser scans through a range of computational and manual techniques. It is widely acknowledged that the nature of the flow conditions at the knickpoint may be an important control on the knickpoint retreat rate (e.g. Gardner, 1983). Therefore, the water depth was calculated for each point in the point cloud using an empirical relationship derived by Gangloff (2014) between water depth and the normalised intensity of the laser return measured by the scanner:

$$I_{norm} = \frac{I_{raw}+1024}{\cos(\theta)} \quad \text{Eqn. 3.1}$$

$$h = \frac{47.43493-(0.1901 \times I_{norm})+(2.9797\times10^{-4} \times {I_{norm}}^2)-(1.63145\times10^{-3} \times {I_{norm}}^3)}{1000} \quad \text{Eqn. 3.2}$$

Where I_{norm} = normalised intensity of laser return, I_{raw} = intensity of laser return measured by laser scanner, θ = incidence angle of laser (in degrees) and h = water depth (in m) (relationship derived by Gangloff, 2014). This empirical relationship is only valid on gently sloping surfaces so the water depth is only calculated upstream and downstream of the knickpoint rather than at the knickpoint itself. Additionally, there is some refraction and change in the light celerity caused by the water which leads to a slight offset between the calculated water depth and the true water depth at each point. However, this is a minor effect and does not alter the calculation of the knickpoint position as the water depth, and thus the offset, is negligible on the steep faces of the knickpoints. Additionally, the slope calculation is unaffected as the degree of offset does not vary over the short distances used to calculate the topographic slope.

The slope of the channel at each point was also calculated over a local area (over 5 mm radius surrounding each point), allowing the subsequent extraction of the shear stress and stream power using the following equations:

$$\tau = \rho g h S \quad \text{Eqn. 3.3}$$

$$\Omega = \rho g Q S \quad \text{Eqn. 3.4}$$

Where τ = shear stress, Ω = stream power, ρ = fluid density (1000 kg m^{-3}), g = acceleration due to gravity (9.81 m s^{-2}), Q = discharge (in m^3 s^{-1}) and S = channel slope (in m/m).

Following the calculation of each of the above parameters, these data were written to new scalar fields in the point clouds for visualisation and analysis in CloudCompare v 2.6.1.beta software.

3.2.3 Channel centre line extraction

The location of the channel in each point cloud was identified through visual analysis of the map of the water depths (Fig. 3.2.3). A line was then drawn along the centre of the channel throughout its length (Fig. 3.2.4A & 3.2.4B), which was used to extract the information required to determine the knickpoint form, knickpoint location and water depth for each point cloud. The centre of the channel was chosen for analysis to ensure that the vector distance calculated for knickpoint movement between scans is consistent and accurate.

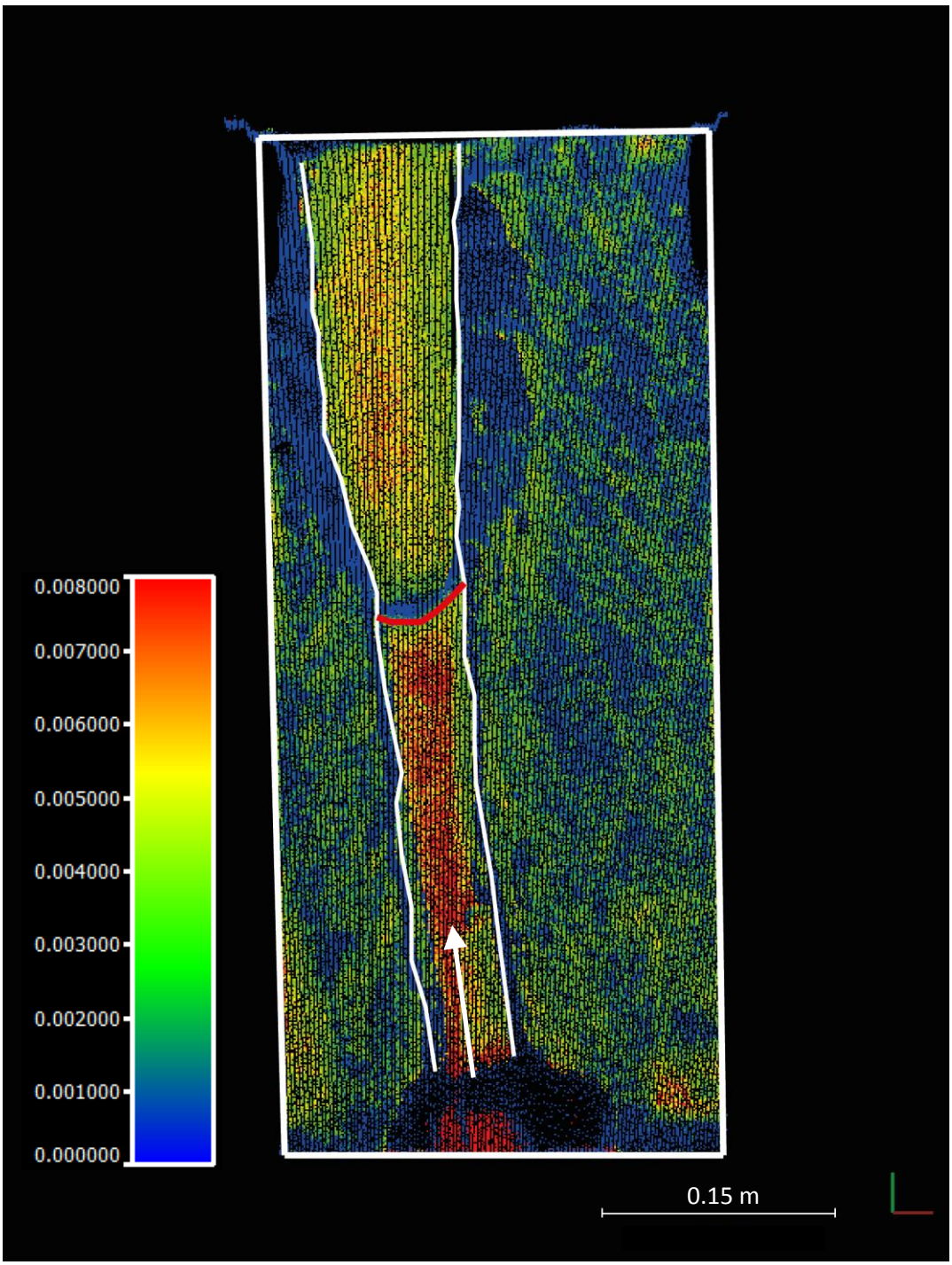

Fig. 3.2.3: Map of water depth, calculated using empirical law derived by Gangloff (2014), for scan number 13 (time = 762 s) of Experiment 22. The colours have been saturated to red above 0.008 m water depth. The channel can be clearly seen in the area of 'hotter' colours with the location of the knickpoint indicated by the red line across the channel. The white lines along the edges of the channel mask and the borders of the flume are shown to allow easy comparison with Fig. 3.2.4A; the white arrow indicates the flow direction. The white scale bar is 0.15 m long.

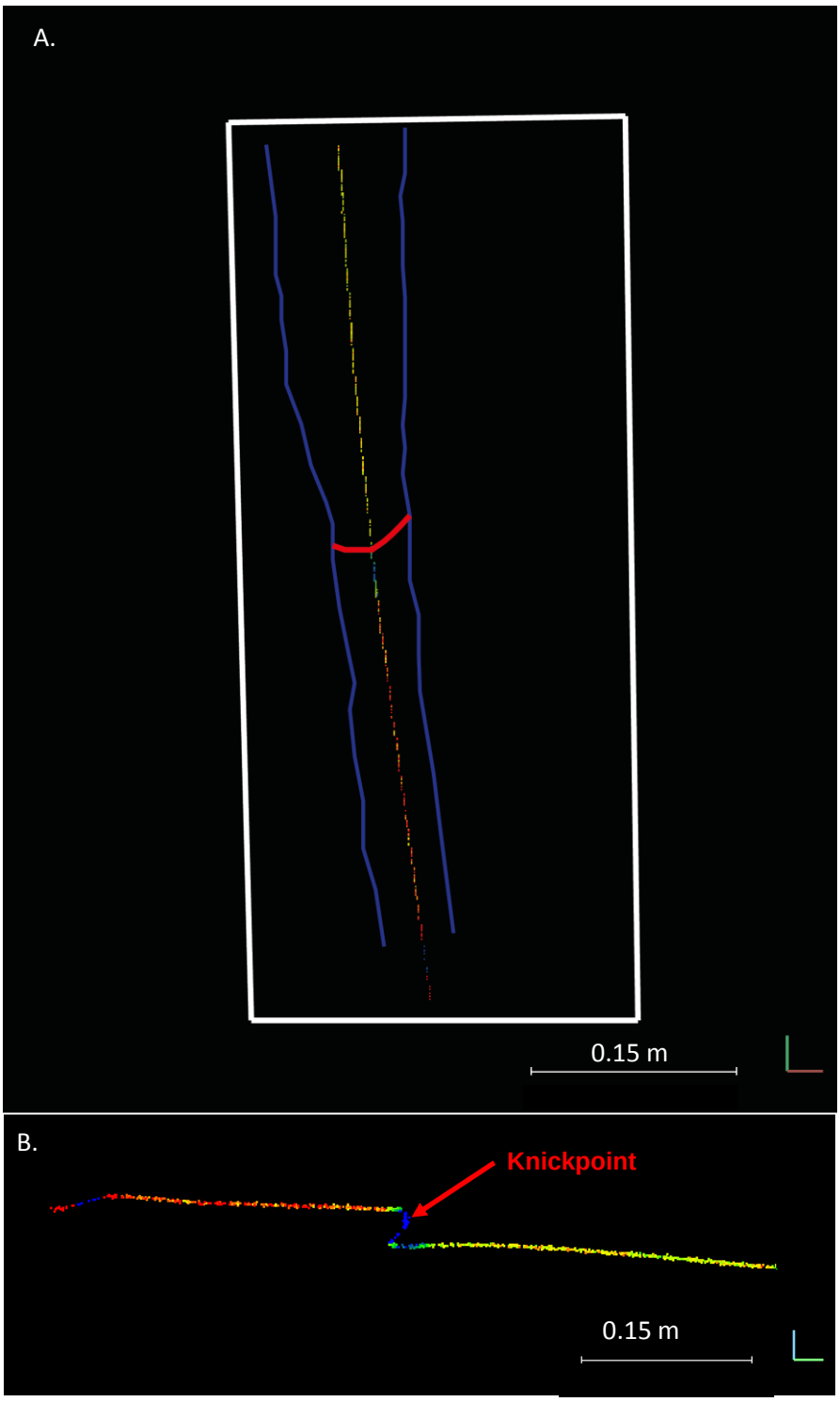

Fig. 3.2.4: A: Plan view of the subsection of the point cloud manually extracted from the centre line of the channel for scan number 13 of experiment 22 using CloudCompare. The white boundary lines and the blue channel edge lines allow direct comparison with Fig 3.2.3. The red line shows the location of the knickpoint which can be clearly seen in the cross-sectional view in **B** (colours still represent the water depth as in Fig. 3.2.3). The white scale bar is 0.15 m long.

3.2.4 Knickpoint form classification

The knickpoints that evolved during the experiments were classified into one of four categories of knickpoint form: (i) Knickpoints that maintained a vertical step and developed an undercutting plunge pool (Fig. 3.2.5A), (ii) Knickpoints that maintained a vertical step at the knickpoint lip, but did not develop an undercutting plunge pool (Fig. 3.2.5B), (iii) Knickpoints that diffused from a vertical step into a reach that was steeper than the slope of the rest of the channel (Fig. 3.2.5C) and (iv) Knickpoints that diffused completely and were no longer visible in the channel profile (Fig. 3.2.5D).

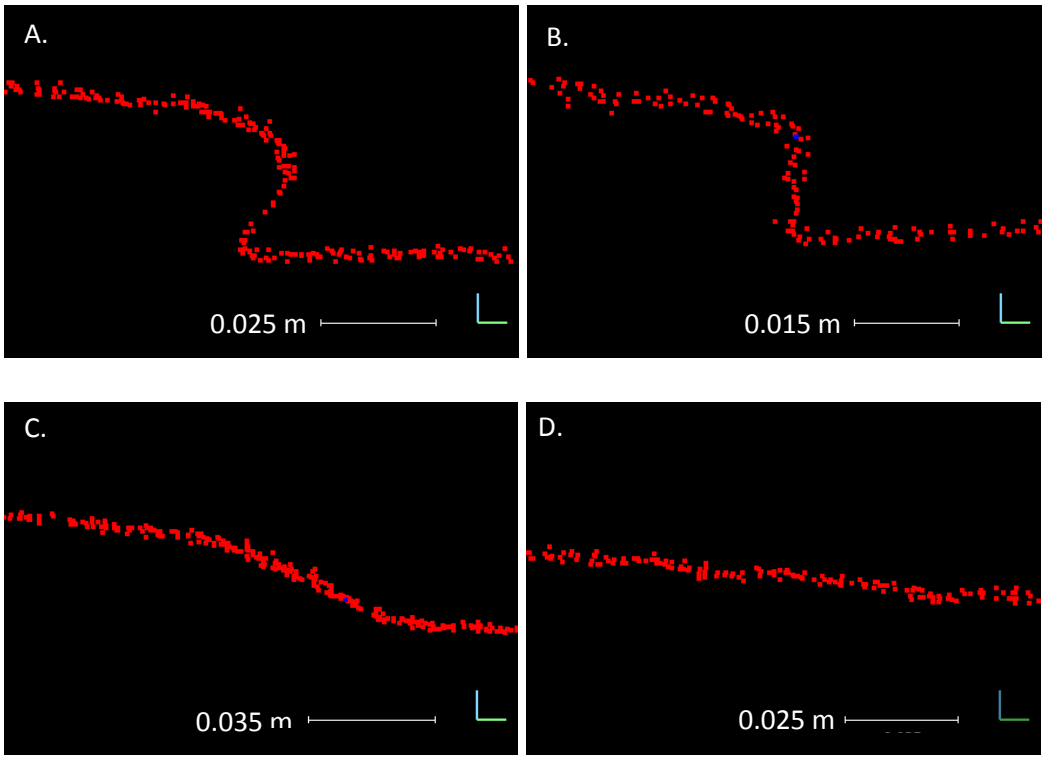

Fig. 3.2.5: The four classification types of knickpoint form seen in the experiments; **A.** Undercutting. **B.** Vertical step. **C.** Steepened reach. **D.** Diffused.

A summary classification of the knickpoint form over the course of a whole experiment was required to allow comparison between different experiments. In some cases, the knickpoint maintained the same form throughout its propagation upstream (Fig. 3.2.6A). In other cases, the form of the knickpoint evolved as it migrated upstream (Fig. 3.2.6B), which made the summary classification more difficult. To maintain consistency between experiments,

the summary classification of the knickpoint form was made when the knickpoint had retreated halfway up the channel length (red arrows in Fig. 3.2.6), to avoid potential boundary effects of the initial base level fall at the channel outlet.

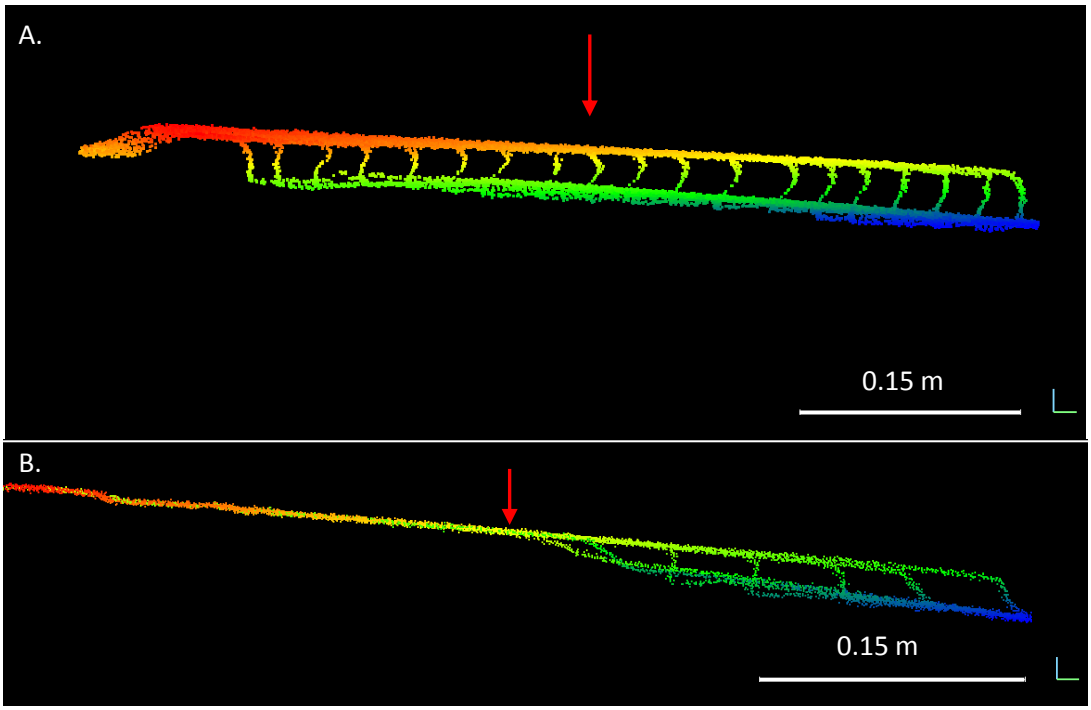

Fig. 3.2.6: Evolution through time of knickpoints from different experiments. Red arrows indicate the location of where the summary knickpoint classification was made at half the channel length. **A.** Experiment 22 (initial knickpoint height: 4 cm), scans 2-20: the knickpoint maintains an undercutting plunge pool throughout the length of the channel, resulting in the summary classification as 'Undercutting'. **B.** Experiment 20 (initial knickpoint height: 2 cm), scans: 3, 5, 7, 9, 11, 13 and 15. The knickpoint starts with a vertical step and then diffused into a steepened reach before diffusing completely before the knickpoint has retreated halfway up the channel length, resulting in the summary classification as 'Diffused'. The red to blue colour spectrum indicates relative height, with warm colours 'higher' than cooler colours.

3.2.5 Vector distance and knickpoint retreat rate

For each point cloud in each experiment, where a knickpoint was present, the upstream and downstream limits (x-, y- and z- coordinates extracted for each) of the knickpoint were manually selected through visual analysis of the channel profiles. An automatic knickpoint detection processing was not used

in this study due to some of the point clouds containing 3D artefacts such as undercutting plunge pools. Normal point cloud to raster interpolation algorithms would not be able to produce Digital Elevation Models (DEMs) that accurately replicated these features so it was decided that all data extraction would take place on the raw point clouds. These data provide information regarding the geometry of the knickpoint as the knickpoint height is calculated as the difference between the z-coordinates of the upstream and downstream knickpoint limits.

The location of the knickpoint in each point cloud was compared with the knickpoint location in the subsequent point cloud in order to calculate the knickpoint retreat rate. The vector distance between the locations of the knickpoint limits between experiments was calculated using the following equation:

$$d = \sqrt{(x_{i+1} - x_i)^2 + (y_{i+1} - y_i)^2 + (z_{i+1} - z_i)^2} \quad \text{Eqn. 3.5}$$

where d = vector distance between knickpoint locations and the indices *i* and *i+1* refer to coordinates in the initial and subsequent point clouds respectively.

Each point cloud has a corresponding time stamp, measured by the laser scanner, which represents the time (in seconds) since the first laser scan of the experiment. The knickpoint retreat rate was therefore calculated using the following equation:

$$KP_{RR} = \frac{d}{(t_{i+1} - t_i)} \quad \text{Eqn. 3.6}$$

Where KP_{RR} = knickpoint retreat rate, t_i = time that the initial point cloud was collected and t_{i+1} = time that the subsequent point cloud was collected. The mean retreat rate between each scan was calculated as the mean of the retreat rates of the upstream and downstream limit of the knickpoints.

Where the knickpoints maintained a vertical step, or developed an undercutting plunge pool (e.g. Fig. 3.2.7A), it was relatively easy to visually

select the location of the upstream and downstream limits of the knickpoint. However, where the knickpoints evolved into a steepened reach (e.g. Fig. 3.2.7B), the selection of the limits was generally harder due to a less abrupt inflection point from the ‘normal’ channel slope to the ‘steepened’ channel slope at the knickpoint. This could potentially lead to some measurement error in the exact position of the upstream and downstream location of the knickpoint which would be difficult to quantify, but care was taken when manually selecting the knickpoint limits in order to be as accurate and as consistent as possible.

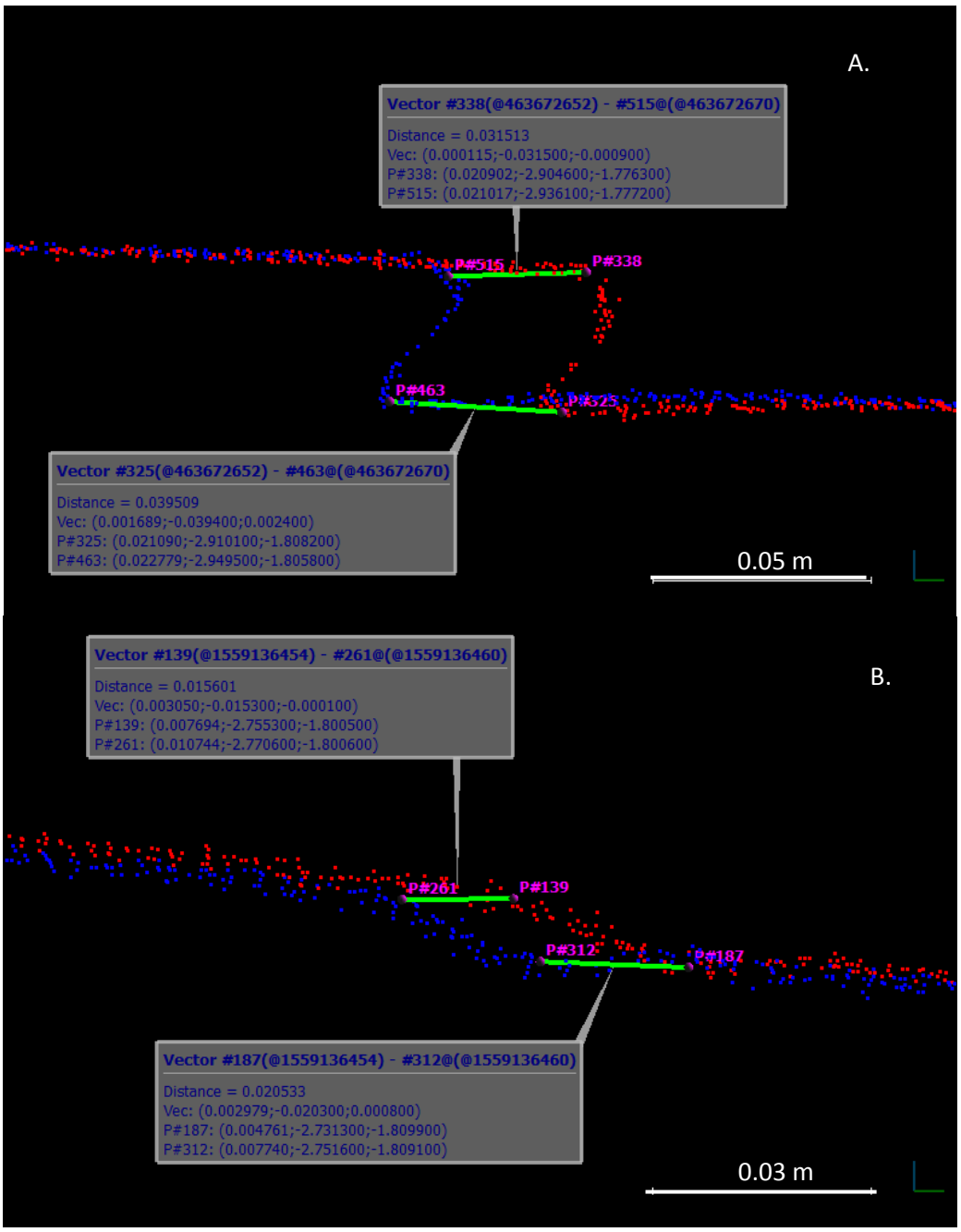

Fig. 3.2.7: A. Example of the selection of the upstream and downstream limits of the knickpoint, and the calculation of the vector distance (in metres) between them (shown by green segments). Experiment 22, scans 13 (in red) and 14 (in blue). **B.** Example of upstream and downstream knickpoint limit selection for a knickpoint that is classified as a steepened reach rather than a vertical step or has an undercutting plunge pool. The inflection point at the upstream limit of the knickpoint is harder to determine, although care was taken to ensure the selection was as accurate and consistent as possible. Experiment 35, scan 9 (in red) and scan 10 (in blue). Colours are used to aid differentiation between the two point clouds.

3.2.6 Water depth extraction

Water depth was calculated for each point in the point cloud using the empirical relationship derived by Gangloff (2014), and included in the point cloud data. The water depth information was stored as “Scalar field #4” and manually extracted from the channel centre line extraction sub-clouds. The depth was extracted for each scan in a similar way to the knickpoint location, with the value taken from a point upstream of the inflection point in the channel at the upstream limit of the knickpoint (Fig. 3.2.8).

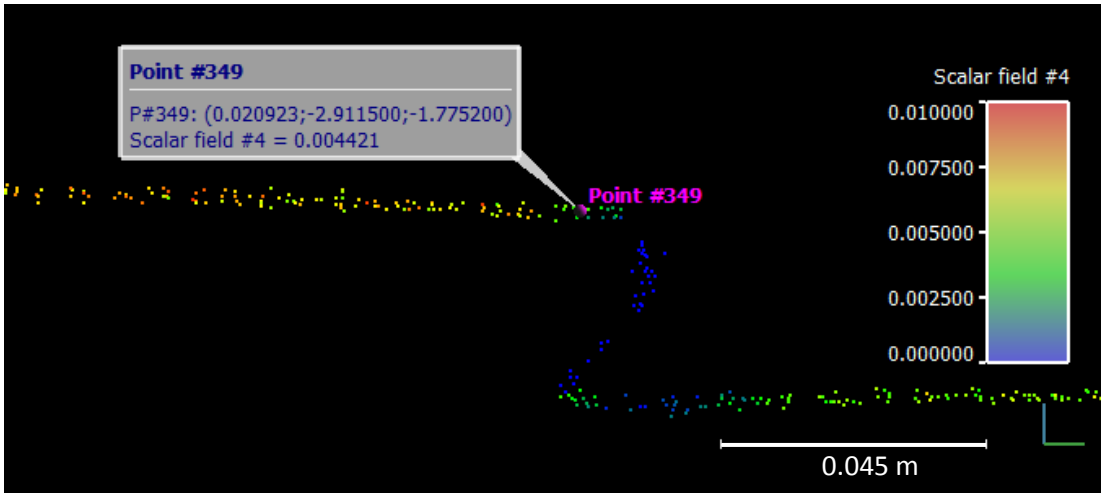

Fig. 3.2.8: Example of extraction of water depth upstream of the knickpoint from the centre channel line point cloud subset. In this case (Experiment 22, scan 13), the extracted water depth was 4.42 mm (“Scalar field #4”).

3.3 Experimental modelling results

This Sub-Chapter documents the results of the experimental modelling study examining the controls on knickpoint form and retreat in a homogenous substrate. Videos of all experiments from the mounted time lapse camera and the evolution of the channel profile extracted from the point clouds are available on the Supplementary Disc.

3.3.1 Hydraulic scaling of the experimental channel

The channel width (*W*) at any given point along the length of a bedrock river, with uniform precipitation, bedrock and incision rate, is supposed to scale with the drainage area (*A*) according to the following relationship:

$$W = k_w A^b \qquad \text{Eqn. 3.3.1}$$

Where k_w is a constant known as the width index and b is the width-area scaling exponent (Lague, 2014). Assuming that drainage area is a proxy for discharge, the average reported value of b from seven different study sites is 0.35 ± 0.11 (data compiled in Lague, 2014 from: Snyder *et al.*, 2003b; Duvall *et al.,* 2004; Whittaker *et al.,* 2007; DiBiase and Whipple, 2011). The channel width was extracted upstream of the knickpoint using the water depth mask for 10 point clouds in each experiment where the discharge magnitude was varied and the initial base level drop (BLD) was maintained constant. The value of b in the experimental channel is 0.37 (Fig. 3.3.1) which suggests that the river geometries in these experiments are relatively consistent with natural bedrock rivers.

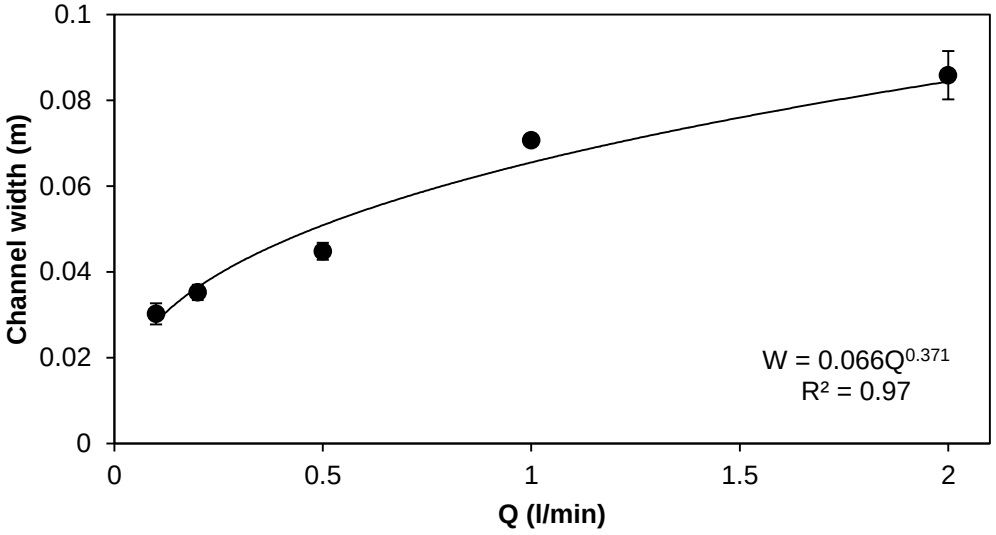

Fig. 3.3.1: Scaling of channel width against discharge in the experimental channel. The value of the width-discharge exponent (0.37) matches the value seen in natural bedrock rivers. The error bars are very small for each experiment, and represent the standard deviation on the measurements of the channel width.

Similar to the channel width, the slope (*S*) of a natural bedrock river is supposed to scale with drainage area according to a power-law relationship:

$$S = k_s A^{-\theta} \qquad \text{Eqn. 3.3.2}$$

where k_s is the channel steepness index and θ is the concavity index (Lague, 2014). The most likely value for the concavity index is still debated, with a range of values for θ between 0.4 to 0.6 often reported for 'steady-state' systems (e.g. Whipple, 2004; Kirby and Whipple, 2012). On the other hand, a previous experimental study of landscape evolution using silica (Turowski *et al.*, 2006) reported that the channel slope was independent of the drainage area (i.e. the channel profile was flat and the concavity index was close to zero). A possible explanation for this observation is the very small scale channels that developed in the 'fogbox' due to the size of the landscape (40 x 60 cm) resulting in very narrow (< 10 mm) and shallow (< 1 mm) channels. At this scale, the flow velocity can be affected by surface tension of the water so the flow hydraulics are not necessarily comparable to natural settings (Turowski *et al.*, 2006). The value of the concavity index θ in the channel in

my experiments is 0.27 (Fig. 3.3.2), which is lower than often reported, although it should be noted that a direct comparison with 'steady-state' systems cannot be made due to the 'transient' nature of the experimental channel as the knickpoints migrate and evolve.

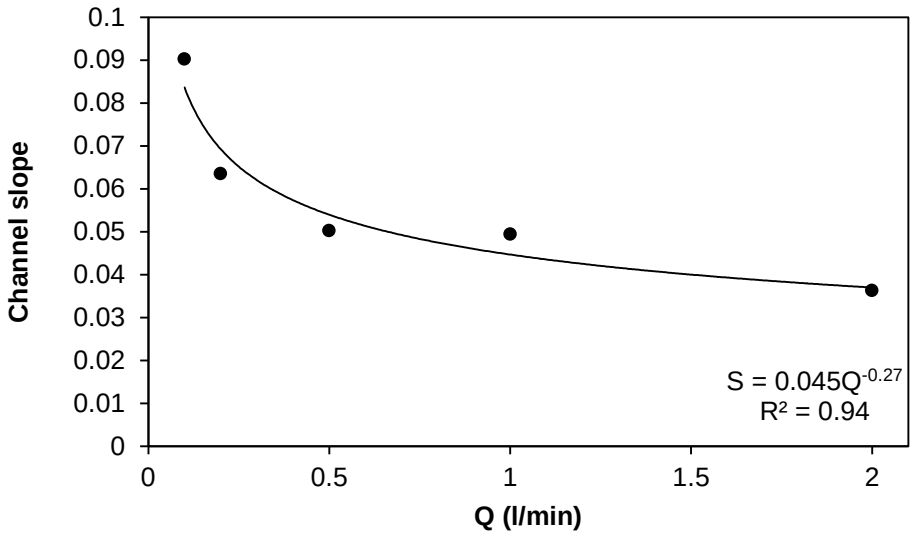

Fig. 3.3.2: Scaling relationship between slope (S) and discharge (Q) in the experimental channel. The value of the concavity index (0.27) is lower than proposed for natural bedrock rivers (between 0.4 to 0.6)

Fig. 3.3.3 shows the relationship between the ratio of channel width to flow depth and the channel slope. Steeper slopes are associated with narrow deeper channels (lower width-depth ratio) while lower slopes are associated with wider shallower channels, which is similar to the findings of Whittaker *et al.* (2007) although the exponent in the equation (-0.82) is higher than that predicted by Whittaker *et al.* (2007) for the Rio Torto in the Apennines, Italy (exponent = -0.34). This difference could be explained by the small number of data points in the experimental study (five) covering a narrow range of slopes (0.036 – 0.09) compared to the Whittaker *et al.* (2007) study that had a range of slopes from 0.0 – 0.4.

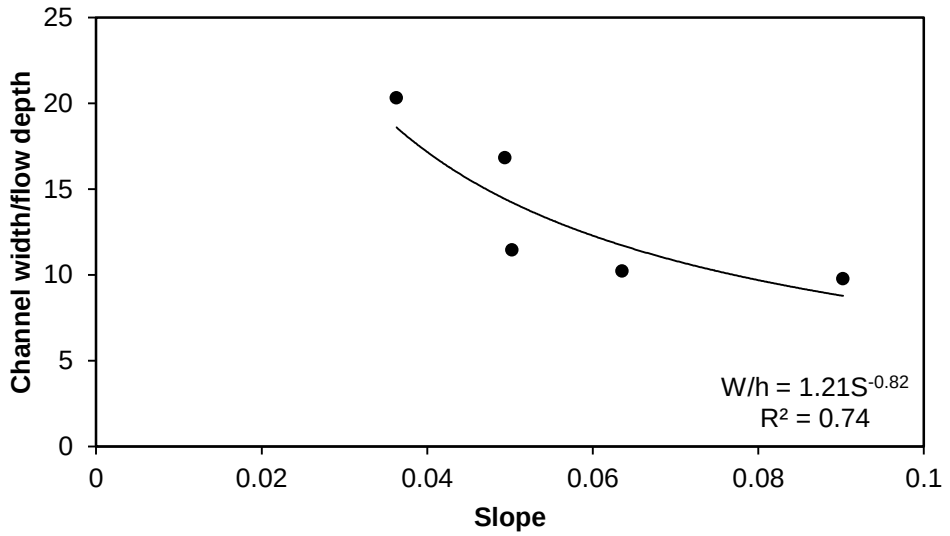

Fig. 3.3.3: Channel width-depth ratio against channel slope for the experimental channel.

The hydraulic scaling relationships in the experimental channel follows the same pattern as those found in natural bedrock rivers, although the exponents in some of the equations are slightly different to those found in other studies (e.g. Whittaker *et al.,* 2007; Kirby and Whipple, 2012; Lague, 2014). Despite this, there is still a qualitative consistency between the knickpoint dynamics and knickpoint forms in the experiments and natural rivers (see Section 3.1.3), so the understanding of the mechanisms of knickpoint retreat developed from the experiments can be used to help identify the important controls on knickpoint retreat in natural bedrock river settings (Turowski *et al.*, 2006).

3.3.2 Controls on knickpoint form retreat rate

3.3.2.1 Effect of knickpoint height on knickpoint form and retreat rate

There is a positive relationship between knickpoint height (KP_H) and knickpoint retreat rate (KP_{RR}) ($KP_{RR} = 0.0067KP_H + 0.00023$) in the experiments where the discharge was kept constant (1 l/min) and the initial base level drop varied (0.01 to 0.04 m) (Fig. 3.3.4). Table 3.3.1 provides the mean height and retreat rate of knickpoints for each experiment. The

correlation between KP_H and KP_{RR} is strong for this summary data (Pearson correlation coefficient = 0.83; Fig. 3.3.4B) suggesting a clear positive relationship between KP_H and KP_{RR} when Q is constant. A possible explanation for this relationship is differences in the knickpoint form (see Fig. 3.2.5 in sub-chapter 3.2 for the definition of the classifications). Generally, initially taller knickpoints (> 30 mm) developed an undercutting plunge pool (e.g. Expt 11; Fig. 3.3.5) and retreated faster than shorter knickpoints (< 20 mm) that diffused from the initial vertical step into a steepened reach (e.g. Expt 12; Fig. 3.3.6); knickpoints that maintained the vertical step generally corresponded to intermediate knickpoint heights and the experiments that diffused completely before the knickpoint reached half of the channel length retreated the slowest (e.g. Expt 35; Fig. 3.3.7)

Table 3.3.1: Summary data of experiments that had a constant discharge of 1 l/min with varying initial Base Level Drops (0.01 – 0.04 m). Data are sorted in ascending order of mean knickpoint height (KP_H) and colour coded according to knickpoint form classification when it had retreated halfway of the channel length. Experiment number 8 is excluded from all further analysis due to large bend that formed in the channel which affected the knickpoint migration (See Supplementary Disc for video of experiments).

Expt no.	Initial Base Level Drop (mm)	Knickpoint height (mm)		Knickpoint retreat rate (mm/s)		KP form
		Mean	St Dev	Mean	St Dev	
35	10	9.77	1.99	0.303	4.13×10^{-2}	Diffused
6	10	9.83	5.55	0.336	4.46×10^{-2}	Steepened
9	15	14.8	2.60	0.343	8.39×10^{-2}	Steepened
16	20	17.4	2.10	0.372	8.66×10^{-2}	Vertical
12	15	21.9	3.78	0.348	1.18×10^{-1}	Steepened
8	*40*	*22.4*	*8.13*	*0.443*	*9.43×10^{-2}*	*Steepened*
36	30	24.8	2.00	0.346	6.20×10^{-2}	Vertical
11	40	29.2	3.82	0.515	8.39×10^{-2}	Undercutting
5	40	32.2	5.39	0.493	1.76×10^{-1}	Vertical

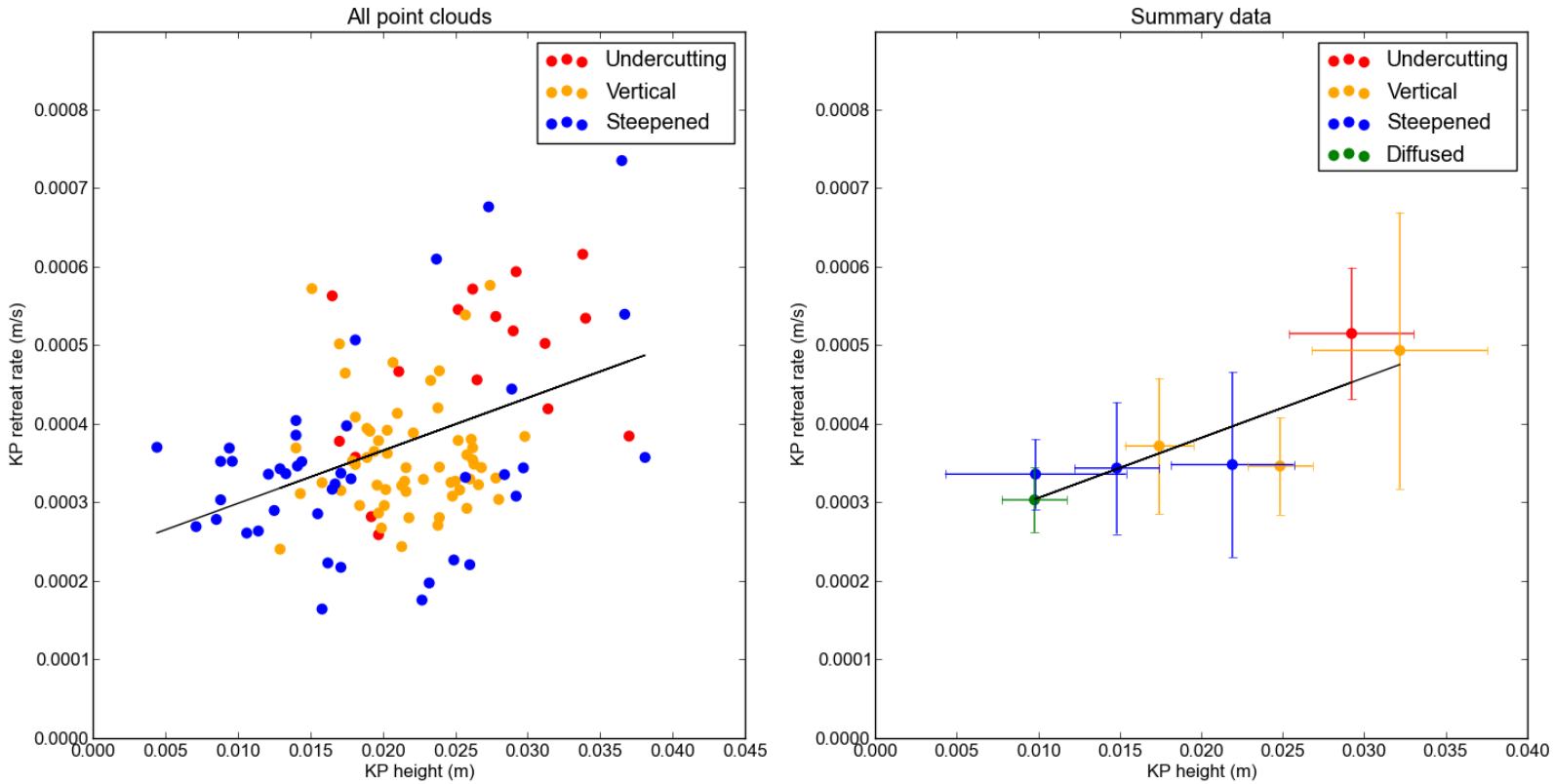

Fig. 3.3.4: Knickpoint height (KP_H) against knickpoint retreat rate (KP_{RR}) for the experiments where the discharge was kept constant and the initial base level drop varied (0.01-0.04 m). Colours indicate the classification of knickpoint form as indicated. **A.** Every point cloud where a knickpoint was present in the experiments (linear regression line: $KP_{RR} = 0.0067KP_H + 0.00023$; $R^2 = 0.16$; Pearson correlation coefficient = 0.40). **B.** Mean knickpoint height and mean knickpoint retreat rate for each experiment, with error bars indicating the standard deviation. The knickpoint form was classified when the knickpoint had migrated half the channel length ($KP_{RR} = 0.0077KP_H + 0.00023$; $R^2 = 0.69$; Pearson correlation coefficient = 0.83).

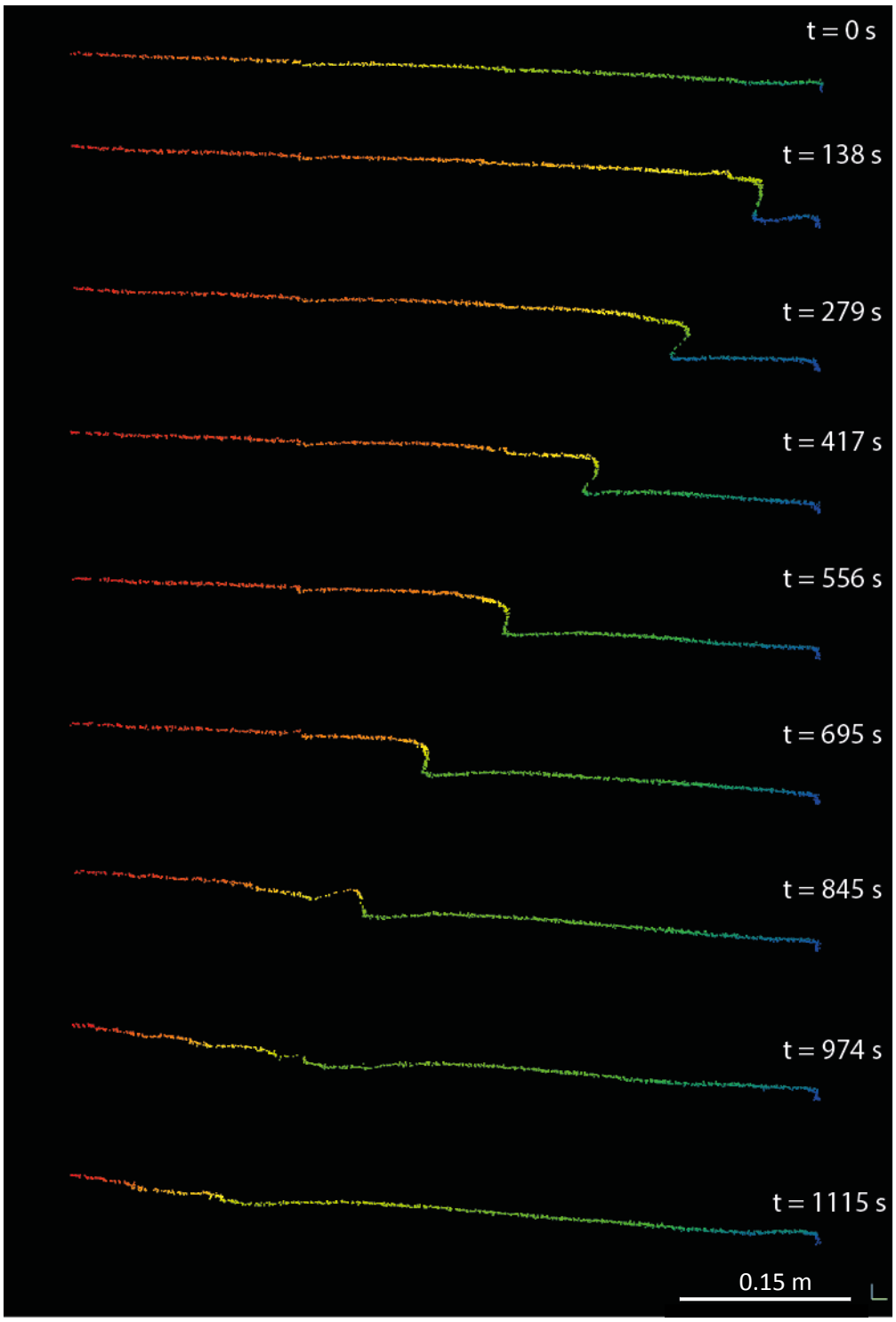

Fig. 3.3.5: Example of the long profile evolution of an experiment where the knickpoint form is classified as 'Undercutting'. (Experiment 11: Q = 1 l/min; Initial BLD = 0.04 m). The red to blue colour spectrum indicates relative height, with warm colours indicating a higher elevation than cooler colours for each scan. At t = 695s, the knickpoint form is classified as 'Vertical'.

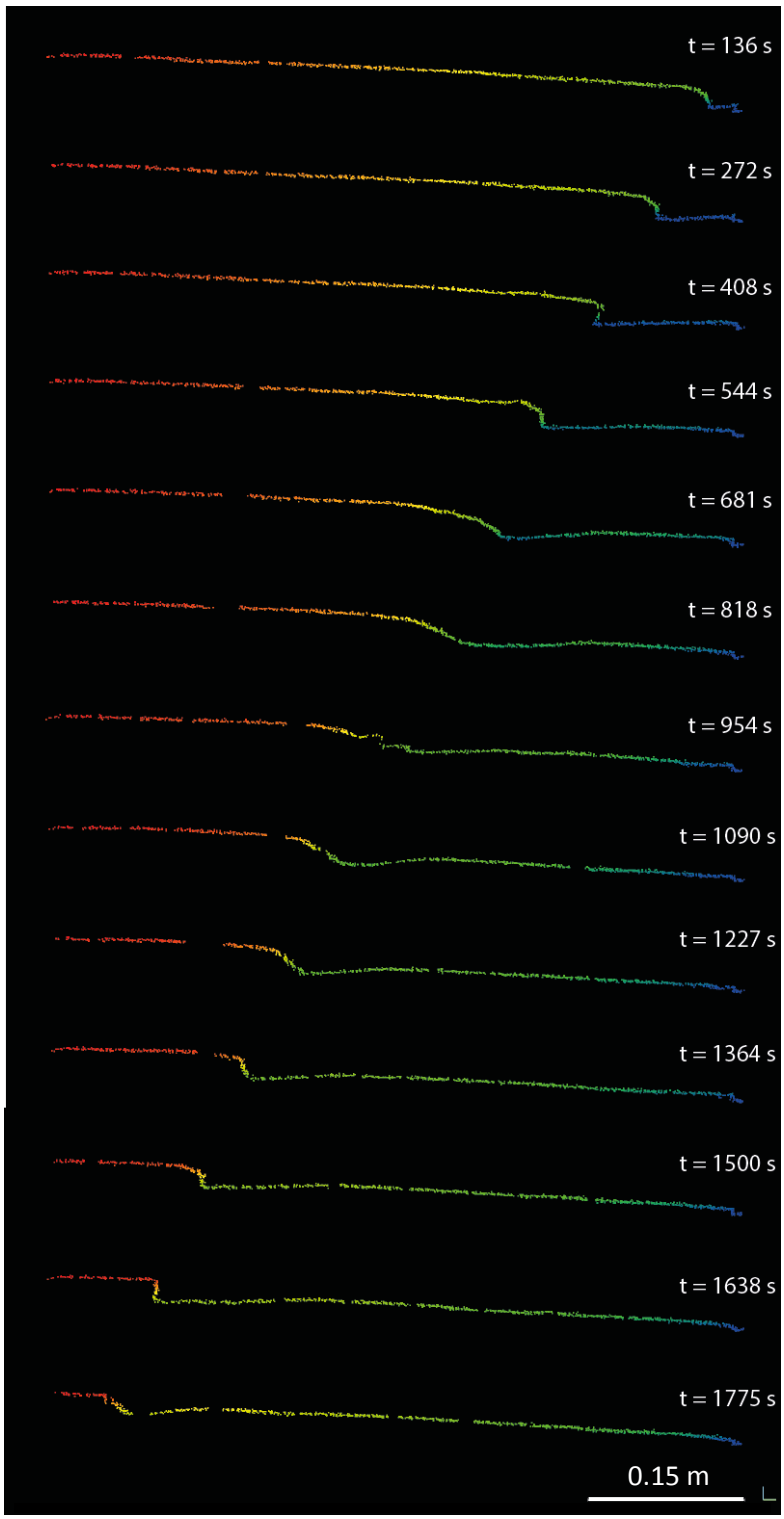

Fig. 3.3.6: Example of the long profile evolution of an experiment where the knickpoint form is classified as ‘Steepened’ (Experiment 12: Q = 1 l/min; Initial BLD = 0.015 m). The red to blue colour spectrum indicates relative height, with warm colours indicating a higher elevation than cooler colours for each scan. Example of a ‘vertical’ knickpoint form can be seen at t = 544s and t = 1638s.

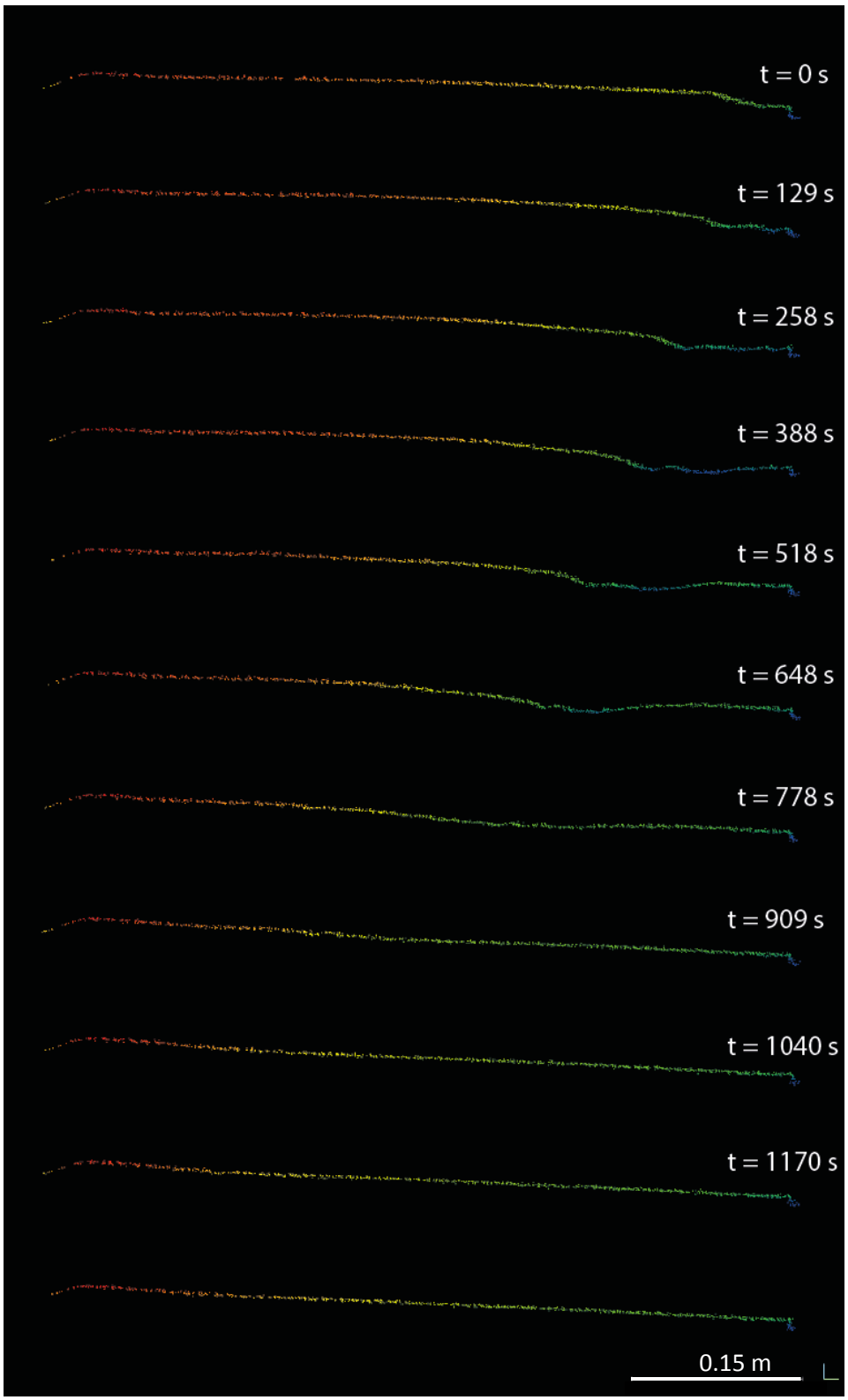

Fig. 3.3.7: Example of the long profile evolution of an experiment where the knickpoint form is classified as 'Diffused' (Experiment 35: Q = 1 l/min; Initial BLD = 0.01 m). The red to blue colour spectrum indicates relative height, with warm colours indicating a higher elevation than cooler colours for each scan.

3.3.2.2 Effect of Discharge magnitude on knickpoint form and retreat rate

The results from the experiments where the initial base level drop was kept constant (at 0.02 m) and the discharge magnitude was varied (0.1 – 2 l/min) (Table 3.3.2) show little to no relationship between the magnitude of the discharge and the knickpoint retreat rate (Fig. 3.3.8). Therefore, on the reach scale of the order of 10-20 channel widths, discharge is not a dominant control on the knickpoint retreat rate.

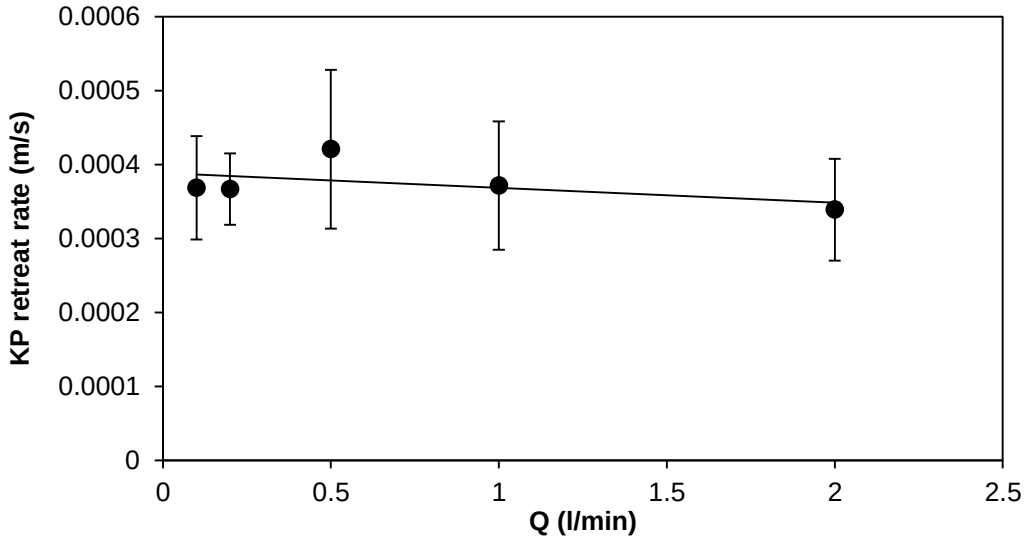

Fig. 3.3.8: Relationship between knickpoint retreat rate and discharge (0.1 to 2 l/min). All experiments (no. 16, 18, 19, 20, 31) were carried out using the same initial base level drop (0.02 m) although the knickpoint height evolved during each experiment. There is no clear trend between knickpoint retreat rate and discharge in these experiments (KP_{RR} = -2.02 x $10^{-5}Q$ + 0.000389; R^2 = 0.28; Pearson correlation coefficient = -0.53)

Table 3.3.2: Summary data of experiments that had a constant initial base level drop (0.02 m) with discharge magnitude varying between 0.1 and 2 l/min. Data are sorted in ascending order of mean knickpoint height (KP_H) and colour coded according to knickpoint form classification when it had retreated halfway of the channel length.

Expt no.	Q (l/min)	Channel width (m)	Knickpoint height (mm)		Knickpoint retreat rate (mm/s)		KP form
			Mean	St Dev	Mean	St Dev	
19	0.2	0.0352	13.0	4.56	0.367	4.83×10^{-2}	Steepened
31	2	0.086	16.5	5.01	0.339	6.88×10^{-2}	Steepened
16	1	0.0701	17.4	2.10	0.372	8.66×10^{-2}	Vertical
20	0.1	0.030	17.4	3.01	0.368	6.98×10^{-2}	Diffused
18	0.5	0.045	19.8	2.94	0.421	1.07×10^{-1}	Diffused

There is some variability within the data (e.g. the higher retreat rate for the experiment with Q = 0.5 l/min). Although the initial knickpoint heights were kept constant at 0.02 m, the knickpoint height varied during the course of each experiment (see videos on Suppl. disc). Therefore the relationship between the knickpoint height and retreat rate was investigated using the same approach as Section 3.3.2.1 to analyse the variability in retreat rate and knickpoint height during an experiment (Fig. 3.3.9; Table 3.3.2). The general relationship between KP_H and KP_{RR} in the constant initial base level drop (BLD) experiments is relatively poor when all the point clouds are considered (R^2 = 0.02; Pearson correlation coefficient = 0.15; Fig. 3.3.9A). However, there is a positive relationship when mean height is plotted against the mean retreat rate (R^2 = 0.36; Pearson correlation coefficient = 0.60; Fig. 3.3.9B).

The classification of knickpoint form in the summary plot (Fig. 3.3.9B) does not follow the same pattern as Fig. 3.3.4B as the two experiments which are classified as having diffused before the knickpoint reached the halfway point in the channel correspond to the taller knickpoints with a higher KP_{RR}. However, the uncertainty on the mean values in these experiments is high so it is hard to identify a true pattern in the data. Another possible explanation for the distribution of points in Fig. 3.3.9B could be the dynamic behaviour in the evolution of the knickpoints leading to the summary knickpoint

classification potentially not being representative of the true nature of the knickpoint form in each of these experiments (see example of Expt 19; Fig. 3.3.10). In experiment 19, the knickpoint evolved from being an initial vertical step when the experiment started to a steepened reach (t = 0 s to 129 s – note that the scan was started at 0 s but, by the time the laser has scanned as far as the channel at the centre of the box flume, the knickpoint had already retreated a short distance). Then, the knickpoint evolved into a vertical step (t = 259 s to 517 s), which could explain the faster retreat in this experiment. The knickpoint then diffused into a steepened reach by the time it reached the halfway point in the channel. Therefore, the summary classification used in Fig. 3.3.9B is not necessarily representative of the true nature of the knickpoint during the entire course of this experiment. However this classification method was maintained in order to achieve consistency between the summary classifications in all experiments. The knickpoints in experiments 16, 18, 20, 31 also evolve through different knickpoint forms during the course of the experiments (see Fig. 3.3.11 for Expt 20 and videos on Suppl. Disc for Experiment's 16, 18 and 31), which could potentially explain the unexpected relationship between knickpoint form and KP_{RR} in Fig. 3.3.9B.

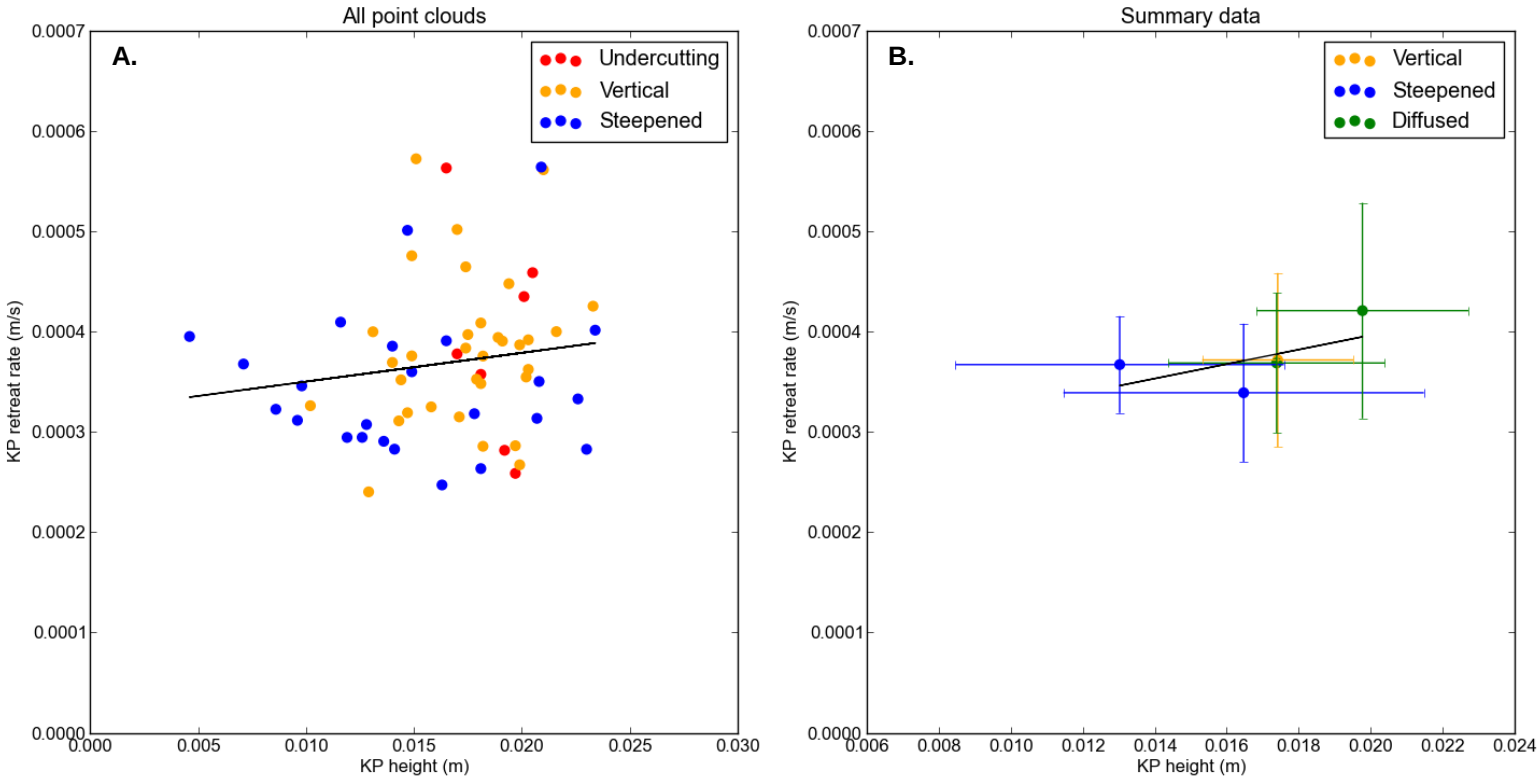

Fig. 3.3.9: Knickpoint height (KP_H) against knickpoint retreat rate (KP_{RR}) for the experiments where the discharge was varied while the initial base level drop was kept constant. Colours indicate the classification of knickpoint form as indicated. **A.** Every point cloud where a knickpoint was present in the experiments (linear regression line: $KP_{RR} = 0.0029KP_H + 0.00032$; $R^2 = 0.02$; Pearson correlation coefficient = 0.15). **B.** Mean knickpoint height and mean knickpoint retreat rate for each experiment, with error bars indicating the standard deviation. The knickpoint form was classified when the knickpoint had migrated half the channel length ($KP_{RR} = 0.0072KP_H + 0.00025$; $R^2 = 0.36$; Pearson correlation coefficient = 0.60)

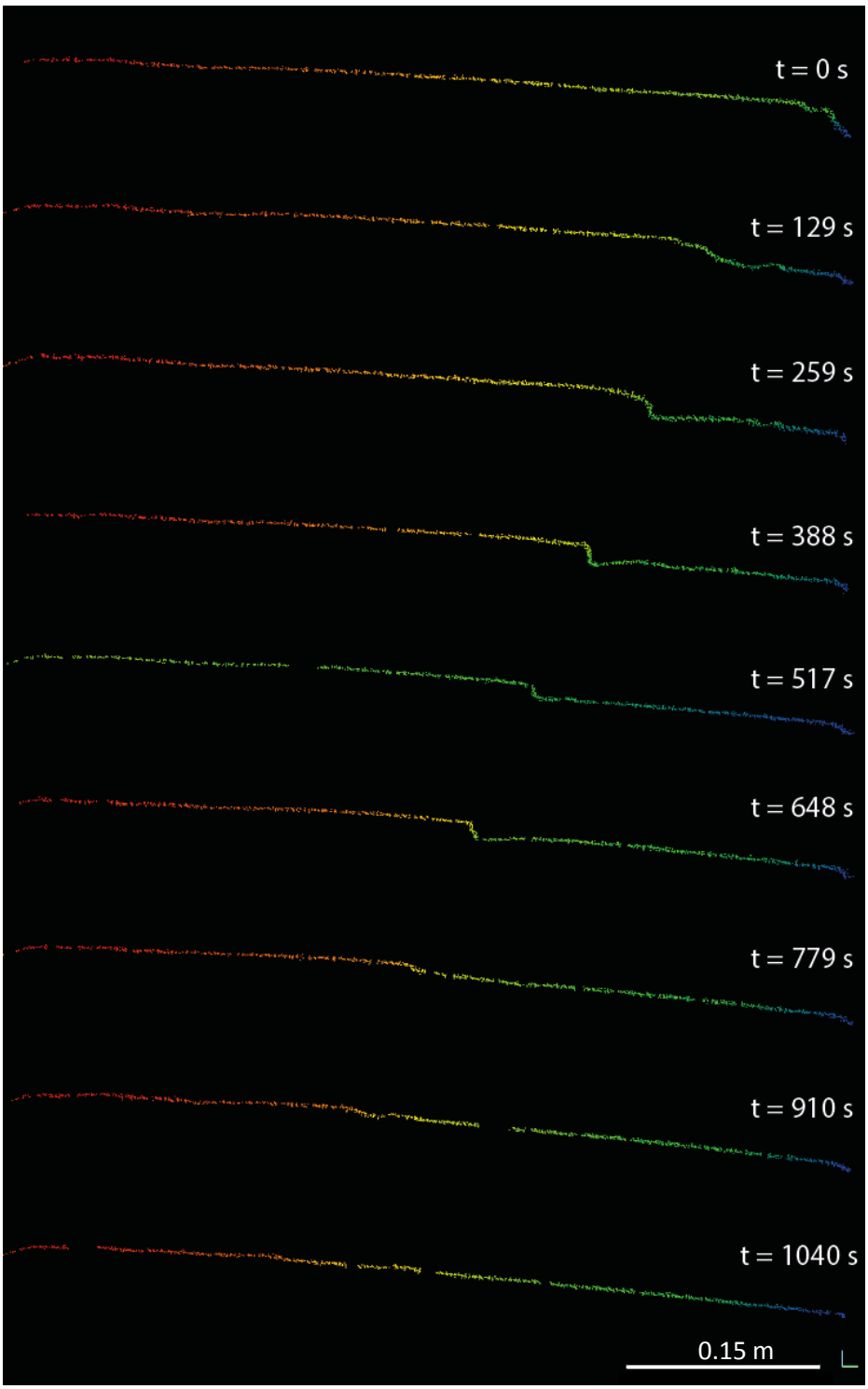

Fig. 3.3.10: Long profile evolution during Experiment 19 (Q = 0.5 l/min; initial BLD = 0.02 m). The summary classification at the halfway point may be misrepresentative due to the dynamic evolution of the knickpoint form from a steepened reach (t = 0 to 129 s) to a vertical step (t = 259 to 517 s) and then back to a steepened reach (t = 648 to 779 s) before diffusing completely (t = 910 to 1040 s). The red to blue colour spectrum indicates relative height, with warm colours indicating a higher elevation than cooler colours for each scan.

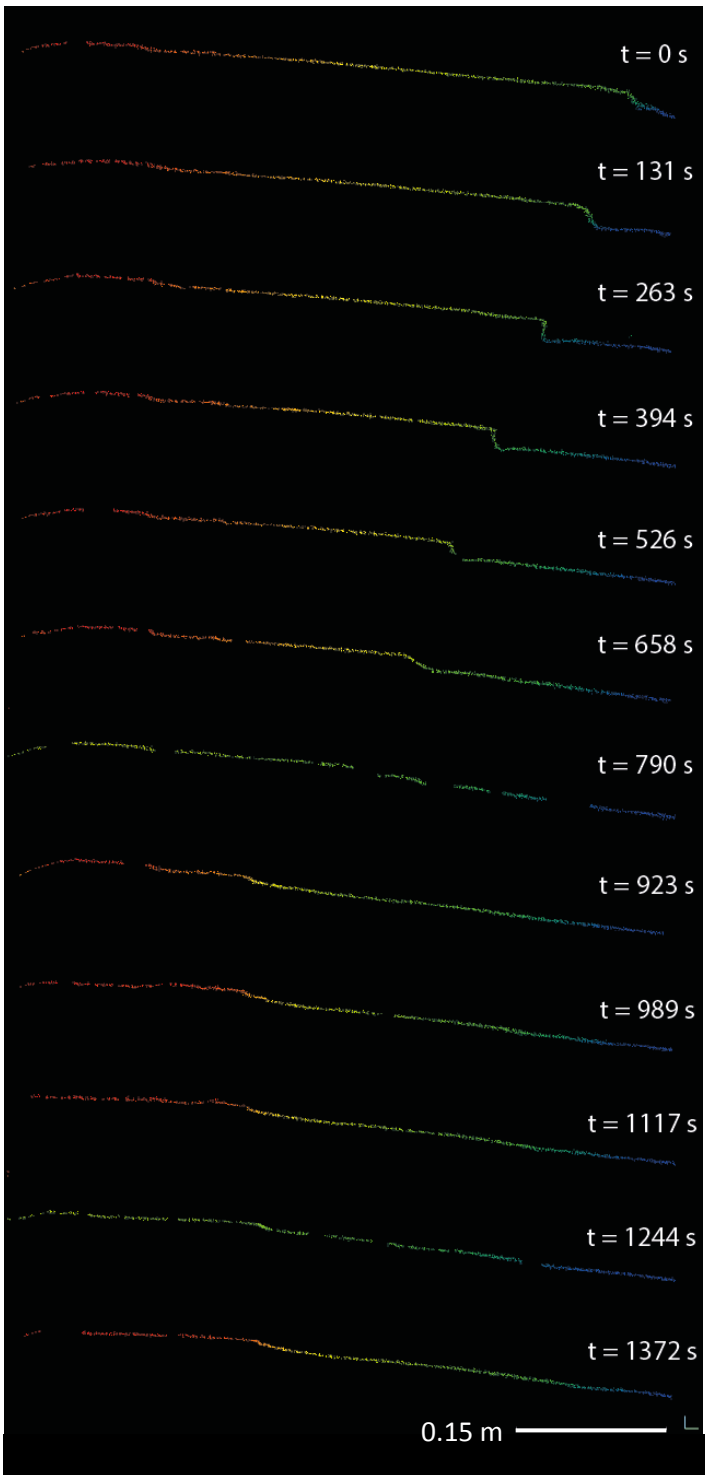

Fig.3.3.11: Long profile evolution during Experiment 20 (Q = 0.11 l/min; Initial BLD = 0.02 m), again demonstrating the variability in the knickpoint form. The summary classification of this experiment is 'Diffused' as the knickpoint was not present after t = 790 s, before it had reached the halfway point. However, in the initial stages of the retreat, the knickpoint was a vertical step with some minor undercutting, which may have led to the high retreat rates for experiment 20 in Fig. 3.3.9. The red to blue colour spectrum indicates relative height, with warm colours indicating a higher elevation than cooler colours for each scan.

Given the apparent similarity in the trends between knickpoint height and knickpoint retreat rate between the two different sets of experiments (Fig. 3.3.4 and 3.3.9), the datasets were combined to further explore the relationship between knickpoint height and retreat rate, shown in Fig. 3.3.12. The datasets plot on top of one another and there is no noticeable difference between them, suggesting that despite variations in discharge over an order of magnitude, the dominant control on the knickpoint retreat rate is the knickpoint geometry (i.e. KP_H). This relationship is set by the mechanism of erosion at the knickpoints which is set by their form; taller knickpoints tend to develop an undercutting plunge pool and in turn retreat faster than knickpoints that diffuse from a vertical step into a steepened reach.

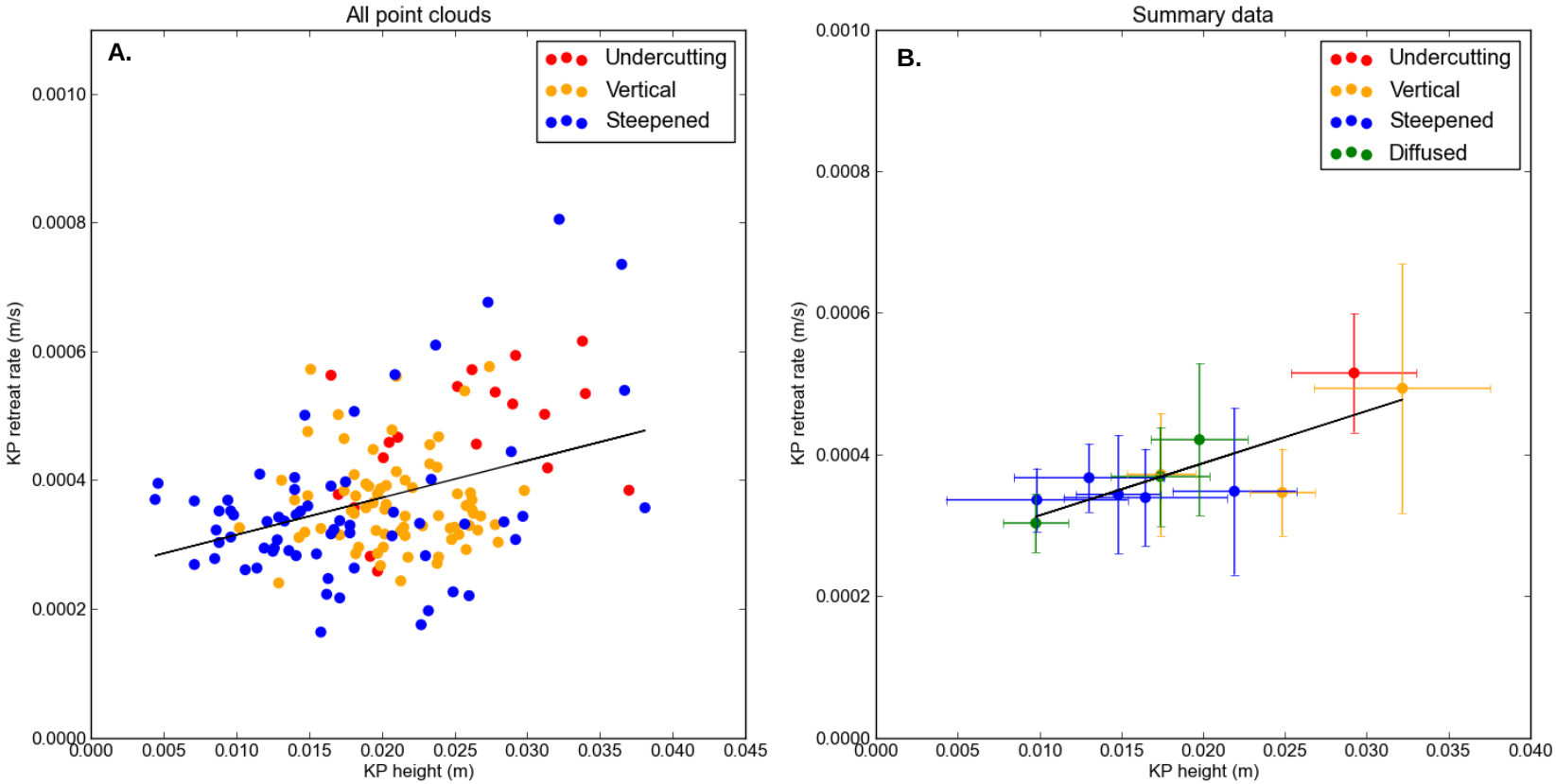

Fig. 3.3.12: Plots of the combined datasets from Figs. 3.3.4 and 3.3.9. **A.** Every point cloud where a knickpoint was present in the experiments (linear regression line $KP_{RR} = 0.0058KP_H + 0.00026$; $R^2 = 0.14$; Pearson correlation coefficient = 0.37). **B.** Mean knickpoint height and mean knickpoint retreat rate for each experiment, with error bars indicating the standard deviation. The knickpoint form was classified when the knickpoint had migrated half the channel length ($KP_{RR} = 0.0074KP_H + 0.00024$; $R^2 = 0.65$; Pearson correlation coefficient = 0.81)

3.3.2.3 Relationships between knickpoint height and water depth on knickpoint form and retreat rate

Despite discharge not scaling with knickpoint retreat rate (Fig. 3.3.8), it is possible that the discharge can influence the knickpoint form through variations in the water depth, which in turn sets the erosion mechanism and the rate of retreat. The ratio of water depth to knickpoint height can vary either through a change in the knickpoint height or a change in discharge leading to a change in the flow depth (Fig. 3.3.3).

Broadly, the faster knickpoint retreat rates correspond to lower values of h/KP_H (Fig. 3.3.13A: $KP_{RR} = -0.00023h/KP_H + 0.00041$: Pearson correlation coefficient = -0.18 when all points clouds are considered) The relationship is a little clearer in the plot of the summary data (Fig. 3.3.13B; $R^2 = 0.42$, Pearson correlation coefficient = -0.65) but there is still significant variability at low values of the h/KP_H ratio, possibly caused by noise within the flow depth measurements.

The most notable feature of Fig. 3.3.13 is at high values of h/KP_H, the knickpoints had all diffused into a steepened reach or diffused completely by the time the knickpoint reached halfway up the experimental channel length. Knickpoints which developed an undercutting plunge pool are grouped at lower values of h/KP_H and vertical stepped knickpoints are broadly in between. As in Fig. 3.3.12, the same relationship holds for both sets of experiments suggesting that while the magnitude of the discharge is not a direct control on the knickpoint retreat rate, it helps set the knickpoint form through variations in the flow depth and therefore influences the retreat rate through the h/KP_H ratio.

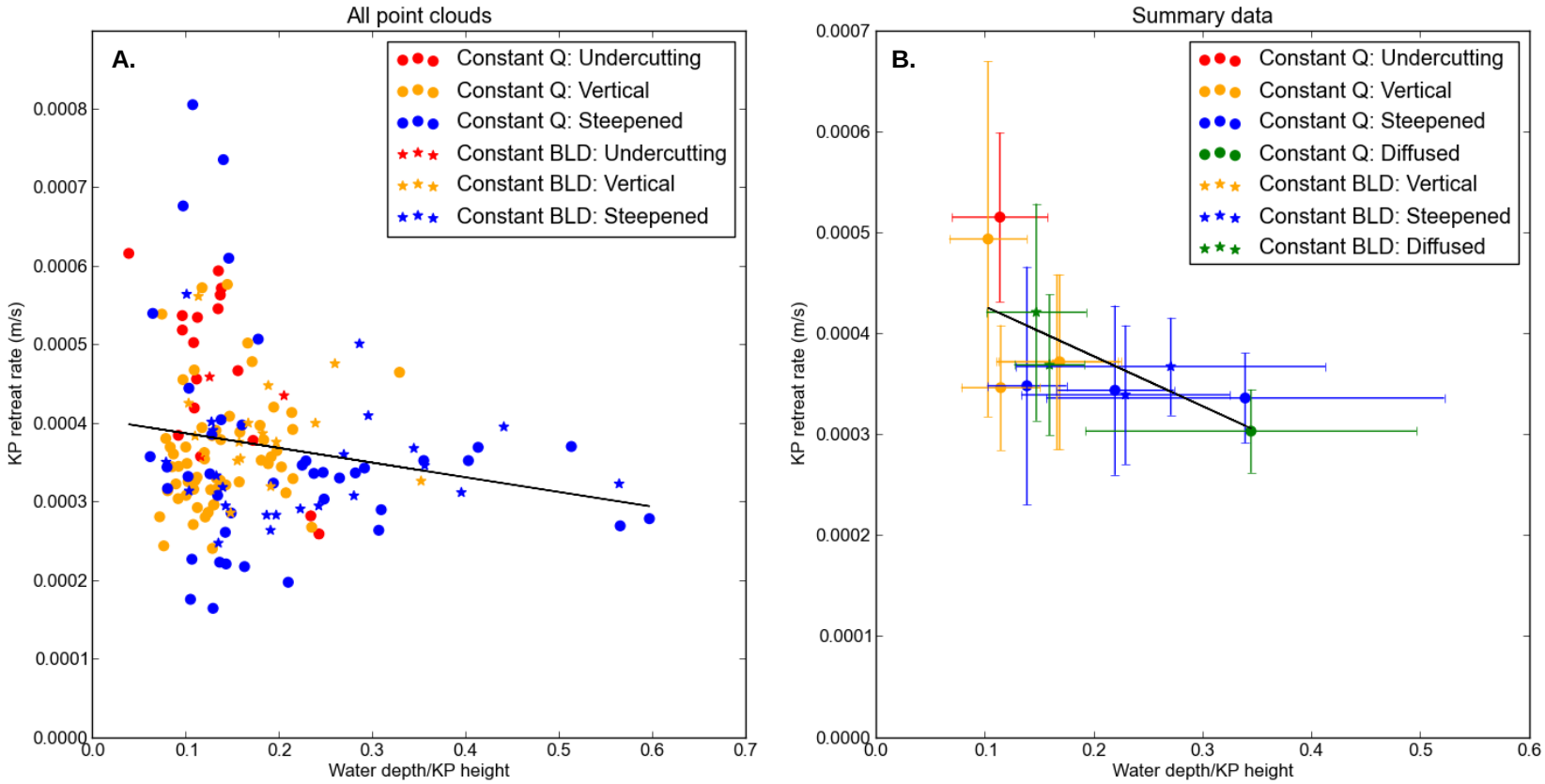

Fig. 3.3.13: Plots of water depth to knickpoint height ratio against knickpoint retreat rate for both the constant *Q* (circles) and constant BLD (stars) experiments. **A.** Every point cloud where a knickpoint was present in the experiments (linear regression line through combined datasets: KP_{RR} = -0.00023h/KP_H + 0.00041; R^2 = 0.03; Pearson correlation coefficient = -0.18). **B.** Mean knickpoint height and mean knickpoint retreat rate for each experiment, with error bars indicating the standard deviation. Linear regression through combined datasets: KP_{RR} = -0.00049h/KP_H + 0.00048; R^2 = 0.42; Pearson correlation coefficient = -0.65).

3.3.2.4 Summary of controls on knickpoint retreat rate

The clear dominant control on the knickpoint retreat rate in these experiments is the knickpoint form, which is controlled by the ratio of flow depth to knickpoint height. However, given the flow depth is relatively constant at discharges over an order of magnitude (Fig. 3.3.3), the knickpoint form is more strongly controlled by the knickpoint height (see Fig. 3.3.14 conceptual diagram in Fig. 3.3.15). At low $KP_{H,}$ the h/KP_H ratio is high and the knickpoint will diffuse from the initial vertical step into a steepened reach as it retreats (Fig. 3.3.15A). As the KP_H increases, the h/KP_H ratio decreases and the knickpoint will either maintain its vertical step or, at very high values of KP_H, will develop an undercutting plunge pool (Fig. 3.3.15B & C). Knickpoints with an undercutting plunge pool have a higher KP_{RR} than knickpoints that diffuse into a steepened reach because material is also removed from the base of the knickpoint through the development of a lateral secondary flow circulation (Fig. 3.3.15C). According to Fig. 3.3.13, the threshold h/KP_H ratio where knickpoints will either diffuse into a steepened reach or completely disappear is > 0.35 and undercutting plunge pools can develop at knickpoints that have a $h/KP_H < 0.2$.

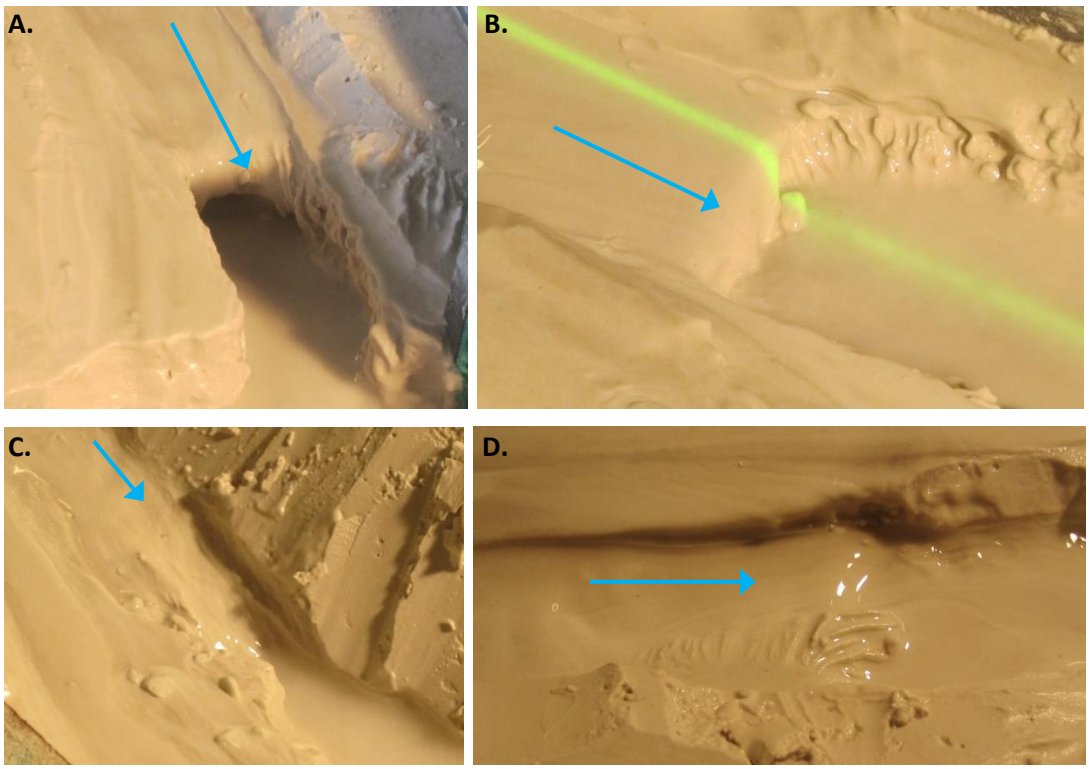

Fig. 3.3.14: Photographs of the four key knickpoint morphologies. **A.** Knickpoint with an undercutting plunge pool. **B.** Vertical stepped knickpoint, with no undercutting: the green line is the laser. **C.** Knickpoint that has diffused into a steepened reach. **D.** Knickpoint that has diffused completely. Blue arrows indicate flow direction. Note the turbid water immediately downstream of the knickpoints in **A**, **B**, and **C**; this sediment has been eroded from the knickpoint as it retreats upstream. For scale, the channel width upstream of the knickpoint is ~ 7 cm.

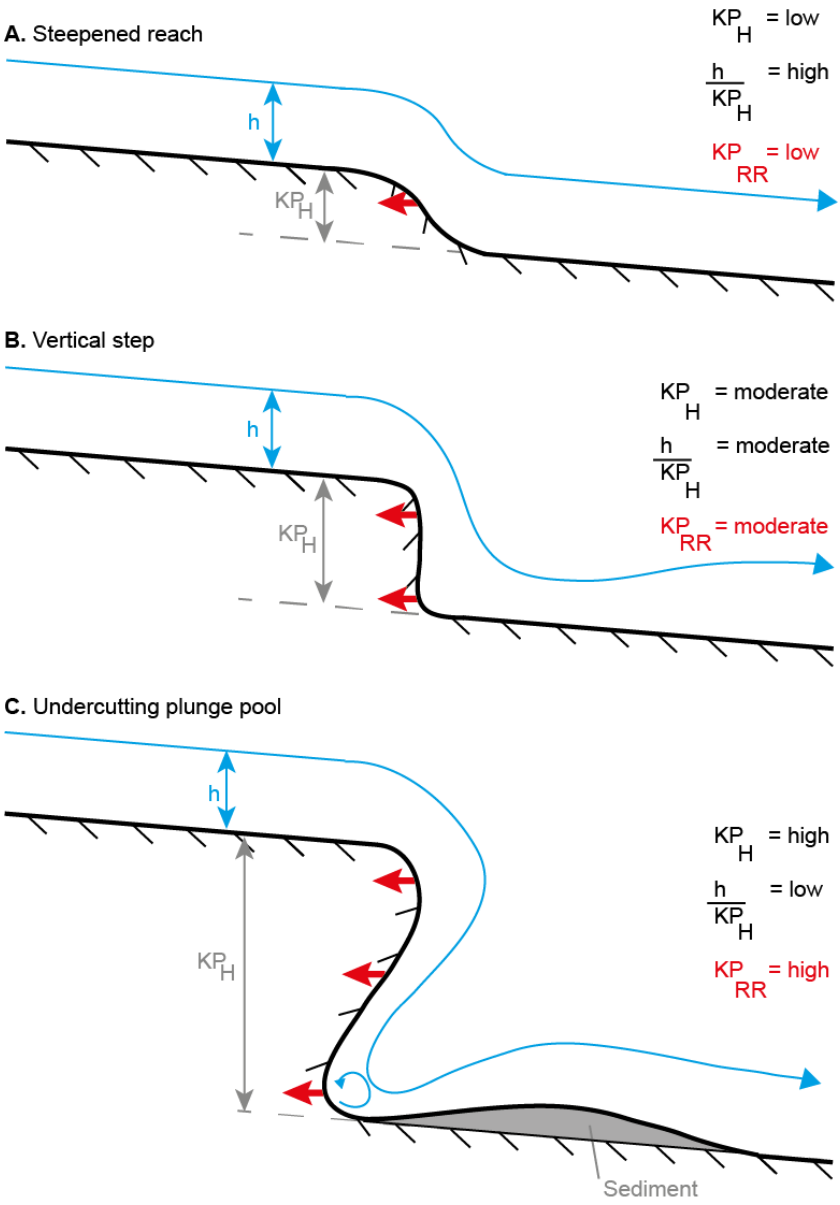

Fig. 3.3.15: Conceptual model (not to scale) showing the controls on knickpoint retreat in the experimental flume. **A.** Smaller knickpoints (with high h/KP_H ratio values; > 0.35) tend to diffuse from the initial vertical step into a steepened reach, where erosion of material from the knickpoint takes place at the lip of the knickpoint (red arrow). **B.** Moderate sized knickpoints in the experiments maintained their vertical steps and material was eroded from the knickpoint lip and from the downstream face of the knickpoint, thus allowing a faster knickpoint retreat rate than steepened reaches. **C.** The largest knickpoints (with low h/KP_H ratios; < 0.2) retreat the fastest as material was eroded from the knickpoint lip, the downstream face and by the undercutting plunge pool due to development of secondary circulation of the flow. The amount of eroded material at the knickpoint exceeded the sediment transport capacity of the channel downstream of the knickpoint, leading to the deposition of a sediment push bar.

3.3.3 Total erosion by knickpoints as they migrate

This section examines the controls on the total volume of erosion (KP_{er}) that takes place as the knickpoints migrated upstream through the experimental channel. The total amount of erosion caused by knickpoint propagation has been shown to be important in landscape evolution in natural settings such as Hawai`i (Mackey *et al.,* 2014) and, in this study, is calculated using the following equation:

$$KP_{er} = W \times KP_H \times KP_{RR} \quad \text{Eqn. 3.3.4}$$

Where KP_H and W are the dimensions of the knickpoint (height and width respectively) and KP_{RR} is the rate at which it migrates upstream.

As $KP_{RR} = f(KP_H)$, demonstrated in Section 3.3.2, it is no surprise that taller knickpoints erode up to four times more material than knickpoints half their size as both the values for knickpoint geometry and the retreat rate are lower (Fig. 3.3.16).

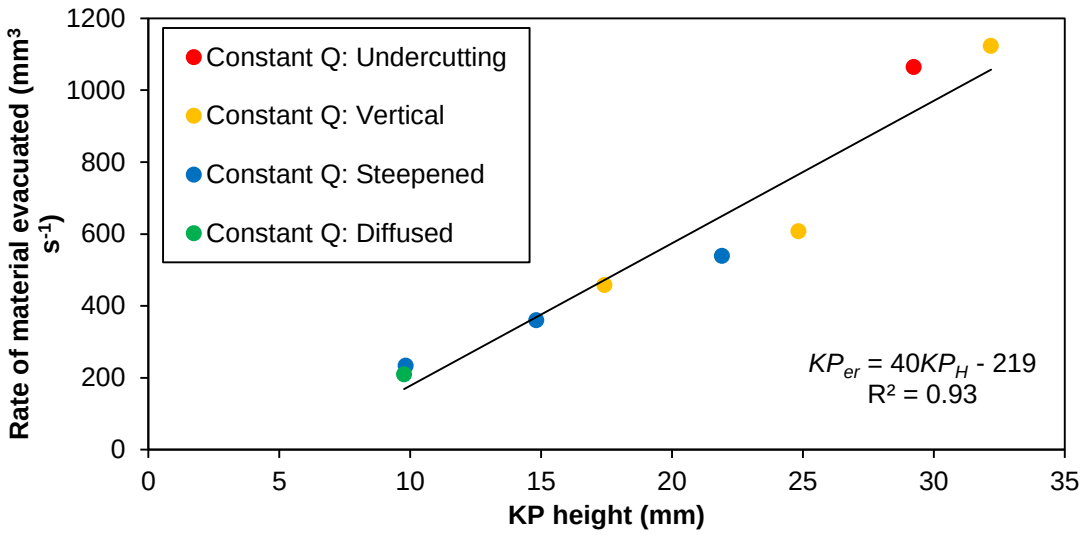

Fig. 3.3.16: Under a constant discharge, taller knickpoints erode more material than smaller knickpoints as both the geometry and the retreat rate of the taller knickpoints are greater.

It was shown in Section 3.3.2 that the discharge magnitude does not have a direct control on the knickpoint retreat rate. However, the discharge does control the geometry of the channel, through variations in the channel width (Fig. 3.3.1):

$$W \propto Q^{0.38} \qquad \text{Eqn. 3.3.5}$$

Therefore, even though the knickpoints are not retreating faster during higher discharges, the total amount of erosion caused by the propagation of the knickpoints does increase as extra material is eroded from the edges of the channel (Fig. 3.3.17; 3.3.18).

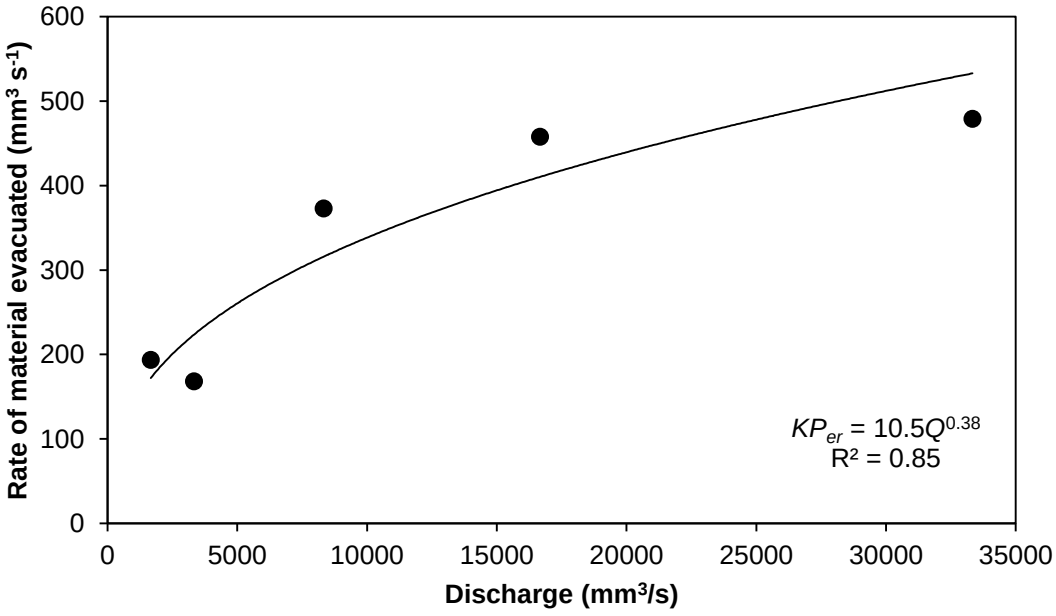

Fig. 3.3.17: Even though the knickpoints do not retreat faster under higher discharge, the total amount of material eroded does increase due to an increase in the channel width (see Fig. 3.3.1); extra material is eroded from the edges of the channel.

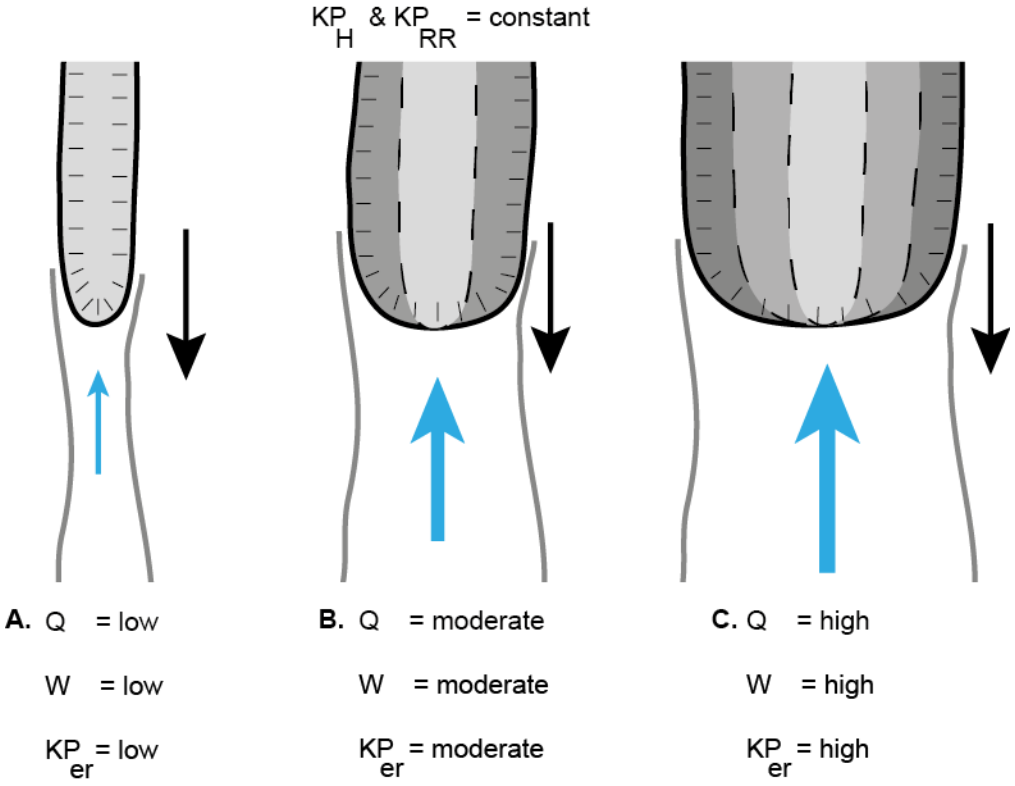

Fig. 3.3.18: Conceptual plan-view diagram of how increasing discharge (size of blue arrow, flowing towards the top of the page) alters the total volume of material eroded from knickpoints (outline of knickpoint indicated by the solid black line), even if the knickpoint retreat rate does not change (solid black arrow, retreating towards the bottom of the page). An increase in the discharge leads to an increase in the channel width ($W \propto Q^{0.38}$; grey lines indicate the banks of the channel), which increases the area of the knickpoint face, thus eroding more material as the knickpoint migrates upstream.

Given $KP_{RR} = 0.0077KP_H + 0.00023$ (Fig. 3.3.4B), the total amount of material eroded from the knickpoint can be estimated solely based on the knickpoint height and width, by substituting this into equation 3.3.4:

$$KP_{er} = W.KP_H(0.0077KP_H + 0.00023) \quad \text{Eqn. 3.3.6}$$

If the total sediment flux from a catchment is known, for example from sediment gauging techniques or using detrital cosmogenic nuclides concentrations in river sediment, the above relationship can be used to estimate the proportion of the total sediment flux that has been sourced from

the erosion of knickpoints as they retreat upstream. Measurements of the knickpoint geometry are relatively easy to obtain through field observations or high-resolution remote sensing techniques such as lidar so this relationship potentially offers a new method for examining the relative importance of knickpoint migration in the wider context of landscape change.

3.3.4 Effect of hydrograph variability

The experiments described in Section 3.3.2 showed that the discharge variations do not lead to variations in the knickpoint retreat rate (Fig. 3.3.8). However, rivers in natural settings rarely experience a constant discharge through time and thus a series of experiments were carried out to explore the impact of temporal variability of discharge using the 'tipping bucket'. The hydrograph during the tipping bucket experiments oscillates between a peak value equivalent to 2 l/min and a minimum value of 0.5 l/min, with the total volume of water equal to 1 l/min (Fig. 3.3.19).

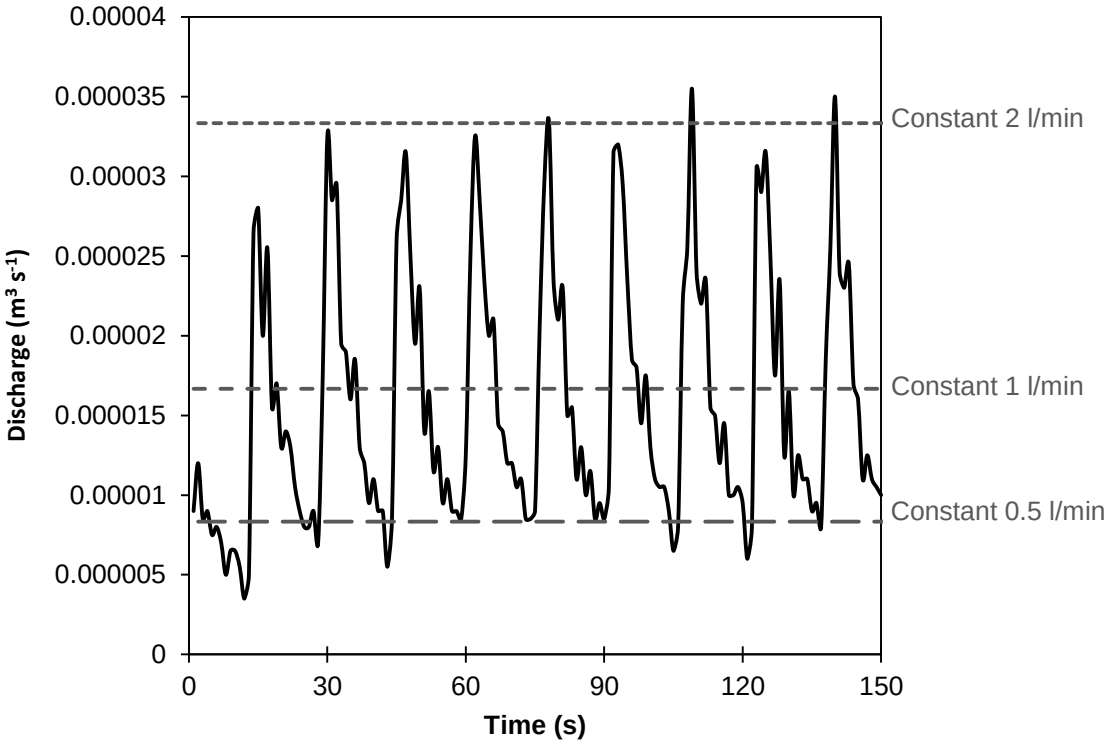

Fig. 3.3.19: Hydrograph during the 'tipping bucket' experiments (in black), with grey dashed lines showing the hydrographs of constant discharge for 0.5, 1 and 2 l/min for comparison. The hydrograph was collected using a balance located at the outlet of experimental channel, monitoring the mass of water flowing out of the channel. The total volume of water was 1 l/min, delivered to the reservoir at the inlet of the experimental channel in five pulses of 200ml every minute. The discharge within the channel oscillated between equivalent constant discharge values of 0.5 and 2 l/min. The minor peaks in the falling limb of each pulse are caused by secondary waves reflecting off the back wall of the reservoir, which were impossible to stop using this experimental set-up.

The evolution of the knickpoints during the tipping bucket experiments followed the same pattern as the other experiments, e.g. Expt 22 developing an undercutting plunge pool (Fig. 3.3.20) and Expt 23 diffusing into a steepened reach (Fig. 3.3.21). Compared to the experiments where discharge was kept constant, a similar relationship was found between knickpoint height and retreat rate in the tipping bucket experiments (KP_{RR} = 0.0068KP_H + 0.00020; R^2 = 0.27; Pearson correlation coefficient = 0.52; Fig. 3.3.22A). This relationship is also true in the summary plot of mean KP_H against KP_{RR} for each experiment (Table 3.3.3; Fig. 3.3.22B). If anything, the pattern of the taller knickpoints developing an undercutting plunge pool which in turn leads to a faster retreat rate is clearer in the tipping bucket experiments than in the constant discharge experiments (Fig. 3.3.4).

Table 3.3.3: Summary data of experiments that had a variable discharge (tipping bucket experiments with mean discharge of 1 l/min) and varying initial BLD (0.005 – 0.04 m), plotted in Fig. 3.3.22B. Data are sorted in ascending order of mean knickpoint height (KP_H) and colour coded according to knickpoint form classification when it had retreated halfway of the channel length. The knickpoints in experiments 32 and 33 diffused instantly and no data of knickpoint retreat was produced. Experiment 28 is excluded from all further analyses due to a falsely high knickpoint retreat rate; experiment 28 had a small initial knickpoint (0.01 m), but was preceded by an experimental that had a large knickpoint (Expt 27: 0.03 m) which developed a large plunge pool which had large deposits downstream. Therefore we suggest the high knickpoint retreat rate in experiment 28 is due to the knickpoint migrating through sediment rather than eroding bedrock and is therefore not a fair representation of the behaviour of a knickpoint that is 0.01m high under variable discharge conditions.

Expt no.	Initial Base Level Drop (mm)	Knickpoint height (mm)		Knickpoint retreat rate (m/s)		KP form
		Mean	St Dev	Mean	St Dev	
32	*5*	-	-	-	-	*Diffused*
33	*5*	-	-	-	-	*Diffused*
24	5	6.18	0.576	0.294	8.28×10^{-2}	Diffused
28	*10*	*11.2*	*1.60*	*0.475*	*6.12×10^{-1}*	*Steepened*
34	10	13.0	3.66	0.309	6.81×10^{-2}	Steepened
23	15	13.1	3.19	0.266	1.17×10^{-1}	Steepened
25	20	18.2	2.52	0.269	8.14×10^{-2}	Steepened
27	30	21.7	7.51	0.334	1.44×10^{-1}	Steepened
22	40	30.7	3.95	0.426	5.04×10^{-2}	Undercutting

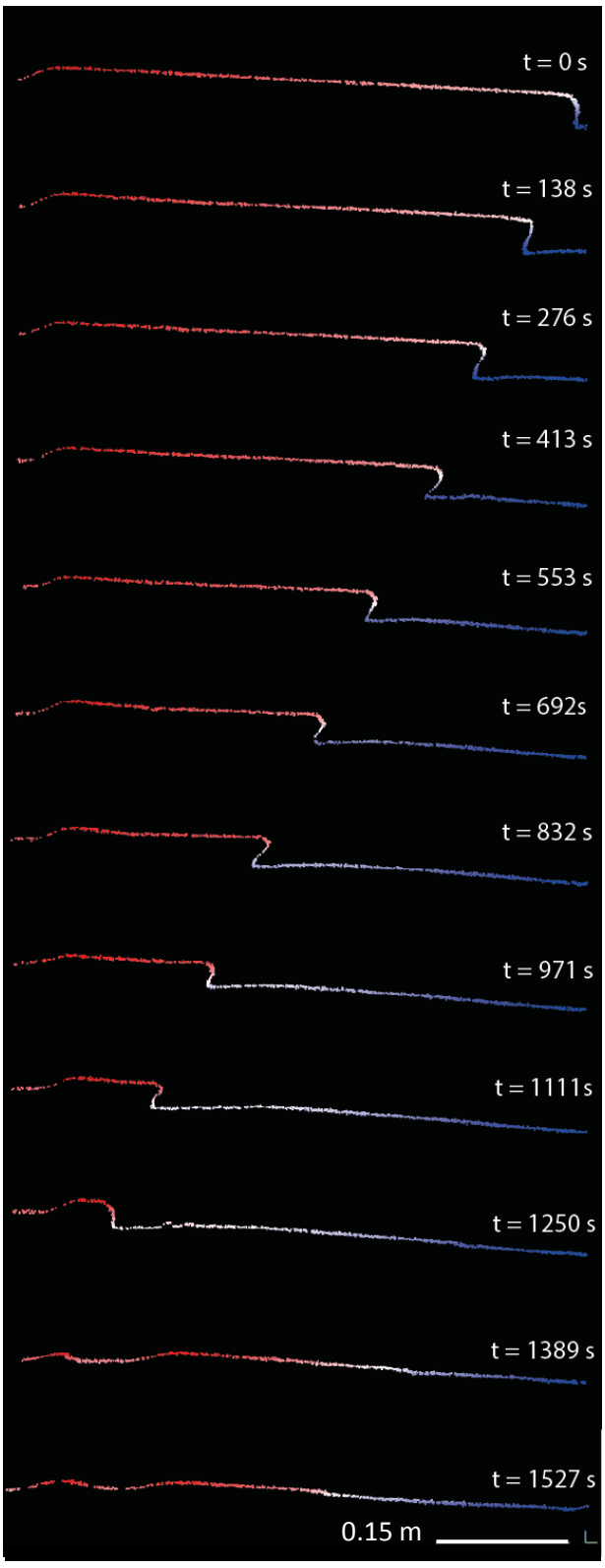

Fig. 3.3.20: Long profile evolution during Experiment 22 (*Q* = 1 l/min (variable); Initial BLD = 0.04 m; Summary knickpoint form classification: Undercutting). The red to blue colour spectrum indicates relative height, with warm colours indicating a higher elevation than cooler colours for each scan.

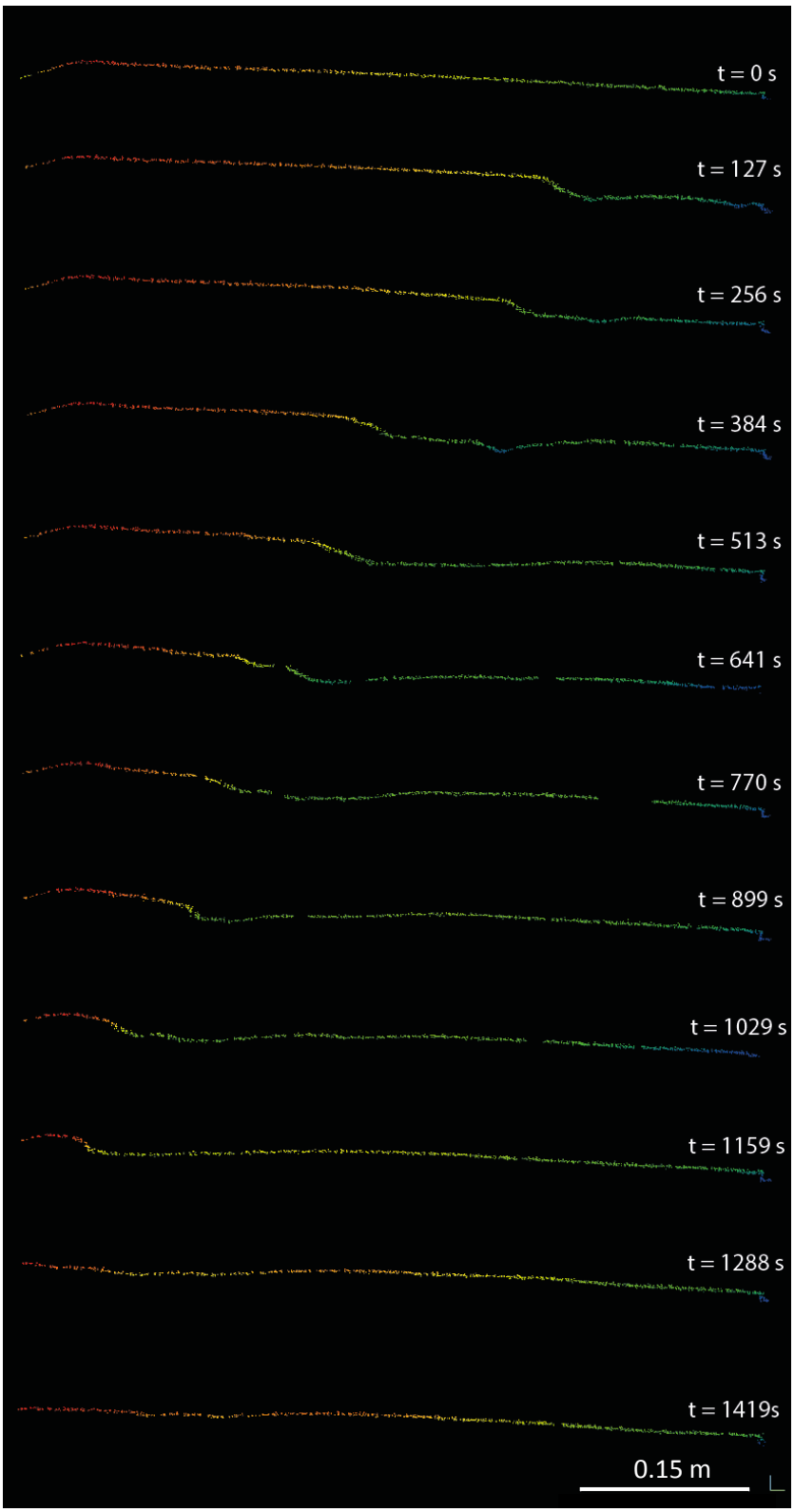

Fig. 3.3.21: Long profile evolution during Experiment 23 (Q = 1 l/min (variable); Initial BLD = 0.015 m; Summary knickpoint form classification: Steepened). The red to blue colour spectrum indicates relative height, with warm colours indicating a higher elevation than cooler colours for each scan.

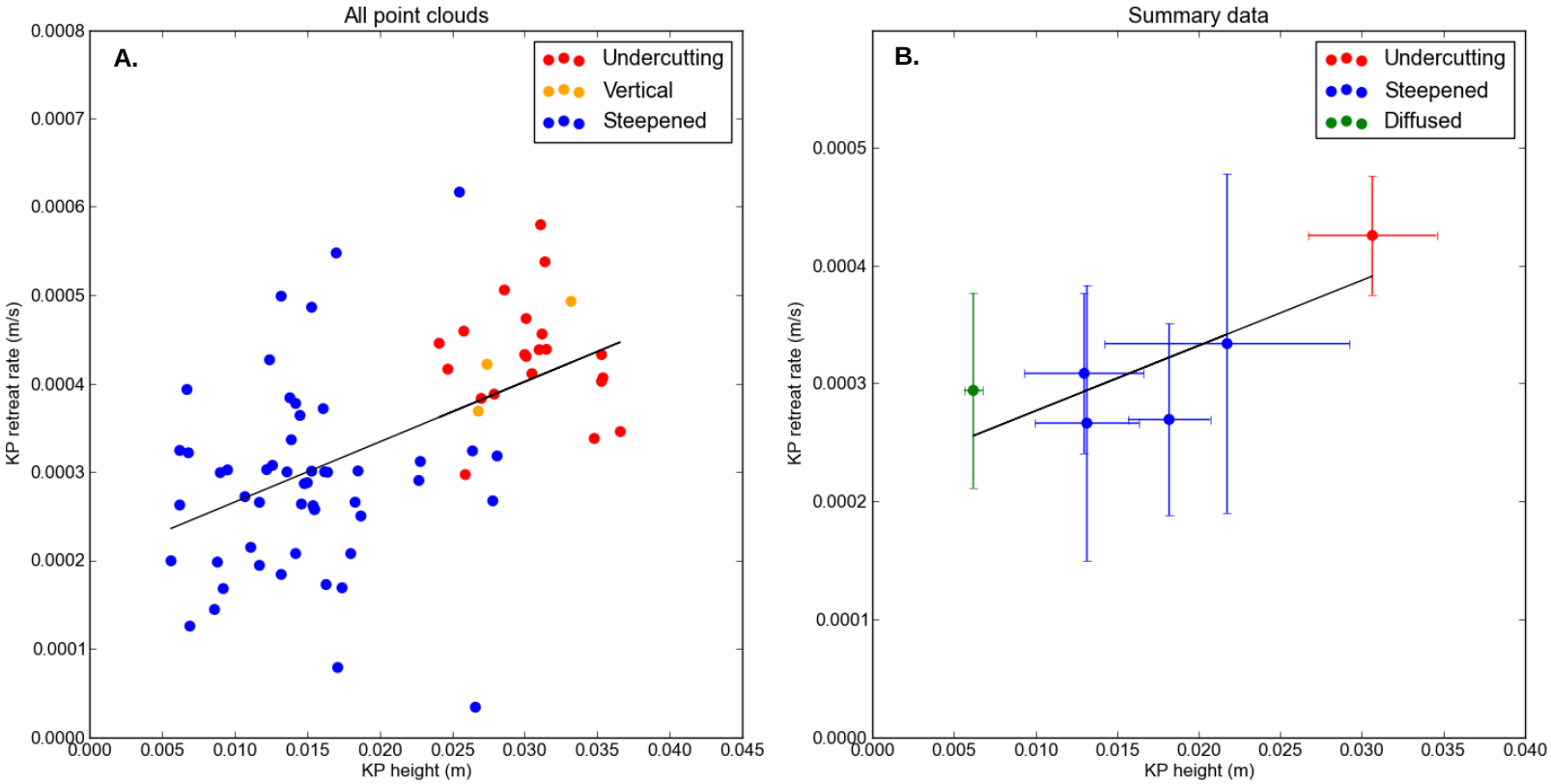

Fig. 3.3.22: Knickpoint height (KP_H) against knickpoint retreat rate (KP_{RR}) for the tipping bucket experiments. Colours indicate the classification of knickpoint form as indicated. **A.** Every point cloud where a knickpoint was present in the experiments (linear regression line $KP_{RR} = 0.0068KP_H + 0.00020$; $R^2 = 0.27$; Pearson correlation coefficient = 0.52). **B.** Mean knickpoint height and mean knickpoint retreat rate for each experiment, with error bars indicating the standard deviation. The knickpoint form was classified when the knickpoint had migrated half the channel length ($KP_{RR} = 0.0055KP_H + 0.00022$; $R^2 = 0.63$; Pearson correlation coefficient = 0.79)

Fig. 3.3.23 shows a comparison of the tipping bucket experiments to the constant discharge experiments to see if temporal hydrograph variability leads to a difference in the knickpoint form or retreat rate. Most noticeably, the pattern of taller knickpoints developing plunge pools that undercut and smaller knickpoints diffusing into a steepened reach is similar in both datasets. The gradient of the trend line for all the point clouds in each set of experiments (solid line = constant discharge, gradient = 0.0067; dashed line = tipping bucket, gradient = 0.0068) are very similar. The gradient of the trend line for the constant discharge experiments (0.0077) in the summary plot is slightly greater than for the tipping bucket experiments (0.0055) but again the datasets are, within the error bars, plotted on top of each other. Therefore, we can suggest that variability in the hydrograph has little effect on the form and retreat rate of knickpoints. The dominant control on knickpoint retreat is set by the knickpoint height through the form and mechanism of knickpoint retreat (i.e. development of an undercutting plunge pool or diffusion into a steepened reach).

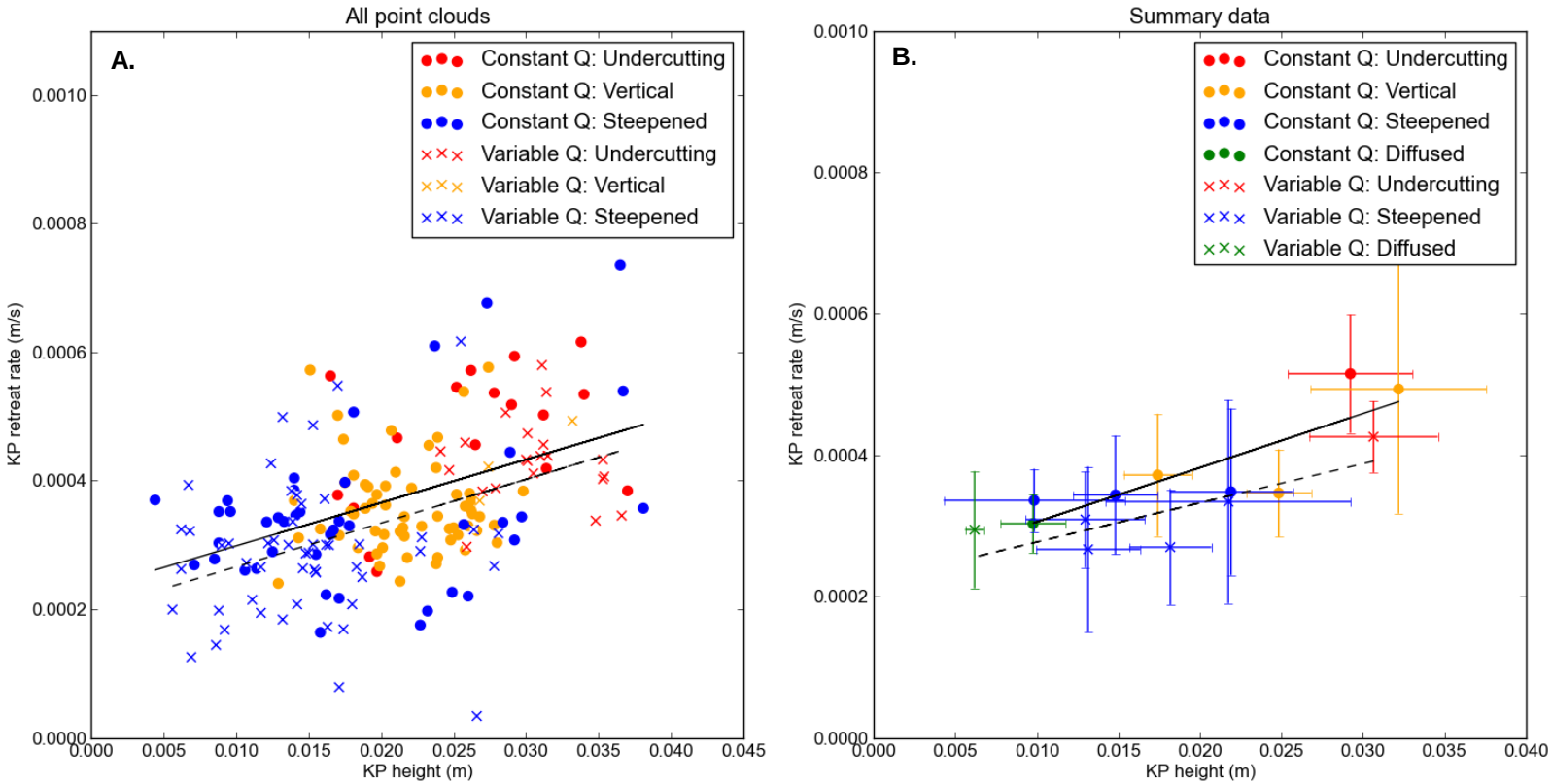

Fig. 3.3.23: Comparison of relationship between knickpoint height (KP_H) against knickpoint retreat rate (KP_{RR}) between the experiments with constant discharge (points; solid trend line) and the variable discharge (tipping bucket experiments; shown by the crosses and dashed trend line). Colours indicate the classification of knickpoint form as indicated. **A.** Every point cloud where a knickpoint was present in the experiments **B.** Mean knickpoint height and mean knickpoint retreat rate for each experiment, with error bars indicating the standard deviation.

The temporally variable delivery of discharge in the tipping bucket experiments also had little influence on the channel width (0.071 m) compared to the constant discharge experiments that had the same mean discharge of 1 l/min (0.070 m). This suggests that long-term mean discharge is more important in setting the channel width than the maximum peak discharge of the hydrograph. This is contrary to Hartshorn *et al.* (2002) who found that the highest magnitude flows during 'Supertyphoon' Bilis acted to widen the LiWu river channel in Taiwan. However, the peak discharge in the tipping buckets was only double the mean discharge, whereas the peak flow during Supertyphoon Bilis was 65 times greater than the daily average discharge so it is possible that the channel widening effect of peak flows was not visible during the experiments due to the relatively smaller difference in magnitude. As the knickpoint retreat rates and the knickpoint geometries are both similar in both the constant discharge and variable discharge experiments, there is also no significant difference in the total volume of material eroded by the knickpoints as they retreated upstream (Fig. 3.3.24)

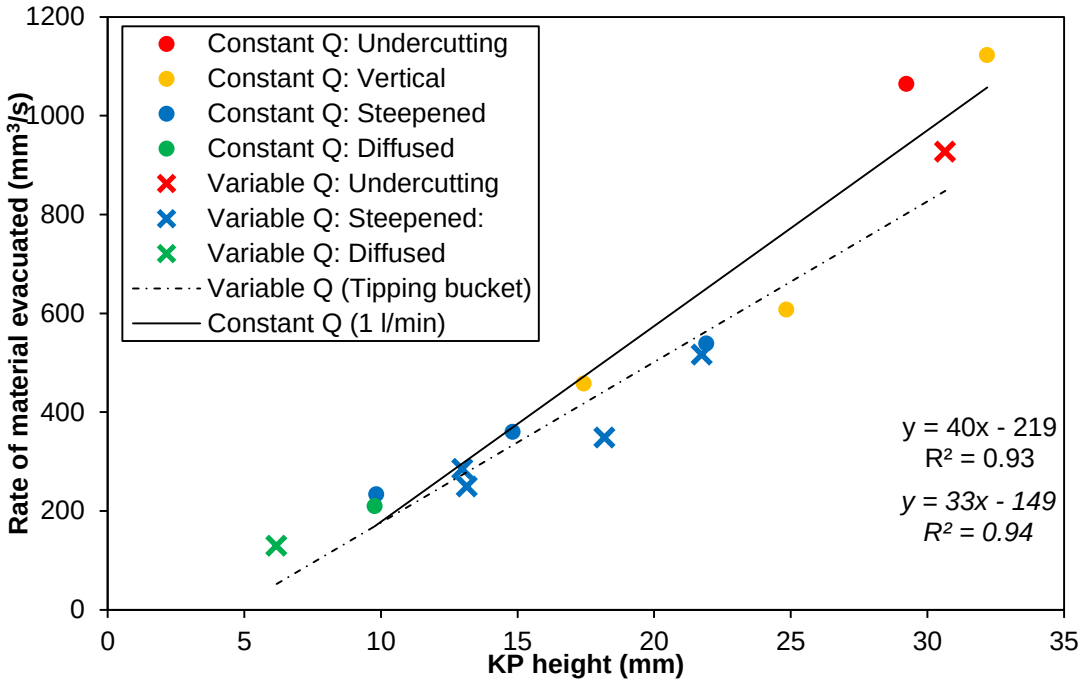

Fig. 3.3.24: Rate of total material eroded by the knickpoints as they retreated upstream. There is very little difference between the constant discharge experiments (circles) and the variable discharge experiments (crosses). Italic equation corresponds to dashed trendline.

Sub-Chapter 3.4: Experimental modelling discussion

3.4.1 Comparison to other experimental studies

The understanding of the temporal evolution of knickpoint form in a homogenous substrate through time has been debated for many decades; Von Engeln (1940) was the first to question whether vertical step knickpoints, such as waterfalls, can be maintained (or even enhanced) as they retreat upstream, when a caprock of resistant material is not present. An experimental study by Gardner (1983) concluded that vertical knickpoints generated by successive drops in base level will diffuse into a gradual slope through knickpoint replacement and subsequent inclination, with this result independent of the magnitude of the base level change or bedrock structure (Fig. 3.4.1).

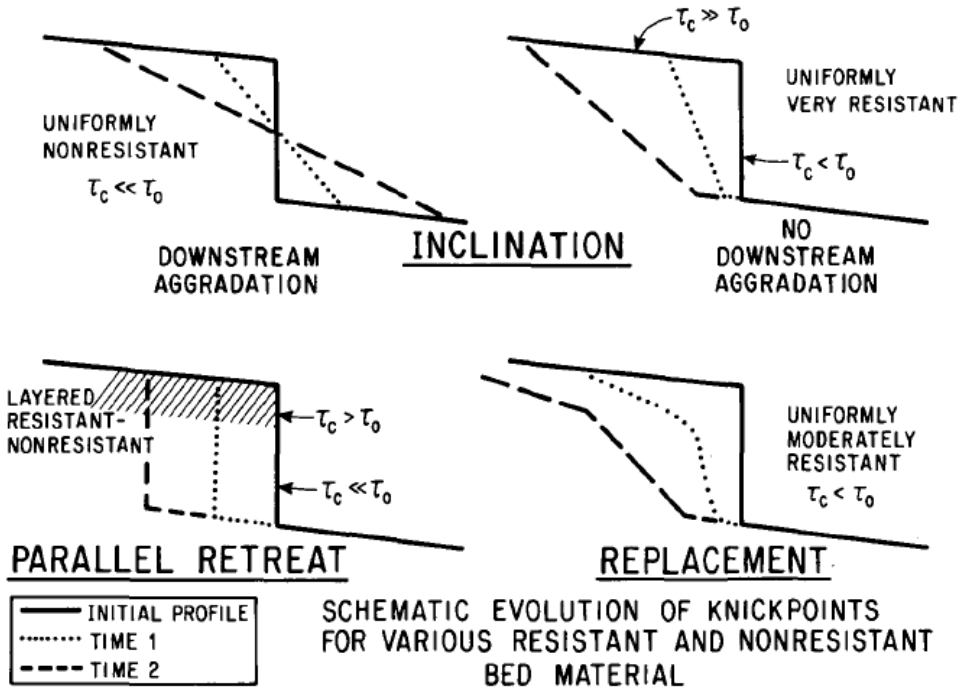

Fig. 3.4.1: Conceptual diagram of knickpoint form evolution through time (Gardner, 1983).

Changes in the morphology of a knickpoint are a function of the relationship between the bed shear stress (τ_o) and the critical shear stress for bedrock erosion (τ_c) at different locations (Gardner, 1983; Stein and Julien, 1993; Rengers and Tucker, 2014); during knickpoint replacement and inclination

the maximum bed shear stress exceeds the critical shear stress in the drawdown reach upstream of the knickpoint and reaches a maximum value at the knickpoint lip. As the erosion rate at the knickpoint face is slower than the erosion rate at the knickpoint lip, the profile of the knickpoint gradually diffuses, which is a process also identified in these experiments where knickpoints diffused into a steepened reach or diffused completely as they retreated upstream.

Gardner (1983) suggests that parallel knickpoint retreat, where a vertical step is maintained as the knickpoint migrates upstream (Fig. 3.4.1), is only possible where three conditions are met: (i) there are layered resistant and non-resistant rocks and the critical shear stress is greater than bed shear stress at the resistant caprock, (ii) the underlying unit of non-resistant material is exposed to erosion where bed shear stress is greater than critical shear stress and (iii) removal of material occurs from the plunge pool that forms at the base of the retreating knickpoint. Leopold *et al.* (1964) suggested the criteria for parallel knickpoint retreat in a homogenous, cohesive, material are: (i) critical shear stress is greater than bed shear stress upstream of the knickpoint face, (ii) flow is sufficient to transport eroded material away from the base of the knickpoint face, (iii) the ratio of knickpoint height to flow depth is greater than 1.

Numerous experiments carried out in this study (e.g. Expt 11; Fig. 3.3.2) either maintained a vertical step or developed an undercutting plunge pool without the presence of alternating bedrock layers of resistant and non-resistant material (similar to Leopold *et al.,* 1964 and Stein and Julien, 1993). The height of the knickpoint relative to the flow depth is crucially important in controlling the knickpoint form, although a higher threshold value is suggested here than in Leopold *et al.* (1964); $h/KP_H = 0.2$, equivalent to a KP_H/h ratio of 5 for undercutting to occur. Therefore, contrary to the experimental study of Gardner (1983), the development of undercutting plunge pools and vertical stepped waterfalls can happen without bedrock

layering and vertical knickpoints can indeed be formed, maintained and even enhanced as they retreat upstream (Von Engeln, 1940).

Undercutting plunge pools develop where the erosion rate at the base of the knickpoint exceeds the erosion rate at the knickpoint lip, possibly induced by a lateral secondary flow circulation at the plunge pool base. The increased removal of more material by the plunge pool accelerates the overall rate of knickpoint retreat (Fig. 3.3.15). The importance of the undercutting plunge pool in the development and evolution of knickpoints was also identified in a series of experiments by Holland and Pickup (1976). Once an undercutting plunge pool had been 'obliterated', the retreat mechanism of the knickpoint changed from parallel retreat, caused by dominant removal of material from the knickpoint base, to rotation and diffusion caused by the switch to dominant removal of material from the knickpoint lip (Fig. 3.4.1). Following reactivation of the undercutting plunge pool and re-onset of parallel retreat, the knickpoint accelerated upstream and even enhanced the knickpoint height (Holland and Pickup, 1976), supporting the findings from this study that knickpoint form and geometry are fundamentally important in setting the retreat rate of knickpoints.

The magnitude of discharge was not important for the retreat rate of the knickpoints in this study, again supporting the previous work of Holland and Pickup (1976). An increase in retreat rate was identified by Holland and Pickup (1976) immediately after the discharge was increased, but the retreat rate then settled back to the original rate even though the higher discharges were maintained. A similar pattern of retreat rate response to a changing discharge was not identified during this study, although this could have been a result of the difference in the temporal resolution of the tipping bucket pulses (five per minute) and the point cloud collection using the laser scanner (one per minute). The acceleration in knickpoint retreat following a sudden increase in discharge (the rising limb of the tipping bucket, for example) may have occurred but over the longer timescale monitored by the laser scanner, the mean discharge and knickpoint geometry is more important in setting the

knickpoint retreat rate. This is consistent with Holland and Pickup (1976) who documented that despite the acceleration of knickpoint retreat over the short term immediately after an increase in discharge, the knickpoint retreat rates in their experiments fluctuated considerably more as a direct result of the particular knickpoint morphology and of the varying resistance to erosion of the substrate rather than the discharge.

3.4.2 Implications for understanding of knickpoint erosion processes in natural settings

3.4.2.1 Importance of thresholds, knickpoint geometry and knickpoint form

The findings from the experiments presented in this thesis are important in terms of understanding how knickpoints retreat and evolve in natural bedrock rivers. The importance of thresholds in the erosion of bedrock channels have already been discussed at length in Sections 1.2.1, 1.2.2, 2.3.1.5 and 2.5.2, and this study further demonstrates their importance in knickpoint erosion mechanisms. A threshold value for the water depth to knickpoint height ratio exists above which the knickpoint form can evolve into a different state (e.g. the development of an undercutting plunge pool); this in turn sets the mechanism and rate of knickpoint retreat. Haviv *et al.* (2010) identified a similar pattern for waterfalls flowing over a resistant caprock: where knickpoints are taller than a threshold height for failure by buckling, the lateral retreat rate is faster than for knickpoints shorter than the threshold height. My experiments show that there are also threshold knickpoint heights for setting the knickpoint form, and hence lateral retreat rate, in settings that have a homogenous substrate as well as where a resistant caprock is present (e.g. Gardner, 1983; Haviv *et al.*, 2010).

Faster retreat rates have also been found to correlate with knickpoint height in numerical modelling studies (e.g. Flores-Cervantes *et al.,* 2006) and in natural bedrock rivers such as the Da`an River gorge in Taiwan (Cook *et al.,*

2013). An increase in the knickpoint retreat rate was identified between 2006 and 2008 which coincided with the amalgamation of two knickpoints into a single larger knickpoint. However, the findings from my experiments do not follow the predictive equation of Hayakawa and Matsukara (2003) who suggested an inverse relationship between retreat rate and bedrock compressive strength and knickpoint height and width, based on a small (nine waterfalls) field dataset from Japan (equation 2.5.1). An explanation of the discrepancy between my experimental results and the predictive equation of Hayakawa and Matsukara (2003) is difficult, although could possibly be the result of the nature of the weak Neogene or Quaternary sedimentary rocks present on the Boso Peninsula, Japan (Hayakawa and Matsukara, 2003). Where the substrate is very weak (e.g. mudstones on the Boso Peninsula), the lithological strength could be the most important factor in controlling knickpoint retreat and as such lead to very high waterfall retreat rates (~0.01 - 0.27 m/yr; Hayakawa and Matsukara, 2003). Equation 2.5.1 may only be applicable in such a context and is possibly not appropriate where the lithological strength is greater and other factors such as knickpoint geometry (e.g. Haviv *et al.,* 2010) or sediment availability (e.g. Jansen *et al.*, 2011; Cook *et al.*, 2013) become important in controlling knickpoint retreat.

Previous studies (e.g. Kirby and Whipple, 2012) have suggested that vertical stepped knickpoints are predominantly anchored in space and often have no direct significance in terms of transmitting transient signals of erosion induced by changes in climate or tectonic activity. This is due to the fact that vertical stepped knickpoints tend to be spatially correlated with discrete heterogeneities in the channel profile such as coarse debris from landslides (Korup, 2006), debris-flows at tributary junctions and/or locally resistant substrate (Kirby *et al.,* 2003). The experimental data suggests that not only are vertical stepped and undercutting knickpoints, where they exist, faster at propagating upstream, but they also erode more material than slope-break knickpoints. The spatial correlation of vertical stepped knickpoints with discrete heterogeneities in the channel profile may be due to these locations exceeding the local threshold value for a change in the knickpoint form. This

could be caused by an increase in sediment size induced by a landslide deposit increasing the local erosion rate (e.g. Sklar and Dietrich, 2001) at the knickpoint base, thus encouraging the development of an undercutting plunge pool, or a change in the local rock strength again changing the h/KP_H ratio required for an undercutting plunge pool to develop.

Additionally, my experiments support the findings of Mackey *et al.* (2014) in demonstrating the potentially important role of vertical and undercutting plunge pools in causing rapid landscape change. They found that, in contrast to the assertion of Kirby and Whipple (2012), a 40 m high vertical waterfall in the Ka`ula`ula valley, Hawai`i, has not been anchored in space through time, as it has retreated a distance of 4 km at a rate of 33 mm/yr in the last 120 ka. The migration of the knickpoint has generated up to 40% of the total relief in just 3% of the time since the volcanic topography was formed (Mackey *et al.*, 2014). Additionally, the retreat rate of the waterfall was also three orders of magnitude higher than the vertical bedrock channel incision rate upstream of the waterfall, illustrating the importance of understanding the controls on knickpoint retreat rate for understanding rapid landscape change. The mechanism of waterfall retreat in the Ka`ula`ula valley is plucking and toppling of basaltic columns which is a very different mechanism compared to the grain detachment by hydraulic stress taking place in the experiments presented in this thesis. However, the similar findings in both studies (rapid propagation and large volumes of material eroded by vertical and undercutting knickpoints) is important as it suggests that knickpoint erosion mechanisms can be independent of the substrate, a conclusion that has also been found by Jansen *et al.* (2011) in a study of knickpoints in Scotland.

3.4.2.2 Role of discharge in knickpoint erosion

At the landscape scale, a relationship between knickpoint retreat rate and discharge has been proposed by many previous studies (e.g. Bishop *et al.*, 2005; Crosby and Whipple, 2006; Jansen *et al.,* 2011; DiBiase *et al.,* 2015) and this relationship has been used by others to predict the location of knickpoints within landscapes (e.g. Crosby and Whipple, 2006; Berlin and

Anderson, 2007). However, my experimental study suggests that, at the reach scale, the discharge magnitude is not a direct control on the knickpoint retreat rate (Fig. 3.3.8). Variations in the flow depth can potentially set the knickpoint form through the h/KP_H ratio but the hydraulic scaling relationships show that increases in discharge alter the channel width more than the flow depth, with the latter only changing a small amount, and thus the knickpoint height is the dominant control on the knickpoint form and retreat rate at the reach scale in these experiments.

Although contradictory to studies that examine knickpoint retreat at the landscape scale, two recent studies of natural rivers support the conclusion that factors other than the discharge control the knickpoint retreat rate at the reach scale (Cook *et al.,* 2013; Mackey *et al.,* 2014). The influence of the knickpoint geometry on the retreat rate on the Da`an River gorge has already been discussed, but the bedrock structure may also be important: when the knickpoint retreat rate peaked between 2006 and 2008, the Da`an River was incising through a section of horizontally bedded strata of weak mud layers beneath stronger sandstone beds (Cook *et al.,* 2013). However, the most important factor in initiating the retreat of the knickpoint in the Da`an River gorge was determined to be the availability of coarse bedload for sediment transport. Immediately following the 1999 Chi-Chi earthquake, there was no knickpoint erosion or gorge formation because sediment was trapped behind the uplifted channel reach. Throughout the knickpoint propagation over a distance of 1.2 km, there was no identifiable relationship between the discharge and the retreat rate.

Mackey *et al.* (2014) specifically examined the ability of drainage area-dependent waterfall-retreat models to explain the knickpoint retreat history in the Ka`ula`ula valley, quantified using cosmogenic nuclide surface exposure and accumulation ages:

$$KP_{RR} = cA^{p} \qquad \text{Eqn. 3.4.1}$$

where *c* and *p* are constants and *A* is drainage area, a proxy for discharge. Previously proposed values of *c* and *p,* based on a positive relationship between retreat rate and discharge (e.g. Rosenbloom and Anderson, 1994; Crosby and Whipple, 2006; Berlin and Anderson, 2007), fail to accurately model the retreat of the 40 m Ka`ula`ula waterfall over the last 120 ka, with the simplest explanation of the retreat history obtained with a constant rate of knickpoint retreat (i.e. $p = 0$), independent of discharge/drainage area (Mackey *et al.,* 2014).

These field-based studies combined with the experimental data from this study suggest that caution should be employed when attempting to model knickpoint retreat using discharge or drainage area. Not only does the magnitude of the discharge have little effect on the retreat rate (Fig. 3.3.8, and the experimental study of Holland and Pickup, 1976), but temporal variability in the hydrograph (Section 3.3.4) also fails to significantly change the longer term rate of knickpoint retreat in the experimental channel compared to an equivalent constant mean discharge, although this relationship requires further exploration using higher resolution measurements to pick out the effect of individual pulses of water. Berlin and Anderson (2007) specifically state that they ignore the complexities of erosion mechanisms at knickpoints in their study of the Roan Plateau, Colorado, in favour of a simple scaling with drainage area/discharge. This experimental study explicitly demonstrates that understanding the complexities of the erosion mechanisms at knickpoints, such as a threshold h/KP_H ratio value for the development of an undercutting plunge pool, is fundamental in understanding the role that knickpoints have in landscape change.

Despite the fact that discharge is not important in controlling the knickpoint retreat rate, discharge is still important in terms of controlling the volume of material eroded by knickpoints as they retreat upstream (Section 3.3.3; Fig. 3.3.17, 3.3.18). The width of the bedrock channel scales with discharge and thus sets the geometry of the knickpoint. Therefore, a channel that has a

higher mean discharge will erode more material through knickpoint retreat than a channel with a lower discharge, even if the height of the knickpoint and the retreat rate remain constant. I propose that the volume of material eroded as a knickpoint migrates upstream is a function solely of the knickpoint geometry, i.e. the height and the width, with the latter set by the discharge. Where sediment flux data is available, it could be possible to further explore the relative significance of erosion of knickpoints in the wider denudation of catchments.

3.4.2.3 Other possible controls on knickpoint retreat not tested in these experiments: bedrock structure/strength and sediment

These experiments have exclusively studied the role of discharge and knickpoint geometry in controlling knickpoint retreat, while maintaining other factors such as sediment availability, bedrock structure and bedrock strength constant. Several studies have documented the importance of bedrock heterogeneity in controlling the mechanisms and retreat rate of knickpoints. For example, regular joint spacing (e.g. columnar basalt) privileges knickpoint retreat through block toppling (Lamb and Dietrich, 2009), potentially leading to rapid propagation rates (Mackey *et al.,* 2014): the presence of resistant caprock can also encourage the development of undercutting plunge pools (e.g. Gilbert, 1907; Haviv *et al.*, 2010). However, the importance of different factors in controlling knickpoint retreat in an environment is set by the balance of several different factors, with the dominant control differing between settings. In Scotland, the dominant control on knickpoint retreat since deglaciation is the supply of coarse sediment, with the location of knickpoints independent of bedrock strength or structure (Jansen *et al.,* 2011). As the supply of sediment has reduced during the Holocene, the rate of knickpoint propagation in these channels has also reduced, with no relationship to knickpoint geometry or discharge (Jansen *et al.*, 2011). The supply of sediment was also crucial for the initiation of knickpoint migration in the Da`an River, Taiwan, which only began once coarse bedload became available for transport (Cook *et al.,* 2013).

The experiments presented in this thesis represent an important empirical baseline for the understanding of knickpoint erosion processes as the erosion mechanisms that are witnessed in natural river settings have been replicated in a homogenous substrate. This baseline understanding can be used in other environmental settings that may be more complex, such as having variations in bedrock strength, because it can help determine the relative importance of each controlling factor on knickpoint retreat rates in different settings. For example, the threshold h/KP_H value in my experiments for the development of an undercutting plunge pool is 0.2 but I hypothesise that this value would vary in different environments. For example, if the silica cement mixture used for the experimental substrate had a lower proportion of spherical beads (Section 3.1.3), it would be stronger and the h/KP_H threshold value for developing an undercutting plunge pool would be lower as more energy would be required from the flow to erode the material at the base of the knickpoint. Overall, this would also have the impact of reducing the knickpoint retreat rate for an equivalent knickpoint geometry. Such a relationship was identified by Wells *et al.* (2009) who found that, where all other conditions were kept constant, headcuts in a weaker experimental substrate developed larger plunge pools and also retreated faster than knickpoints in a stronger substrate. Thus, the fastest knickpoint retreat rates in natural rivers would be expected where tall knickpoints coincide with a weaker substrate. Additionally, the threshold h/KP_H ratio value for the development of undercutting plunge pools in a weaker substrate would be higher (i.e. smaller knickpoints relative to the flow depth), which would for a given distribution of knickpoint heights mean that more would develop undercutting plunge pools and hence retreat faster.

3.4.3 Conclusions and further work

The rate of knickpoint retreat in any setting is set by the balance of different factors such as knickpoint geometry, discharge, sediment supply and the nature of the bedrock. These experiments represent an important empirical

baseline for environments where bedrock is homogenous, demonstrating that the dominant control on the knickpoint retreat is the mechanism of knickpoint retreat (e.g. relative rates of removal of material from the lip and base of the knickpoint) which is set by the knickpoint form (e.g. undercutting). The form of the knickpoint is controlled by the ratio of the flow depth to the knickpoint height, with the threshold values for development of undercutting plunge pools or diffusion into a steepened reach of 0.2 and 0.35 in these experiments, respectively. This concept is applicable beyond this discrete set of experiments because I propose that variations in bedrock strength would simply alter the threshold h/KP_H values required for different forms of the knickpoint to develop. Bedrock heterogeneity adds a complexity to the controls on knickpoint retreat, but it could be expected that where bedrock layering of weak and strong rocks exists, this may act to encourage the development of undercutting plunge pools at a higher h/KP_H ratio value (i.e. smaller knickpoints) when all other factors are kept constant. At the reach scale, these experiments demonstrate that discharge is not the dominant control on knickpoint retreat, but can control the amount of material eroded by knickpoints as they retreat upstream through changing the width of the channel and thus total area that the knickpoint works over.

However, additional experiments could be carried out to further improve the understanding of the role of bedrock heterogeneities (e.g. joint spacing) in knickpoint retreat. Questions remain whether regular joint spacing would dominate the balance over other factors and act to encourage higher rates of knickpoint migration, due to the relative ease of erosion through block plucking/toppling in these environments compared to other settings (Lamb and Dietrich, 2009). The same set of experiments could also be carried out using homogenous substrates of varying strengths to see if this has a noticeable impact on the threshold values of h/KP_H ratio for setting different knickpoint form. Further variations in the hydrograph (i.e. different tipping bucket regimes) could also be examined to see if the acceleration on knickpoint retreat rate immediately following a rise in discharge identified by Holland and Pickup (1976) is also present in these experiments.

Chapter 4: Synthesis

4.1. Summary of findings in relation to research objectives

This chapter aims to bring together the work presented in Chapters 2 and 3 in respect to the main research objectives provided in Section 1.3

4.1.1 Impact of discrete flood events in landscape evolution

The 'geomorphic effectiveness' of high magnitude flood events that occur on 10^0 to 10^2 year timescales has been well-documented in previous studies, such as channel widening during peak flows (e.g. Hartshorn *et al.,* 2002) and the plucking of large blocks from the channel bed (e.g. Snyder *et al.,* 2013a). The effects of these events tend to be focussed within the channel system. This study has shown that extreme flood events, that occur on $\geq 10^3$ year timescales, can lead to catastrophic change both within the bedrock channel and the wider landscape, such as large canyon formation and drainage reorganisation (Sub-Chapters 2.3 and 2.4).

The first research objective of this study was to quantify the impact of extreme flood events over longer term bedrock erosion processes in landscape evolution. This study is unique in directly quantifying the impact of multiple discrete extreme flood events on the evolution of a bedrock landscape, rather than using sedimentary deposits to infer the action of the extreme floods (e.g. Waitt, 2002). To successfully achieve this, the short term impact of extreme flood events was identified in Sub-Chapters 2.3 and 2.4. Surface exposure ages have identified that large knickpoints have retreated distances from hundreds of metres to in excess of 2.5 km in very short periods of time, eroding canyons that are demonstrably too wide to have been formed by annual peak flows along the Jökulsá á Fjöllum. A flood in the early Holocene eroded ~ 0.14 km^3 of material from Ásbyrgi canyon at the downstream end of the Jökulsárgljúfur canyon. However, this only partly achieves the first research objective as the impact of discrete events has also to be considered over multiple timescales, including a comparison to the action and impact of 'background' erosion processes between flood events, discussed below.

4.1.2 Long-term impact of multiple extreme flood events on landscape evolution

Previous studies of erosion during extreme flood events (e.g. Lamb *et al.*, 2008b; 2014) have focussed on the impact of single events in the development of canyons. This study of the Jökulsárgljúfur canyon is the first to identify the evolution of a canyon system through time as a result of multiple discrete extreme flood events, quantifying the relative impact of the flood events compared to 'background' non-flood periods (the second part of the first research objective). Sub-Chapters 2.3 and 2.4 showed that erosion during these extreme events has dominated the long term evolution of the landscape, with the combined effect resulting in a 28 km long, up to 100 m deep, canyon while also forming additional abandoned features such as Ásbyrgi and the Klappir scablands. This illustrates the importance of extreme flood events in shaping the Earth's surface at a large spatial scale (i.e. across a whole landscape). By contrast, the geomorphic work that takes place during high magnitude floods that occur on $10^0 – 10^2$ years timescale, such as Supertyphoon Bilis (Hartshorn *et al.,* 2002), is mainly focussed within the already established channel system. Thus, another possible definition of an 'extreme flood event' is one that has an impact on a spatial scale beyond the channel itself (Section 1.2.3.2.1).

After a transient perturbation, such as an extreme flood event, a landscape has a characteristic timescale of recovery before it returns to its background state, assuming that it is not perturbed again before recovery is complete (Brunsden and Thornes, 1979; Allen, 2008; Duller *et al.,* 2014). The typical 'recovery' of a bedrock landscape that has experienced an extreme flood event is the gradual diffusion of the vertical headwalls of knickpoints through abrasion and the plucking of individual blocks (Lamb *et al.*, 2014). Despite the landscape recovery timescale of knickpoints in the Jökulsárgljúfur canyon not being known, the experimental study of knickpoint processes (Chapter 3) provides an insight into how the Jökulsárgljúfur canyon may evolve during 'background' non-flood periods. The experiments show that tall knickpoints

(with flow depth to knickpoint height ratio values less than 0.2) are more likely to maintain a vertical headwall or develop an undercutting plunge pool than short knickpoints (flow depth to knickpoint height ratio values greater than 0.35), which are more likely to diffuse through time. The exact values for the thresholds in setting the knickpoint form in the Jökulsárgljúfur canyon may be different than in the experiments, due to differences in the bedrock structure/strength, but the general concept suggests that Selfoss (13 m high) is more likely to diffuse from a waterfall with a vertical headwall into a steepened reach than Hafragilsfoss (20 m high) or Dettifoss (54 m high). This is corroborated by the fact that there are rapids 500 m upstream of Selfoss, of the order of a couple of metres in elevation that appear to have diffused. Thus, the 'landscape recovery time' following a transient perturbation such as an extreme flood event is dependent on the landforms created during the extreme flood event, with the recovery times increasing with increasing knickpoint height.

Unlike Pointed Canyon, Idaho (Lamb *et al.*, 2014), there is also a possibility that extreme flood events may have permanently shifted the 'landscape state' of the Jökulsárgljúfur canyon, and it may never 'recover' to its original state. For example, during peak annual flows (flow depth ~3 m; Section 2.3.2.2), the ratio of the flow depth to knickpoint height at Dettifoss is very low at 0.06. Experimental knickpoints with similar h/KP_H ratios maintained their vertical step throughout the channel length as they retreated upstream (Fig. 3.3.13B), so it is possible that Dettifoss will never diffuse, even if another extreme flood event does not occur. Therefore, not only do extreme flood events lead to catastrophic landscape change in short periods of time; they can also have a long lasting legacy on the landscape morphology with characteristic vertical headwalls maintained for long periods after extreme flood events (the first research objective).

4.1.3 Knickpoint erosion processes

Thresholds exist in bedrock channels that switch erosion mechanisms from one regime to another. For example, it is well known that a critical shear

stress value is required to put bed sediment into motion to act as tools for abrasion (e.g. Buffington and Montgomery, 1997) and also for whole blocks to be detached and transported through plucking (Snyder *et al.*, 2003a). However, as discussed in Chapter 1, the role of thresholds between erosion regimes is commonly ignored in models of bedrock erosion, especially erosion at knickpoints, so the findings from Sub-Chapter 2.3; where the dominant erosion process during extreme flood events in the Jökulsárgljúfur canyon was the toppling and transportation of whole bedrock columns at knickpoints once a threshold flow depth had been exceeded (second research objective), combined with the identification of important thresholds for determining knickpoint form and long term retreat rate in Chapter 3 has highlighted the importance of thresholds for the different mechanisms of knickpoint retreat in bedrock channels; the third research objective in this study, discussed in detail below. These complexities should be considered and integrated into models of landscape evolution in order to accurately predict how landscapes evolve over long and short timescales in response to changes in external forcing such as tectonics or climate, or the impact of extreme events.

Where bedrock columns exist, a simple flow depth threshold exists between an erosion regime characterised by the plucking of individual blocks and one of whole rock column toppling (Lamb and Dietrich, 2009). Not only does this lead to the formation of waterfalls that have vertical headwalls, it is possible to achieve rapid rates of knickpoint retreat in short periods of time when this threshold is exceeded (Sub-Chapter 2.3). The limiting factor on the rate of knickpoint retreat through block toppling is often the ability for material, once toppled, to be transported away from the base of the knickpoint (Mackey *et al.*, 2014). This is unlikely to be a problem in the Jökulsárgljúfur canyon given the high sediment transport capacity of extreme flood events (e.g. Carling, 2013; Attal, 2015); it can therefore be assumed that, in settings such as the Jökulsárgljúfur canyon, knickpoint retreat will occur when the threshold flow depth is exceeded.

Once the flow depth for column toppling (set by the joint spacing of the rock) is exceeded, the retreat rate is independent of discharge magnitude, with the duration of the flood likely to determine the total distance that the knickpoint erodes. Therefore the > 2.5 km of knickpoint retreat identified in the Jökulsárgljúfur canyon could indicate a prolonged period of heightened discharge slightly above the threshold value (> 3250 m^3 s^{-1}; Sub-Chapter 2.3) rather than a short pulse of extreme discharge of the order of 10^5-10^6 m^3 s^{-1}. This would be possible given the triggering mechanism and floodwater source beneath Vatnajökull; a prolonged fissure-type eruption, similar to the Bárðarbunga/Holuhraun eruption in 2014/2015, located beneath the ice would continually generate high volumes of floodwater for a long period of time, potentially causing knickpoints in the Jökulsárgljúfur canyon to retreat large distances. For example, the 140 jökulhlaups over a period of 30 days led to significant landscape change in the proglacial area (Dunning *et al.,* 2013) despite the peak discharge of the largest flood estimated at 5,000-15,000 m^3 s^{-1} (Magnússon *et al.*, 2012) rather than on the order of 10^5 to 10^6 m^3 s^{-1}. Additionally, a prolonged period of heightened discharge could be triggered through a 'jökulhlaup cycle' (Evans and Clague, 1994), where an ice-dammed lake periodically releases large volumes of water as the ice-dam weakens through downwasting and retreat and a critical threshold is reached where the water in the lake can no longer be continuously supported behind the dam. The ice-dammed lake then becomes 'self-dumping' where it drains and refills on a regular basis until either the glacier re-advances and re-forms a stronger dam or retreats far enough so it no longer blocks water in a lake (Evans and Clague, 1994). A period of repeat jökulhlaups triggered in this way could also generate a prolonged period of heightened discharge, causing knickpoints in the Jökulsárgljúfur canyon to retreat large distances.

The magnitude of the discharge affects the total material eroded during knickpoint retreat, as a higher discharge leads to a wider channel, thus cutting a wider canyon as the knickpoint migrates upstream (Fig. 3.3.16). This process is evident in the morphology of the Jökulsárgljúfur canyon as the extreme floods led to the development of an overwidened gorge, with the

present day river channel not filling the base of the canyon (Fig. 2.3.1; 2.3.2C). I hypothesise that the magnitude of the peak discharge of the floods in the Jökulsárgljúfur canyon are manifested in the canyon width, rather than the knickpoint retreat rate, and thus the overwidened canyon morphology could be diagnostic of the peak discharge of the extreme flood events while the length of knickpoint retreat could be diagnostic of the flood duration.

Once the knickpoints have developed as a result of extreme flood event(s), thresholds are also important in controlling how the knickpoints will evolve through time during background 'non-flood' periods. If the ratio of the typical flow depth to the knickpoint height is low enough (< 0.2 in the experimental channel), then the knickpoint can maintain a vertical headwall, or develop an undercutting plunge pool, and the knickpoint is unlikely to diffuse into a steepened reach or 'slope-break' knickpoint. On the other hand, if the knickpoint height is smaller relative to the flow depth (ratio > 0.35), the knickpoint is more prone to diffusion and could be lost from the long profile as it migrates upstream.

The threshold h/KP_H values for knickpoint form are determined from the experimental study that was carried out using a cohesive homogenous substrate representative of bedrock without any structure. The presence of bedrock columns in the knickpoints in Iceland make them more prone to both rapid rates of knickpoint retreat and vertical headwalls due to the relative ease with which they can be toppled (Lamb and Dietrich, 2009; Lamb *et al.*, 2014; Mackey *et al.*, 2014). I therefore hypothesise that the threshold h/KP_H value for maintaining a vertical headwall as the waterfalls migrate would be higher in the study area (i.e. relatively smaller knickpoints would be maintained) where the bedrock contains vertical jointing. A future series of experiments could be carried out in order to test the importance of bedrock structure (e.g. columns) in setting the threshold value in the ratio of water depth to knickpoint height in order to maintain a vertical headwall/develop an undercutting plunge pool.

Chapter 5: Conclusions and Wider Implications

5.1 Conclusions

The conclusions from this study are wide reaching and important, from the detailed evolution of a large canyon system in Iceland caused by extreme flood events to an improved process-based understanding of knickpoint dynamics and the consideration of these erosion processes in models of landscape evolution. The important conclusions from this study are:

1. Bedrock erosion during extreme flood events can lead to catastrophic landscape change in very short periods of time. Within the Jökulsárgljúfur canyon, erosion is caused by the upstream migration of knickpoints once a threshold flow depth for column toppling has been exceeded. During discrete periods of rapid canyon cutting, approximately 5000 and 2000 years ago, multiple knickpoints at different elevations have retreated distances from hundreds of metres to in excess of 2.5 km (Fig. 5.1), incising the Jökulsárgljúfur canyon by more than 100 m.

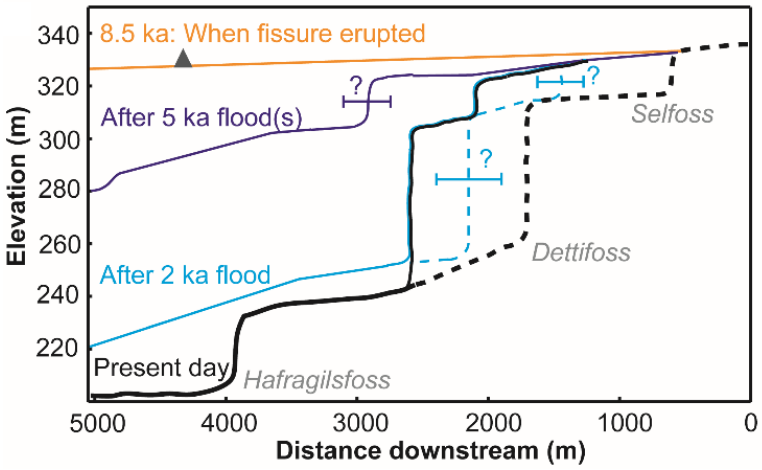

Fig. 5.1: Proposed evolution of the Jökulsárgljúfur canyon during the Holocene. The strath terraces and exposure ages have been used to reconstruct the long profile of the Jökulsá á Fjöllum when the fissure erupted (in orange), after the 5 ka flood event(s) (in dark blue) and after the 2 ka flood event (in light blue). There has been no subsequent erosion since the 2 ka extreme flood event within the overspill channel. Bars with question marks indicate uncertainty on the position of knickpoints (palaeo-Dettifoss at 2 ka ago is likely to be where the gorge over-widens).

2. Extreme flood events can dominate landscape evolution over timescales that are much greater than the duration of the flood events. During the Holocene, floods which occur on a millennial timescale initiated, lengthened, widened and deepened the Jökulsárgljúfur canyon while very little geomorphic activity occurred during background 'non-flood' periods between events. The legacy of extreme flood events is maintained within the landscape morphology, as the timescale of 'landscape recovery' is much greater than the frequency of the extreme flood events; leading to the persistence of the perturbed landscape morphology (vertical headwalls of knickpoints; Fig. 5.1; and abandoned canyons; Fig. 5.2) over long timescales (> 10^4 years).

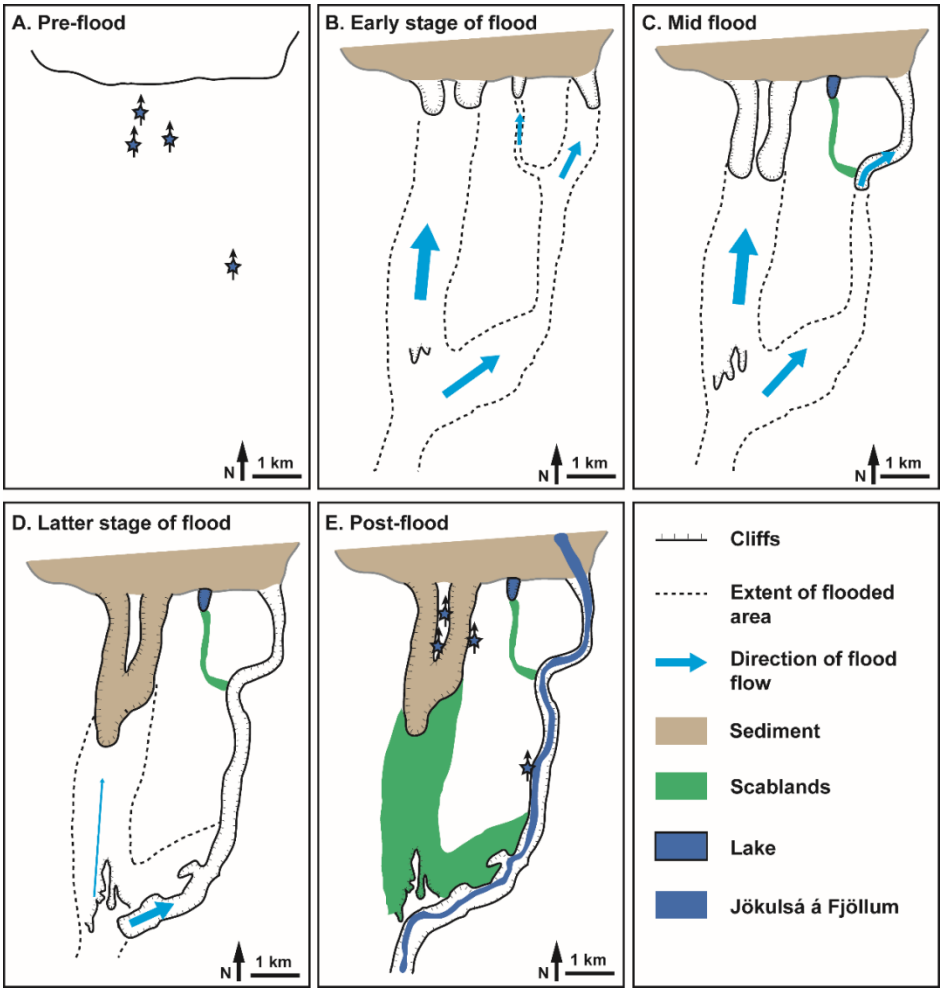

Fig. 5.2: Proposed macroform evolution of the lower Jökulsárgljúfur canyon during an extreme flood event in the early Holocene. **A.** Before the flood, the precise course of the Jökulsá á Fjöllum is impossible to determine; but fluvially sculpted surfaces on the top of

Ásbyrgi Island, the eastern rim of Ásbyrgi and the western rim of the main canyon at Landsbjörg indicate that a river once flowed here before the canyons were formed. The locations of the fluvially sculpted surfaces are shown by the blue stars (also shown in E for comparison), with direction of palaeo-flow shown by the black lines. **B.** In the early stages of the flood, the floodwaters follow the course of the pre-flood river and also spread to the east. At the northern limit of the lava surface, four canyons begin to be incised. Through time, the floodwaters flowing into the canyon that currently contains Lake Ástjörn are captured by the faster retreat of the canyon to the east **(C.)** while the two Ásbyrgi canyons continue to retreat until they coalesce. The western canyon of Ásbyrgi continues to retreat and, eventually, the large canyon to the east retreats far enough to also capture the floodwaters flowing across the Klappir scablands into Ásbyrgi. During the waning flow, a thin layer of sediment is deposited in the bottom of Ásbyrgi **(D.)**. The headwall in the main canyon continues to retreat, disconnecting Ásbyrgi and Klappir from the course of the Jökulsá á Fjöllum leading to the outstanding preservation of the landforms **(E.)**. Subsequent floods along the Jökulsá á Fjöllum are channelled in the main canyon, although some potential minor reoccupation of Klappir may have occurred, which stripped some of the soils (Waitt, 2002). The main canyon at Landsbjörg is drawn here assuming that all the erosion in this main canyon occurred during the early Holocene flood, although additional reworking of the canyon morphology during later floods cannot be ruled out.

3. The dominant control on knickpoint retreat rate is the form of the knickpoint which sets the mechanism of retreat (Fig. 5.3). Knickpoints with a low flow depth to knickpoint height ratio are more likely to develop an undercutting plunge pool, which causes them to retreat faster than knickpoints that diffuse into a steepened reach. Taller knickpoints therefore retreat faster than smaller knickpoints; they do not necessarily require heterogeneity in bedrock structure such as layering or jointing to maintain a vertical headwall or develop an undercutting plunge pool as they retreat.

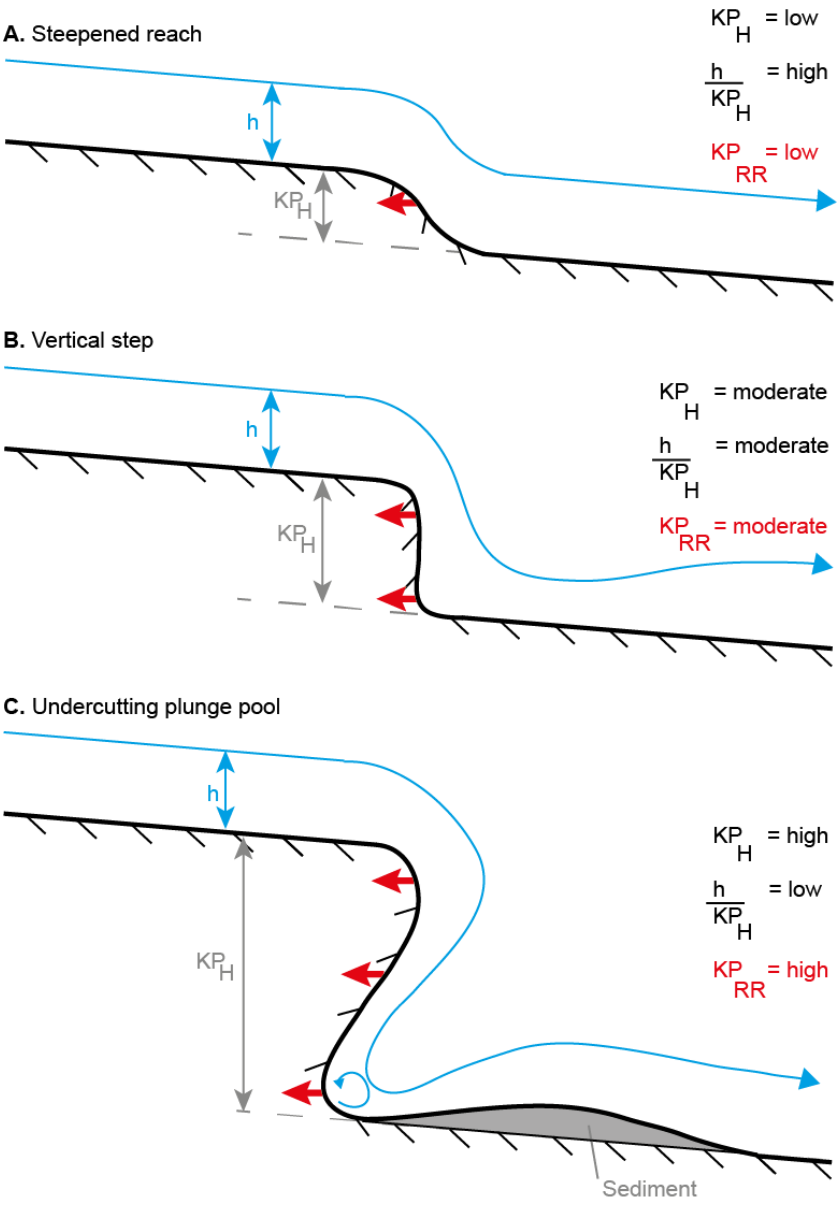

Fig. 5.3: Conceptual model (not to scale) showing the controls on knickpoint retreat in the experimental flume. **A.** Smaller knickpoints (with high h/KP_H ratio values; > 0.35) tend to diffuse from the initial vertical step into a steepened reach, where erosion of material from the knickpoint takes place at the lip of the knickpoint (red arrow). **B.** Moderate sized knickpoints in the experiments maintained their vertical steps and material was eroded from the knickpoint lip and from the downstream face of the knickpoint, thus allowing a faster knickpoint retreat rate than steepened reaches. **C.** The largest knickpoints (with low h/KP_H ratios; < 0.2) retreat the fastest as material was eroded from the knickpoint lip, the downstream face and by the undercutting plunge pool due to development of secondary circulation of the flow. The amount of eroded material at the knickpoint exceeded the sediment transport capacity of the channel downstream of the knickpoint, leading to the deposition of a sediment push bar.

4. Knickpoint retreat rate is independent of variations in mean discharge, but high discharges do lead to more material being eroded as the knickpoint retreats upstream (Fig. 5.4). Higher discharges create wider knickpoints that erode more material from the banks of the canyon as they retreat upstream. During extreme flood events, this can result in the formation of canyons that are significantly wider than what would be expect to be formed during periods of 'background' flow.

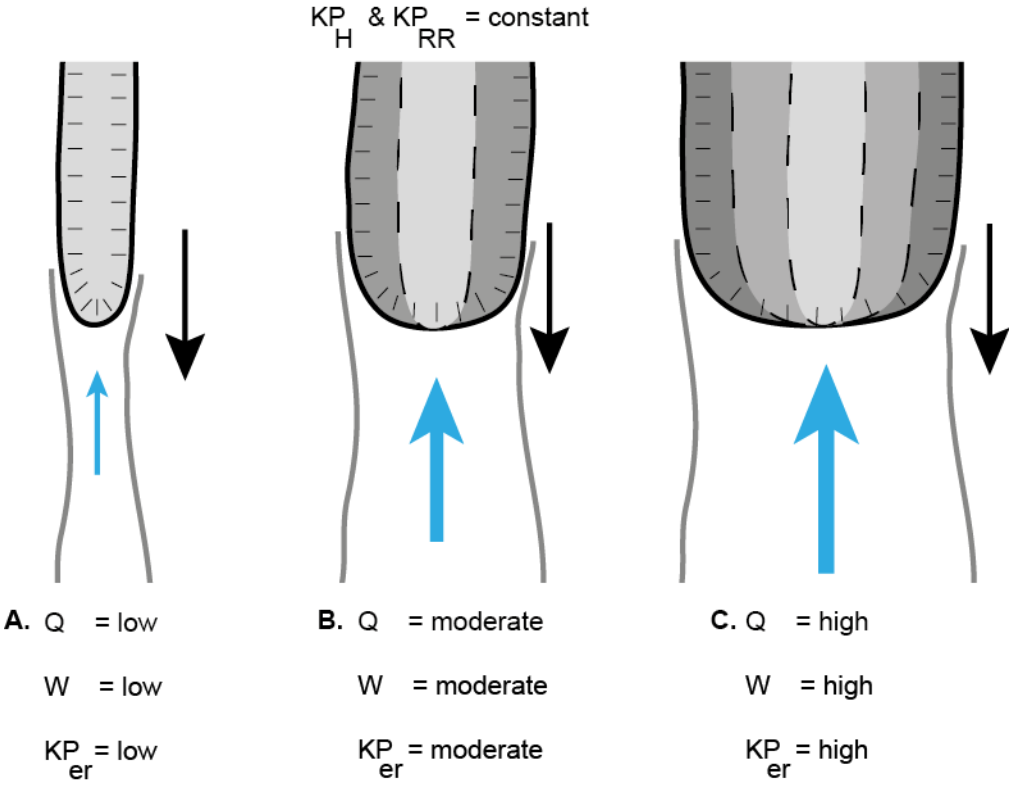

Fig. 5.4: Conceptual plan-view diagram of how increasing discharge (size of blue arrow, flowing towards the top of the page) alters the total volume of material eroded from knickpoints (outline of knickpoint indicated by the solid black line), even if the knickpoint retreat rate does not change (solid black arrow, retreating towards the bottom of the page). An increase in the discharge leads to an increase in the channel width ($W \propto Q^{0.38}$; grey lines indicate the banks of the channel), which increases the area of the knickpoint face, thus eroding more material as the knickpoint migrates upstream.

5. In order to fully understand the wider role of bedrock erosion in landscape evolution, the mechanisms of erosion and thresholds between different

erosion mechanism regimes need to be considered. Simplifications such as the stream power model do not satisfactorily resolve the complexities of bedrock erosion at the reach scale where a detailed understanding of the physics of erosion mechanisms is required in order to accurately model the past, present and future response of bedrock channels to transient forcing mechanisms.

5.2 Wider implications of the research

5.2.1 Terrestrial analogue for understanding landscape evolution on Mars

A key aim of previous work that has studied bedrock erosion and canyon formation during extreme flood events (e.g. Lamb *et al.,* 2008b; 2014) has been to determine a diagnostic link between landform morphology and the processes that formed them, in order to infer and understand the formation processes of morphologically similar landscapes (Fig. 4.1.1). The surface of Mars contains extensive areas that are characterised by large cataracts and multiple bedrock terraces such as the Ares Vallis and Valles Marineris regions, thought to have been formed during extreme flood events in the Hesperian epoch of Martian geological history, ~3.7 billion years ago (Warner *et al.* 2010; 2013). The occurrence of extreme flood events at this time has major implications for the understanding of the hydrosphere in early Martian history as they could indicate the presence of large water bodies on the surface of the planet (Warner *et al.,* 2010; 2013).

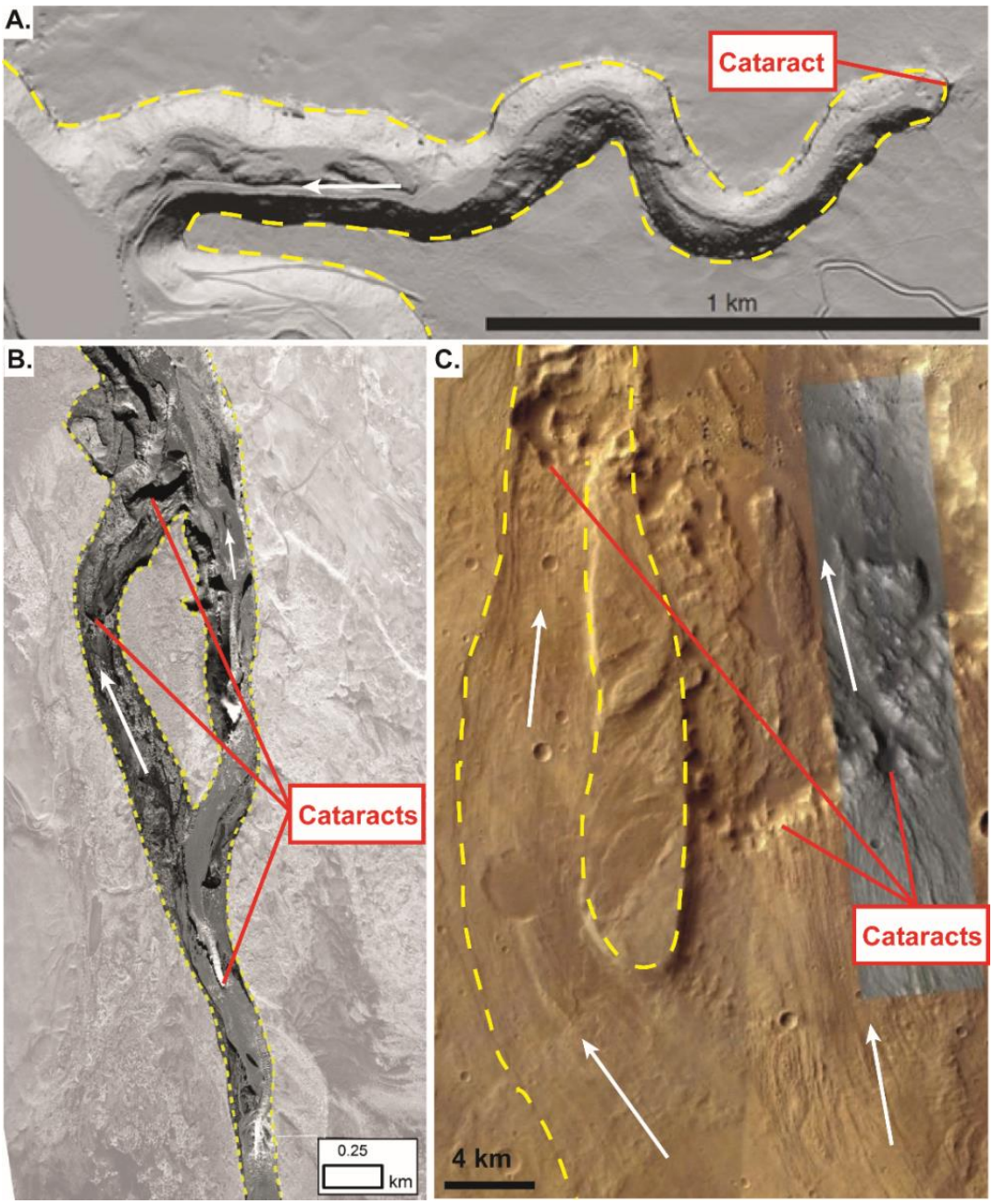

Fig. 4.1.1: Example of the similarity in landforms on the surface of Earth and Mars, illustrating the potential for understanding of erosion processes in extra-terrestrial environments: **A**: Box Canyon, Idaho; (study area of Lamb *et al.,* 2008b). **B**: the Jökulsárgljúfur canyon (this study). **C**: Ares Vallis tributary outflow channel, Mars (study area of Warner *et al.*, 2010, image from Google Mars). Dry vertical knickpoints (cataracts) are present in all the landscapes, as well as multiple channels eroded into bedrock. Assuming landscape form is diagnostic of the processes that formed it, the understanding of bedrock erosion during extreme flood events developed from the study of the Jökulsárgljúfur canyon can help understanding the evolution of landscapes on Mars such as Ares Vallis. White arrows indicate the flow direction and yellow dashed lines indicate the flow limits.

If we can assume that a diagnostic link does exist between landscape processes and form, the understanding of knickpoint erosion processes and landscape evolution developed in this study could be applied to Martian landscapes such as Ares Vallis (Warner *et al.*, 2010) or Valles Marineris (Warner *et al.,* 2013). For example, Warner *et al.* (2010) suggested a simple time evolution of canyon formation in a tributary valley flowing into the main Ares Vallis trunk channel following a sequence of base-level change (Fig. 4.1.2). However, Sub-Chapter 2.3 in this study has shown that high resolution geochronological techniques (surface exposure dating, equivalent to crater-age distributions on Mars) can identify the timing and specific impacts of individual flood events in landscape evolution. The morphology of the Martian cataracts can also be used to estimate the magnitude of the flood events that formed them, as a similar relationship between discharge and canyon width identified in Chapter 3 would also be expected on Mars. There remains a need for quantitative studies of landscapes on Mars to understand how they were formed, and with the ever-increasing resolution of imagery data and DEMs of the surface, there is a possibility that the concepts and understanding developed in this study could be applied to Mars in the future.

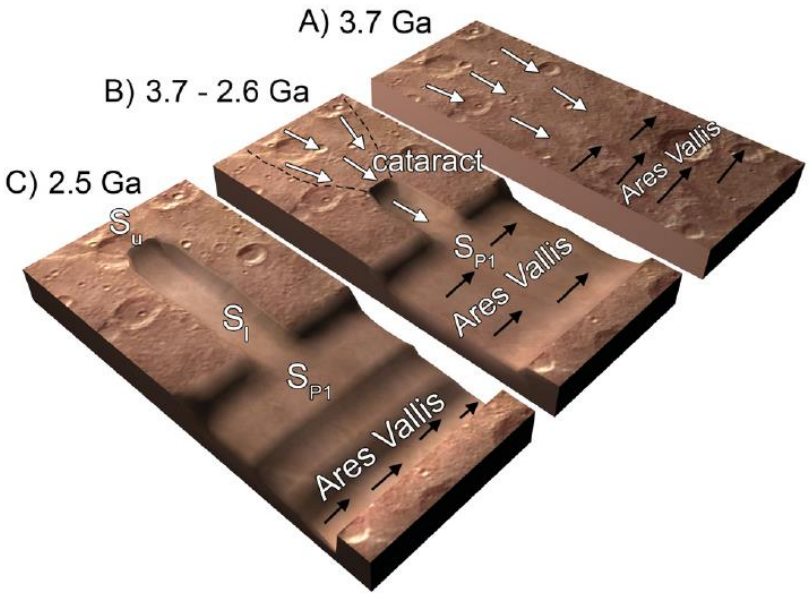

Fig. 4.1.2: Conceptual diagram of Warner *et al.* (2010) showing the proposed evolution of a cataract during floods in a tributary channel following base-level fall in the main Ares Vallis

trunk channel. High resolution geochronological information of the age of surfaces along the profile of the tributary (and main) canyon could possibly isolate the erosive impact of individual flood events. The timing of these flood events would help understanding the early hydrosphere of Mars as large surface water bodies would have had to be present to act as the source of the floodwaters.

5.2.2 Future research questions/areas for research

There are a few avenues of potential future research, both field-based and experimental, that could be conducted in the future, building on the findings of this research. The joint spacing of the lava flows at the knickpoints is important in setting the threshold flow depth required for the knickpoints to begin retreating (Appendix A.2.2) yet the lava flows that the Jökulsárgljúfur canyon is cut into do not all have the same characteristic joint-spacing. The impact of these variabilities could be investigated by assessing the joint structure at each of the three major knickpoints (Selfoss, Dettifoss and Hafragilsfoss) and using the Lamb and Dietrich (2009) model to see which requires the lowest flow depth in order to start migrating. If, for example, Dettifoss were to start retreating while Selfoss was still stable, eventually these two knickpoints could combine to form a single larger (67 m high) knickpoint. Additional work could also explore the fact that the Jökulsá a Fjöllum drops the height of three lava flows at Dettifoss, each exhibiting different joint spacing characteristics; the Lamb and Dietrich (2009) model does not currently take this into account as it assumes that the columns at the knickpoint headwall are free-standing and uniform.

If possible, the additional samples for surface exposure dating collected from the Ásbyrgi and Klappir region should be analysed (Fig. 2.1.12). These samples should provide additional confirmation on whether Ásbyrgi was formed during a single event; under the scenario proposed in Fig. 2.4.12, I would expect all of the surface exposure ages to be clustered in the early Holocene (~9-10 ka ago). A younger age could be expected from the sample collected from a boulder deposited within the western canyon of Ásbyrgi if it

had been transported during later floods that overtopped the Klappir scablands.

The most outstanding future experimental work would include heterogeneity in the bedrock substrate. The work presented here provides an important empirical baseline of how knickpoints evolve in a homogenous substrate but it would be essential to test how factors such as bedrock layering or jointing increase or decrease the threshold h/KP_H ratio required for vertical headwalls to be maintained or diffuse as they retreat upstream. The same suite of experiments could also be carried out using a stronger/weaker homogenous substrate to test how this controls the thresholds for knickpoint form and whether knickpoints would retreat faster in a weaker substrate. Holland and Pickup (1976) identified a response in the knickpoint retreat rate immediately after a change in the discharge and this could be investigated by improving the temporal resolution of the point cloud collection relative to the frequency of the pulses of flow induced by the tipping bucket. In my experiments, there were five pulses per point cloud, and any short term variability in the knickpoint retreat rate caused by the tipping bucket was not resolved, although the long term retreat rate of the knickpoints was found to be set by the mean discharge, irrelevant of its temporal variability. These future experiments would help understanding how knickpoints evolve through time and assessing the importance of knickpoint erosion in studies of long term landscape evolution.

6. References

Alho P, Russell AJ, Carrivick JL, Käyhkö J (2005) Reconstruction of the largest Holocene jökulhlaup within Jökulsá á Fjöllum, NE Iceland. *Quaternary Science Reviews* 24, 2319-34

Alho P, Roberts MJ, Käyhkö J (2007) Estimating the inundation area of a massive, hypothetical jökulhlaup from northwest Vatnajökull. *Natural Hazards* 41, 21-42

Allen PA (2008) Time scales of tectonic landscapes and their sediment routing systems. In Gallagher K, Jones SJ, Wainwright J (Eds.) *Landscape Evolution: Denudation, Climate and Tectonics Over Different Time and Space Scales*. Special Publication of Geological Society of London 296, 7-28

Anderson RS (1986) Erosion profiles due to particles entrained by wind: Application of an eolian sediment-transport model. *GSA Bulletin* 97, 1270-8

Andrews JT, Hardardóttir J, Helgadóttir G, Jennings AE, Geirsdóttir Á, Sveinbjörnsdóttir ÁE, Schoolfield S, Kristjánsdóttir GB, Smith LM, Thors K, Syvitski JPM (2000) The N and W Iceland Shelf: insights into Last Glacial Maximum ice extent and deglaciation based on acoustic stratigraphy and basal radiocarbon AMS dates. *Quaternary Science Reviews* 19, 619-631

Arndt RE and Maines BH (1994) Vortex cavitation: A progress report. In: O'Hern TJ (Ed.) *Cavitation and gas-liquid flow in fluid machinery and devices*, ASME Fluids Engineering Division Summer Meeting, v. FED-190, 99-117

Attal M (in press) Linkage between sediment transport and supply in mountain rivers. *Gravel Bed Rivers 8 conference: Gravel Bed Rivers and Disasters.*

Attal M, Lavé J (2006) Changes of bedload characteristics along the Marsyandi River (central Nepal): Implications for understanding hillslope sediment supply, sediment load evolution along fluvial networks, and denudation in active orogenic belts. In: Willett SD, Hovius N, Brandon MT and Fisher D (Eds.) *Tectonics, Climate, and Landscape Evolution*, Geological Society of America Special Paper 398, 143-171

Attal M, Lavé J (2009) Pebble abrasion during fluvial transport: Experimental results and implications for the evolution of the sediment load along rivers. *Journal of Geophysical Research* 114, F04023

Attal M, Cowie PA, Whittaker AC, Hobley D, Tucker GE, Roberts GP (2011) Testing fluvial erosion models using the transient response of bedrock rivers to tectonic forcing in the Apennines, Italy. *Journal of Geophysical Research* 116, F02005

Bagnold RA (1966) An approach to the sediment transport problem from general physics. *US Geological Survey Professional Paper 422-I*

Baker VR (1973) Palaeohydrology and sedimentology of Lake Missoula flooding in eastern Washington. *Geological Society of America Special Paper* 144, 1-79

Baker VR (1988) Flood erosion. In: Baker VR, Kochel RC, Patton PC (Eds.) *Flood Geomorphology*. Wiley, New York, pp. 81-95

Baker VR (2002) The Study of Superfloods. *Science* 295, 2379-2380

Baker VR (2009) Overview of megaflooding: Earth and Mars. In: Burr DM, Carling PA, Baker VR (Eds.) *Megaflooding on Earth and Mars*. Cambridge University Press, Cambridge. pp. 1-12

Baker VR, Bunker, RC (1985) Cataclysmic late Pleistocene flooding from glacial lake Missoula: a review. *Quaternary Science Reviews* 4, 1-41

Baker VR, Kale VS (1998) The Role of Extreme Floods in Shaping Bedrock Channels. In: Tinkler KJ, Wohl EE (Eds.) *Rivers Over Rock: Fluvial Processes in Bedrock Channels*, AGU Geophysical Monograph 107

Baker VR, Benito G, Rudoy AN (1993) Paleohydrology of Late Pleistocene Superflooding. Altay Mountains, Siberia. *Science* 259, 348-350

Barnes HL (1956) Cavitation as a Geological Agent. *American Journal of Science* 254, 493-505

Baynes ERC, Attal M, Niedermann S, Kirstein LA, Dugmore AJ, Naylor M (2015) Erosion during extreme flood events dominates Holocene canyon evolution in North-East Iceland. *Proceedings of the National Academy of Sciences* 112 (8), 2355-2360

Baynes ERC, Attal M, Dugmore AJ, Kirstein LA, Whaler KA (2015) Catastrophic impact of extreme flood events on the morphology and evolution of the lower Jökulsá á Fjöllum (northeast Iceland) during the Holocene. *Geomorphology,* doi: 10.1016/j.geomorph.2015.05.009

Benito G (1997) Energy expenditure and geomorphic work of the cataclysmic Missoula flooding in the Columbia River gorge, USA. *Earth Surface Processes and Landforms* 22, 457-472

Bennett SJ (1999) Effect of slope on the growth and migration of headcuts in rills. *Geomorphology* 30, 273-290

Berlin MM, Anderson RS (2007) Modeling of knickpoint retreat on the Roan Plateau, western Colorado. *Journal of Geophysical Research* 112, F03S06

Berlin MM, Anderson RS (2009) Steepened channels upstream of knickpoints: Controls on relict landscape response. *Journal of Geophysical Research* 114, F03018

Bishop P, Hoey TB, Jansen JD, Artza IL (2005) Knickpoint recession rate and catchment area: The case of uplifted rivers in Eastern Scotland. *Earth Surface Processes and Landforms* 30, 767-778

Björnsson H (2002) Subglacial lakes and jökulhlaups in Iceland. *Global and Planetary Change* 35, 255-271

Björnsson H (2009) Jökulhlaups in Iceland: sources, release and drainage. In: Burr DM, Carling PA, Baker VR (Eds.) *Megaflooding on Earth and Mars*. Cambridge University Press, Cambridge. pp. 50-64

Björnsson H, Pálsson F (2008) Glaciers in Iceland. *Jökull* 58, 365-386

Blard P-H, Farley KA (2008) The influence of ^{4}He on cosmogenic ^{3}He determinations in volcanic olivine and pyroxene. *Earth and Planetary Science Letters* 276, 20-29

Bonnet S (2009) Shrinking and splitting of drainage basins in orogenic landscapes from the migration of the main drainage divide. *Nature Geoscience* 2, 766-771

Boulton SJ, Stokes M, Mather AE (2014) Transient fluvial incision as an indicator of active faulting and Plio-Quaternary uplift of the Moroccan High Atlas. *Tectonophysics* 633, 16-33

Braun J, Willett SD (2013) A very efficient *O(n)*, implicit and parallel method to solve the stream power equation governing fluvial incision and landscape evolution. *Geomorphology* 180-181, 170-179

Brader MD (2012) *Lateglacial to Holocene relative sea-level changes at Stykkishólmur, northern Snæellsnes, Iceland.* Durham University: Unpublished Masters Thesis

Bretz JH (1923) The channeled scabland of the Columbia Plateau. *The Journal of Geology* 31, 617-649

Brunsden D, Thornes JB (1979) Landscape Sensitivity and Change. *Transactions of the Institute of British Geographers* 4 (4), 463-484

Buffington JM, Montgomery DR (1997) A systematic analysis of eight decades of incipient motion studies, with special reference to gravel-bedded rivers. *Water Resources Research* 33 (8), 1993-2029

Burbank DW, Leland J, Fielding E, Anderson RS, Brozovic N, Reid MR, Duncan C (1996) Bedrock incision, rock uplift and threshold hillslopes in the northwestern Himalayas. *Nature* 379, 505-510

Burke MJ, Woodward J, Russell AJ, Fleisher PJ (2009) Structural controls on englacial proto-esker sedimentation: Skeiðarárjökull, Iceland. *Annals of Glaciology* 50, 85-92

Burke MJ, Woodward J, Russell AJ (2010a) Sedimentary architecture of large-scale, jökulhlaup-generated, ice-block obstacle marks: Examples from Skeiðarársandur, SE Iceland. *Sedimentary Geology* 227 (1-4), 1-10

Burke MJ, Woodward J, Russell AJ, Fleisher PJ, Bailey PK (2010b) The sedimentary architecture of outburst flood eskers: A comparison of ground-penetrating radar data from Bering Glacier, Alaska and Skeiðarárjökull, Iceland. *GSA Bulletin* 122 (9-10), 1637-1645

Carling PA (1996) Morphology, sedimentology and palaeohydraulic significance of large gravel dunes, Altai Mountains, Siberia. *Sedimentology* 43, 647-664

Carling PA (2013) Freshwater megaflood sedimentation: What can we learn about generic processes? *Earth Science Reviews* 125, 87-113

Carling PA, Kirkbride AD, Parnachov S, Borodavko PS, Berger GW (2002) Late Quaternary catastrophic flooding in the Altai Mountains of south-central Siberia: a synoptic overview and an introduction to flood deposit sedimentology. In: Martini PI, Baker VR, Garzon G (Eds.) *Flood and Megaflood Processes and Deposits: Recent and Ancient Examples*. Special Publications of the International Association of Sedimentologists. Blackwell Science, Oxford. 17-35

Carling PA, Burr DM, Johnsen TF, Brennand TA (2009a) A review of open-channel megaflood depositional landforms on Earth and Mars. In: Burr DM, Carling PA, Baker VR (Eds.) *Megaflooding on Earth and Mars*. Cambridge University Press, Cambridge. pp. 33-49

Carling PA, Herget J, Lanz JK, Richardson K, Pacifici A (2009b). Channel-scale erosional bedforms in bedrock and in loose granular material: character, processes and implications. In: Burr DM, Carling PA, Baker VR (Eds.) *Megaflooding on Earth and Mars*. Cambridge University Press, Cambridge. pp. 13-32

Carling PA, Martini IP, Herget J, Borodavko P, Parnachov S (2009c). Megaflood sedimentary valley fill: Altai Mountains, Siberia. In: Burr DM, Carling PA, Baker VR (Eds.) *Megaflooding on Earth and Mars*. Cambridge University Press, Cambridge. pp. 243-264

Carrivick JL (2006) Application of 2D hydrodynamic modelling to high magnitude outburst floods: An example from Kverkfjöll, Iceland. *Journal of Hydrology* 321, 187-99

Carrivick JL (2007) Hydrodynamics and geomorphic work of jökulhlaups (glacial outburst floods) from Kverkfjöll volcano, Iceland. *Hydrological Processes* 21, 725-740

Carrivick JL, Russell AJ, Tweed FS (2004) Geomorphological evidence for jökulhlaups from Kverkfjöll volcano, Iceland. *Geomorphology* 63, 81-102

Carrivick JL, Tweed FS, Carling PA, Alho P, Marren PM, Staines K, Russell AJ, Rushmer EL, Duller R (2013) Discussion of 'Field evidence and hydraulic modelling of a large Holocene jökulhlaup at Jökulsá á Fjöllum channel, Iceland' by Douglas Howard, Sheryl Luzzadder-Beach and Timothy Beach, 2012. *Geomorphology* 201, 512-519

Cenderelli DA, Wohl EE (2001) Peak discharge estimates of glacial-lake outburst floods and 'normal' climatic floods in the Mount Everest region, Nepal. *Geomorphology* 40, 57-90

Chambers JE, Wilkinson PB, Wardrop D, Hameed A, Hill I, Jeffrey C, Loke MH, Meldrum PI, Kuras O, Cave M, Gunn DA (2012). Bedrock detection beneath river terrace deposits using three-dimensional electrical resistivity tomography. *Geomorphology* 177-178, 17-25

Chanson H (2002) *The hydraulics of Stepped Chutes and Spillways*. Swets & Zeitlinger BV, Lisse

Claerbout JF, Muir F (1973) Robust modelling with erratic data. *Geophysics* 38 (5), 826-844

Clague JJ, Evans SG (1997) The 1994 jökulhlaup at Farrow Creek, British Columbia, Canada. *Geomorphology* 19, 77-87

Clarke AO (1996) Estimating probable maximum floods in the Upper Santa Ana Basin, Southern California, from stream boulder size. *Environmental and Engineering Geoscience* 2, 165-182

Clayton JJ, Knox JC (2008) Catastrophic flooding from Glacial Lake Wisconsin. *Geomorphology* 93, 382-97

Cook KL, Turowski JM, Hovius N (2013) A demonstration of the importance of bedload transport for fluvial bedrock erosion and knickpoint propagation. *Earth Surface Processes and Landforms* 38, 683-695

Cook KL, Turowski JM, Hovius N (2014) River gorge eradication by downstream sweep erosion. *Nature Geoscience* 7, 682-686

Coppus R, Imeson AC (2002) Extreme events controlling erosion and sediment transport in a semi-arid Sub-Andean valley. *Earth Surface Processes and Landforms* 27, 1365-75

Costa JE (1983) Paleohydraulic reconstruction of flash-flood peaks from boulder deposits in the Colorado Front Range. *Geological Society of America Bulletin* 94 (8), 986-1004

Craddock WH, Burbank DW, Bookhagen B, Gabet EJ (2007) Bedrock channel geometry along an orographic rainfall gradient in the upper Marsyandi River valley in central Nepal. *Journal of Geophysical Research* 112, F03007

Crosby BT, Whipple KX (2006) Knickpoint initiation and distribution within fluvial networks: 236 waterfalls in the Waipaoa River, North Island, New Zealand. *Geomorphology* 82, 16-38

Crosby BT, Whipple KX, Gasparini NM, Wobus C (2007) Formation of fluvial hanging valleys: Theory and simulation. *Journal of Geophysical Research* 112, F03S10

Dadson SJ, Hovius N, Chen H, Dade WB, Hsieh M-L, Willett DS, Hu J-C, Horng M-J, Chen M-C, Stark CP, Lague D, Lin J-C (2003) Links between erosion, runoff variability and seismicity in the Taiwan orogen. *Nature* 426, 648-651

DiBiase RA, Whipple KX (2011) The influence of erosion thresholds and runoff variability on the relationships among topography, climate and erosion rate. *Journal of Geophysical Research* 116, F04036

DiBiase RA, Whipple KX, Lamb MP, Heimsath AM (2015) The role of waterfalls and knickzones in controlling the style and pace of landscape adjustment in the western San Gabriel Mountains, California. *GSA Bulletin* 127 (3-4), 560-583

Doetsch J, Linde N, Pessognelli M, Green AG, Günther T (2012) Constraining 3-D electrical resistance tomography with GPR reflection data for improved aquifer characterization. *Journal of Applied Geophysics* 78, 68-76

Duller RA, Mountney NP, Russell AJ, Cassidy NC (2008) Architectural analysis of a volcaniclastic jökulhlaup deposit, southern Iceland: sedimentary evidence for supercritical flow. *Sedimentology* 55, 939-964

Duller RA, Warner NH, McGonigle C, De Angelis S, Russell AJ, Mountney NP (2014) Landscape reaction, response, and recovery following the catastrophic 1918 Katla jokulhlaup, southern Iceland. *Geophysical Research Letters* 41, 4214-4221

Dunai TJ (2000) Scaling factors for production rates of in situ produced cosmogenic nuclides: a critical reevaluation. *Earth and Planetary Science Letters* 176, 157-169

Dunai TJ (2010) *Cosmogenic Nuclides: Principles, Concepts and Applications in the Earth Surface Sciences.* Cambridge University Press, Cambridge

Dunning SA, Large ARD, Russell AJ, Roberts MJ, Duller R, Woodward J, Meriaux A-S, Tweed FS, Lim M (2013) The role of multiple glacier outburst floods in proglacial landscape evolution: The 2010 Eyjafjallajökull eruption, Iceland. *Geology* 41 (10), 1123-1126

Dunning SA, Rosser NJ, Petley DH, Massey CR (2006) Formation and failure of the Tsatichhu landslide dam, Bhutan. *Landslides* 3, 107-113

Duvall A, Kirby E, Burbank DW (2004) Tectonic and lithologic controls on bedrock channel profiles and processes in coastal California. *Journal of Geophysical Research* 109, F03002

Eliasson S (1974) Eldsumbrot i Jökulsárgljúfrum [Eruptions in Jökulsárgljúfur]. *Náttúrufræðingurinn* 44, 52-70.

Eliasson S (1977) Molar um Jökulsárhlaup og Ásbyrgi. *Náttúrufræðingurinn* 47, 160-179

Evans SG, Clague JJ (1994) Recent climatic change and catastrophic geomorphic processes in mountain environments. *Geomorphology* 10, 107-128

Fay H (2002) Formation of kettle holes following a glacial-outburst flood (jökulhlaup), Skeiðarársandur, southern Iceland. In: Snorasson A, Finnsdottir HP, Moss M, (Eds.) *The Extremes of the Extremes: Extraordinary Floods*. IAHS Publication, vol. 271. IAHS Press, Oxford. pp. 205-210

Fairbanks RG (1989) A 17,000-year glacio-sea level record: influence of glacial melting rates on the Younger Dryas event and deep-ocean circulation. *Nature* 342, 637-642.

Ferrier KL, Huppert KL, Perron JT (2013) Climatic control of bedrock river incision. *Nature* 496, 206-211

Finnegan NJ, Roe G, Montgomery DR, Hallet B (2005) Controls on the channel width of rivers: Implications for modelling fluvial incision of bedrock. *Geology* 33, 229-232

Flint J-J (1973) Experimental development of headward growth of channel networks. *GSA Bulletin* 84 (3), 1087-1094

Flores-Cervantes JE, Istanbulluoglu JE, Bras R (2006) Development of gullies on the landscape: A model of headcut retreat resulting from plunge pool erosion. *Journal of Geophysical Research* 111, F01010

Frankl A, Poesen J, Deckers J, Haile M, Nyssen J (2012) Gully head retreat rates in semi-arid highlands of Northern Ethiopia. *Geomorphology* 173-174, 185-195

Gangloff A (2014) *Numerical and analogical modelisation in fluvial dynamics*. Masters thesis. Universite de Rennes 1

Garcia-Castellanos D, Estrada F, Jimenez-Munt I, Gorini, C, Fernandez M, Verges J, De Vicente R (2009) Catastrophic flood of the Mediterranean after the Messinian salinity crisis. *Nature* 462, 778-781

Gardner TW (1983) Experimental study of knickpoint and longitudinal profile evolution in cohesive, homogenous material. *GSA Bulletin* 94, 664-672

Gasparini NM, Whipple KX, Bras RL (2007) Predictions of steady state and transient landscape morphology using sediment-flux-depended river incision models. *Journal of Geophysical Research* 112, F3, doi: 10.1029/2006/JF000567

Geirsdottir A, Miller GH, Andrews JT (2007) Glaciation, erosion and landscape evolution of Iceland. *Journal of Geodynamics* 43 (1), 170-186

Georgsson LS, Friðleifsson GÓ, Ólafsson M, Sigurðsson Ó, Hafstad þH (1989) *Aquaculture condition in Öxarfjörður. Ground water, ground sea, geothermal systems and research drilling*. *Aquaculture Project 1987-1988.* Orkustofnun report OS-89041/JHD-08. pp. 61 (In Icelandic.

Geotomo (2001) *Res2Dinv Electrical Resistivity Tomography processing software*. Version 3.4

Gilbert GK (1877) *Report on the geology of the Henry Mountains*. US Geographical and geological survey of the Rocky Mountain region, Department of the Interior, Government Printing Office, Washington D.C.

Gilbert (1896) *Niagara Falls and their history.* National Geographic Society/American Book Company, New York

Gilbert GK (1907) *Rate of recession of Niagara Falls*. USGS Bull No. 306. Available at http://pubs.usgs.gov/bul/0306/report.pdf. Accessed April 14, 2014

Goehring BM, Kurz MD, Balco G, Schaefer JM, Licciardi J, Lifton N (2010) A reevalution of in situ cosmogenic ^{3}He production rates. *Quaternary Geochronology* 5, 410-418

Gosse JC, Phillips FM (2001) Terrestrial in situ cosmogenic nuclides: theory and application. *Quaternary Science Reviews* 20, 1475-1560

Graf WH (1977) *Hydraulics of sediment transport*. McGraw-Hill, New York

Gudmundsson MT, Larsen G, Hoskuldsson A, Gunnar Gyljason A (2008) Volcanic hazards in Iceland. *Jokull* 58, 251-268

Gupta S, Collier JS, Palmer-Felgate A, Potter G (2007) Catastrophic flooding origin of shelf valley systems in the English Channel. *Nature* 448, 342-345

Hancock GS, Anderson RS, Whipple KX (1998) Beyond power: bedrock river incision processes and form. In: Tinkler KJ, Wohl EE (Eds.) *Rivers over rock: fluvial processes in bedrock channels.* American Geophysical Union Monograph 107, 35-60

Hartshorn K, Hovius N, Dade WB, Slingerland RL (2002) Climate-Driven Bedrock Incision in an Active Mountain Belt. *Science* 297, 2036-2038

Hasbargen LE, Paola C (2000) Landscape instability in an experimental drainage basin. *Geology* 28 (12), 1067-1070

Haviv I, Enzel Y, Whipple KX, Zilberman E, Matmon A, Stone J, Fifield KL (2010) Evolution of vertical knickpoints (waterfalls) with resistant caprock: Insights from numerical modelling. *Journal of Geophysical Research* 115, F03028

Hayakawa Y, Matsukara Y (2003) Recession rates of waterfalls in Boso Peninsula, Japan, and a predictive equation. *Earth Surface Processes and Landforms* 28, 675-684

Helgason J (1987) Jarðfræðirannsóknir á Vatnasviði Jökulsár á Fjöllum við Möðrudal [Geological Investigations of the Jökulsá á Fjöllum drainage basin at Modrudalur]. Report OS-87005/VOD-01: Orkustofnun Reykjavík. Available here: http://www.os.is/gogn/Skyrslur/OS-1987/OS-87005.pdf. Accessed October 6, 2014. Icelandic

Heritage GL, Large ARG, Moon BP, Jewitt G (2004) Channel hydraulics and geomorphic effects of an extreme flood event on the Sabie River, South Africa. *Catena* 58, 151-181

Hjort C, Ingólfsson Ó, Norðdahl H (1985) Late Quaternary geology and glacial history of Hornstrandir, Northwest Iceland: a reconnaissance study. *Jökull* 35, 9-29

Holland WN, Pickup G (1976) Flume study of knickpoint development in stratified sediment. *GSA Bulletin* 87 (1), 76-82

Howard AD, Kerby G (1983) Channel changes in Badlands. *GSA Bulletin* 94, 739-752

Howard AD, Dietrich WE, Seidl MA (1994) Modeling fluvial erosion on regional to continental scales. *Journal of Geophysical Research* 99 (B7), 13971-13986

Howard DA, Luzzader-Beach S, Beach T (2012) Field evidence and hydraulic modelling of a large Holocene Jökulhlaup at Jökulsá á Fjöllum channel, Iceland. *Geomorphology* 147-148, 73-85

Hsu H-L, Yanites BJ, Chen C-C, Chen Y-G (2010) Bedrock detection using 2D electrical resistivity imaging along the Peikang River, central Taiwan. *Geomorphology* 114, 406-414

Hubbard A, Sugden D, Dugmore AJ, Norddahl H, Petursson HG (2006) A modelling insight into the Iceland Last Glacial Maximum ice sheet. *Quaternary Science Reviews* 25, 2283-2296

Hydrologic Engineering Centre (2001) *HEC-RAS River analysis system. Hydraulic Reference Manual ver. 3.0.* Army Corps of Engineering, Davis, California

Ingólfsson Ó (1991) A review of the Late Weichselian and early Holocene glacial and environmental history of Iceland. In Caseldine C, Maizels JK (Eds) *Environmental Change in Iceland: Past and Present,* Dordrecht, Kluwer pp. 13-29

Ingólfsson Ó, Norðdahl H (2001) High relative sea level during the Bølling Interstadial in Western Iceland: a reflection of ice-sheet and extremely rapid glacial unloading. *Arctic, Antarctic and Alpine Research* 33 (2), 231-243

Ingólfsson Ó, Norðdahl H, Schomacker A (2010) Deglaciation and Holocene Glacial History of Iceland. In Schomacker A, Krüger J, Kjær KH (Eds.) *The Mýrdalsjökull Ice Cap, Iceland: Glacial Processes, Sediments and Landforms on an active volcano Developments in Quaternary Science* 13 pp. 51-68

Ísaksson SP (1985) Stórhlaup í Jökulsá á Fjöllum á fyrri hluta 18. Aldar [Big floods in the Jökulsá á Fjöllum in the first half of the 18th Century]. *Náttúrufræðingurinn* 54 (4-5), 165-191. Icelandic

Jansen JD, Fabel D, Xu S, Schnabel C, Codilean AT (2011) Does increasing paraglacial sediment supply slow knickpoint retreat? *Geology* 39, 543-546

Jennings A, Syvitski J, Gerson L, Grönvold K, Geirsdóttir Á, Hardardóttir J, Andrews J, Hagen S (2000) Chronology and palaeoenvironments during the late Weichselian deglaciation of the south west Iceland shelf. *Boreas* 29, 167-183

Jerolmack DJ, Paola C (2010) Shredding of environmental signals by sediment transport. *Geophysical Research Letters* 37, L19401

Jóhannesson H, Sæmundsson K (1999) *Geological map 1:1.000.000*. Icelandic Institute of Natural History, Reykjavik

Jónsson J (1982) Notes of Katla volcanological debris flows. *Jökull* 32, 61-68

Kataoka KS (2011) Geomorphic and sedimentary evidence of a gigantic outburst flood from Towada caldera after the 15 ka Towada-Hachinohe ignumbrite eruption, northeast Japan. *Geomorphology* 125 (1), 11-26

Kehew AE, Lord ML (1986) Origin and large-scale erosional features of glacial-lake spillways in the northern Great Plains. *GSA Bulletin* 97, 162-177

Kirby E, Whipple KX (2012) Expression of active tectonics in erosional landscapes. *Journal of Structural Geology* 44, 54-75

Kirby E, Whipple KX, Tang W, Chen Z (2003) Distribution of active rock uplift along the eastern margin of the Tibetan plateau: inferences from bedrock channel longitudinal profile. *Journal of Geophysical Research* 108, 2217

Kirkbride MP, Dugmore AJ, Brazier V (2006) Radiocarbon dating of mid-Holocene megaflood deposits in the Jökulsá á Fjöllum, north Iceland. *The Holocene* 16 (4), 605-609

Komar PD (1984) The lemniscate loop-comparisons with the shapes of streamlined landforms. *Journal of Geology* 92, 133-146

Korup O (2006) Rock-slope failure and the river long profile. *Geology* 34, 45-48

Kurz MD (1986) Cosmogenic helium in a terrestrial igneous rock. *Nature* 320, 435-439

Lague D (2014) The stream power river incision model: evidence, theory and beyond. *Earth Surface Processes and Landforms* 39, 38-61

Lague D, Crave A, Davy P (2003) Laboratory experiments stimulating the geomorphic response to tectonic uplift. *Journal of Geophysical Research* 108 (B1), 2008

Lague D, Hovius N, Davy P (2005) Discharge, discharge variability and the bedrock channel profile. *Journal of Geophysical Research* 110: F04006

Lal D (1988) In situ-produced cosmogenic isotopes in terrestrial rocks. *Annual Review of Earth and Planetary Sciences* 16, 355-388

Lal D (1991) Cosmic ray labeling of erosion surfaces: in situ nuclide production rates and erosion models. *Earth and Planetary Science Letter*s 104, 424-439

Lamb MP, Dietrich WE (2009) The persistence of waterfalls in fractured bedrock. *GSA Bulletin* 121 (7-8), 1123-1134

Lamb MP, Howard AD, Dietrich WE, Perron JT (2007) Formation of amphitheater-headed valleys by waterfall erosion after large-scale slumping on Hawaii. *GSA Bulletin* 119 (7), 805-822

Lamb MP, Dietrich WE, Sklar LS (2008a) A model for fluvial bedrock incision by impacting suspended and bed load sediment. *Journal of Geophysical Research* 113, F03025

Lamb MP, Dietrich WE, Aciego SM, DePaolo DJ, Manga M (2008b) Formation of Box Canyon, Idaho, by Megaflood: Implications for Seepage Erosion on Earth and Mars. *Science* 320 (5879), 1067-1070

Lamb MP, Fonstad MA (2010) Rapid formation of a modern bedrock canyon by a single flood event. *Nature Geoscience* 3, 477-481

Lamb MP, Mackey BH, Farley KA (2014) Amphitheater-headed canyons formed by megaflooding at Malad Gorge, Idaho. *Proceedings of the National Academy of Sciences* 111 (1), 57-62

Lamb MP, Finnegan NJ, Scheingross JS, Sklar LS (2015) New insights into the mechanics of fluvial bedrock erosion through flume experiments and theory. *Geomorphology,* doi:10.1016/j.geomorph.2015.03.003

Lane SN, Reid SC, Tayefi V, Yu D, Hardy RJ (2008) Reconceptualising coarse-sediment delivery problems in rivers as catchment-scale and diffuse. *Geomorphology* 98, 227-249

Lapotre MGA, Lamb MP (2015) Hydraulics of floods upstream of horseshoe canyons and waterfalls. *Journal of Geophysical Research: Earth-Surface.* doi: 10.1002/2014JF003412.

Lavé J, Avouac JP (2000) Active folding of fluvial terraces across the Siwaliks Hills, Himalayas of central Nepal. *Journal of Geophysical Research* 105 (B3), 5735-5770

Lavé J, Avouac JP (2001) Fluvial incision and tectonic uplift across the Himalayas of central Nepal. *Journal of Geophysical Research* 106 (B11), 26561-26591

Leopold LB, Wolman MG, Miller JP (1964) *Fluvial processes in Geomorphology*. Freeman, San Francisco

Leske (1963) Die Umlenkung eines frei herabfallenden eben Strahls an einer horizontalen Sohle. *Wissehnschaftliche Seitschrift TU Dresden* 12 (6), 1749-1765

Licciardi JM, Kurz MD and Curtice JM (2006) Cosmogenic ^{3}He production rates from Holocene lava flows in Iceland. *Earth and Planetary Science Letters* 246, 251-264

Licciardi JM, Kurz MD and Curtice JM (2007) Glacial and volcanic history of Iceland table mountains from cosmogenic 3He exposure ages. *Quaternary Science Reviews* 26, 1529-1546

Lloyd JM, Norðdahl H, Bentley M,J Newton AJ, Tucker O, Zong Y (2009) Lateglacial to Holocene relative sea-level changes in the Bjarkarlundur area near Reykhólar, North West Iceland. *Journal of Quaternary Science* 24 (7), 816-831

Loke MH, Acworth I, Dahlin T (2003) A comparison of smooth and blocky inversion methods in 2D electrical imaging surveys. *Exploration Geophysics* 34, 182-187

Mackey BH, Scheingross JS, Lamb MP, Farley KA (2014) Knickpoint formation, rapid propagation, and landscape response following coastal cliff retreat at the last interglacial sea-level highstand: Kaua'i, Hawai'i. *GSA Bulletin* 126 (7-8), 925-942

Magilligan FJ (1992) Thresholds and the spatial variability of flood power during extreme floods. *Geomorphology* 5, 373-390

Magilligan FJ, Gomez B, Mertes LAK, Smith LC, Smith ND, Finnegan D, Garvin JB (2002) Geomorphic effectiveness, sandur development, and the pattern of landscape response during jökulhlaups: Skeiðarársandur, southeastern Iceland. *Geomorphology* 44, 95-113

Magnusson E, Gudmundsson MT, Roberts MJ, Sigurdsson G, Hoskuldsson F, Oddsson B (2012) Ice-volcano interactions during the 2010 Eyjafjallajökull eruption, as revealed by airborne imaging radar. *Journal of Geophysical Research* 117, B07405

Maizels JK (1991) Origin and evolution of Holocene sandurs in areas of jokulhlaup drainage, south Iceland. In: Maizels JK, Caseldine C (Eds.) *Environmental Change in Iceland: Past and Present.* Kluwer Academic Publishers

Maizels JK (1993) Lithofacies variations within sandur deposits: the role of runoff regime, flow dynamics and sediment supply characteristics. *Sedimentary Geology* 85, 299-325

Maizels JK (1995) Sediments and landforms of modern proglacial terrestrial environments. In: Menzies JE, (Ed.) *Modern Glacial Environments.* Butterworth-Heinemann, Oxford. p. 365-416

Maizels JK (1997) Jökulhlaup deposits in proglacial areas. *Quaternary Science Reviews* 16, 793-819

Malverti L, Lajeunesse E, Metivier F (2008) Small is beautiful: Upscaling from microscale laminar to natural turbulent rivers. *Journal of Geophysical Research* 113, F04004.

Margold M, Jansson KN, Stroeven AP, Jansen JD (2011) Glacial Lake Vitim, a 3000-km^3 outburst flood from Siberia to the Arctic Ocean. *Quaternary Research* 76, 393–396

Marren PM, Russell AJ, Rushmer EL (2009) Sedimentology of a sandur formed by multiple jökulhlaups, Kverkfjöll, Iceland. *Sedimentary Geology* 213, 77-88

Martinez-Lopez J, Rey J, Duenas J, Hidalgo C, Benavente J (2013) Electrical Tomography applied to the detection of subsurface cavities. *Journal of Cave and Karst Studies* 75 (1), 28-37

Masarik J, Reedy RC (1995) Terrestrial cosmogenic-nuclide production systematics calculated from numerial simulations. *Earth and Planetary Science Letters* 136, 381-395

Mitrovica JX, Tamisiea ME, Davis JL, Milne GA, (2001) Recent mass balance of polar ice sheets inferred from patterns of global sea-level change. *Nature* 409, 1026-1029

Montgomery DR, Hallet B, Yuping L, Finnegan N, Anders A, Gillespie A, Greenberg HM (2004) Evidence for Holocene megafloods down the Tsangpo River gorge, southeastern Tibet. *Quaternary Research* 62, 201-207

Morche D, Schmidt K-H (2012) Sediment transport in an alpine river before and after a dambreak flood event. *Earth Surface Processes and Landforms* 37, 347-353

Morche D, Schmidt K-H, Heckmann T, Haas F (2007) Hydrology and geomorphic effects of a high-magnitude flood in an Alpine river. *Geografiska Annaler Series A* 89 (1), 5-19

Mudd SM, Attal M, Milodowski DT, Grieve SWD, Valters DA (2014) A statistical framework to quantify spatial variation in channel gradients using the integral method of channel profile analysis. *Journal of Geophysical Research* 119 (2), 138-152

Murai H, Nishi S, Shimizu S, Murakami Y, Hara Y, Kuroda T, Yaguchi S (1997) Velocity dependence of cavitation damage (sheet-type cavitation). *Transactions of the Japan Society of Mechanical Engineers, Part B* 63 (607), 750-756

Niedermann S (2002) Cosmic-Ray-Produced Noble Gases in Terrestrial Rocks: Dating Tools for Surface Processes. *Reviews in Mineralogy and Geochemistry* 47, 731-784

Niedermann S, Bach W, Erzinger J (1997) Noble gas evidence for a lower mantle component in MORBs from the southern East Pacific Rise: Decoupling of helium and neon isotope systematics. *Geochimica et Cosmochimica Acta 61* (13), 2697-2715

Norðdahl H (1991) Late Weichselian and Early Holocene deglaciation history of Iceland. *Jökull* 40, 27-50

Norðdahl H, Pétursson HG (2005) Relative sea-level changes in Iceland: new aspects of the Weichselian deglaciation of Iceland. In, Caseldine C, Russell A, Harðardóttir J, Knudsen O (eds.) *Iceland: Modern Processes and Past Environments Amsterdam*: Elsevier pp. 25-78

O'Connor JE (1993) Hydrology, hydraulics, and geomorphology of the Bonneville flood. *GSA Special Paper* 274, 83

O'Connor JE, Baker VR (1992) Magnitudes and implications of peak discharges from glacial Lake Missoula. GSA Bulletin 104, 267-79

Oberteuffer JA (1974) Magnetic Separation: A Review of Principles, Devices and Applications. *IEEE Transactions on Magnetics* 10 (2), 223-238

Olafsson M, Friðleifsson GÓ, Eiriksson J, Sigvaldason H, Ármannsson H (1993) *On the origin of organic gas in Öxarfjörður, NE-Iceland.* Orkustofnun (Icelandic National Energy Authority Geothermal Division) report OS-93015/JHD-05. Reykjavik. pp. 76

Ortega JA, Wohl E, Livers B (2013) Waterfalls on the eastern side of Rocky Mountain National Park, Colorado, USA. *Geomorphology* 198, 37-44

Paola C, Parker C, Seal R, Sinha SK, Southard JB, Wilcock PR (1992) Downstream fining by selective deposition in a laboratory flume. *Science* 258, 1757-1760

Rathburn SL (1993) Pleistocene cataclysmic flooding along the Big Lost River, east central Idaho. *Geomorphology* 8 (4), 305-19

Rengers FK, Tucker GE (2014) Analysis and modelling of gully headcut dynamics, North American high plains. *Journal of Geophysical Research: Earth Surface* 119, 983-1003

Rengers FK, Tucker GE (2015) The evolution of gully headcut morphology: a case study using terrestrial laser scanning and hydrological monitoring. *Earth Surfaces Processes and Landforms*

Repka JL, Anderson RS, Finkel RC (1997) Cosmogenic dating of fluvial terraces, Fremont River, Utah. *Earth and Planetary Science Letters* 152, 59-73

Reusser L, Bierman P, Pavich M, Larsen J, Finkel R (2006) An episode of rapid bedrock channel incision during the last glacial cycle, measured with ^{10}Be. *American Journal of Science* 306, 69-102

Richardson K, Carling PA (2005) A typology of sculpted forms in open bedrock channels. *GSA Special Paper* 392

Roberts M (2005) Jokulhlaups: A reassessment of floodwater flow through glaciers. *Reviews of Geophysics* 43, RG1002

Robinson ZP, Fairchild IJ, Russell AJ (2010) Hydrogeological implications of glacial landscape evolution at Skeiðarársandur, SE Iceland. *Geomorphology* 97, 218-236

Roering JJ, Kirchner JW, Sklar LS, Dietrich WE (2001) Hillslope evolution by nonlinear creep and landsliding: An experimental study. *Geology* 29 (2), 143-146.

Rosenbloom NA, Anderson RS (1994) Hillslope and channel evolution in a marine terraced landscape, Santa Cruz, California. *Journal of Geophysical Research* 99, 14013-14029

Rudoy AN (2002) Glacier-dammed lakes and geological work of glacial superfloods in the late Pleistocene, Southern Siberia, Altai Mountains. *Quaternary International* 87, 119-140

Rundgren M, Ingólfsson Ó, Björck S, Jiang H, Hafliðason H (1997) Dynamic sea-level change during the last deglaciation of northern Iceland. *Boreas* 26, 201-215

Rushmer EL (2002) Sedimentological and Geomorphological impacts of the jökulhlaup (glacial outburst flood) in January 2002 at Kverkfjöll, Northern Iceland. *Geografiska Annaler Series A- Physical Geography* 88, 43-53

Russell AJ, Roberts MJ, Fay H, Marren PM, Cassidy NJ, Tweed FS, Harris T (2006) Icelandic jökulhlaup impacts: Implications for ice-sheet hydrology, sediment transfer and geomorphology. *Geomorphology* 75, 33-64

Russell AJ, Tweed FS, Roberts MJ, Harris TD, Gudmundsson MT, Knudsen O and Marren PM (2010) An unusual jökulhlaup resulting for subglacial volcanism, Sólheimajökull, Iceland. *Quaternary Science Reviews* 29, 1363-81

Russell AJ, Knudsen Ó (2002) Jökulhlaup deposits at the Ásbyrgi Canyon, northern Iceland: sedimentology and implications for flow type. In: Snorasson A, Finnsdóttir HP, Moss, M, (Eds.), *The Extreme of the Extremes: Extraordinary Floods*. Proceedings Symposium at Reykjavik, Iceland, July 2000, 271. IAHS Publication 271, pp. 107–112.

Sæmundsson K (1973) Straumrákaðarklappir I kringum Ásbyrgi. *Náttúrufræðingurinn* 43, 52-60

Saemundsson K, Hjartarson A, Kaldal I, Sigurgeirsson MA, Kristinsson SG, Vikingsson S (2012) *Geological Map of the Northern Volcanic Zone, Iceland. Northern Part. 1: 100,000*. Iceland GeoSurvey and Landsvirkjun, Reykjavik

Scheingross JS, Brun F, Lo DY, Omerdin K, Lamb MP (2014) Experimental evidence for fluvial bedrock incision by suspended and bedload sediment. *Geology* 42 (6), 523-526

Schumm SA (1973) Geomorphic thresholds and complex response of drainage systems. In: Morisawa M (Ed.) *Fluvial Geomorphology*. George Allen and Unwin, London, pp. 299-310

Schumm SA (1979) Geomorphic Thresholds: The Concept and its Applications. *Transactions of Institute of British Geographers* 4 (4), 485-515

Schumm SA and Lichty RW (1965) Time, space and casuality in geomorphology. *American Journal of Science* 263, 110-119

Schunke E (1985) Sedimenttransport und fluviale Abtragung der Jökulsá á Fjöllum im periglazialen Zentral-Island [Sediment transport and fluvial erosion of Jökulsá Fjöllum in periglacial Central Iceland]. *Erdkunde* 39 (3), 197-205. German

Seidl MA, Dietrich WE (1992) The problem of channel erosion into bedrock. *Catena Supplement* 23, 101-24

Seidl MA, Finkel RC, Caffee MW, Hudson GB, Dietrich WE (1997) Cosmogenic isotope analyses applied to river longitudinal profile evolution: Problems and interpretations. *Earth Surface Processes and Landforms* 22, 195-290

Seong YB, Owen LA, Bishop MP, Bush A, Clendon P, Copland L, Finkel RC, Kamp U, Shroder Jr JF (2008) Rates of fluvial bedrock incision within an actively uplifting orogeny: Central Karakoram Mountains, northern Pakistan. *Geomorphology* 97, 27-286

Shakesby RA (1985) Geomorphological effects of jökulhlaups and ice-dammed lakes, Jotunheimu, Norway. *Geografisk Tidaskrift* 39, 1-16

Shennan I, Milne G, Bradley S (2012) Late Holocene vertical land motion and relative sea-level changes: lessons from the British Isles. *Journal of Quaternary Science* 27, 64-70

Siewert MB, Krautblatter M, Christiansen HH, Eckerstorfer M (2012) Arctic rockwall retreat rates estimated using laboratory-calibrated ERT measurements of talus cones in Longyeardalen, Svalbard. *Earth Surface Processes and Landforms* 37, 1542-1555

Sigbjarnarson G (1996) Norðan Vatnajökuls III. Eldstöðvar og hraun frá nútíma. *Náttúrufræðingurinn* 65, 199-212

Sklar LS, Dietrich WE (2001) Sediment and rock strength controls on river incision into bedrock. *Geology* 29, 1087-1090

Sklar LS, Dietrich WE (2004) A mechanistic model for river incision into bedrock by saltating bed load. *Water Resources Research* 40, W06301

Smith KT, Dugmore AJ (2006) Jökulhlaups circa Landnám: Mid- to Late first millennium AD floods in South Iceland and their implications for landscapes of settlement. *Geografiska Annaler A* 88 (2), 165-176

Smith LC, Alsdorf DE, Magilligan FJ, Gomez B, Mertes LAK, Smith ND, Garvin JB (2000) Estimation of erosion, deposition, and net volumetric change caused by the 1996 Skeiðarársandur jökulhlaup, Iceland, from synthetic aperture radar interferometry. *Water Resources Research* 36 (6), 1583-94

Snyder NP, Whipple KX, Tucker GE, Merritts DJ (2003a) Importance of a stochastic distribution of floods and erosion thresholds in the bedrock river incision problem. *Journal of Geophysical Research* 108, B2, 2117

Snyder NP, Whipple KX, Tucker GE, Merritts DJ (2003b) Channel response to tectonic forcing: DEM analysis of stream profiles in the Mendocino triple junction region, northern California. *GSA Bulletin* 112, 1250-1263

Stein OR, Julien PY (1993) Criterion delineating the mode of headcut erosion. *Journal of Hydraulic Engineering* 119 (1), 37-50

Stein OR, Julien PY, Alonso CV (1993) Mechanics of jet scour downstream of a headcut. *Journal of Hydraulic Research* 31 (6), 723-738

Stock JD, Montgomery DR (1999) Geologic constraints on bedrock river incision using the stream power law. *Journal of Geophysical Research* 104, 4983-93

Stokes M, Griffiths JS, Mather A (2012) Palaeoflood estimates of Pleistocene coarse grained river terrace landforms (Rio Almanzora, SE Spain). *Geomorphology* 149-150, 11-26

Striberger J, Bjorck S, Holmgren S, Hamerlik L (2012) The sediments of Lake Logurinn – A unique proxy record of Holocene glacial meltwater variability in eastern Iceland. *Quaternary Science Reviews* 38, 76-88.

Telford WM, Geldart LP, Sheriff ER (1990) *Applied Geophysics*, Second Edition. Cambridge University Press, Cambridge

Thórarinsson S (1950) Jökulhlaup og eldgos á jökulvatnasvæði Jökulsár á Fjöllum [Glacial floods and eruptions in the drainage basin of Jökulsá á Fjöllum]. *Náttúrufræðingurinn* 20, 113-133. Icelandic

Thors K, Helgadóttir G (1991) Evidence from south west Iceland of low sea-level in Flandrian times. In Maizels JK, Caseldine C (Eds.) *Environmental Change in Iceland: Past and Present.* Kluwer Academic: Dordrecht pp. 93-104

Tomasson H (1973) Hamfarahlaup i Jökulsá á Fjöllum [Catastrophic floods in Jökulsá á Fjöllum]. *Náttúrufræðingurinn* 43, 12-34. Icelandic

Tómasson H (1996) The jökulhlaup from Katla in 1918. *Annals of Glaciology* 22, 249-54

Tómasson H (2002) Catastrophic floods in Iceland. In: Snorasson A, Finnsdóttir HP, Moss M (Eds.) *The Extremes of the Extremes: Extraordinary Floods*, International Association of Hydrological Sciences Publication no. 271, 121-128

Tucker GE, Hancock GR (2010) Modelling landscape evolution. *Earth Surface Processes and Landforms* 35, 28-50

Tucker GR, Lancaster ST, Gasparini NM, Bras DL, Rybarczyk SM (2001) An object-oriented framework for distributed hydrologic and geomorphic modeling using triangulated irregular networks. *Computers and Geosciences* 27 (8), 959-973

Turowski JM, Lague D, Crave A, Hovius N (2006) Experimental channel response to tectonic uplift. *Journal of Geophysical Research* 111, F03008

Turowski JM, Lague D, Hovius N (2007) Cover effect in bedrock abrasion: A new derivation and its implications for the modelling of bedrock channel morphology. *Journal of Geophysical Research* 112, F04006

Turowski JM Hovius N, Hseih M-L, Lague D, Chen M-C (2008) Distribution of erosion across bedrock channels. *Earth Surface Processes and Landforms* 33, 353-363

Turowski JM, Lague D, Hovius N (2009) Response of bedrock channel width to tectonic forcing: Insights from a numerical model, theoretical considerations, and comparison with field data. *Journal of Geophysical Research* 114, F03016

Turowski JM, Badoux A, Leuzinger J, Hegglin R (2013) Large floods, alluvial overprint, and bedrock erosion. *Earth Surface Processes and Landforms* 38, 947-958

Tushingham AM, Peltier WR (1991) Ice-3G: a new global model of Late Pleistocene deglaciation based upon geophysical prediction of post-glacial relative sea level change. *Journal of Geophysical Research* 96, 4497-4523.

Tweed FS, Russell AJ (1999) Controls on the formation and sudden drainage of glacier-impounded lakes: implications for jökulhlaup characteristics. *Progress in Physical Geography* 23 (1), 79-110

Vishcer DL, Hager WH (1995) *Energy Dissipaters*, Rotterdam, AA Balkema

Von Engeln OS (1940) A particular case of knickpunkte. *Annals of the American Association of Geographers* 30, 268-271

Waitt RB (1998) *Cataclysmic flood along Jökulsá a Fjöllum, north Iceland, compared to repeated colossal jökulhlaups of Washington's channelled scabland*. 15th International Sedimentology Congress, Alicante, Abstracts, 811-812

Waitt RB (2002) Great Holocene floods along the Jökulsá á Fjöllum, north Iceland. In: Martini PI, Baker VR, Garzon G (Eds.) *Flood and Megaflood Processes and Deposits: Recent and Ancient Examples,* Special Publications of International Association of Sedimentologists pp. 37-51

Ward DJ, Spotila JA, Hancock GS, Galbraith JM (2005) New constraints on the late Cenozoic incision history of the New River, Virginia. *Geomorphology* 72, 54-72

Warner NH, Gupta S, Kim J-R, Lin S-Y, Muller J-P (2010) 'Retreat of a giant cataract in a long-lived (3.7-2.6 Ga) martian outflow channel. *Geology* 38 (9), 791-794

Warner NH, Sowe M, Gupta S, Dumke A, Goddard K (2013) Fill and spill of giant lakes in the eastern Valles Marineris region of Mars. *Geology* 41 (6): 675-678

Waythomas CF, Walder JS, McGimsey RG, Neal CA (1996) A catastrophic flood caused by drainage of a caldera lake at Aniakchak Volcano, Alaska, and implications for volcanic hazards assessment. *GSA Bulletin* 108, 861-71

Weissel JK, Seidl MA (1998) Inland propagation of erosional escarpments and river profile evolution aross the southeast Australian passive continental margin. In: Tinkler J, Wohl EE (Eds.) *Rivers over Rock: Fluvial Processes in Bedrock Channels*. AGU Geophysical Monograph Series 107, 189-206

Wells RR, Alonso CV, Bennett SJ (2009) Morphodynamics of Headcut Development and Soil Erosion in Upland Concentrated Flows. *Soil Science Society of America Journal* 73, 521-530

Whipple KX (2001) Fluvial landscape response time: how plausible is steady-state denudation? *American Journal of Science* 301, 313-325

Whipple KX (2004) Bedrock rivers and the geomorphology of active orogens. *Annual Reviews of Earth and Planetary Sciences* 32, 151-185

Whipple KX, Tucker GE (1999) Dynamics of the stream-power river incision model: Implications for height limits of mountain ranges, landscape response timescales, and research needs. *Journal of Geophysical Research* 104 (B8), 17661-74

Whipple KX, Parker G, Paola C, Mohrig D (1998) Channel dynamics, sediment transport, and the slope of alluvial fans: Experimental study. *The Journal of Geology* 106, 677-693

Whipple KX, Hancock GS, Anderson RS (2000) River incision into bedrock: mechanics and relative efficacy of plucking, abrasion and cavitation. *GSA Bulletin* 112 (3), 490-503

Whittaker AC, Boulton SJ (2012) Tectonic and climatic controls on knickpoint retreat rates and landscape response times. *Journal of Geophysical Research* 1117, F02024

Whittaker AC, Cowie PA, Attal M, Tucker GE, Roberts GP (2007) Bedrock channel adjustment to tectonic forcing: implications for predicting river incision rates. *Geology* 35, 103-106

Wiedmer M, Montgomery DR, Gillespie AR, Greenberg H (2010) Late Quaternary megafloods from Glacial Lake Atna, Southcentral Alaska, U.S.A. *Quaternary Research* 73, 412-424

Willgoose G, Bras RL, Rodriguez-Iturbe I (1991) A coupled channel network growth and hillslope evolution model, 1, Theorys. *Water Resources Research* 27 (7), 1671-84

Wilson A, Hovius N, Turowski JM (2013) Upstream-facing convex surfaces: Bedrock bedforms produced by fluvial bedload abrasion. *Geomorphology* 180-181, 187-204

Wilson A, Lavé J (2014) Convergent evolution of abrading flow obstacles: Insights from analogue modelling of fluvial bedrock abrasion by coarse bedload. *Geomorphology* 208, 207-224

Wobus CW, Tucker GE and Anderson RS (2006) Self-formed bedrock channels. *Geophysical Research Letters* 33, L18408

Wohl E (1992) Gradient irregularity in the Herbert Gorge of Northeastern Australia. *Earth Surface Processes and Landforms* 17, 69-84

Wolman MG, Gerson R (1978) Relative scales of time and effectiveness of climate in watershed geomorphology. *Earth Surface Processes* 3, 189-208

Wolman MG, Miller JP (1960) Magnitude and Frequency of Forces in Geomorphic Processes. *The Journal of Geology* 68 (1), 54-74

Yanites BJ, Tucker GE (2010) Controls and limits on bedrock channel geometry. *Journal of Geophysical Research* 115, F04019

You Y, Yu Q, Pan X, Wang X, Guo L (2013) Application of electrical resistivity tomography in investigating depth of permafrost base and permafrost structure in Tibetan Plateau. *Cold Regions Science and Technology* 87, 19-26

Zweck C, Zreda M, Desilets D (2013) Snow shielding factors for cosmogenic nuclide dating inferred from Monte Carlo neutron transport simulations. *Earth and Planetary Science Letters* 379, 64-71

7: Appendices

Appendix A. Supplementary information for Sub-Chapter 2.3

A.1 Surface exposure dating

Tables A1 and A2 provide information relevant for the calculations of the surface exposure age ranges. Table A1 shows general sample information, He isotope data and calculated exposure ages. Table A2 provides information used for the estimate of radiogenic ^{4}He production from the decay of uranium and thorium. The eruption age of the basalt lava flows from which the samples were collected is not known other than “younger than 800 ka” (Sæmundsson, 2012); however based on radiogenic ^{4}He production rates, the total amount of ^{4}He measured in our samples could have been produced within ~30-150 ka (Table A2), which means we cannot exclude that up to 100% of total ^{4}He may be radiogenic in origin. If the basalt eruption age is higher than 30-150 ka, then an unknown fraction of radiogenic ^{4}He would have been lost from the samples. Nevertheless, the crushing extractions show that magmatic He is present as well and has certainly not been completely degassed prior to the melting extractions. Therefore, the ^{4}He measured in the samples may be anything between purely magmatic and purely radiogenic in origin. We therefore give the maximum range in which the true surface exposure age may lie, using a 0% and 100% fraction of radiogenic ^{4}He to total ^{4}He, respectively, as the lower and upper limit.

Assuming no radiogenic ^{4}He, the lower limit on the surface exposure age range is calculated by subtracting the $(^{3}He/^{4}He)_{Crushed}$ ratio from the $(^{3}He/^{4}He)_{Melt}$ ratio in order to determine the $(^{3}He_{Cosmogenic}/^{4}He)$ ratio (e.g. ref. 1). Assuming all the ^{4}He is radiogenic in origin, the upper limit on the surface exposure age range is calculated assuming all of the ^{3}He in the melt measurement is cosmogenic. The production rate was calculated using the Dunai (2000) scaling scheme with a sea-level high-latitude rate of 124 at g^{-1} yr^{-1} (Goehring *et al.*, 2010). The true exposure age for each sample lies between the upper and lower limits, with the exception of DW8 where only a maximum age limit is possible due a contamination of the sample with basalt matrix (as evidenced by $(^{3}He/^{4}He)_{Melt} < (^{3}He/^{4}He)_{Crushed}$).

Table A3 provides all the information regarding the dip measurements of all the samples, as well as the topographic shielding measurements. As all measurements of dip and shielding are low, there is a negligible correction required for the production rate of cosmogenic ^{3}He. This is due to the cosmic ray flux being greatest from directly above the sample location as there is less atmosphere to pass through so shielding blocks/topography located at a low angle on the horizon have a very small impact on the overall production rate (see Fig. 2.2.10). Figs A1-A9 are photographs of each of the sampling locations within the Jökulsárgljúfur canyon processed in this study.

Table A1: Sample information and He isotope data used to determine the surface exposure ages. The $(^{3}He/^{4}He)_{Crushed}$ ratio was measured after the samples were crushed *in vacuo*, releasing the gases contained within fluid and melt inclusions within the olivine and pyroxene samples. These gases are magmatic in origin so need to be corrected for when calculating the abundance of $^{3}He_{Cosmogenic}$. The $(^{3}He/^{4}He)_{Melt}$ ratio was measured after the samples were melted in a furnace at 1750 ^{o}C, releasing the gases contained in the crystal lattice of the olivine and pyroxene. The column of $^{4}He_{Melt}$ is the concentration of ^{4}He per gram of sample measured in the melt extraction. Assuming no radiogenic ^{4}He, the $(^{3}He/^{4}He)_{Crushed}$ ratio is subtracted from the $(^{3}He/^{4}He)_{Melt}$ ratio in order to determine the $(^{3}He_{Cosmogenic}/^{4}He)$ ratio (e.g. Niedermann, 2002). Assuming all the ^{4}He is radiogenic in origin, all of the ^{3}He in the melt measurement is cosmogenic and this concentration is used to estimate the exposure age.

* weighted mean of two samples (DW5, DW7) was used for samples of a single lava flow.

Sample Name	Sample Mass (g)	Sample elevation (m)	Longitude and Latitude (WGS84)	$(^3He/^4He)_{Crushed}$ (10^{-6})	$(^3He/^4He)_{Melt}$ (10^{-6})	$^4He_{Melt}$ (10^{-10} cm^3 STP g^{-1})	$^3He_{Cosmo}$ (10^6 at g^{-1}) – assuming no radiogenic ^4He	$^3He_{Cosmo}$ (10^6 at g^{-1}) – assuming 100% radiogenic ^4He	$^3He_{Cosmo}$ Production rate (at g^{-1} yr^{-1})	Exposure age assuming no radiogenic ^4He (years)	Exposure age assuming all ^4He is radiogenic (years)
DW2	0.91494	320	16.398593 °W 65.818129 °N	30.3 ± 3.0	84.7 ± 9.2	1.90 ± 0.14	0.278 ± 0.049	0.432 ± 0.048	166.0	1700 ± 300	2600 ± 300
DW3	0.80676	324	16.395168 °W 65.822557 °N	11 ± 18	258 ± 41	1.49 ± 0.18	0.99 ± 0.18	1.03 ± 0.17	166.7	5900 ± 1100	6200 ± 1000
DW4	0.61308	298	16.391800 °W 65.822469 °N	17 ± 17	40.8 ± 5.0	3.23 ± 0.25	0.21 ± 0.15	0.351 ± 0.049	162.7	1300 ± 900	2200 ± 300
DW5	0.90612	253	16.389620 °W 65.823888 °N	11.9 ± 4.4 *	38 ± 11	2.74 ± 0.20	0.193 ± 0.086	0.281 ± 0.081	156.1	1200 ± 500	1800 ± 500
DW6	1.17064	255	16.391407 °W 65.826340 °N	11.9 ± 4.4 *	30.1 ± 6.8	4.43 ± 0.23	0.217 ± 0.097	0.358 ± 0.083	156.4	1400 ± 600	2300 ± 500
DW7	0.80786	244	16.405153 °W 65.833584 °N	11.9 ± 4.4 *	28.7 ± 3.9	4.16 ± 0.31	0.188 ± 0.065	0.321 ± 0.044	154.8	1200 ± 400	2100 ± 300
DE1	0.89070	309	16.391552 °W 65.831073 °N	28 ± 12	85.1 ± 8.8	6.65 ± 0.43	1.03 ± 0.27	1.52 ± 0.17	164.3	6300 ± 1600	9300 ± 1000
AR1	0.72338	131	16.514544 °W 65.997324 °N	17.0 ± 3.6	86 ± 12	6.70 ± 0.49	1.23 ± 0.22	1.54 ± 0.21	139.2	8800 ± 1600	11000 ± 1500
DW8	*0.83574*	*279*	*16.416389 °W* 65.839065 °N	*11 ± 10*	*4.6 ± 0.6*	*61.4 ± 3.1*		*0.754 ± 0.099*	*159.8*		*4700 ± 700*

Table A2: U, Th and Li concentrations in the olivine/pyroxene separates and the basalt matrix as obtained using ICP-MS at GFZ Potsdam. Li concentrations (except in the contaminated sample DW8) are low and do not require a correction for thermal neutron-produced cosmogenic or nucleogenic ^{3}He (Dunai *et al.*, 2007). U and Th concentrations have been used to estimate the production of radiogenic ^{4}He following Blard and Farley (2008). The production rate of radiogenic ^{4}He is dependent on the phenocryst size, and we use a value of 400 µm, as we sieved our samples to between 300 and 500 µm before mineral separation. The time required for all measured ^{4}He to have been produced through U and Th decay is shown (cf. Table A1); all of these values are below the upper age limit on the eruption age of the basalt (800 ka), so we must consider the possibility that all ^{4}He in the samples is radiogenic in origin. We therefore present a lower and upper age limit for the exposure ages (assuming that there is no radiogenic ^{4}He and all ^{4}He is radiogenic, respectively). The time to produce total He by U/Th decay is not shown for sample DW8 due to a contamination of the sample with basalt matrix (cf. Table A1 caption).

Sample Name	**^{238}U ol + px (ppm)**	**^{232}Th ol + px (ppm)**	**^{7}Li ol + px (ppm)**	**^{238}U Basalt matrix (ppm)**	**^{232}Th Basalt matrix (ppm)**	**^{7}Li Basalt matrix (ppm)**	**Radiogenic ^{4}He production rate (10^{5} at/g/yr)**	**Total ^{4}He measured (10^{-10} cm^{3} STP g^{-1})**	**Time for Total ^{4}He measured to be produced through U and Th decay (ka)**
DW2	0.02	0.01	2.0	0.13	0.53	4.6	1.26	1.90 ± 0.14	40.5 ± 3.3
DW3	0.02	0.01	2.3	0.14	0.55	4.2	1.17	1.49 ± 0.18	34.1 ± 4.6
DW4	0.02	0.01	12	0.21	0.83	5.6	1.74	3.23 ± 0.25	49.4 ± 4.3
DW5	0.02	0.01	4.9	0.09	0.40	3.8	1.22	2.74 ± 0.20	60.2 ± 4.7
DW6	0.07	0.02	4.0	0.09	0.35	3.8	2.53	4.43 ± 0.23	47.0 ± 2.5
DW7	0.02	0.01	3.4	0.09	0.37	3.7	1.17	4.16 ± 0.31	95.8 ± 7.6
DE1	0.03	0.02	3.8	0.22	0.84	5.3	2.07	6.65 ± 0.43	86.1 ± 6.1
AR1	0.02	0.02	5.9	0.08	0.26	3.3	1.22	6.70 ± 0.49	148 ± 11
DW8	*0.04*	*0.06*	*62.0*	*0.22*	*0.84*	*5.7*	*2.65*	*61.4 ± 3.1*	

Table A3: Sample information regarding dip of the bedrock surface and topographic shielding measurements at each sampling location. As all measurements of dip and shielding are low, there is a negligible correction required for the production rate of cosmogenic ^{3}He (Fig 2.2.10).

Sample Name	Bedrock surface dip (degrees)	Topographic shielding measurements	
		Direction of shielding block (degrees)	Inclination of shielding block (degrees)
DW2	15	0	7.6
		10	5.0
		355	17.9
		310	15.0
		285	16.1
		265	9.4
		240	7.7
		210	5.1
DW3	0	50	4.0
		0	11.8
		270	9.8
		250	5.4
DW4	12	65	10.0
		100	17.2
		160	12.2
		200	7.8
		230	3.6
		245	5.8
		250	9.6
		310	10.9
		340	25.0
DW5	0	0	1.5
		355	10.6
		345	17.6
		330	16.8
		320	19.1
		300	25.0
		275	16.1
		250	14.2
		220	19.3
		190	30.8
		180	16.5
		160	10.2
		150	10.1
		130	15.4
		100	16.9
		70	14.4
		50	9.1

		30	6
		10	3
DW6	0	340	2.6
		330	9.6
		325	9.8
		315	17.8
		310	16.9
		295	30.2
		230	27.5
		260	55.7
		215	7.8
		200	10.0
		165	8.8
		145	12.2
		120	16.2
		90	17.2
		60	13.1
		30	6.9
		0	4.7
DW7	0	0	2.1
		345	3.5
		320	5.6
		305	11.5
		290	14.4
		275	23
		245	26
		220	27
		195	18
		190	12.3
		175	8.8
		165	2.7
		150	4.6
		135	7.2
		115	8.9
		80	13.1
		55	15.9
		30	15.6
		15	9.2
DW8	0	340	5.1
		310	13.5
		265	17
		220	15
		180	6
		150	17.2
		115	12.4
		85	12.8
		50	8.7
		15	3.4

		0	1.6
DE1	20	100	17.0
		45	11.3
		15	7.7
		10	3.9
		340	2.8
		310	1.1
		270	4.6
		220	2.8
		180	4.7
		150	7.2
AR1	0	*N/A*	

Fig. A1: Photograph of Sample AR1 location. Plucked block that was sampled has the red penknife on top of it.

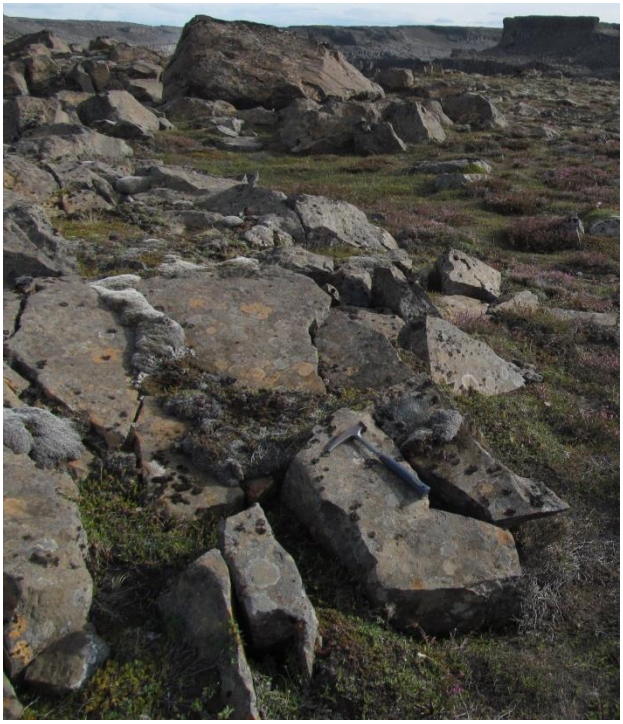

Fig. A2: Photograph of Sample DE1 location. Hammer for scale, Plucked block that was sampled is located above the hammer in the photo.

Fig. A3: Photograph of Sample DW2 location. Plucked block that was sampled has the penknife on top of it for scale.

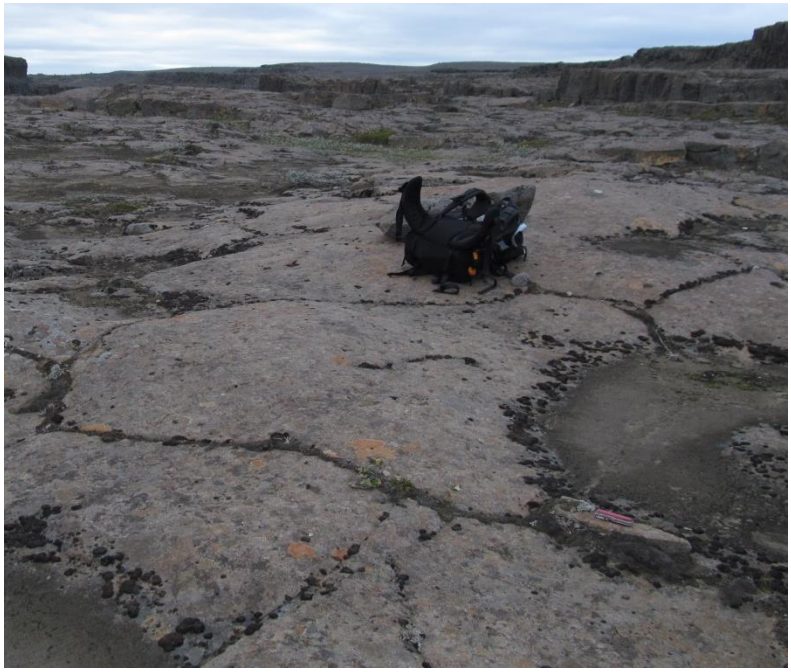

Fig. A4: Photograph of Sample DW3 location. Plucked block that was sampled has the penknife on top of it for scale, in the bottom right of the photograph.

Fig. A5: Photograph of Sample DW4 location. Plucked block that was sampled has the penknife on top of it for scale, in the bottom right of the photograph.

Fig. A6: Photograph of Sample DW5 location. Plucked block that was sampled has the penknife on top of it for scale, at the bottom of the photograph.

Fig. A7: Photograph of Sample DW6 location. Plucked block that was sampled has the penknife on top of it for scale, at the bottom of the photograph.

Fig. A8: Photograph of Sample DW7 location. Plucked block that was sampled is located to the left of the penknife and hammer.

Fig. A8: Photograph of Sample DW8 location. Plucked block that was sampled is located to the left of the penknife.

A.2 Hydraulic calculations

A.2.1 Calculation of flow depth during peak annual flow

We use a location immediately upstream of Selfoss as a reference for the calculation. The active bankful channel width (*W*) at this location is 150 m, mapped from clear channel boundaries using aerial photos and measured in the field. We assume that the channel cross-section is triangular in shape as channel cross-section data are not available at Selfoss and a triangular shape assumption will provide a maximum estimate of flow depth for a given discharge.

First, we estimate the flow depth of the Jökulsá á Fjöllum during annual peak flow. Between 1973 and 1979, the maximum discharge *Q* recorded at the Grimsstadir gauging station, 25 km upstream of Selfoss, was 470 $m^3 s^{-1}$ (Schunke, 1985, Data from Icelandic Met Office). The drainage area of the Jökulsá á Fjöllum increases by 15 % between Grimsstadir and Selfoss but most of the water is produced from glacial melt; we therefore assume that discharge does not increase noticeably between Grimsstadir and Selfoss and use a 500 $m^3 s^{-1}$ maximum discharge as a conservative estimate.

An average flow velocity *V* of 2 m/s was measured in 2001 between the Grimsstadir gauging station and Selfoss over a wide range of discharges (Henriksen, 2005). We use this value as a minimum estimate of flow velocity at Selfoss, considering that flow will probably accelerate at the lip of the waterfall. We calculate the maximum flow depth *D* at Selfoss during the maximum peak discharge of 500 $m^3 s^{-1}$ using the minimum flow velocity, the bankful width and the conservative assumption that the channel cross-section is triangular (cross section area $A = WD/2$):

$$D = \frac{2Q}{VW} = 3.3\ m \qquad \text{Eqn. A1}$$

A.2.2 Calculation of threshold flow depth and discharge for basalt column toppling

We used Lamb and Dietrich's (2009) method to calculate the threshold flow depth required for the basaltic columns to topple. This method calculates the flow depth required for column toppling based on the bedrock joint spacing, the height of the column, the angle of the column from horizontal and the channel slope (equations 11-13 in Lamb and Dietrich, 2009). We measured the spacing of the joints in the field (average 0.65 m) as well as the height of the lava flow at Selfoss (13 m). We use a channel slope of 0.002 and the columns are vertical.

Full list of parameters used in calculations:
H = 13 m; H is height of columns (measured in the field).
L = 0.65 m; L is width/length of rock columns (measured in the field).
S = 0.002; S is channel bed slope (the drop in elevation of the Jökulsá á Fjöllum between Grimsstadir and Selfoss is ~45 m over 25 km, which is equivalent to an average slope of 0.002 m/m).
θ = 0; θ is the tilt angle of rock column from horizontal. The columns in the study area are vertical (measured in the field).
ρ_r/ρ = 2.8; ρ_r is the density of basalt (2800 kg m^{-3}), ρ is density of water (1000 kg m^{-3}).
η/L = 0.1; η is the protrusion length scale. Although the rock columns do not protrude into the flow, this value takes into account the form drag induced from the roughness of the top surfaces (Lamb and Dietrich, 2009). Value for η/L is taken from Lamb and Dietrich, 2009 as column widths in Idaho are similar to those of our study area.
C_d = 1; C_d is the drag coefficient (value same as used by Lamb and Dietrich, 2009).
C_{f1} = 0.005; C_{f1} is the friction coefficient for the depth-averaged flow (value same as used by Lamb and Dietrich, 2009, representative of a gravel-bed river).

C_{f2} = 0.005; C_{f2} is the friction coefficient for the flow over the protrusion distance η (value same as that used by Lamb and Dietrich, 2009, representative of a gravel-bed river).
Fr = 0.63; Fr is the Froude number upstream of the waterfall = $(S/C_{f1})^{0.5}$ (Lamb and Dietrich, 2009).

The threshold flow depth (D) for block toppling at Selfoss is calculated to be 8.1 m.
The flow velocity and discharge at this threshold flow condition was then calculated for both an assumed triangular and rectangular channel cross-section. The triangular cross-section represents the most conservative estimate of the discharge, as the true shape of the gorge lies somewhere between triangular and rectangular in cross-section, but topographic data do not currently exist. Flow velocity is calculated using the following equation:

$$V = Fr\sqrt{gd} \qquad \text{Eqn. A2}$$

where d is the hydraulic diameter (equivalent to D in a rectangular channel and $D/2$ in a triangular channel) and g is the acceleration due to gravity. Discharge is calculated using the following equation:

$$Q = VA \qquad \text{Eqn. A3}$$

where $A = WD$ for a rectangular channel and $A = WD/2$ for a triangular channel. W increases to ~200 m for a flow depth of 8.1 m, measured from topographic data in the field. For a triangular channel cross-section, the flow velocity is 4.0 m/s and the discharge is 3250 $m^3\ s^{-1}$. For a rectangular channel cross-section, the flow velocity is 5.7 $m\ s^{-1}$and the discharge is 9200 $m^3\ s^{-1}$. The most conservative estimate of the threshold discharge for block toppling (3250 $m^3\ s^{-1}$) is more than six times greater than annual peak flow measured between 1973 and 1979 (Schunke, 1985, Data from Icelandic Met Office) and twice the discharge of floods which occur approximately twice a century (Helgason, 1987).

A sensitivity analysis was performed to assess the influence of the following three key parameters on the calculated threshold flow depth for toppling and associated flow velocity and discharge: L (width of rock columns), θ (tilt angle

of column from horizontal) and *S* (channel slope); results are shown in Tables A4, A5 and A6 respectively. In the absence of detailed topographic data, we assume that width increases linearly with depth, from 150 m for *D* = 3.3 m to 200 m for *D* = 8.1 m, before calculating discharge under the two assumptions of a triangular and a rectangular channel. The results are very sensitive to column width: columns 10 cm thinner or wider than the measured 65 cm lead to a 1 m decrease or increase in the threshold flow depth, respectively (Table A4). Tilt angle has a lesser impact, with a tilt angle of 30 degrees causing a 1 m reduction in threshold flow depth (Table A5). An increase in channel slope from 0.002 to 0.003 reduces the threshold flow depth by 1 m, whereas a reduction in channel slope from 0.002 to 0.001 increases the depth by 2 m (Table A6).

We note that if the rock columns were 0.20 - 0.25 m wide, block toppling and therefore knickpoint retreat would occur under peak annual flow conditions (~500 m^3 s^{-1}; Schunke, 1985, Data from Icelandic Met Office), assuming a triangular channel cross-section (Table A4). Floods which occur approximately twice per century (1500 m^3 s^{-1}; Helgason, 1987), would cause knickpoint retreat if the rock columns were ~0.4 m wide. The mean rock column width measured at Selfoss is 0.65 m which requires a flow of 3250 m^3 $s^{-1}$for block toppling to occur, supporting the argument that knickpoint retreat during extreme flood events is the dominant erosion mechanism. While there is some variability in the 21 individual rock column measurements at Selfoss (lower quartile: 0.5 m; upper quartile: 0.8 m), we believe using the mean column width is appropriate for determining a conservative estimate of the discharge required for block toppling to occur because while a lower discharge would be required to topple the smaller columns, these columns are interspersed with larger columns (> 1 m) that require a larger discharge to topple (Table A4).

Table A4: Influence of rock column widths (*L*) on the calculated threshold flow depth for block toppling and associated flow velocity and discharge at Selfoss, with all other parameters unchanged. An average column width of 65 cm was measured in the field.

Width of column (m)	Threshold flow depth *D* (*m*)	Triangular cross-section		Rectangular cross-section	
		Flow velocity (m s^{-1})	Discharge (m^3 s^{-1})	Flow velocity (m s^{-1})	Discharge (m^3 s^{-1})
0.2	2.8	2.3	462	3.3	1305
0.25	3.5	2.6	684	3.7	1934
0.3	4.1	2.9	935	4.0	2644
0.35	4.8	3.1	1211	4.3	3427
0.4	5.4	3.3	1511	4.6	4274
0.45	6.0	3.4	1830	4.8	5176
0.5	6.6	3.6	2167	5.1	6130
0.55	7.1	3.7	2519	5.3	7125
0.6	7.6	3.9	2886	5.5	8162
0.65	8.1	4.0	3250	5.7	9200
0.7	8.6	4.1	3651	5.8	10328
0.75	9.1	4.2	4048	6.0	11449
0.8	9.6	4.3	4452	6.1	12593
0.85	10.0	4.4	4863	6.3	13754
0.9	10.4	4.5	5279	6.4	14932
0.95	10.8	4.6	5700	6.5	16121
1.0	11.2	4.7	6122	6.6	17317

Table A5: Influence of rock column tilt angle (θ) on the calculated threshold flow depth for block toppling and associated flow velocity and discharge at Selfoss, with all other parameters unchanged. Columns are vertical at Selfoss ($\theta = 0$).

Tilt angle of column (degrees)	Threshold flow depth *D* (*m*)	Triangular cross-section		Rectangular cross-section	
		Flow velocity (m s^{-1})	Discharge (m^3 s^{-1})	Flow velocity (m s^{-1})	Discharge (m^3 s^{-1})
0	8.1	4.0	3250	5.7	9200
5	8.1	4.0	3239	5.6	9161
10	8.0	4.0	3167	5.6	8959
15	7.9	3.9	3050	5.6	8628
20	7.6	3.9	2892	5.5	8180
25	7.4	3.8	2697	5.4	7628
30	7.0	3.7	2471	5.3	6990
35	6.6	3.6	2222	5.1	6285
40	6.2	3.5	1957	4.9	5536
45	5.7	3.4	1684	4.7	4763

Table A6: Influence of channel slope (*S*) on the calculated threshold flow depth for block toppling and associated Froude number (*Fr*), flow velocity and discharge at Selfoss, with all other parameters unchanged. Average slope of the Jökulsá á Fjöllum is 0.002 between Grimsstadir and Selfoss.

Channel slope *S* *(m/m)*	Froude number	Threshold flow depth *D* (*m)*	Triangular cross-section		Rectangular cross-section	
			Flow velocity (m s^{-1})	Discharge (m^3 s^{-1})	Flow velocity (m s^{-1})	Discharge (m^3 s^{-1})
0.0010	0.45	10.0	3.1	3420	4.4	9674
0.0012	0.49	9.5	3.3	3394	4.7	9599
0.0014	0.53	9.1	3.5	3364	5.0	9514
0.0016	0.57	8.7	3.7	3331	5.2	9421
0.0018	0.60	8.4	3.9	3298	5.5	9328
0.0020	0.63	8.1	4.0	3250	5.7	9200
0.0022	0.66	7.9	4.1	3229	5.8	9133
0.0024	0.69	7.7	4.3	3194	6.0	9035
0.0026	0.72	7.5	4.4	3160	6.2	8938
0.0028	0.75	7.3	4.5	3126	6.3	8842
0.0030	0.78	7.1	4.6	3092	6.5	8746

A.3 Knickpoint retreat rates assuming progressive migration

The surface exposure ages fit within two distinct clusters; three samples overlap between 5.4 and 4.8 ka and five samples overlap between 2.3 and 1.4 ka, suggesting periods of rapid knickpoint retreat and canyon formation during these time periods, possibly associated with extreme flood events. Here, we test the alternative hypothesis that the terraces have been abandoned through the steady migration of knickpoints by calculating the possible rates of knickpoint retreat assuming that retreat between two sample locations is progressive rather than the result of discrete events. On a given terrace, point *A* at location d_A is exposed by waterfall retreat at time t_A and point *B* at location d_B is exposed by the retreat of the same waterfall at time t_B, where times t_A and t_B are identified from the surface exposure ages of the samples. The rate of knickpoint retreat (KP_{RR}) between points *A* and *B* is given by:

$$KP_{RR} = \frac{(d_B - d_A)}{(t_B - t_A)}$$ Eqn. A4

Fig. A10 shows the possible knickpoint retreat rates that could explain the distribution of the surface exposure ages from our samples, with the range in the retreat rates a result of the uncertainty in the surface exposure ages.

Even under the assumption that the knickpoints retreat progressively, there are large differences in retreat rates during different periods of the Holocene (Fig. A10). There is a phase of rapid exposure of the upper terrace postdating the fissure eruption, which overlaps with a period of rapid exposure of the middle terrace between 5.4 and 4.8 ka. There is an additional phase of rapid exposure of the lower terrace in the early Holocene between 2.3 and 0.8 ka. If we assume that the knickpoints are steadily retreating, there is a period of much slower exposure of the upper and middle terraces between 4.8 and 2.3 ka. This analysis therefore identifies two periods of rapid canyon cutting associated with knickpoint retreat. Given the overlap of surface exposure ages across multiple terraces, the nature of the bedrock (lack of evidence for incision through abrasion or diffusion of knickpoint headwalls; susceptibility for column toppling above a threshold flow depth), and the lack of progressive knickpoint retreat in historical times between 1953 and 1988, we privilege a scenario where intense erosion and rapid knickpoint retreat occurred as a result of discrete extreme flood events between 5.4 and 4.8 ka and 2.3 and 1.4 ka.

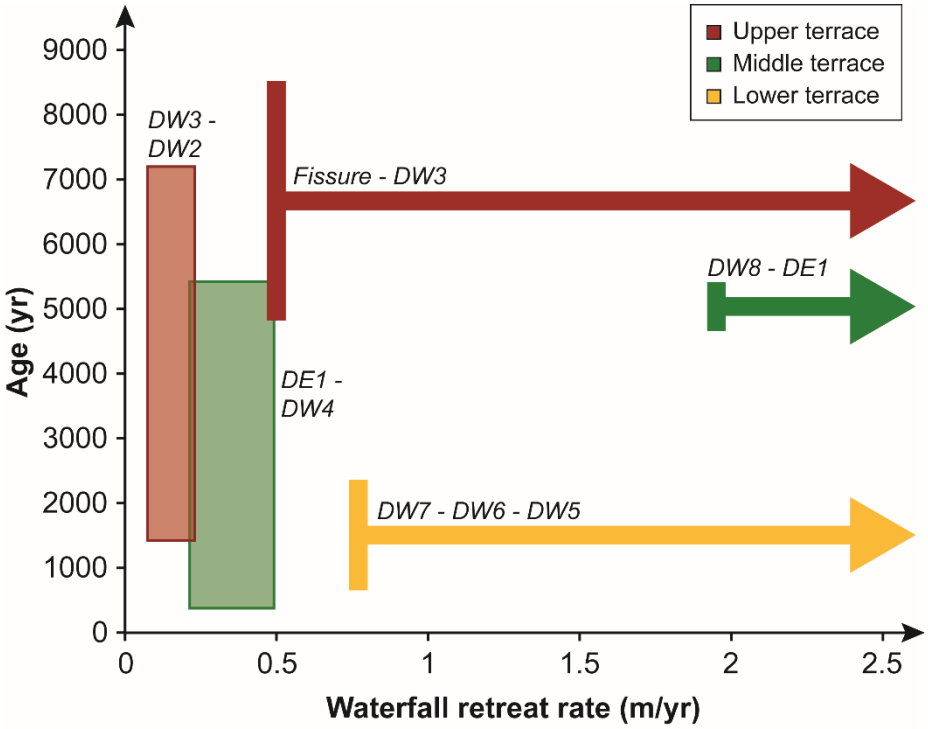

Fig. A10: Range of possible knickpoint retreat rates that could explain the age difference between samples on each terrace level, assuming that retreat between two sample locations is progressive rather than the result of discrete events. Ranges are indicated by boxes or arrows when there is no upper limit on the maximum retreat rate during these periods (the exposure ages overlap so they may have been exposed at nearly the same time e.g. following an extreme flood). For each box or arrow, the name of the samples considered in the calculation is indicated (see location of samples on Fig. 2.3.3B). Calculation of the retreat rates is explained in the text of Appendix A.3. Note that minimum retreat rates are a result of the assumption that rate is constant between the exposure of the points considered; knickpoints could have been static for periods of time if large swaths of the terraces had been exposed during discrete high magnitude events.

Appendix B. Supplementary Information for Sub-Chapter 2.4

B.1 Palaeo-flow estimates using maximum boulder size

We used the method described in Stokes *et al.* (2012) to calculate the palaeo-discharge necessary to transport the largest boulders found within the Ásbyrgi canyon. The calculation requires the following information: maximum boulder diameter, relict channel width, relict channel slope and density of the boulder material. This section provides the values of the parameters we used in the calculation and a sensitivity analysis for the effect of different values of channel slope and boulder size in both the East and West canyons of Ásbyrgi.

List of parameters used:

Boulder diameter (B): 1.49 m for East canyon, 3.75 m for West canyon. These values were measured in the field using a tape measure. Sensitivity analysis for different values of B is shown in Table 2.4.2.

Channel width (W): 410 m for East canyon. 420 m for West canyon. The canyon width was defined as the distance between the canyon walls, determined from aerial imagery. The value used is the mean of seven individual measurements for each canyon.

Channel slope (β): ~0.002 m/m. This value was derived from the Digital Elevation Model of the canyon floor, but are not well constrained due to the accuracy of the DEM. Hence, a sensitivity analysis for different values of S is shown in Table 2.4.3.

Boulder density (σ): 2800 kg m^{-3}. This value is representative of basalt.

Fluid density (ρ): 1150 kg m^{-3}. This value is typical of water containing sediment, as would be expected during a jökulhlaup.

Lift coefficient of cubic boulder (Cl_c): 0.178 (same value used as in Stokes *et al.,* 2012)

Lift coefficient of round boulder (Cl_r): 0.2 (same value used as in Stokes *et al.,* 2012)

Drag coefficient of cubic boulder (Cd_c): 1.18 (same value used as in Stokes *et al.,* 2012)

Drag coefficient of round boulder (Cd_r): 0.2 (same value used as in Stokes *et al.,* 2012)

Manning's roughness coefficient (n): 0.0283. n is defined as 0.295 $(\tan\beta)^{0.377}$. The sensitivity analysis of different values of the channel slope takes into account the resulting variability of n (Table 2.4.3).

The minimum discharge required to transport the largest boulder in the Eastern canyon is calculated to be 12,000 $m^3\ s^{-1}$.

The minimum discharge required to transport the largest boulder in the Western canyon is calculated to be 39,000 $m^3\ s^{-1}$.

Table B2 shows the results from the sensitivity analysis for different values of the maximum boulder diameter (B) for the palaeo-discharge estimate in each the East and West canyons, keeping all the other parameters constant. The results are very sensitive to boulder size; a 10 cm change in the boulder diameter leads to a change in the discharge of the order of $10^3\ m^3\ s^{-1}$. For smaller boulders (e.g. the East canyon), a change of 10 cm in the boulder size has a proportionally larger impact on the discharge magnitude; a boulder of 0.6 m requires 20% more discharge to be transported than a boulder with a diameter of 0.5 m.

Table B1 shows the results from the sensitivity analysis for different values of the channel slope (β) for the palaeo-discharge estimate in each the Eastern and Western canyons, keeping all the other parameters constant. The effect of varying the channel slope on Manning's roughness coefficient is also shown in Table 2.4.3. Channel slope has a lesser impact on the palaeo-discharge estimate, as increasing the slope by 50% from 0.002 to 0.003 in the Western channel decreases the discharge by 8% (3072 $m^3\ s^{-1}$).

Decreasing the slope by 50% from 0.002 to 0.001 increases the discharge by 12% (5554 m^3 s^{-1}).

Table B1: Sensitivity analysis for different boulder sizes (*B*) on the minimum palaeo-flow discharge estimate for both the West and the East Ásbyrgi canyons. The measured maximum boulder size was 3.75 m in the West canyon and 1.49 m in the East canyon. The channel slope was held constant at 0.002 m/m. The channel width in the West canyon was 420 m and the channel width in the East canyon was 410 m.

West canyon		East canyon	
Max. boulder size (m)	**Discharge (m^3 s^{-1})**	**Max. boulder size (m)**	**Discharge (m^3 s^{-1})**
2.5	23811	0.5	3109
2.6	25007	0.6	3905
2.7	26215	0.7	4734
2.8	27434	0.8	5594
2.9	28664	0.9	6482
3.0	29905	1.0	7394
3.1	31156	1.1	8330
3.2	32418	1.2	9287
3.3	33689	1.3	10264
3.4	34970	1.4	11260
3.5	36260	1.5	12274
3.6	37560	1.6	13306
3.7	38868	1.7	14353
3.8	40186	1.8	15416
3.9	41512	1.9	16494
4.0	42847	2.0	17586
4.1	44190	2.1	18692
4.2	45541	2.2	19811
4.3	46901	2.3	20943
4.4	48268	2.4	22087
4.5	49643	2.5	23244

Table B2: Sensitivity analysis for different channel slopes (β) on the minimum palaeo-flow discharge estimate for both the West and the East Ásbyrgi canyons. The measured slope, by extracting profiles from the DEM, was 0.002 m/m. For the West canyon calculations, the boulder size was 3.75 m and the channel width was 420 m. For the East canyon, the boulder size was 1.49 m and the channel width was 410 m.

Channel slope (m/m)	Manning's roughness coefficient (*n*)	Discharge ($m^3 s^{-1}$)	
		West canyon	East canyon
0.0010	0.0218	45080	13882
0.0012	0.0234	43557	13414
0.0014	0.0248	42306	13028
0.0016	0.0260	41246	12702
0.0018	0.0272	40331	12420
0.0020	0.0283	39526	12172
0.0022	0.0294	38809	11951
0.0024	0.0304	38163	11753
0.0026	0.0313	37577	11572
0.0028	0.0322	37040	11407
0.0030	0.0330	36454	11254
0.004	0.0368	34531	10634
0.005	0.0400	33018	10168
0.006	0.0429	31809	9796
0.007	0.0454	30805	9486
0.008	0.0478	29945	9222
0.009	0.0500	29193	8990
0.010	0.0520	28526	8784